Examining molecular interactions and dynamics in centrosome and centriole assembly



Lisa Gartenmann
Lincoln College
University of Oxford

A thesis submitted for the degree of
Doctor of Philosophy

Trinity Term 2018

Acknowledgments

First and foremost I would like to thank Jordan. Thank you for being the best supervisor I could ask for in the world. Thank you for creating the best lab environment to work in, for 'taking me in' and letting me restart my DPhil in your lab - I am deeply grateful for this. Thank you for always being cheerful, understanding, interested, motivating and always having your door open. I really appreciate all the time you made for me and all the support, advice and guidance you have provided.

I would like to thank the EPA Trust for funding my DPhil and the Dunn School staff and admin members for all the amazing support they provided through out my time here. In particular, thank you Lucinda. I would also like to thank all the members of Micron for all their help, chats and technical support. A massive thanks goes to Ian: thanks for all your time, help, for sharing your knowledge and for always managing to fix the OMX V2 when it inevitably broke down again.

I want to thank everyone in the Raff lab, both past and present members – you have all been such a pleasure to get to know and work with. In particular, thank you, Zsofi for taking so much time to teach, advise and train me, particularly in the initial period of my DPhil. Without your help, I would have never been as independent that quickly. Thank you for all your help, support and chats along the way! A really big thanks goes to Alan: thank you for teaching and training me in all things flies and microscopes, for all the help on all the projects and for sticking with me on the SAPs…! Thanks for always being encouraging, having time to talk and for sharing your knowledge and ideas. Thanks to Ines for always being there to share a laugh, for supporting me, to share geeky things with and coming to gym/boxing with me! Sorry for forcing you to eat more vegetables…! Thank you Anna for all your help, support, and our great conversations, and for helping organize the social side of the lab! Additionally, I would like to thanks all those in and outside of the lab who helped me get through this thesis and viva. Finally, a thank you goes to all members of Cake Team - thanks for letting me bake to my hearts content. Thank you everyone in the lab for creating such a friendly, open, kind and fun place to work!

I am so grateful for all the amazing friends that I have met along the way. To Anna, Ben, Chris, Neele, Julia and Christy: you have all made my time in Oxford fantastic and a laugh – thank you for all the great great memories we got to share. Thank you for keeping me going when the going got tough. I am so happy and lucky that I have gotten to know you all.

The biggest thanks goes to David – I am so lucky to have met such a wonderful, fun, clever and kind person at the start of my time in Oxford. Thank you for always being there for me during the best and worst times in this crazy DPhil ride. Thanks for always being at my side and being the best of partners. To many more great times ahead together.

Letztlich, danke Mami und Papi für alle eure Unterstützung, Liebe und Zeit. Ich hätte diese Doktorarbeit nie ohne euch geschafft – danke, dass ihr mich seit klein auf immer gefordert, unterstützt und geliebt habt. Danke, dass ihr immer Zeit hattet mit mir zu reden, dass ihr mich besucht habt, und dass meine Ferien zu Hause immer so toll waren – ihr seid die besten Eltern! Ich danke euch von ganzem Herzen!

Abstract

Examining molecular interactions and dynamics in centrosome and centriole assembly

Lisa Gartenmann, Lincoln College

Centrioles are cellular organelles that give rise to the centrosome, a structure composed of a pair of centrioles surrounded by pericentriolar material. Centrosomes perform a variety of different cellular functions: they are the main microtubule organising centre in animal cells and are important signalling hubs. The centrosome is composed of hundreds of different proteins, but only a handful are essential. In *Drosophila*, Sak/Plk4, Ana2, Sas-6, Sas-4 and Asl are required for centriole assembly and Spd-2 and Cnn are indispensable for PCM assembly. Many questions remain regarding how these proteins behave, interact and are regulated, as genetic analysis of these processes is often complicated by the absence of centrioles when these proteins are mutated.

In this thesis, I apply recent technological advancements and a biological model system to the study of essential centriole proteins. Using newly developed fluorescent proteins, I am able to localise Sak over the cell cycle in live embryos. Developing and applying a correlative microscopy approach, I was able to localise the protein termini of Ana2 and Sas-6 with nanometre precision to the centriole cartwheel. With the further characterisation and utilization of an *in vivo* centriole model system, I shed light on the direct contribution of Sak, Asl and Sas-4 on the Ana2/Sas-6 interaction, definitively identify the role of Asl in Spd-2 and Cnn recruitment, and develop a protein-protein interaction assay. The latter led me to identify novel Cdk1/Cyclin B phosphorylation sites on Ana2, providing a possible insight into the cell cycle and centriole duplication cycle link.

Publications resulting from this Thesis

Gartenmann, L., Wainman, A., Qurashi, M., Kaufmann, R., Schubert, S., Raff, J.W., and Dobbie, I.M. (2017). A combined 3D-SIM/SMLM approach allows centriole proteins to be localised with a precision of approximately 4-5 nm. *Current Biology*: *CB 27*, R1054-R1055.

Novak, Z.A., Wainman, A., **Gartenmann, L.**, and Raff, J.W. (2016). Cdk1 Phosphorylates *Drosophila* Sas-4 to Recruit Polo to Daughter Centrioles and Convert Them to Centrosomes. *Developmental Cell 37*, 545-557

Post thesis submission:

Aydogan, M. G., Steinacker, T.L., **Gartenmann, L.,** Wainman, A., Saurya, S., Conduit, P.T., Boemo, M.A., Raff, J.W. (2018). A free-running oscillator times and executes centriole biogenesis. *Nature, under review*.

Gartenmann, L. et al., 2018-2019 (*manuscript in preparation*)

Figure Titles

Figure 1.1 *Centriole architecture in different species*

Figure 1.2 *Centrioles are composed of a central cartwheel, and peripheral microtubules*

Figure 1.3 *The structure of the* Trichonympha *basal body*

Figure 1.4 *Cellular structures that arise from centrioles*

Figure 1.5 *The centriole duplication cycle*

Figure 1.6 *A conserved pathway of centriole and mitotic centrosome assembly*

Figure 1.7 *Five proteins are essential for centriole assembly in* Drosophila

Figure 1.8 *Sas-6 molecules appear to form the centriole cartwheel*

Figure 1.9 *Centriole duplication and the cell cycle*

Figure 1.10 *PCM organization and assembly in Interphase and Mitosis*

Figure 3.1 *Schematic illustration of the mRNA injection procedure*

Figure 3.2 *mNeonGreen seems brighter than GFP in the mRNA injection assay*

Figure 3.3 *mKate2 and mCardinal can fluoresce in the mRNA injection assay*

Figure 3.4 *Self-labelling enzymes exhibit high levels of background*

Figure 3.5 *mNeonGreen-Cnn performs well in our OMX-V3 3D-SIM system*

Figure 3.6 *Brightness and stability quantification of mNeonGreen and GFP*

Figure 3.7 *mRuby2 does not mature quickly enough to allow imaging in the early* Drosophila *embryo*

Figure 3.8 *Asl-mKate2 can be imaged using 3D-SIM*

Figure 3.9 *mKate2 is brighter than mCherry*

Figure 3.10 *mKate2 is more stable than mCherry*

Figure 3.11 *Sak-mNeonGreen is present as a dot at centrioles from early S-phase to early-M-phase*

Figure 3.12 *Sak-mNeonGreen is present as a ring at centrioles in late M-phase*

Figure 4.1 *Summary of localisation data of centriole and centriole wall proteins*

Figure 4.2 *Images of wing disc centrioles taken with different microscopy modes*

Figure 4.3 *A schematic model of different possible modes of interaction between the Ana2 tetramer and the Sas-6 cartwheel*

Figure 4.4 *Schematic summary of the initial selection of well-oriented centrioles*

Figure 4.5 *Summary of the procedure for the alignment of the SIM and SMLM data*

Figure 4.6 *Summary of the data processing and the calculation of the radii of the SMLM data*

Figure 4.7 *Calculations of the radial distribution of several centriole proteins*

Figure 4.8 *Precise localisation of the N-terminus of Asl using SIM and SMLM*

Figure 4.9 *The N- and C-termini of Ana2 are located towards the periphery of the cartwheel*

Figure 4.10 *Fusion-protein expression levels do not affect the localisation of Sas-4-GFP*

Figure 5.1 *The co-overexpression of Sas-6 and Ana2 leads to SAP formation*

Figure 5.2 *SAPs in* Drosophila *eggs*

Figure 5.3 *Centriole and centrosome protein organization at SAPs and centrioles*

Figure 5.4 *The organization of centriole and centrosome proteins is similar at centrioles and SAPs*

Figure 5.5 *The distribution of centriole and centrosome proteins is similar between SAPs and centrioles*

Figure 5.6 *Schematic illustration of the key centriole interaction residues and domains analysed in this study*

Figure 5.7 *Analysis of the expression levels of mutant protein in transgenic flies*

Figure 5.8 *SAP assembly appears to require the same Ana2 and Sas-6 domains and residues as centriole assembly*

Figure 5.9 *The interaction between Ana2 and Sas-4 is required for efficient SAP assembly*

Figure 5.10 *Phosphorylation of the Ana2 STAN domain is required for efficient SAP assembly*

Figure 5.11 *Quantification of SAP assembly when the Ana2 STAN domain is mutated*

Figure 5.12 *The generation of 'cilia rescue' eggs that lack Asl and Sas-4*

Figure 5.13 *mRNA injections assay to generate SAPs*

Figure 5.14 *Efficient SAP assembly requires Sas-4 and Asl, but not Sak*

Figure 5.15 *Schematic of the different Asl proteins produced by different* asl *mutations*

Figure 5.16 *The requirement of Asl and Spd-2 in PCM recruitment*

Figure 6.1 *SAPs can be formed by mRNA injection*

Figure 6.2 *Titration of the concentration of mRNA needed to generate SAPs only when both mRNA species are present*

Figure 6.3 *SAPs generated by mRNA injection require the same protein-protein interaction domains and regulatory residues to form as in transgenic eggs*

Figure 6.4 *The identification of conserved putative Cdk sites in Ana2*

Figure 6.5 *The conserved putative Cdk sites S284 and T301 could have a role in preventing centriole duplication in M-phase*

Figure 6.6 *Transgenic Ana2-2E-Cdk and Ana2-2A-Cdk mutants can form SAPs*

Figure 6.7 In vitro *kinase assay to assess the ability of Cdk1/Cyclin B to phosphorylate peptides containing the putative Ana2 Cdk sites*

Figure 6.8 *Ana2-GFP incorporation dynamics during nuclear cycle 12*

Figure 6.9 *Ana2-S284E,T301E-GFP incorporation dynamics during nuclear cycle 12*

Figure 6.10 *Ana2-S284A,T301A-GFP incorporation dynamics during nuclear cycle 12*

Figure 6.11 *Analysis of cell cycle and centriole assembly parameters during nuclear cycle 12*

Figure 7.1 *Schematics of thesis findings in context*

Abbreviations

aa	*Amino acid*
Ana	*Anastral spindle*
APC	*Anaphase-promoting complex*
A.U.	*Arbitrary units*
Asl	*Asterless*
Asp	*Abnormal simple protein*
AurA	*Aurora-A kinase*
BBS	*Bardet-Biedl Syndrome*
Bld	*Bald*
bp	*Base pair*
BSA	*Bovine Serum Albumin*
CC	*Coiled-coil*
CCA	*Coiled-coil Alanine substitution*
CCD	*Charge-Coupled Device*
ΔCC	*Coiled-coil deletion*
Cdk	*Cyclin-dependent kinase*
Cep	*Centrosomal protein*
CLEM	*Combined light microscopy and EM*
Cnn	*Centrosomin*
CPAP	*Centrosomal P4.1-associated protein*
C-terminal/terminus	*Carboxyl-terminal/terminus*
Da	*Dalton*
DNA	*Deoxyribonucleic Acid*
FRAP	*Fluorescence Recovery After Photobleaching*
e	*Endogenous*
EM	*Electron Microscopy*
ET	*Electron Tomography*
GFP	*Green Fluorescent Protein*
hr	*Hours*
IF	*Immunofluorescence*
k	*Kilo*
M	*Molar*
m	*Monomeric*
MCPH	*Autosomal primary recessive microcephaly*
MGS	*Meckel-Gruber syndrome*
min	*Minutes*
msec	*Milliseconds*
mM	*Milimolar*
MT	*Microtubule*
MTOC	*Microtubule organising centre*
N-terminal/terminus	*Amino-terminal/terminus*
nm	*Nanometre(s)*
PB	*Polo Box*
PBS	*Phosphate Buffered Saline*
PCM	*Pericentriolar material*

PCNT	*Pericentrin*
PCR	*Polymerase Chain Reaction*
PD	*Primordial Dwarfism*
pH	*Peotential Hydrogen*
PISA	*Present In Sas-6*
Plk	*Polo-like kinase*
Plp	*Pericentrin-like protein*
RFP	*Red Fluorescent Protein*
RNA	*Ribonucleic Acid*
ROI	*Region Of Interest*
mRNA	*Messenger RNA*
SAP	*Sas-6 Ana2 Particle*
Sas	*Spindle assembly abnormal*
s.d.	*Standard deviation*
SDS-PAGE	*Sodium Dodecyl Sulphate-Polyacrylamide Gel Electrophoresis*
Spd-2	*Spindle-defective protein 2*
STAN	*STIL/Ana2 Domain*
STED	*Stimulated Emission Depletion*
STIL	*SCL TAL1 Interrupting Locus*
STORM	*Stochastic Optical Reconstruction Microscopy*
3D-SIM	*3 dimensional Structured Illumination Microscopy*
SMLM	*Single Molecule Localisation Microscopy*
TACC	*Transforming Acidic Coiled-Coil*
WF	*Widefield*
WT	*Wild type*
UAS	*Upstream Activating Sequence*
Ubq	*Ubiquitin*
µl	*Microliter*
µm	*Micrometres*
unc	*Uncoordinated*
YFP	*Yellow Fluorescent Protein*

Table of Contents

1. Introduction 1

1.1. Centrioles, centrosomes and cilia 1

1.1.1. Centriole: functions and structure 2

1.1.2. Centrosomes 8

1.1.3. Cilia 13

1.1.4. Centrosomes and cilia in human diseases 15

1.2. Centriole and centrosome duplication 19

1.2.1. The essential centriole duplication proteins 21

1.2.1.1. Plk4/Sak 22

1.2.1.2. Ana2/STIL 27

1.2.1.3. Sas-6 28

1.2.1.4. Sas-4 32

1.2.1.5. Asl 34

1.2.2. Centrosome duplication regulation 36

1.3. PCM structure and recruitment 40

1.3.1.1. Organization of PCM 41

1.3.1.2. Essential PCM assembly component: Spd-2 and Cnn 43

1.4. Thesis outline 44

2. Material and methods 46

2.1. Fly Husbandry 46

2.1.1. Fly handling 46

2.1.2. *Drosophila melanogaster* stocks 46

2.1.3. Generation of transgenic lines 49

2.2. Bioinformatics 49

2.2.1. Jalview 49

2.3. Molecular Biology 50

2.3.1. PCR reactions for DNA amplification and diagnostics 50

2.3.2. Site-directed mutagenesis on plasmids....50
2.3.3. DNA sequencing....50
2.3.4. Constructions of plasmids for the generation of transgenic *Drosophila* lines ...50
2.3.5. Genetic screening and diagnostic PCRs for genetic recombination events 52
2.3.6. Constructions of plasmids for *in vitro* mRNA generate for injection into *Drosophila* eggs and embryos 52
2.3.7. *In vitro* mRNA transcription 54
2.4. Biochemistry and Cell biology 55
2.4.1. *Drosophila* embryo and egg fixation for immunoprecipitation 55
2.4.1.1. Conventional fixation 55
2.4.1.2. Formaldehyde fixation for fluorophore conservation....55
2.4.2. SDS-PAGE and western blotting 56
2.4.3. *In vitro* kinase assay and dot blotting....57
2.4.3.1. Peptides production 57
2.4.3.2. *In vitro* kinase assay 57
2.4.3.3. Biotin dot blot – loading control 58
2.4.4. *Drosophila* egg and embryo staining for immunofluorescence 58
2.4.5. Primary antibodies used in this study....59
2.4.6. Staining wing discs for 3D-SIM/SMLM....59
2.5. Microscopy and Image analysis....60
2.5.1. Microinjection of mRNA into living *Drosophila* embryos or eggs 60
2.5.2. Live imaging of *Drosophila* embryos and eggs 61
2.5.2.1. Imaging on Spinning Disc microscopes....61
2.5.2.2. Imaging on the Zeiss 880 Airyscan microscope....62
2.5.2.3. Imaging on the OMX V3 Blaze 3D-Structured Illumination Microscope....63
2.5.3. Photoconversion of fluorophores in live embryos 64
2.5.3.1. Photoconversion on the Perkin Elmer Spinning Disk 64
2.5.3.2. Photoconversion on the Zeiss 880 Airyscan 64
2.5.3.3. Photoconversion on the OMX V3 65

2.5.4. Fluorophores brightness and stability assessment on the OMX V3 Blaze.....65
2.5.5. Imaging fixed and stained *Drosophila* samples 67
2.5.5.1. Imaging fixed eggs on the Perkin Elmer ERS Spinning Disc 67
2.5.5.2. Imaging fixed samples on the OMX V3 Blaze with 3D-SIM 67
2.5.5.3. Imaging fixed and stained samples on the OMX V2 with 3D-SIM/SMLM 67
2.5.6. Image processing and presentation.....69
2.5.6.1. Using fastSPDM for SMLM image generation.....69
2.5.6.2. Radial profile analysis 70
2.5.6.3. Tracking Ana2-GFP centrioles with TrackMate 70
3. Evaluation of fluorophores for centriole and centrosome research in the early *Drosophila* embryo 72
3.1. Introduction.....72
3.1.1. Key findings 76
3.2. Results.....76
3.2.1. An mRNA injection screen to identify potentially useful fluorescent proteins .76
3.2.2. Evaluation of new fluorophores using transgenic lines.....83
3.2.2.1. Evaluation of green fluorescent protein mNeonGreen.....86
3.2.2.2. Evaluation of red fluorophores mRuby2 and mKate2.....89
3.2.2.3. Evaluation of the self-labelling enzyme SNAP-tag.....94
3.2.3. Using mNeonGreen: Protein dynamics of Sak in the early *Drosophila* embryo 97
3.3. Discussion 99
4. A correlative SIM/SMLM pipeline to examine the localisation of proteins within centrioles with nanometre precision.....104
4.1. Introduction.....104
4.1.1. Key findings 109
4.2. Results.....110
4.2.1. Selection of *Drosophila* fly lines, sample tissue and staining methods 110

4.2.2. Developing a new analysis method to image the relative position of centriole proteins with 3D-SIM/SMLM 113

4.2.2.1. 3D-SIM/SMLM proof of principle using Asl 120

4.2.3. Precise localisation of the centriole cartwheel proteins 122

4.3. Discussion 126

4.3.1. Future Directions 131

5. SAPs as a model for centriole and centrosome biogenesis 133

5.1. Introduction 133

5.1.1. Key findings 134

5.2. Results 135

5.2.1. Centriole and centrosome proteins display a strikingly similar organization at SAPs and at bona fide centrioles/centrosomes 135

5.2.2. SAP assembly requires the same molecular interactions required for centriole assembly 139

5.2.3. Using SAPs to probe the centriole assembly pathway 146

5.2.4. Using SAPs to probe the pathway of centrosome assembly 154

5.3. Discussion 163

6. SAPs: a model for identifying interaction required for centriole assembly 167

6.1. Introduction 167

6.1.1. Key findings 168

6.2. Results 169

6.2.1. Generating SAPs by mRNA injections 169

6.2.2. Identification of potential Cdk phosphorylation sites in Ana2 175

6.3. Discussion 187

7. General discussion and conclusion 191

7.1. Summary 191

7.2. Fluorescent probes - technical limitations for centriole research in *Drosophila* 191

7.3. Super-resolution microscopes – new perspectives on centrioles 195

7.4. SAPs – a model for centriole and PCM assembly, and as a protein-protein interaction assay 196

8. Appendix 199

8.1. Evaluation of the fluorophore mMaple3 199

8.1.1. Discussion 203

9. References 206

1. Introduction

1.1. Centrioles, centrosomes and cilia

Centrioles are 9-fold radially symmetric microtubule based structures (**Figure 1.1**). They form the basis for two different cellular structures: the centrosome, which consists of a pair of centrioles surrounded by a cloud of pericentriolar material (PCM) that functions as the major microtubule organizing centre (MTOC) in animal cells, and the basal body that gives rise to the cilium, an essential cellular structure for both motility and sensing environmental cues. The centriole is an ancient cellular organelle that has a remarkably conserved structure and it is found in all major eukaryotic groups (Cavalier-Smith, 2002). The last eukaryotic common ancestor is thought to have had centrioles. However, centrioles are not found in all present-day eukaryotes (Carvalho-Santos et al., 2011; Cavalier-Smith, 2002). The centriole's role at the base of the cilia is thought to have emerged first, as seen by the co-distribution of centrioles and basal bodies throughout eukaryotes (Azimzadeh, 2014). All species that have centrioles at some point in their life cycle, will also, at some point, have cilia and vice versa (Marshall, 2009). Cilia are involved in a variety of sensory functions and locomotion, suggesting an ancient and conserved function in organisms, whereas the centrosome is thought to be a more recent development as it is not always found in organisms that contain centrioles/cilia (Azimzadeh, 2014).

Centrosomes and cilia play a number of different roles in animal cells and mutations in genes encoding several centrosome and cilia proteins have been linked to a variety of human diseases and developmental disorders (Chavali et al., 2014; Nigg et al., 2014; Nigg and Holland, 2018; Nigg and Raff, 2009). It is therefore important to identify proteins that comprise the centriole, and understand how these proteins

function and interact with one another. This thesis will focus on *Drosophila* centrioles and centrosomes.

1.1.1. Centriole: functions and structure

The centriole's 9-fold symmetric structure is highly conserved – it has been proposed that the 9-fold symmetry is the result of evolutionary optimization for the development of motile cilia (Carvalho-Santos et al., 2011). However, details of the centrioles architecture, assembly and size differ between tissues and species (Carvalho-Santos et al., 2011). The diameter of centrioles is approximately 250 nm, whereas the length can typically vary between 150-500 nm (Winey and O'Toole, 2014)—and in some cases, such as in *Trichonympha*, the basal body can be ~1500 nm long (Guichard et al., 2012). In *Drosophila*, centrioles are typically ~180-200 nm long and ~200 nm in diameter (although the basal bodies in spermatocytes can be much larger – see below), whereas in humans centrioles are typically ~450-500mn long and ~200-250 nm in diameter (Nigg and Holland, 2018; Winey and O'Toole, 2014) (**Figure 1.1**).

The canonical centriole contains a 9-fold radially symmetric cartwheel in the centre. This structure contains a central hub, from which nine, evenly spaced spokes radiate outward (**Figure 1.1**). These 9-fold symmetric structures organize into ring-link units that are stacked on top of each other, each unit consists of paired rings (**Figure 1.2A**). Elegant cryo-electron tomography (ET) studies in *Trichonympha* (Guichard et al., 2013) show how ordered the centriole cartwheel is (**Figure 1.3A)**. The ring-like cartwheel units stack on top of each other and are joined to the centriole MTs by the "pinhead" (**Figure 1.3B**). The centriole microtubules can be singlets, doublets or triplets, depending on the species and the cell type (**Figure 1.3C**) (Guichard et al.,

2013). The centriole cartwheel and the centriole itself has only been visualized to date with this resolution and technique in *Trichonympha* (Guichard et al., 2013) (the centriolar microtubules have been visualised using a similar technique in *Drosophila* and vertebrate cells (Greenan et al., 2018)). It remains to be seen if the structure and all its features are conserved in other species. In *Drosophila*, the cartwheel is present in mother and daughter centrioles, whereas in mammalian cells the cartwheel is disassembled as the daughter centriole matures into a mother (see section 1.2 for details of the centriole duplication cycle).

The cartwheel is the earliest discernable structure formed during the assembly of a new daughter centriole and it is thought to dictate the 9-fold radial symmetry of centrioles (Gonczy, 2012). In particular, Sas-6/SAS-6/HsSas-6 (*Drosophila/C. elegans*/human nomenclature) appears to be the main structural component of the cartwheel (see 1.2.1.3 for more details). Sas-6 is one of the first proteins to be recruited to the site of centriole formation (Delattre et al., 2006; Leidel et al., 2005; Pelletier et al., 2006; Rodrigues-Martins et al., 2007a). Sas-6 has been shown in a variety of species to contain a N-terminal globular domain that allows for the oligomerisation of Sas-6 dimers (Cottee et al., 2015; Kitagawa et al., 2011; van Breugel et al., 2011; van Breugel et al., 2014). Nine of these Sas-6 dimers are thought to compose one cartwheel unit. Sas-6 has also been shown to self-assemble into symmetric, cartwheel unit-like structures *in vitro* (Guichard et al., 2017; Kitagawa et al., 2011; van Breugel et al., 2011). However other proteins are thought to facilitate the 9-fold symmetry *in vivo* (Cottee et al., 2011; Hilbert et al., 2016). Even though the centriole cartwheel structure is conserved throughout eukaryotes, there are some exceptions such as *C. elegans*. The *C. elegans* centriole contains a central tube,

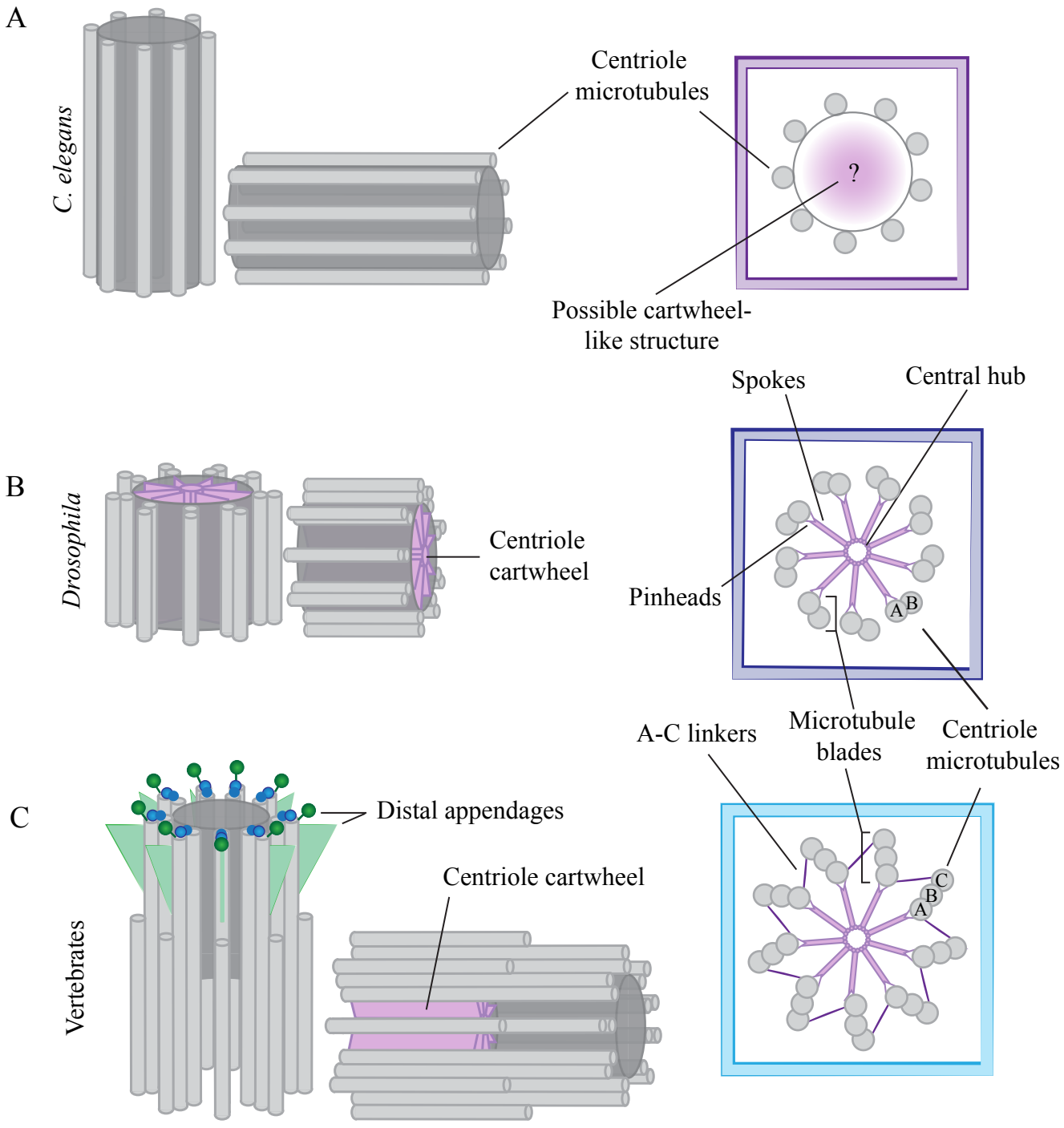


Figure 1.1: Centriole architecture in different species. Schematics illustrate a side-on (left) and end-on (right) view of a typical centriole pair in *C. elegans* (~100 nm x ~150 nm) (**A**), *Drosophila* (~200 nm x ~180-200 nm) (**B**), and vertebrates (~200-250 nm x ~450-500 nm) (**C**). The mother centriole is oriented vertically and the daughter is shown in an orthogonal, engaged, configuration. Several features of centriole architecture are highlighted.

instead of a canonical cartwheel *in vivo* (Pelletier et al., 2006), which leads to a 9-fold symmetric microtubule arrangement. Interestingly, *C. elegans* SAS-6 can oligomerise and these oligomers from a helical structure, not a stack of canonical cartwheel rings (Hilbert et al., 2013). Whether or how these observations in *in vitro* assembly properties translates into a real difference in *in vivo* cartwheel structure remains uncertain.

One feature of the centriole is the 9-fold symmetric centriolar microtubule blades that surround the cartwheel. When viewed from the proximal end of the centriole, the blades are twisted in an anti-clockwise manner (Winey and O'Toole, 2014). The number of microtubules per blade varies depending on the species and the cell type (**Figure 1.1A**). *C. elegans* centrioles contain singlet microtubules, whereas *Drosophila* centrioles contain doublet microtubules in most cells (Winey and O'Toole, 2014) (apart from spermatid cell and sensory neuron cells, which contain triplets) (Callaini et al., 1997) (**Figure 1.1B**). In vertebrates, centriole microtubule blades contain microtubule triplets at the proximal region of the centriole, whereas the distal regions contains only doublet microtubules (Gonczy, 2012) (**Figure 1.1C**).

Microtubules are cytoskeletal building blocks that play a variety of essential roles inside the cell, ranging from intracellular transport and organization, cell motility and chromosome segregation (Zhang et al., 2015). Additionally, they are important components of the centriole and have been implicated in centriole stability and inheritance (Wang et al., 2017). Microtubules consist of α- and β-tubulin, which stack head-to-tail into polar protofilaments. ~13 protofilaments associate in parallel to form a hollow, polar tube (Zhang et al., 2015) (**Figure 1.2B**). Each centriole microtubule

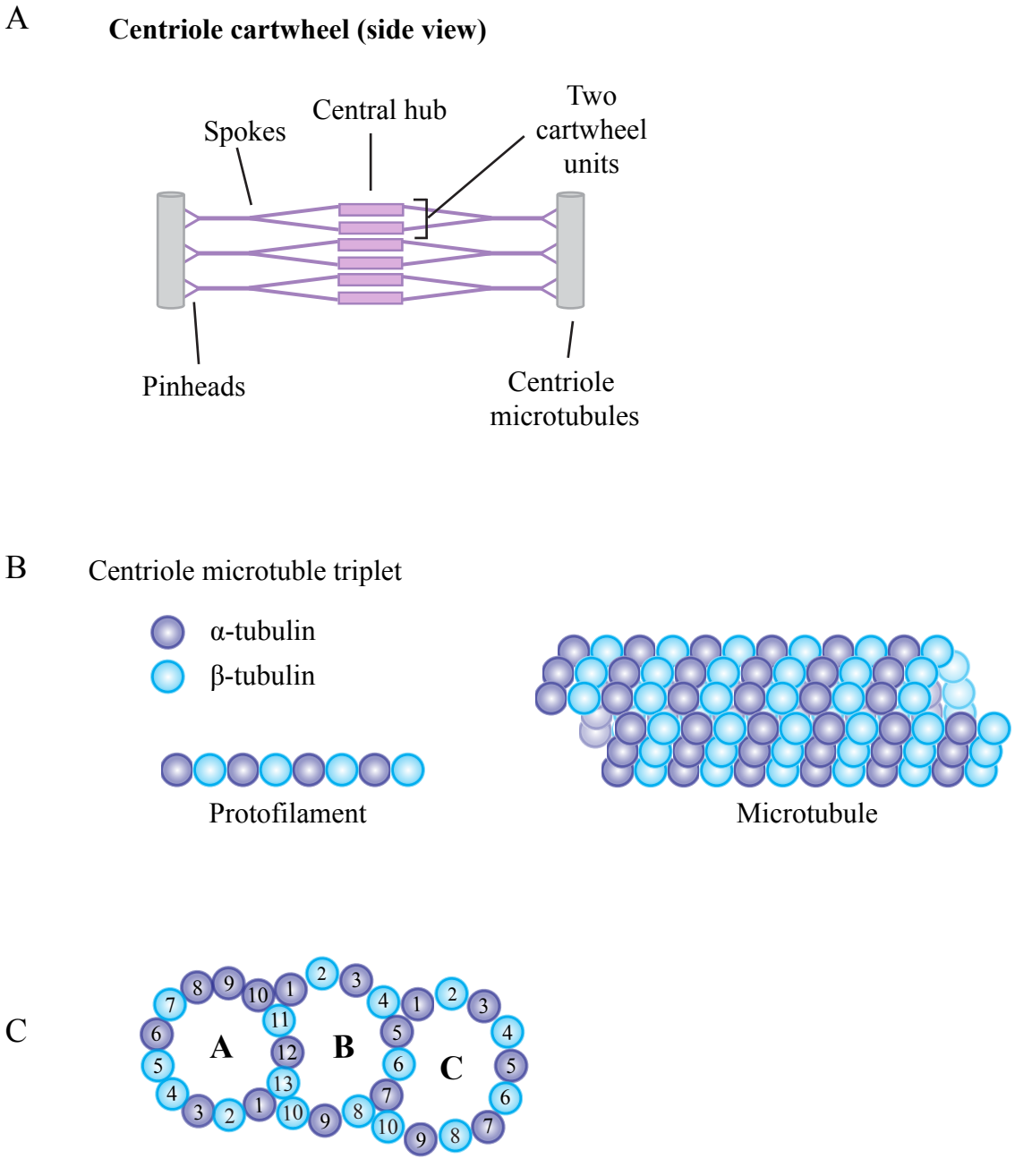


Figure 1.2: Centrioles are composed of a central cartwheel, and peripheral microtubules. Schematic illustrate several aspects of centriole and microtubule architecture. **A**) A side-on view of the centriole cartwheel and peripheral MTs . The central hubs align in the center, with the spokes radiating outward, and ending in a pinhead structure. **B**) Dimers of α- and β-tubulin monomers assemble into microtubule protofilaments. 13 protofilaments usually align to generate a microtubule **C**) A cross-section of a centriolar triplet microtubule blade. A-, B- and C-tubules, are present, with different numbers and arrangements of the protofilaments.

blade, as mentioned above, exists as triplet, doublet or singlets. In centrioles with triplet microtubules, the inner A-tubule consists of 13 protofilaments, whereas the B- and C-tubules consist only of 10 protofilaments (Winey and O'Toole, 2014) (**Figure 1.2C**). An A-tubule is connected to a cartwheel spoke through a structure called a pinhead, and neighbouring A- and C-tubules on different clockwise blades are connected via a structure named A-C-linker (Guichard et al., 2013) (**Figure 1.1C and 1.3C**). In flies, neighbouring blades are connected via A-A tubule linkers (Greenan et al., 2018). The centriolar microtubules are very stable and resistant. This increased stability is associated with several chemical tubulin modifications, which include acetylations and polyglutamylations. The precise functions of many of these tubulin modifications are not clear (Winey and O'Toole, 2014).

In vertebrates, the distal ends of the microtubule blades on the mother centriole are decorated with a variety of different appendage proteins that appear to be important for ciliogenesis in vertebrate cells. There are two types of appendages present on the mother centriole: distal appendages, involved in recruitment of the basal body to the cell membrane, and sub-distal appendages, which play a role in anchoring the microtubules to the cell membrane (Kobayashi and Dynlacht, 2011). A recent 3D-single molecule localisation microscopy (SMLM) study showed that these appendages are complex nanoscale structures (Yang et al., 2018). The presence of the appendage proteins on the mother explains why only mother centrioles can from basal bodies in vertebrates (Kobayashi and Dynlacht, 2011; Nigg and Holland, 2018). Interestingly enough, *Drosophila* centrioles do not appear to have any appendage structures (Callaini et al., 1997), even though they contain homologous a few appendage proteins (Azimzadeh et al., 2012). However, the presence of daughter-

centriole-specific protein centrobin is key to preventing the daughter centriole from forming a basal body (Gottardo et al., 2015). It is unknown if additional mechanisms exist in *Drosophila* to ensure that only the mother centriole can from a basal body.

1.1.2. Centrosomes

Centrosomes are cellular structures that consist of a pair of centrioles, surrounded by an organized matrix of PCM (**Figure 1.4A**). The PCM consists of many hundreds of proteins (Alves-Cruzeiro et al., 2014; Andersen et al., 2003): in *Drosophila* the PCM consists of an underlying scaffold, primarily made of the proteins Spd-2 and Cnn, on to which most other mitotic PCM proteins bind (Conduit et al., 2014b). Some of the subsequently recruited proteins are important for cell signalling, cell cycle regulation and microtubule nucleation; this latter role as a MTOC is believed to be the key function of centrosomes. PCM can recruit γ- tubulin ring complexes, which are responsible for microtubule nucleation, along with a variety of proteins that facilitate microtubule formation and stability. More details on the assembly and organization of the PCM can be found in section 1.3.

Centrosomes normally play an important part in the assembly of the bipolar mitotic spindle but, surprisingly, they are not essential for cell division or chromosome segregation (Basto et al., 2006). Many female oocytes do not contain any centrioles naturally (centrioles are eliminated during oogenesis in *Drosophila* (Mahowald and J.M., 1970; Riparbelli and Callaini, 2003; Rodrigues-Martins et al., 2007b)). Thus female meiotic spindle assembly and cell division occur in a centrosome-independent fashion. This has also been shown to be true for *C. elegans*, *Xenopus*, chickens, rodents and humans (Dumont and Desai, 2012). Interestingly, even in somatic cells,

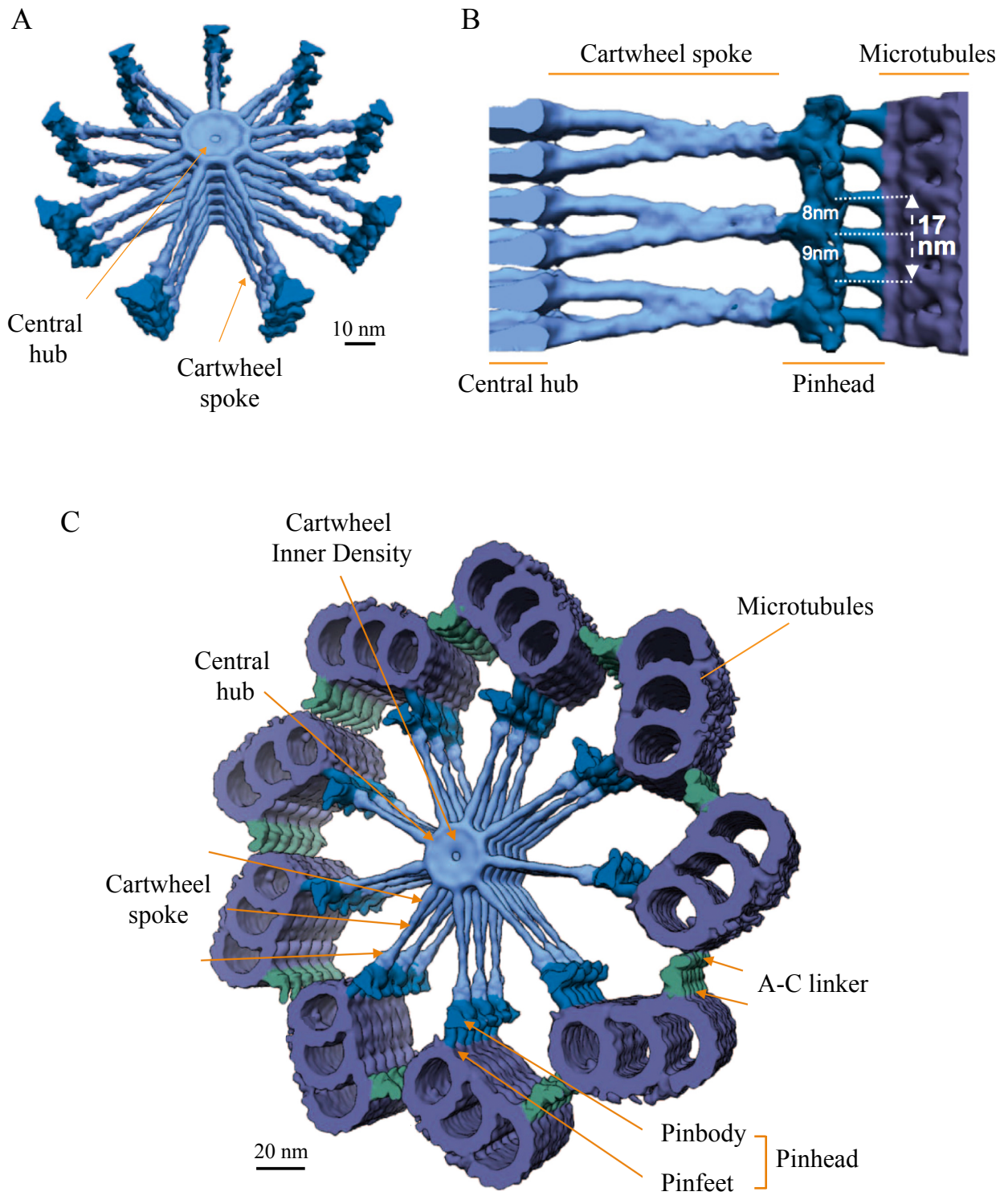


Figure 1.3: The structure of the *Trichonympha* basal body. Schematics illustrate electron cryotomography reconstructions of the *Trichonympha* basal body. **A**) Image of the cartwheel. **B**) Side view of the cartwheel spoke connections to the pinhead and microtubules. **C**) Complete image of the basal body including the cartwheel and the microtubule triplet blades. All images are adapted from Guichard et al. (2013).

centrosomes are not required for spindle pole formation. Laser microsurgery was used to selectively ablate centrosomes in somatic mammalian cells. It was shown that focused and functional spindle poles could form in the absence of one or both centrosomes during prophase (Gonzalez et al., 1990; Khodjakov et al., 1999). Similarly, centrosomes are not required for spindle assembly in *Xenopus* egg extract (Heald et al., 1997).

Nevertheless, centrosomes are important for the organization and efficiency of spindle assembly. In *Xenopus* it was shown that centrosomes are important for spindle pole organization by providing a dominant and focused assembly site (Heald et al., 1997). When microtubules are disassembled, they quickly and preferentially re-grow from the centrosome (Reider et al., 2001). Mitotic spindle orientation, defined by the centrosomes' position, is central in defining the division plane of cells. For many cells, such as stem cells, symmetric or asymmetric cell divisions define the fate of the daughter cells (Conduit, 2013; Knoblich, 2008). In a human brain organoid model of autosomal primary recessive microcephaly (MCPH) (see section 1.1.4), a mutation that impaired the centrosomes ability to form PCM, lead to changes in the division planes of cells. This was thought to lead to a reduction in the stem cell pool, resulting in small brain size (Lancaster et al., 2013). Indeed, it is striking that mutations in several key centriole and centrosome assembly proteins lead to microcephaly and/or dwarfism in humans, although the reason for this is not clear (Nigg and Raff, 2009). Chromosome instability was also found to be increased in vertebrate cell lines that do not have centrosomes (Sir et al., 2013). Additionally, acentrosomal cells often have prolonged cytokinesis due to the lack of astral microtubules nucleated from the centrosome; suggesting centrosomes play a role in ensuring the fidelity of this process

(Savoian et al., 2000). Taken together, these studies suggest that centrosomes are not essential for normal cell function, but influence cellular organization, spindle orientation and spindle pole assembly.

However, in certain developmental stages, centrioles are essential, such as in the early *Drosophila* embryo. Fly embryos that lack Sas-4, Asl or Sas-6 (essential centriole proteins, see section 1.2.1), failed to undergo embryonic development (Stevens et al., 2007; Varmark et al., 2007). This is due to lack of efficient spindle assembly (the first 13 embryonic *Drosophila* cell cycles last between ~10-20min, there are no gap phases (Foe and Alberts, 1983)) or the failure to degrade Cyclin B at the spindle pole, leading to mitotic arrest (Huang and Raff, 1999; Wakefield et al., 2000). However, it was shown that only this initial embryonic development requires centrioles: if the embryo has a maternal contribution of Sas-4, it is able to develop into adult fly with near normal timings (Basto et al., 2006). The adult flies die soon after pupation due to a lack of sensory cilia brought on by the absence of centrioles/basal bodies (Basto et al., 2006). In vertebrate development, centrosomes are indispensible as they form the basis of the cilia – which are essential (see 1.1.3 for more detail). The lack of centrosomes leads to the slow activation of the p53-dependent apoptotic pathway (Lambrus et al., 2015), however centrosomes per se were found not to be required for chromosome segregation (Bazzi and Anderson, 2014; Insolera et al., 2014).

Additionally, centrosomes act as signalling hubs. Centrosomes are extensively regulated by cell cycle cues (such as Cyclin B) and developmental stimuli, and have been known to play a role in DNA damage response. It has been suggested that

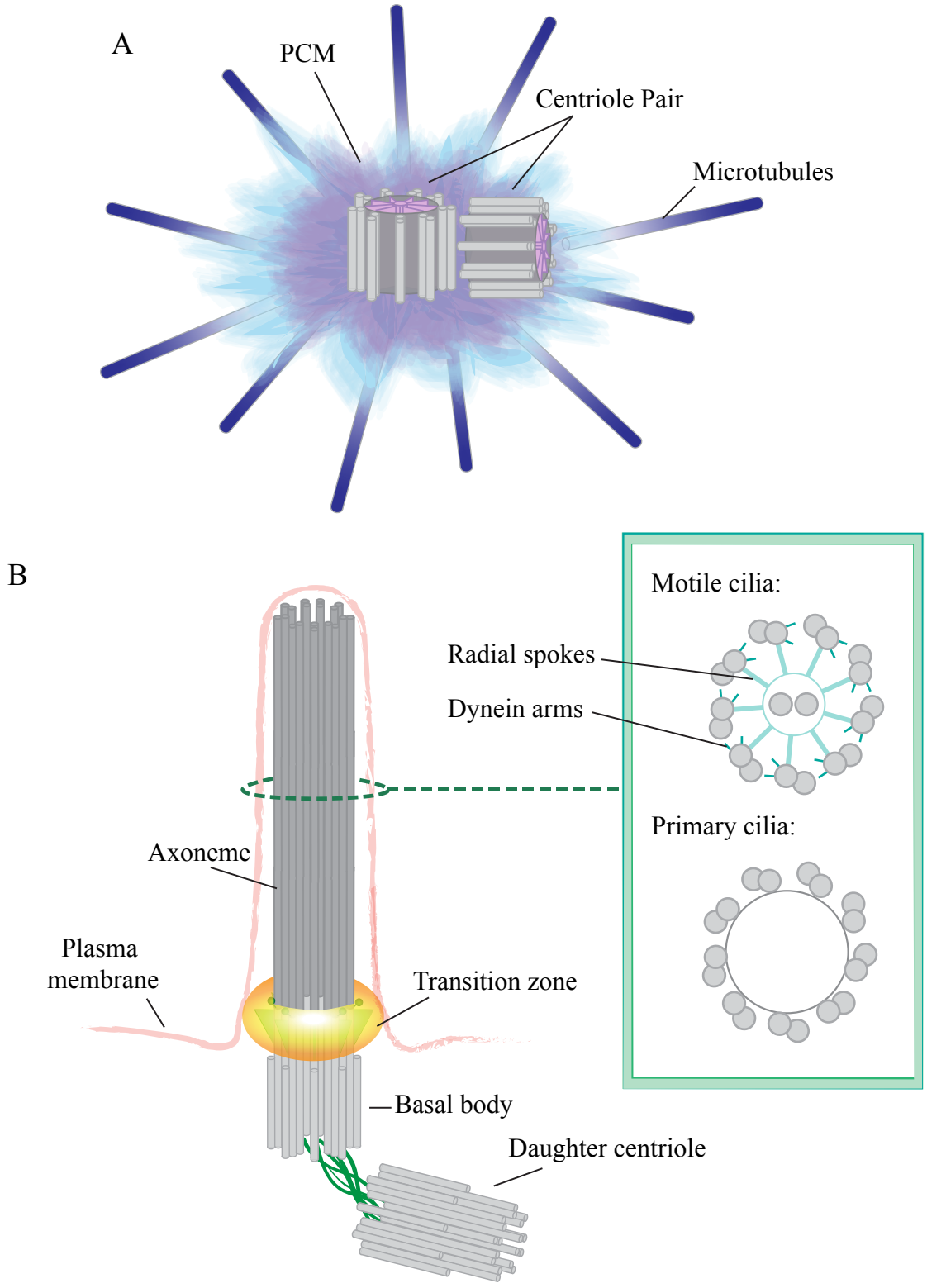


Figure 1.4: Cellular structures that arise from centrioles. A) Schematic of a centrosome consisting of a pair of centrioles (mother and daughter) surrounded by PCM that nucleates microtubules. **B**) Schematic of a cilium (left), and a cross-section of the axoneme in motile and primary cilia (right). The axoneme consists of microtubule doublets in a 9-fold symmetric arrangement. Motile cilia also contain a central doublet, radial spokes and dynein arms.

centrosomes function as a hub where different signalling pathways integrate (Arquint et al., 2014).

Taken together it appears that centrosomes are not essential for cell division, but they have important roles in spindle assembly, development and in a variety of signalling pathways. However, centrioles are essential for their ability to form cilia. This is in line with the evolutionary link between the co-existence of centriole with cilia, but not centrosomes. Perhaps centrosomes initially evolved to ensure the equal partitioning of the two centriole pairs between the two daughter cells, as the centrioles are required for cilia assembly.

1.1.3. Cilia

In many non-dividing cells, the centrioles will migrate to the cell surface, where the mother centriole become anchored at the cell membrane and form the basal body (Reiter et al., 2012). The basal body can become decorated with a variety of structures that facilitate the formation of a functioning cilium. It then initiates the growth of the microtubules form the core of the cilium, called the axoneme (**Figure 1.4B**) (Carvalho-Santos et al., 2011) with the transition zone forming the interface between the basal body. The axoneme and its components have been shown to be involved in many human diseases, such as Meckel-Gruber syndrome (MGS) and nephronophthsis (Reiter et al., 2012).

There are two types of cilia, broadly speaking, motile cilia and primary cilia. Motile cilia, or flagella, consist of a ring of 9 symmetric microtubule doublets with a central pair of microtubules (**Figure 1.4B**). Primary cilia usually non-motile and consist of a

ring 9 microtubule doublets, but do not contain a central pair of microtubules (**Figure 1.4B**) (Nigg and Raff, 2009).

Primary cilia are critical for the function of many cell types, such as sensory neurons (including photoreceptors, mechanosensory, olfactory and chemosensory neurons) (Singla and Reiter, 2006). In *Drosophila*, the ability to form cilia is indispensible for Type I sensory neuron function (Jana et al., 2016). Flies lacking centrioles, thus cilia, are uncoordinated and are unable to survive as adults (Basto et al., 2006).

In vertebrates, most quiescent cells form a primary cilium (Singla and Reiter, 2006). Mouse embryos that were genetically null for CPAP, the Sas-4 homologue in mammals, arrested very early in development, exhibited very high levels of apoptosis and small body size, but no increased chromosomal missegregation, aneuploidy or DNA damage (Bazzi and Anderson, 2014; David et al., 2014). However, if p53 (a pro-apoptotic protein) was also knocked out, the mice died later in development due to the lack of cilia (Bazzi and Anderson, 2014). Primary cilia are important signal transducers in vertebrates where, for example, they are essential for Hedgehog (Corbit et al., 2005; Huangfu et al., 2003) and modulate Wnt signal transduction (Corbit et al., 2008). Hedgehog signalling is important for many developmental processes such as regulating tissue patterning and cell proliferation with defects leading to birth defects in humans and cancer (Singla and Reiter, 2006). Wnt signalling is partially mediated by the cilia (Corbit et al., 2008) and is involved in cell proliferation and differentiation (Mitchison and Valente, 2017). However, in *Drosophila*, these signalling pathways do not appear to require cilia as flies develop normally from embryos to adults in the absence of cilia (Basto et al., 2006). In mammalian

embryonic development, motile primary cilia play another important role: the cilia exhibit a twirling motion that moves the surrounding fluid. This flow is essential for the development of the left-right axis (Nonaka et al., 1998). Overall, primary cilia are necessary for vertebrate development.

Motile cilia exhibit movement such as beating and gliding (Azimzadeh, 2014). Many cell types and unicellular organisms use motile cilia as a means of locomotion, for example sperm cells and aquatic protozoan species, such as *Chlamydomonas* (Zhou and Roy, 2015). Certain cell types nucleate multiple motile cilia, which function to generate a directional fluid flow, such as in epithelial cells in found in the mammalian airways (Mitchison and Valente, 2017). Dysfunction in motile cilia have been linked to a variety of different disorders (Brooks and Wallingford, 2014; Mitchison and Valente, 2017) (See section 1.1.4).

1.1.4. Centrosomes and cilia in human diseases

The human diseases that link to centrioles fall into three broad categories: deregulation of the centriole numbers, mutations in the centriole and centrosome proteins, and structural aberrations that lead to ciliary defects (Nigg and Raff, 2009), causing a wide range of developmental and adulthood diseases (Nigg and Raff, 2009). One very striking aspect of these centrosome and cilia defects is that they affect certain tissues, but not others.

Most cells in the human body are ciliated and therefore, defects in ciliary structure and function cause a plethora of disorders and syndromes, collectively named ciliopathies. Ciliopathies seem to mostly involve retinal degeneration, renal disease, cerebral anomalies, liver problems, diabetes, obesity and skeletal dysplasias (Water

and Beales, 2011). Mutations in over 30 proteins have been identified as causes of ciliopathies, of which many localise to centrosomes and basal bodies (Chavali et al., 2014). However very few proteins have had their functions elucidated including Cep290, OFD1, Cep120 and BBS4. The disease phenotypes are often manifestations of aberrant signal transduction through cilia (Joseph et al., 2018; Water and Beales, 2011). One bewildering aspect of ciliopathies is the diversity of their phenotypes - for example Bardet-Biedl syndrome (BBS) and MGS are both usually associated with polycystic kidney disease, however MGS is also associated with shortened limbs, whereas BBS is associated with obesity (Mitchison and Valente, 2017). It is thought that different mutations perturb different features of cilia, thus leading to such a plethora phenotypes (Nigg and Raff, 2009).

Autosomal recessive primary microcephaly (MCPH) is a genetic, neurodevelopmental disorder characterized by a non-progressive mental retardation accompanied by a reduction in head size circumference at birth (Mahmood et al., 2011; Naveed et al., 2018). MCPH affects brain development (Chavali et al., 2014) through mutations in the MCPH genes leading to either a loss of neural progenitor cells (Lancaster et al., 2013; Nigg et al., 2014) or defect in cellular migration (Chavali et al., 2014). More frequent asymmetric division caused by inappropriate spindle positioning in the neural stem and progenitor cells is thought to cause the loss of progenitor cells (by premature differentiation) (Lancaster et al., 2013; Nigg et al., 2014). So far, mutations in 13 genes have been found in MCPH patients - 10 genes code for centriole or centrosome proteins. The remaining three genes code for proteins that are associated with the spindle pole or in spindle assembly check points (Chavali et al., 2014; Gilmore and Walsh, 2013; Tsutsumi et al., 2016) (see Table 1). Several important

centriole biogenesis proteins are present, including Cep152, CPAP, Cep135, Plk4 and STIL. It could be possible that these mutations lead to protein deregulation (Arquint and Nigg, 2014), thus decreasing the number of centrosomes per cell or the number of daughter cells formed during a developmental time period (Chavali et al., 2014; Lancaster et al., 2013; Tsutsumi et al., 2016). It is unclear to date, if all MCPH gene mutations lead to MCPH through the same cellular mechanism (Nigg et al., 2014).

Table 1 Key centriole and centrosomes genes involved with disease

Drosophila *protein*	*Gene Locus*	*Human protein*	*Cellular location*	*Disease*
-	*MCPH1*	Microcephalin	Centrosome	Microcephaly
-	*MCPH2*	WDR62	Centrosome	Microcephaly
Asp	*MCPH5*	ASPM	Centrosome	Microcephaly
-	*SCKL6*	Cep63	Centrosomes	Primordial Dwarfism
Cnn	*MCPH3*	CDK5RAP2	Centrosome	Microcephaly
Cep135	*MCPH 8*	Cep135	Centriole	Microcephaly
Asl	*MCPH9*	Cep152	Centrosome	Microcephaly
	SCKL5			Primordial Dwarfism
Sas-4	*MCPH6*	CPAP	Centriole	Microcephaly
	SCKL4			Primordial Dwarfism
Plp	*MOPD2*	PCNT	Centrosome	Primordial Dwarfism
Ana2	*MCPH7*	STIL	Centriole	Microcephaly
				Tumorigenesis
Sak	*PLK4*	Plk4	Centriole wall	Microcephaly
				Primordial Dwarfism
				Tumorigenesis
Sas-6		HsSas-6	Centriole	

Primordial dwarfism (PD) is defined as a group of disorders that are autosomal recessive and are characterized by a pre- and post-natal growth failure. The most common diseases are Seckel syndrome, mircocephalic osteodysplastic PD type I and II, and Meier-Gorlin syndrome. Several different genes have been implicated in PD, four of which code for centrosome proteins Asl, Sas-4, pericentrin (PCNT), and Cep63 (see Table 1) (Chavali et al., 2014). All other proteins have been shown to be involved in DNA replication or DNA damage response (Klingseisen and Jackson, 2011). For most of the mutations in centrosome protein coding genes, it is not clear how they lead to a reduction in body and organ size. In pericentrin mutations, it was shown that cellular proliferation was impaired, leading to a reduction in the overall number of cells. It is thought that this is due to the failure to recruit enough PCM and impaired γ-tubulin recruitment (Klingseisen and Jackson, 2011). Overall, it appears that all PD genes appear to be involved in regulating cellular proliferation, although possibly through different mechanisms (Klingseisen and Jackson, 2011).

Centrosomes have long been implicated in cancer. Centrosome amplification or defects are a ‘hallmark’ of solid and haematological cancer and are linked to poor patient prognosis (Chan, 2011). Centrosomes anomalies can stem from either numerical alterations (centrosome amplification) or from structural defects (Chan, 2011; Schnerch and Nigg, 2016). Centrosome amplification can lead to multipolar mitotic spindles causing chromosome instability. The resulting aneuploidies and extensive chromosome missegregation promote tumorigenesis (Ganem et al., 2009; Nigg and Holland, 2018). Centrosome amplification is caused by a variety of factors which include deregulation of centriole duplication, perturbation of cell cycle progression, DNA damage, failures in cell division or deregulation of oncogenes or

tumour suppressor genes (Nigg and Holland, 2018). *In vitro*, centrosome amplification increases the activity of Rac1, a small GTPase. This disrupts normal cell-to-cell contacts and leads to cell invasion (Godinho et al., 2014). In mice and *Drosophila*, centrosome amplification induced by Plk4 overexpression is sufficient to promote spontaneous tumorigenesis, apparently by generating chromosome missegregation and aneuploidy (Basto et al., 2008; Levine et al., 2017). However, other studies in mice have found that centrosome amplification due to Plk4 over-expression, only leads to tumour formation in the absence of the tumour suppressor gene *p53* (Vitre et al., 2015). Tumour development by centrosome amplification appears complex and potentially tissue dependent (Nigg and Holland, 2018). Recently, it has been shown that structural abnormalities in centrosome structure can lead to tumorigenesis with overexpression of Ninein-like protein leading to a misregulation of microtubule nucleation. This disrupts epithelial cell polarity by mislocalisation of adhesion and junction proteins and down-regulates the tumour suppressor Scribble (Schnerch and Nigg, 2016). Overall, there are strong, yet unclear, links between centrosome abnormalities and cancer.

1.2. Centriole and centrosome duplication

Centriole duplication is tightly controlled. It is essential that centrioles, and thus centrosomes, duplicate only once during each cell cycle to ensure that each mitotic cell contains only two centrosomes. This ensures that only a resulting in a bi-polar spindle is formed which ensures the inheritance of the correct number of chromosomes and centrosomes. Centrioles can be formed *de novo* (Peel et al., 2007; Rodrigues-Martins et al., 2007b) or through a canonical duplication pathway. This thesis will discuss canonical duplication.

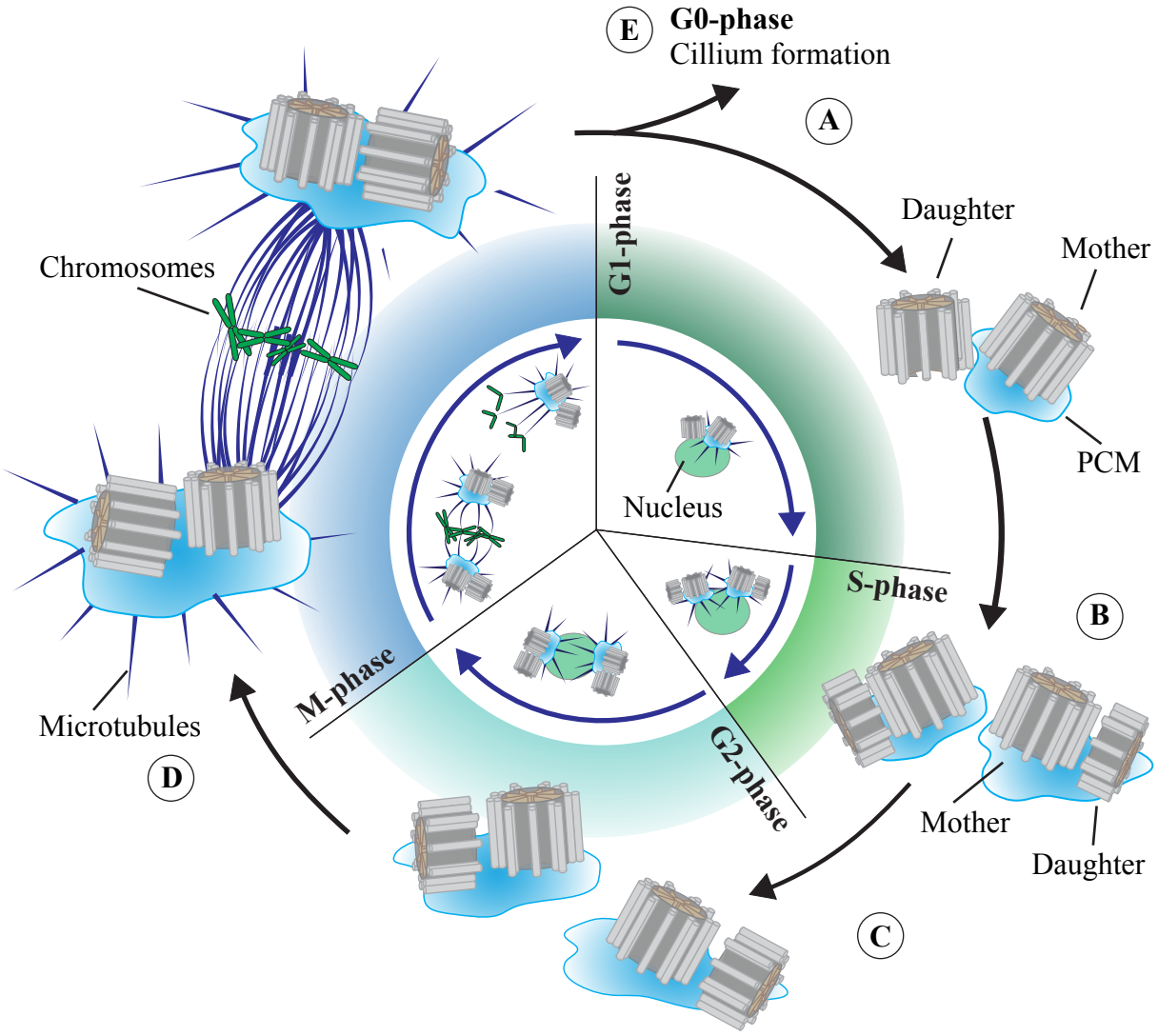


Figure 1.5: The centriole duplication cycle. A) In G1-phase, centrosome consists of a disengaged mother and daughter centriole. The mother centriole typically nucleates a small amount of PCM. **B**) At the beginning of S-phase, the centriole pair separates (both are now mother centrioles) and both centrioles initiate the assembly of a daughter centriole. Daughter centrioles will reach their full length by G2/M. **C**) In G2-phase, the two centrosomes migrate to opposite sides of the nucleus. The centrosomes rapidly expand their PCM. **D**) M-phase begins with the breakdown of the nuclear envelope. The mother and daughter centrioles disengage, and each centrosomes nucleate many microtubules and form the bipolar mitotic spindle. Thus, one centrosome is inherited by each daughter cell. **E**) When cells exit the cell cycle and enter G0-phase, the centriole pair usually migrates to the cell surface where the mother centriole initiates cilia formation.

Centrosome duplication occurs by duplicating existing centrioles (**Figure 1.5**). In G1-phase, after mitosis and cytokinesis, each daughter cell contains one centrosome, consisting of a pair centrioles (**Figure 1.5A**): an older mother centriole and younger daughter centriole. As the cell enters S-phase (**Figure 1.5B**), the daughter becomes as new mother centriole, and both centrioles start to assemble a daughter centriole on their sides, in a tightly apposed "engaged" configuration. The daughter centrioles grow throughout S-phase. At the start of G2-phase (**Figure 1.5C**), the two centrosomes migrate to opposite sides of the nucleus, and the two mother centrioles rapidly expand their PCM. The enlargement of the PCM allows the centrosomes to nucleate sufficient numbers of microtubules for spindle pole formation. In early M-phase (**Figure 1.5D**), the two centrosomes form the poles of the bipolar spindle. Sometime during mitosis, the mother and daughter centrioles disengage, but remain in close proximity to one another. Toward the end of mitosis, each is segregated into a daughter cell. If the cell continues to proliferate, the centrioles and centrosomes continue this cycle (**Figure 1.5A-D**). However, if cells enter G0-phase (**Figure 1.5E**), the centrosomes will form cilia.

1.2.1. Essential centriole duplication proteins

Proteomic studies have identified many hundreds of proteins that are present at centrosomes in human cells, *Clamydomonas* and *Drosophila* (Andersen et al., 2003; Keller et al., 2005; Muller et al., 2010). Genome-wide RNAi screens identified a number of proteins important for centriole assembly. A breakthrough came from research in *C. elegans* embryos where only five genes (SPD-2, ZYG-1, SAS-5, SAS-6, SAS-4) were found to be essential for centriole assembly (Delattre et al., 2004; Kirkham et al., 2003; Leidel et al., 2005; Leidel and Gonczy, 2003; O'Connell et al., 2001; Pelletier et al., 2004). These proteins were recruited sequentially and were

interdependent on one another for their centriolar localisation (Delattre et al., 2006; Pelletier et al., 2006). The *C. elegans* embryo biology was key to making this discovery: the meiotically arrested oocytes naturally do not contain any centrioles. Upon fertilization, the sperm provided a pair of centrioles that initiated the first cellular division. Thus, if the mother was mutant for an essential centriole assembly gene, the oocyte will only contain the two paternal centrioles after the first cellular division (instead of two pairs of centrioles), and so organise a monopolar spindle during the second round of division. It was shown that SPD-2 recruited ZYG-1, ZYG-1 then recruits SAS-6 and SAS-5 to the centriole, which then allow the recruitment of SAS-4 (Delattre et al., 2006; Pelletier et al., 2006) (**Figure 1.6A**).

This spurred the field to identify the essential centriole assembly proteins in other organisms. The following five homologues and orthologous in *Drosophila* and human were identified: Sak/Plk4, Ana2/STIL, Sas-6/HsSAS-6, Sas4/CPAP and Asl/Cep152 (Basto et al., 2006; Bettencourt-Dias et al., 2005; Blachon et al., 2008; Dobbelaere et al., 2008; Goshima et al., 2007; Leidel et al., 2005; Peel et al., 2007; Stevens et al., 2010a) (**Figure 1.6B,C**). All of these proteins appear to be essential. The assembly pathways shown in **Figure 1.6B,C** are widely accepted, but are not definitively proven in flies or vertebrates as in these systems the mutation of any of these essential genes leads to the absence of centrioles. Thus, it has not been possible to recapitulate the precise assembly pathway, shown *C. elegans*. Below, I discuss the current knowledge about each of these 5 essential proteins.

1.2.1.1. Plk4/Sak

Plk4, the vertebrate homologue of Sak in *Drosophila* and the functional orthologue of ZYG-1 in *C. elegans,* is a member of the polo-like-kinase (Plk) family, a family of

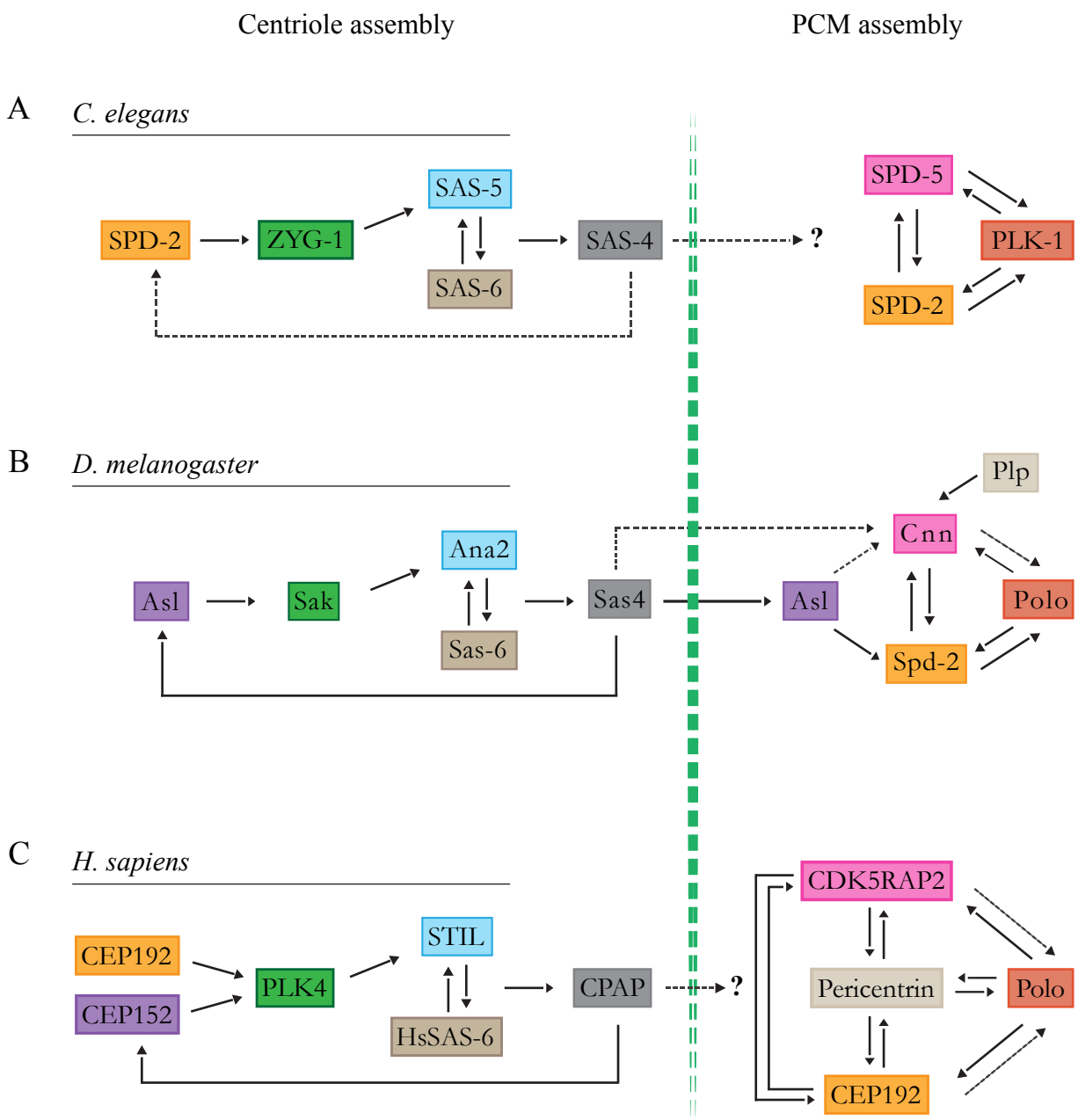


Figure 1.6: A conserved pathway of centriole and mitotic centrosome assembly. Schematics show the proposed centriole and mitotic PCM assembly pathways in *C. elegans* (**A**), *D. melanogaster* (**B**) and *H. sapiens* (**C**). The colored boxes indicate homologues or functional orthologous in the different species. Adapted from Conduit et al., (2015).

Ser/Thr protein kinases. Plks are present in all branches of the animal kingdom. A common feature of Plk family members is the presence of polo boxes (PBs), which can be key to activity, localisation and function (Zitouni et al., 2014). All Plks share a similar architecture: a N-terminal catalytic kinase domain (Carvalho-Santos et al., 2010) and PBs in the C-terminal region (Zitouni et al., 2014). The kinase domain of Plk4/Sak is divergent in sequence from the rest of the Plk family and its C-terminus contains a cryptic PB (comprising PB1 and PB2) and a third PB3 (Slevin et al., 2012) (**Figure 1.7A**). The Plk1 PB domain normally interacts with other proteins that have been phosphorylated on S-S/T(P) sites (Eila et al., 2003), but the cryptic PB in Plk4/Sak does not contain a phosphate-recognition cavity, suggesting that any interaction with its targets will be phosphorylation-independent (Slevin et al., 2012). The cryptic PB localises the kinase to the centrosome (Cizmecioglu et al., 2010; Dzhindzhev et al., 2010; Kim et al., 2013; Sonnen et al., 2013) and is important for homo-dimerization of Plk4/Sak. PB3 is known to self-associate when Plk4/Sak dimerises.

In flies, Sak is recruited to the centrosome by the protein Asl, (Dzhindzhev et al., 2010) in *C. elegans*, ZYG-1 is recruited by SPD-2 (Delattre et al., 2006; Pelletier et al., 2006), and in humans, Plk4 is recruited by the human homologues of both proteins (Cep152 and Cep192, respectively) (Sonnen et al., 2013).

Sak/Plk4 levels must be tightly controlled to prevent centriole overduplication (Habedanck et al., 2005). The Sak/Plk4 protein, a low abundance protein (Cunha-Ferreira et al., 2009; Habedanck et al., 2005; Rogers et al., 2009), is subjected to ubiquitin-dependent degradation by the proteasome E3 ubiquitin ligase complex

SCF^{Slimb} (or $SCF^{\beta TrCP}$ in vertebrates) (Cunha-Ferreira et al., 2009; Guderian et al., 2010; Sillibourne et al., 2010). The SCF^{Slimb} complex recognises its substrate by specific phosphorylation of a conserved degron motif. Sak/Plk4 is a 'suicide kinase' that upon homodimerization via the cryptic PB, *trans*-phosphorylates its own degron at two specific residues thereby marking it for protein degradation (Cunha-Ferreira et al., 2013; Guderian et al., 2010; Holland et al., 2012; Sillibourne et al., 2010). The phosphorylation of the degron has been found to depend on the autophosphorylation of other residues (Cunha-Ferreira et al., 2013; Holland et al., 2010; Klebba et al., 2013). To allow control of Sak/Plk4 activity during mitosis, Sak/Plk4 is dephosphorylated by the protein phosphatase 2A/Twins (Brownlee et al., 2011) stabilising Sak/Plk4 in mitosis.

Interestingly, in fixed human (Kim et al., 2013; Ohta et al., 2014; Sonnen et al., 2012) and *Drosophila* cells (Dzhindzhev et al., 2017) Sak/Plk4 localises as a ring around the mother centriole in G1-phase that then resolves into a single "dot" that marks the site of daughter centriole assembly. It is unclear how this ring-to-dot-transition occurs. STIL appears to be is a key player in this process by protecting Plk4 from degradation and stimulating its activity in a small area (i.e. the dot) (Ohta et al., 2018).

Plk4/Sak begins a new round of centriole duplication by binding to and phosphorylating Ana2/STIL, a step is essential for centriole biogenesis (Arquint et al., 2015; Lopes et al., 2015; Moyer et al., 2015; Ohta et al., 2014). Upon binding to Ana2/STIL, Plk4/Sak is activated and then phosphorylates Ana2/STIL (Nigg and Holland, 2018) in an ordered and sequential fashion at various places (McLamarrah et al., 2018). One important region that is phosphorylated is the STIL/Ana2 Domain

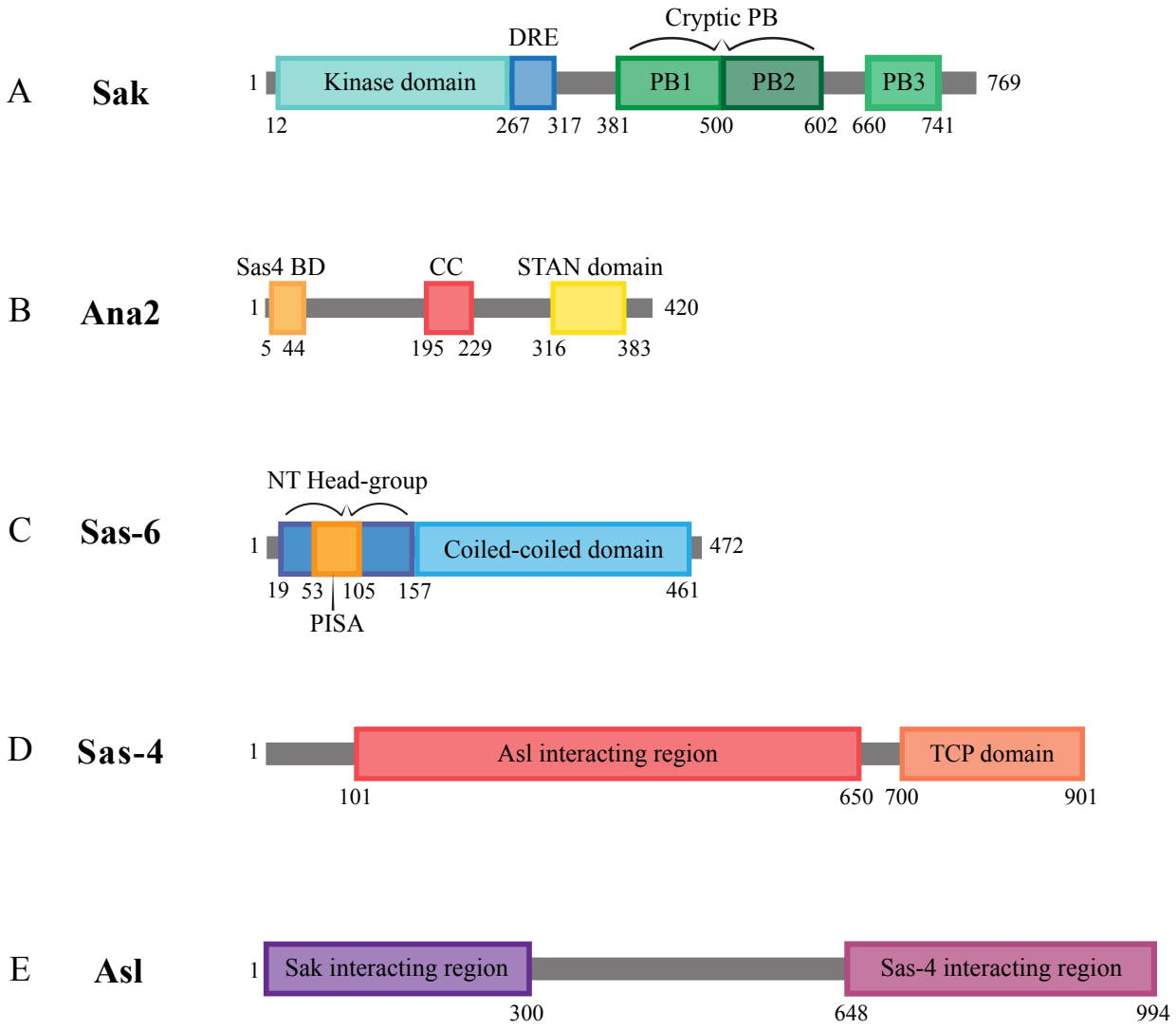


Figure 1.7: Schematic illustration of the five proteins essential for centriole duplication in *Drosophila*. **A**) the kinase Sak; **B-D**) the cartwheel proteins Ana2, Sas-6, and Sas-4; **E**) the outer centriole protein Asl. Details of protein domains and their functions are described in the main text. Abbreviations: DRE, Downstream REgulatory region (the phospho-degron in Plk4); PB, Polo-box; BD, binding domain; CC, central coiled-coil domain; STAN, STil/ANa2 domain; PISA, Present in Sas-6; TCP, T complex 10 (the region of Sas-4 that binds to Ana2).

(STAN) of Ana2 (Dzhindzhev et al., 2014; McLamarrah et al., 2018), which allows Ana2 to recruit Sas-6.

For all the experiments performed in this thesis, Sak/Plk4 will be referred to as Sak.

1.2.1.2. Ana2/STIL

Drosophila Ana2 is the homologue of STIL in humans and SAS-5 in *C. elegans* (Stevens et al., 2010a). It was first discovered in flies (Goshima et al., 2007) and it was later found to be the homologue of SAS-5 (Stevens et al., 2010a). The protein STIL is significantly larger than SAS-5 and Ana2, but they all share 2 conserved domains: a central coiled-coil (CC) domain near the middle of the protein and a STAN domain located at the C-terminus (Stevens et al., 2010a) (**Figure 1.7B**). The CC domain is required for Ana2 homodimerization (Cottee et al., 2015) and the STAN has been shown to be essential for centriole assembly and has been implicated in the interaction between Ana2 and Sas-6 (Cottee et al., 2015; Dzhindzhev et al., 2014; Moyer et al., 2015; Ohta et al., 2018). Ana2 is a critical component of the centriole cartwheel, whose precise localisation and orientation within this structure has not been determined.

Ana2/STIL is essential for centriole duplication (Arquint et al., 2012; Stevens et al., 2010a; Vulprecht et al., 2012). Ana2/STIL can lead to centriole overduplication when overexpressed (Arquint et al., 2012) and therefore its protein levels and expression are regulated by the cell cycle. Specifically, STIL is degraded upon passage through mitosis by APC/$^{CCdc20\text{-}Cdh1}$ (Arquint et al., 2012). In *C. elegans*, ZYG-1 is upstream of SAS-5 (Delattre et al., 2006; Pelletier et al., 2006), and there is strong evidence that this holds true for Sak/Plk4 and Ana2/STIL. The CC domain of STIL is required and

sufficient for the interaction with Plk4 (Arquint et al., 2015; Kratz et al., 2015; Moyer et al., 2015; Ohta et al., 2014). However, the precise mode of interaction between the two proteins is unclear and it does not seem to be conserved between humans and *Drosophila* (Cottee et al., 2017). The phosphorylation of Ana2/STIL by Sak/Plk4 is important for centriole duplication. Recent work in *Drosophila* S2 cells suggests the following order of phosphorylation and their proposed affects (McLamarrah et al., 2018): first, Sak/Plk4 phosphorylations on Ana2 promote binding of the two proteins (Dzhindzhev et al., 2017; McLamarrah et al., 2018), and relieve Sak/Plk4 auto-inhibition—allowing it become an active kinase (Arquint et al., 2015; Klebba et al., 2015; Moyer et al., 2015). Second, the N-terminal phosphorylation of Ana2 induces a conformational change, which enhances Sak/Plk4's ability to phosphorylate the STAN domain. Finally, Sak/Plk4 phosphorylates residues in the central region of Ana2, leading to the release of Sak/Plk4 (McLamarrah et al., 2018). The phosphorylation of the STAN domain is essential to subsequent centriole assembly. In flies, four conserved residues, S318, S365, S370 and S373, have been shown to be essential for Sas-6 recruitment and centriole formation (Dzhindzhev et al., 2014), in humans, the site S1116 was found to be important (Kratz et al., 2015; Ohta et al., 2014).

1.2.1.3. Sas-6

SAS-6 was first identified as a protein required for centriole duplication by an RNAi screen in *C. elegans* by two independent groups (Dammermann et al., 2004; Leidel et al., 2005). Homologues were identified in humans and *Drosophila*, HsSas-6 and Sas-6, respectively, and their role in centriole duplication and localisation confirmed (Leidel et al., 2005; Mennella et al., 2012; Peel et al., 2007; Rodrigues-Martins et al., 2007a; Sonnen et al., 2012).

Sas-6/HsSas-6/SAS-6 all share two conserved domains: a globular N-terminal region that contains the conserved PISA (present in Sas-6) domain, and an extended coiled-coil region (Leidel et al., 2005); the very C-terminal region is predicted to be unstructured (Guichard et al., 2017). **(Figure 1.7C**). The coiled-coil region allows two Sas-6 molecules to form a parallel homodimer (**Figure 1.8A**). These homodimers are then able to interact with other homodimers via their N-terminal head-groups (Kitagawa et al., 2011; van Breugel et al., 2011) (**Figure 1.8B**). In flies, the residue F143 is critical to the interaction between to Sas-6 homodimers (Cottee et al., 2015; Kitagawa et al., 2011; van Breugel et al., 2011; van Breugel et al., 2014). Each cartwheel ring is made up of nine homodimers of Sas-6. The N-terminus of Sas-6 is thought to form the cartwheel hub and its C-terminus radiating outwards to form the cartwheel spokes (Cottee et al., 2015; Kitagawa et al., 2011; van Breugel et al., 2011; van Breugel et al., 2014) (**Figure 1.8C**).

Even the moderate overexpression of Sas-6 in *Drosophila* embryos can lead to centriole overduplication (Peel et al., 2007). In human cell lines, similar results were seen upon overexpression of HsSas-6, mother centrioles gave rise to multiple daughter centrioles (the same phenotype is seen in Sak/Plk4 overexpression) (Strnad et al., 2007).

Sas-6 has been suggested to be the main protein that confers symmetry onto the centriole structure (Guichard et al., 2017; Kitagawa et al., 2011): evidence from *in vitro* experiments preformed using recombinant Bld12p protein (Sas-6 homologue in *Chlamydomonas reinhardtii*) showed that the protein can homodimerizes and assemble into multi-fold symmetric structures that resemble a cartwheel

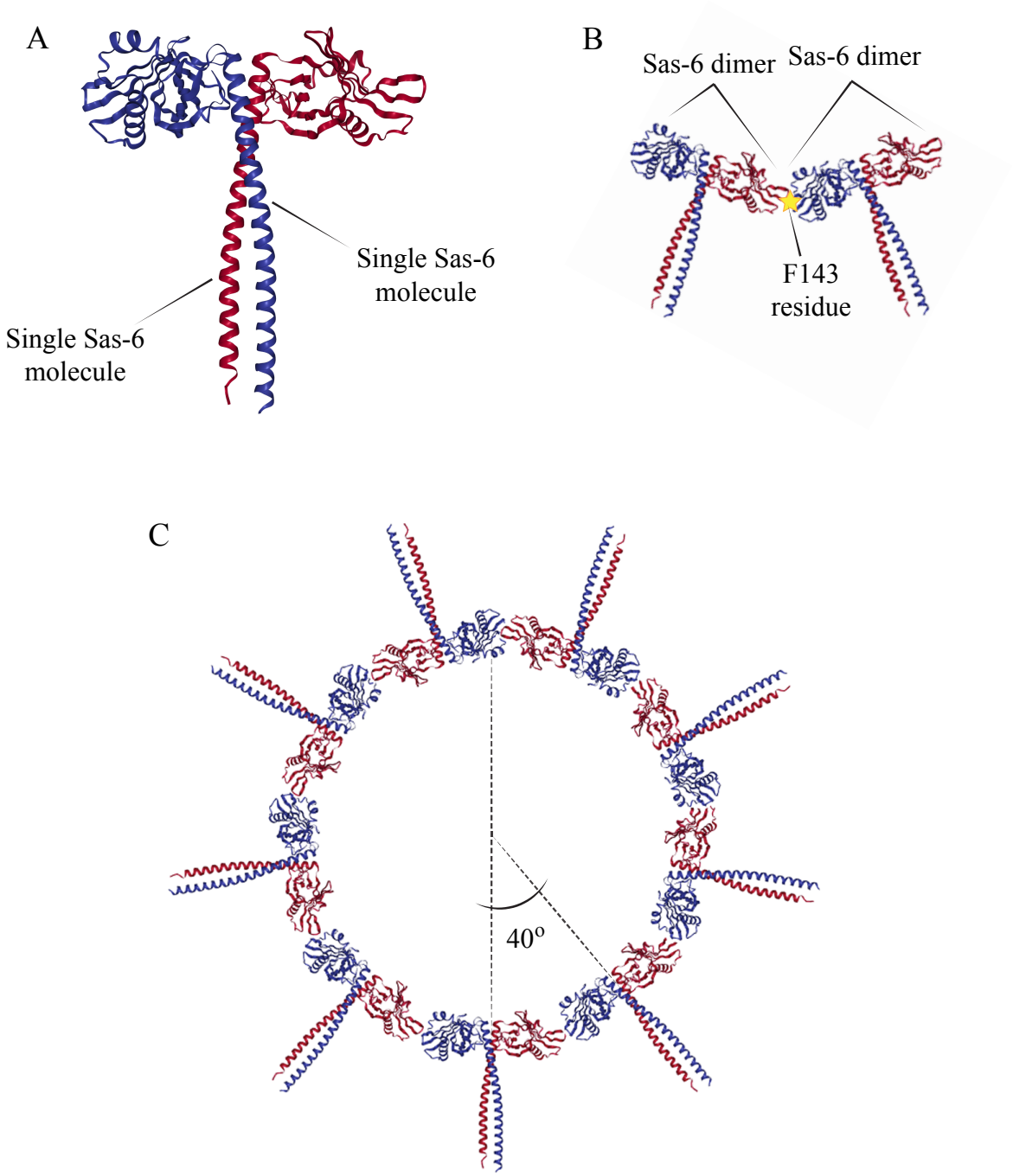


Figure 1.8: Sas-6 molecules form the centriole cartwheel. Structures depicted here are based on the Sas-6 crystal structure from Kitagawa et al. (2011). **A**) Two Sas-6 molecules dimerize via their coiled-coil domains. **B**) Homodimerisation of two Sas-6 dimers via their N-terminal domains (the F143 residue essential for this interaction in flies is highlighted by the yellow star). **C**) Assembly of Sas-6 dimers into a 9-fold symmetric ring, each dimer is 40° offset from its neighbor.

(Guichard et al., 2017; Kitagawa et al., 2011; van Breugel et al., 2011). However, Bld10, the homologue of human Cep135, is able to bias Bld12p's assembly into more 9-fold

symmetric structures (Guichard et al., 2017). Cep135 has been shown to bind HsSas-6 at the central coiled-coil region (Lin et al., 2013). *In vitro*, Bld12p cartwheels can assemble into stacks in the presence of Bld10, that looks strikingly like a centriole cartwheel (Guichard et al., 2017). Interestingly, it was suggested that HsSas-6's ability to homodimerize is not critical to induce symmetry: *in vivo* evidence from human cells suggest only the C-terminus of Sas-6 is required for this despite being an 'error prone mechanism' – consequently the centriole-like structures that were formed in the presence of this protein are not always 9-fold symmetric or always complete (Wang et al., 2015). In *Drosophila*, Sas-6's structural role is clearly seen in spermatocytes: the overexpression of Sas-6 and Ana2 leads to the formation of elongated tube like structures that bear a striking resemblance to the cartwheel (Stevens et al., 2010b). Sas-6 is likely the main component of the centriole cartwheel and has an intrinsic ability to form symmetric structures, facilitated by the other proteins decorating this core structure. This suggestion is largely in agreement with the beautiful cryo-ET structure of the *Trichonympha* basal body (Guichard et al., 2013) (**Figure 1.3**).

The Ana2 STAN phosphorylations are the driving force for Sas-6 recruitment to and assembly into a growing cartwheel (Dzhindzhev et al., 2014; Kratz et al., 2015; Moyer et al., 2015; Ohta et al., 2014). The precise mechanism of interaction between Ana2 and Sas-6 is still to be identified. In *Drosophila*, evidence from a yeast-two hybrid screen suggests that Ana2 and Sas-6 can interact directly (Stevens et al.,

2010a) which is supported by pull-down experiments in S2 cells (Tang et al., 2011). Similarly, in *C. elegans*, SAS-5 forms a complex with SAS-6 (Leidel et al., 2005). However, in humans, CPAP seems to be required to pull down both Ana2 and Sas-6 *in vivo* (Tang et al., 2011). This is supported by later findings that identify CPAP and Cep135 as important Sas-6 interactors (Lin et al., 2013). Cep135 could be immunoprecipitated with CPAP and HsSas-6 in a complex *in vivo* (Lin et al., 2013). Most of the coiled-coil region in HsSas-6 and some of the region upstream were shown to bind to Cep135, which can directly bind microtubules at its N-terminus (Kraatz et al., 2016; Lin et al., 2013). Conflictingly, other studies performed in human cells have failed to show STIL and HsSas-6 a in stable complex by pull down studies, even in the presence of CPAP (Arquint et al., 2012). More research is required to understand the Ana2/STIL:Sas-6 interaction and the potential role of Sas-4/CPAP in this interaction.

1.2.1.4. Sas-4

Sas-4 (**Figure 1.7D**) is the homologue of SAS-4 in *C. elegans* and of CPAP in humans. SAS-4 was first identified in an RNAi screen as a protein that is essential for centriole duplication (Leidel and Gonczy, 2003). Sas-4 has also been identified as a key centriole duplication component in *Drosophila* (Basto et al., 2006; Peel et al., 2007) and in human cells (Gopalakrishnan et al., 2011; Hung et al., 2000; Tang et al., 2009).

Unlike the Sak/Plk4, Ana2 and Sas-6, Sas-4 appears unable to induce centriole over-duplication when moderately overexpressed in flies (Peel et al., 2007). Interestingly, the depletion of CPAP in human cells suppresses the ability of Plk4 to induce centriole over-duplication upon over-expression (Tang et al., 2009). Taken

together, these results suggest that Sas-4/CPAP functions downstream of Sak/Plk4, Ana2/STIL and Sas-6/HsSas-6, as was shown in *C. elegans* (Delattre et al., 2006; Pelletier et al., 2006).

Sas-4/CPAP has been shown to localised to the centriole by light microscopy. Its N-terminus localises as a tight toroid around the centriole in both *Drosophila* (Fu and Glover, 2012; Gopalakrishnan et al., 2011; Mennella et al., 2012) and human cells (Lawo et al., 2012). The C-terminus of CPAP localises to the outer PCM (Sonnen et al., 2012). However, another study seems at odds with this finding based on crystal structure studies suggesting that the C-terminus of Sas-4 interacts with the N-terminus of Ana2 (Cottee et al., 2013), inferring that the C-terminus of Sas-4 would localise near to the centriole cartwheel. This is consistent with data suggesting that in *Drosophila*, the C-terminus of Sas-4 localise to an area smaller than what can be resolved with structured illumination microscopy (SIM)(i.e. 100-150 nm) (Novak et al., 2014).

Sas-4 has been implicated in a variety of functions at the centriole and centrosome.
As mentioned above, Sas-4/CPAP may be required for the cartwheel formation by allowing Ana2 and Sas-6 to interact (Tang et al., 2011). Additionally, CPAP appears to be important for centriole microtubule nucleation (Schmidt et al., 2009; Tang et al., 2009). The N-terminus of CPAP can bind to α/β tubulin dimers (Hung et al., 2004; Hung et al., 2000; Sharma et al., 2016). However, its precise role at the centriole still needs to be clarified. In *Drosophila*, it has been suggested that Sas-4 forms complexes in the cytoplasm with PCM proteins and then recruits these complexes to the centriole/centrosome (Gopalakrishnan et al., 2011). However, in the early *Drosophila*

embryo, studies suggest that although Sas-4 may have a role in anchoring PCM components to the centriole, it is not forming cytoplasmic complexes with these proteins that are then recruited to centrioles (Conduit et al., 2010; Conduit et al., 2015a). Another essential role of Sas-4 is recruiting Asl. Asl/Cep152 and Sas-4/CPAP are able to interact with one another both *in vivo* and *in vitro* (Cizmecioglu et al., 2010; Dzhindzhev et al., 2010). The C-terminus of Asl can interact with the first half of Sas-4 (Dzhindzhev et al., 2010). In vertebrates, this interaction is critical, as down regulation of Asl leads to failures of CPAP recruitment (Cizmecioglu et al., 2010; Dzhindzhev et al., 2010). However, the requirement of Asl to recruit CPAP is not conserved in *Drosophila* (Dzhindzhev et al., 2010). Sas-4 ultimately recruits Asl to the daughter centriole allowing for the centriole-to-centrosome conversion (Novak et al., 2014). The mitotic kinase Cdk1/Cyclin B phosphorylates Sas-4 at a single residue (Thr200), generating a Polo kinase docking site. The recruitment of Polo then promotes Asl recruitment to the daughter centriole (Novak et al., 2016). This elegant mechanism explains why new daughter centrioles have to pass through mitosis before they can mature into mothers as Asl is required for centriole duplication and mitotic PCM recruitment.

1.2.1.5. Asl

The *asl* gene was discovered in a *Drosophila* screen as a gene affecting male sterility (Bonaccorsi et al., 1998) and its human homologue, Cep152, was later identified (Andersen et al., 2003; Blachon et al., 2008). To date there has been no Asl/Cep152 orthologue or homologue identified in *C. elegans.* Asl was first identified as a central player in PCM recruitment (Bonaccorsi et al., 1998; Varmark et al., 2007), and was later shown to be essential for centriole duplication (Blachon et al., 2008) (**Figure 1.7E**).

In *Drosophila*, Asl is recruited to the centriole by Sas-4 (as mentioned above) (Dzhindzhev et al., 2010; Novak et al., 2016) with the protein Ana1 has also being implicated. Ana1 depletions leads to reduced levels of Asl at the centriole suggesting that Ana1 is important either to its recruitment or maintenance at the centriole (Fu et al., 2016). In another study Ana1 was shown to be mainly responsible for Asl maintenance at the centriole, not its recruitment (Saurya et al., 2016).

Asl and Cep152 have been precisely located to toroids that surround the centrioles using super-resolution microscopy with C-terminus is being more proximal to the centriole than the N-terminus (Fu and Glover, 2012; Lawo et al., 2012; Mennella et al., 2012; Saurya et al., 2016; Sonnen et al., 2012; Wegel et al., 2016). Asl is thought to locate between the outer centriole wall and the inner PCM, and to extend outwards into the intermediate PCM (Sonnen et al., 2012). In *Drosophila*, Asl is distributed along the whole length of the centriole (Fu and Glover, 2012; Mennella et al., 2012; Wegel et al., 2016) whereas in human cells, Cep152 only coats the proximal end of the centriole (Lawo et al., 2012; Sonnen et al., 2012).

The main roles of Asl/Cep152 include facilitating the centriole-to-centrosome conversion (Novak et al., 2016) and recruiting Sak/Plk4 to the centriole. The presence of Asl on the daughter centriole allows for the subsequent recruitment of Sak/Plk4 (to initiate the next round of centriole duplication) and begin PCM recruitment (Conduit et al., 2010; Fu et al., 2016; Nigg and Holland, 2018; Novak et al., 2014; Novak et al., 2016). The role of Asl/Cep152 in recruiting Sak/Plk4 is critical. Sak/Plk4 and Asl/Cep152 interact *in vivo* and *in vitro* in human cells*, Drosophila* and *Xenopus* (Cizmecioglu et al., 2010; Dzhindzhev et al., 2010; Hatch et al., 2010). In *Drosophila*,

the first 300 amino acids of Asl are essential to this interaction (Dzhindzhev et al., 2010). Asl/Cep152 is able to localise to the centriole independently of Plk4/Sak (Dzhindzhev et al., 2010; Hatch et al., 2010). Conversely, it is less clear if Sak/Plk4 can localise to the centriole in the absence of Asl/Cep152. Some studies show that in the absence of Cep152 (Cizmecioglu et al., 2010), or in the presence of the Asl Sak-binding mutant which is missing the residues required for the interaction (Dzhindzhev et al., 2010), Sak/Plk4 recruitment is impaired. Whereas another study has shown that Plk4 can localise to the centriole independently of Cep152 and that the expression of N-terminal region of Cep152 is enough to prevent Plk4's localisation to the centriole (Hatch et al., 2010). Taken together, Asl/Cep152 is likely to play a fundamental role in the recruitment of Sak/Plk4 to the centriole but the mechanism remains unclear.

1.2.2. Centrosome duplication regulation

Centrosome duplication must be tightly controlled in space and time. Cell cycle regulation must ensure that both DNA and centriole duplication cycles are controlled (Nigg, 2007). Misregulation can led to incorrect centrosome numbers leading to the formation of mono- or multipolar mitotic spindles, thus resulting in chromosome missegregation (Nigg, 2007). For centrosomes there are three levels of control that will be briefly outlined below: temporal control, number control and centrosome maturation licensing.

Centrioles duplicate only in S-phase. This temporal restriction is thought to be created by three key kinases: Cdk2, Plk4 and Cdk1 (**Figure 1.9**). Cdk2 is considered the master regulator of the G1/S-phase transition (when complexed with Cyclin E) and ensures S-phase progression (when in complex with Cyclin A) (Nigg and Holland, 2018). Cdk2, when in complex with Cyclin E or A, has been shown to be crucial for

allowing centriole duplication in *Xenopus* and mammalian cells (Hinchcliffe et al., 1999; Lacey et al., 1999; Matsumoto et al., 1999; Meraldi et al., 1999). However, the precise role of Cdk2 at the centrosome has not yet been elucidated. Presumably, Cdk2 either directly phosphorylates centriole proteins, or it may simply drive the cell into a cell cycle state that is permissive for centriole duplication. It is likely that Cdk2 stabilises proteins such as HsSas-6, CPAP and STIL by inactivating proteins that lead to their degradation (Arquint et al., 2012; Strnad et al., 2007; Tang et al., 2009).

Sak/Plk4 is the master kinase that initiates centriole duplication. In early *Drosophila* embryos, Sak/Plk4 has been shown to oscillate over the nuclear cycles with levels being lowest in metaphase and increasing from late mitosis until early S-phase, (**Figure 1.9**) (Aydogan et al., 2018). Degradation was found to be crucial to centriole duplication regulation, with two residues on the Sak/Plk4 degron required for the full and efficient destruction of Plk4 (Cunha-Ferreira et al., 2013). It has been postulated that this requirement for two phosphorylations may provide a time window in which Sal/Plk4 is active and can phosphorylate STIL/Ana2 before it gets degraded (Cunha-Ferreira et al., 2013). However, more research is required to fully understand this. In M-phase, when Sak/Plk4 levels are high, the Sak/Plk4 *trans* autophosphorylations are removed by the protein phosphatase 2A (PP2A), protecting Plk4 from degradation and allowing it to be active (Brownlee et al., 2011).

Additionally, Cdk1/Cyclin B is a central player in the control of Plk4 activity in mammalian cells and *Xenopus* (Zitouni et al., 2016) (**Figure 1.9**). Cdk1/Cyclin B was found to bind to STIL/Ana2 in late G2-phase and M-phase, preventing Sak/Plk4 from phosphorylating it. As the cell moves into late M-phase and early G1-phase, Cdk1

levels decrease, leading to a release of STIL/Ana2 and allowing it to be bound and phosphorylated by Sak/Plk4 in mid-G1-phase. This initiates the formation of a new centriole (Zitouni et al., 2016). These findings demonstrate the Plk4 activity is strongly restricted in space and time to prevent unscheduled centriole duplication.

Centriole duplication is also numerically restricted so that each mother centriole only gives rise to one daughter centriole. One aspect of this control is the role of centriole engagement – the tight orthogonal arrangement of mother and daughter centriole. It is known that the centriole pair is tightly engaged from centriole duplication initiation in S-phase until late mitosis/early G1-phase, when they become disengaged and lose their strict orthogonal relationship (**Figure 1.9**) (Loncarek et al., 2008; Tsou and Stearns, 2006). The disengagement was found to require the anaphase-promoting complex (APC) (Shukla et al., 2016). The physical engagement blocks centriole re-duplication. Accordingly, removal of the daughter centriole by laser ablation (Loncarek et al., 2008) or by Plk1 overexpression (leading to premature centriole disengagement) (Loncarek et al., 2010) can to induced centriole reduplication.

An additional layer of centriole duplication control is provided by tightly regulating Plk4, STIL and Sas-6 protein levels. All of these proteins have been shown to induce centriole over-duplication when overexpressed (Arquint et al., 2012; Kleylein-Sohn et al., 2007; Peel et al., 2007; Rodrigues-Martins et al., 2007b; Stevens et al., 2010a; Strnad et al., 2007). The protein levels of Sas-6, STIL and CPAP are regulated over the cell cycle with cytoplasmic protein levels falling in mitosis and then gradually increasing in S-phase (Arquint et al., 2012; Strnad et al., 2007; Tang et al., 2009).

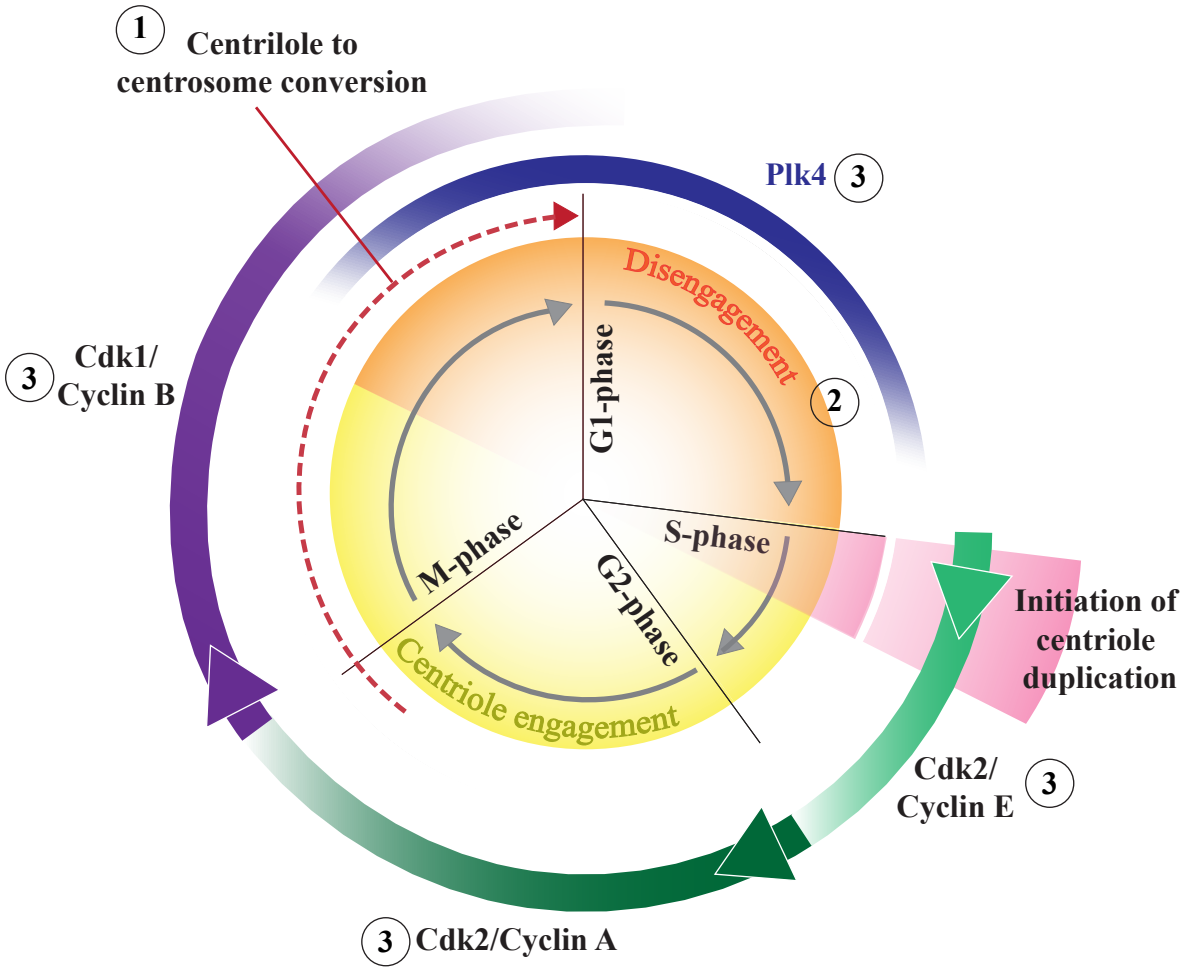


Figure 1.9: Centriole duplication during the cell cycle. Several cell-cycle-regulated events are required for the initiation of centriole duplication (highlighted by the pink box, right hand side): **1**) the maturation of the daughter centriole (centriole-to-centrosome conversion) (red dotted arrow); **2**) the disengagement of the mother and daughter centrioles; **3**) the presence of the kinases Plk4 (blue), Cdk2 (greens) and Cdk1 (purple). See the main text for details.

The regulated degradation of these proteins has been found to prevent centriole over-duplication (Arquint et al., 2012; Strnad et al., 2007).

Finally, another step in centriole duplication control is the regulated centriole-to-centrosome conversion step, allowing the daughter centriole to have the capacity to recruit PCM and duplicate (Nigg and Holland, 2018). Cdk1 and Polo/Plk1 regulate this conversion (Novak et al., 2016; Wang et al., 2011). It had been shown in *Drosophila* that Cdk1 phosphorylates Sas-4 at a single site, leading to the recruitment of Polo kinase (Novak et al., 2016). Polo is required to sequentially recruit Cep135, Ana1 and Asl, in both mammalian cells and *Drosophila* during late interphase and mitosis (**Figure 1.9**) which subsequently leads to the recruitment of PCM (Fu et al., 2016; Novak et al., 2014; Saurya et al., 2016). It has been shown in *Drosophila* that Asl only loads onto the daughter centriole once the centriole pair has disengaged (Novak et al., 2014).

1.3. PCM structure and recruitment

The centrosome is comprised of a pair of centrioles surrounded by organized PCM. Centrioles are essential for robust PCM assembly in many cell types (Basto et al., 2006; Varmark et al., 2007) (**Figure 1.10A**). The degree of PCM formation differs between cell types and cell cycle stages (Conduit et al., 2015b). In many post-mitotic cells, the centrioles organise only small amounts of PCM that nucleates few microtubules. In proliferating cell centrosomes organize larger amounts of PCM and nucleate many more microtubules when in interphase (Haren et al., 2009; Zhu et al., 2008). When these cells enter into mitosis, the PCM is rapidly expanded, which dramatically increase the number of microtubules that are being nucleated. The drastic PCM expansion is a hallmark of centrosome maturation (Conduit et al., 2015b;

Mennella et al., 2014). PCM assembly, similar to centriole assembly, is largely conserved between different species (**Figure 1.6 A-C**). For the purpose of this thesis, I will focus on PCM structure and briefly outline its assembly.

1.3.1.1. Organization of PCM

The PCM is composed of many hundreds of different centrosomal proteins with over 1000 identified in human and 300 in *Drosophila* (Alves-Cruzeiro et al., 2014). The PCM exists in two states, an interphase state, in which the PCM is small and highly organized (Fu and Glover, 2012; Lawo et al., 2012; Mennella et al., 2012; Sonnen et al., 2012), and a mitotic state, in which the PCM has drastically expanded and is able to nucleate sufficient microtubules for mitotic spindle formation. The highly organised interphase PCM structure is lost upon PCM expansion (Sonnen et al., 2012).

A variety of studies, using 3D-SIM, have examined the interphase PCM in *Drosophila* and human cells, and attempted to localise the position and/or the orientation of important PCM proteins (Fu and Glover, 2012; Fu et al., 2016; Lawo et al., 2012; Mennella et al., 2012; Sonnen et al., 2012). It appears consistent that all PCM proteins localised around the centriole in toroids of different sizes, ranging in diameters from ~150-500 nm in human cells (Lawo et al., 2012; Sonnen et al., 2012) and from ~120-400 nm in *Drosophila* (Fu and Glover, 2012; Fu et al., 2016; Mennella et al., 2012). Even though the size of the localised toroid of a protein is different between human and *Drosophila* centrosomes, the organisation order is maintained (see **Figure 1.10B**). Interestingly enough, some of the centrosome proteins are strictly oriented in relation to the centriole in interphase with their N- or C-terminus localised

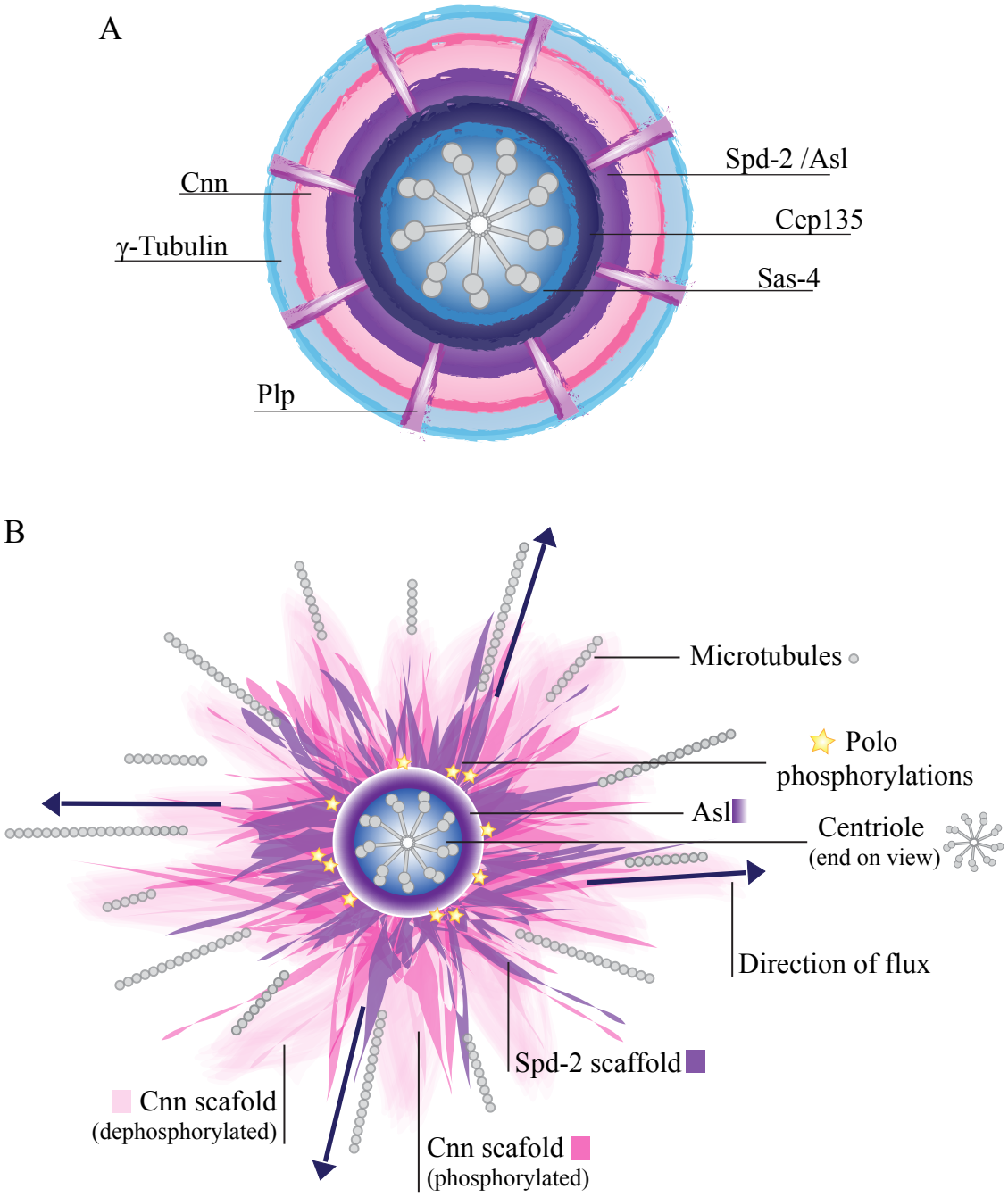


Figure 1.10: PCM organization and assembly in interphase and mitosis. A) Schematic of the general positions of several PCM proteins during interphase. At this stage of the cell cycle many centrosomal proteins are arranged in a toroids that surround the mother centriole, and several of them exhibit strict orientations with respect to the centriole. **B**) A simplified schematic of the mitotic PCM in *Drosophila*. Asl (dark purple/white) recruits Spd-2 (purple), which is then phosphorylated and fluxes outwards away from the mother centriole. The Spd-2 can recruit Cnn (pink) and Polo, which phosphorylates (yellow stars) Cnn, allowing it to assemble into a scaffold. This, in embryos at least, fluxes outwards along the centrosomal MTs (grey). The Cnn gradually gets dephosphorylated (light pink) towards the periphery of the PCM, where the scaffold starts to disassemble.

to differently sized toroids, examples include Asl, Cep135, Sas-4, Plp, Cnn and Spd-2 (Lawo et al., 2012; Mennella et al., 2012; Sonnen et al., 2012).

1.3.1.2. Essential PCM assembly component: Spd-2 and Cnn

In *Drosophila* and in *C. elegans*, the assembly of the mitotic PCM is relatively simple and involves two proteins: Spd-2/SPD-2 and Cnn/SPD-5 in *Drosophila* and *C. elegans*, respectively. For simplicity, I will focus on *Drosophila* Spd-2 and Cnn, but SPD-2 and SPD-5 appear to have a similar role in PCM assembly in worms (Conduit et al., 2015b).

Cnn and Spd-2 are the two essential players required for PCM assembly in flies (Conduit et al., 2014b). Flies lacking Spd-2 have a strongly decreased ability to recruit other PCM proteins to the mitotic centrosome (Conduit et al., 2014b; Dix and Raff, 2007; Giansanti et al., 2008). Conversely, the absence of Cnn also leads to a large reduction in the levels of other PCM proteins at the centrosome (Lucas and Raff, 2007; Megraw et al., 2001; Megraw et al., 1999). However, if both Spd-2 and Cnn are absent, there is a complete loss of PCM at the mitotic centrosome (Conduit et al., 2014b). Additionally, both Spd-2 and Cnn are incorporated into the PCM near the centriole wall and then subsequently slowly flux outwards (Conduit et al., 2014a; Conduit et al., 2014b) (**Figure 1.10B**). It has been shown that the rate of Cnn incorporation into the PCM helps to set the 'size' of the mitotic PCM (Conduit et al., 2010).

The recruitment of Spd-2 and Cnn and their subsequent scaffold formation is illustrated schematically in **Figure 1.10B**. Asl is an important player in initiating the recruitment of Spd-2 and Cnn (Conduit et al., 2010), and this process requires Polo

kinase (Dobbelaere et al., 2008; Fu and Glover, 2012). Polo is thought to phosphorylate Spd-2 specifically at the centrosome (Alvarez Rodrigo et al., 2018). Phosphorylated Spd-2, is then able to recruit Cnn, which in turn helps maintain Spd-2 at that the centrosome (Conduit et al., 2014b). If Spd-2 cannot be phosphorylated by Polo, all three proteins – Spd-2, Cnn and Polo – are recruited to the centrosome, but they fail to expand into a PCM scaffold around the mother centriole (Alvarez Rodrigo et al., 2018). Polo phosphorylates Cnn to allow it to assemble into a scaffold (Conduit et al., 2014a; Feng et al., 2017). Cnn is dephosphorylated in the outer regions of the PCM, resulting in the breakdown of the peripheral PCM. It appears that Spd-2, Polo and Cnn form a positive feedback loop which allows for the robust and efficient expansion of PCM in mitosis (Alvarez Rodrigo et al., 2018).

1.4. Thesis outline

Even though centrioles have been studied for decades, many questions still remain unanswered, often due to technical limitations. Fundamental questions regarding the localisation (Ana2) and protein dynamics of centriole proteins (Sak) have not been answered to date due to the lack of sufficiently advanced microscopic techniques. The recently developed high resolution imaging techniques, and sufficiently bright fluorescent protein labels have not yet been applied to these centriole proteins. In addition, aspects of the precise roles, interaction requirements and domain functions of the essential centriole proteins remain elusive. Here, the problems lie in the inherent lack of centrioles when the essential proteins are perturbed. Important questions include: what is the role of Asl in recruiting PCM? Is Sas-4 required for Ana2 and Sas-6 to interact? Which domains and amino acids are essential for centriole formation? The goal of this thesis was applying recent technological advances to centriole research in *Drosophila* embryos in order to gain deeper insight

into centriole proteins and processes previously inaccessible. This thesis focuses on the implementation of three different technological advances (1) new fluorescent probes, (2) single molecule localisation microscopy and (3) a recently identified *in vivo* centriole model system.

Due to the small size of centrioles and the low abundance of certain proteins, it was prudent to identify brighter and more stable fluorescent probes in multiple colours that are applicable in *Drosophila*. The identification of fluorescent proteins, allowed me to further investigate the behaviour and precise functions of essential centriole duplication proteins (Chapter 3).

Recent developments in the field of super-resolution microscopy allow researchers to image cellular structures in much greater detail. Single-molecule localisation microscopy (SMLM) is now more widely available and allows one to localise individual fluorophores with nanometre precision. Such technology can be used to shed light on to the structure and organization of the centriole cartwheel (Chapter 4).

Finally, the development of an *in vivo* model system that serves as a proxy for *bona fide* centriole assembly (Stevens et al., 2010b; Vicente, 2013) allowed me to probe the pathway of centriole and centrosome assembly. This model system, which does not rely on the presence of centrioles, can provide new insights into the roles and regulation of these key proteins (Chapter 5). Finally, this model system can be utilized as a protein-protein interaction assay that allows for the efficient identification of new protein domains and regulatory sites (Chapter 6).

2. Material and methods

2.1. Fly Husbandry

2.1.1. Fly handling

The flies were kept at 25 °C and 18 °C on *Drosophila* culture medium (5.5% glucose, 5% yeast extract, 3.5% wheat extract, 1% pen/strep, 0.75% agar, 0.4% propionic acid and 0.25% nipagen) in vials or in bottles. Embryos were collected on fruit juice plates (25% cranberry-raspberry juice, 2% sucrose and 1.8% agar) with a drop of yeast paste. Fly handling techniques were used as described in Roberts (1986).

2.1.2. *Drosophila melanogaster* stocks

Oregon R flies were used in all experiments as the wild type (WT) stock. All balancer chromosomes and markers used have been described previously (Lindsley and Zimm, 1992). The complete list of fly lines I used in this thesis are listed in Table 2.

Table 2: Drosophila lines used in this thesis

Chapter	*Fly Line Genotype*	*Description*	*Source/Stock #*
3	w;; eAsl-mCherry/TM6C	Asl-mCherry under an endogenous (e) promoter	T1233
3	w;; eAsl-GFP, asl^{B46}	Asl-GFP under an endogenous promoter	T1302
3	w;; pUbq-Dendra2-Cnn/TM6C	Dendra2-Cnn under a ubiquitin (Ubq) promoter	T1098
3	w;; pUbq-Maple3-Cnn/TM6C	Maple3-Cnn under a ubiquitin promoter	*This Thesis*
3	w;; eAsl-mKate2(14-10), asl^{B46}	Asl-mKate2 under an endogenous promoter in a full mutant Asl (asl^{B46}) background	*This Thesis*
3	w;; Asl-mKate2(18-5), asl^{B46}	Asl-mKate2 under an endogenous promoter in a full mutant Asl (asl^{B46}) background	*This Thesis*
3	w;; Asl-mKate2(19-11), asl^{B46}	Asl-mKate2 under an endogenous promoter in a full mutant Asl (asl^{B46}) background	*This Thesis*
3	w;; Asl-mRuby2(4-2), asl^{B46}/TM6C	Asl-mRuby2 under an endogenous promoter in heterozygous mutant Asl (asl^{B46}) background	*This Thesis*

3	w;; Asl-mRuby2(11-2), *asl*^{B46}/TM6C	Asl-mRuby2 under an endogenous promoter in heterozygous mutant Asl (*asl*^{B46}) background	*This Thesis*
3	w;; Asl-mRuby2(5-2), *asl*^{B46}/TM6C	Asl-mRuby2 under an endogenous promoter in heterozygous mutant Asl (*asl*^{B46}) background	
3	w; pUbq-mNeonGreen-Cnn, Cnn^{f}/SM6a	mNeonGreen-Cnn under a ubiquitin promoter with one allele mutant Cnn (*Cnn*^{f}) allele	*This Thesis*
3	w; pUbq-GFP-Cnn#8/SM6^{TM6}	GFP-Cnn under a ubiquitin promoter with one allele mutant Cnn (*Cnn*^{f}) allele	T054
3	w;; eAsl-mRuby2(11-2), *asl*^{B46}/ TM6C	Asl-mRuby2 under an endogenous promoter	*This Thesis*
3	w;; Sak-mNeonGreen, *Sak*^{aa74}	Sak-mNeonGreen in a full mutant Sak (*Sak*^{aa74}) background	*This Thesis*
3	w; eAslmKate2(1-2)/CyO; Sak-mNeonGreen, *Sak*^{aa74}	Sak-mNeonGreen, in a full mutant background, expression Asl-mKate2	*This Thesis*
4	w; pUbq-Sas-4-GFP	Sas-4-GFP under an ubiquitin promoter	(Cottee et al., 2013)
4	w; eSas-4-GFP#6; eSas-4-GFP#8, *Sas4*^{m}	4 copies of Sas-4-GFP under an endogenous promoter in a full mutant Sas-4 (*Sas-4*^{S2214}) background	(Novak et al., 2016)
4	YFP-Asl^{FL}	Full length mYFP-Asl	(Varmark et al., 2007)
4/5	w; pUbq-GFP-Ana2#3F/SM5	GFP-Ana2 under a ubiquitin promoter	(Stevens et al., 2010b)
4/5	w; pUbq-GFP-Sas-6#^{89L}/SM5	GFP-Sas-6 under a ubiquitin promoter	(Peel et al., 2007)
4	w; *ana2*^{169}, eAna2-GFP#2 rec#8/SM5	Ana2-GFP under an endogenous promoter with a mutant Ana2 (*ana2*^{169}) allele	N. Muschalik *The Thesis*
4	w; *ana2*^{719}, eAna2-GFP#2 rec#15/SM5	Ana2-GFP under an endogenous promoter with a mutant Ana2 (*ana2*^{719}) allele	N. Muschalik *The Thesis*
4	w;; *sas-6*, e, eSas-6-GFP#1/TM6C (rec#3)	Sas-6-GFP under an endogenous promoter with a mutant Sas-6 (*sas-6*^{e02901}) allele	N. Muschalik *The Thesis*
4	w;; *sas-6*, e, eSas-6-GFP#7/TM6C (rec#5)	Sas-6-GFP under an endogenous promoter with a mutant Sas-6 (*sas-6*^{e02901}) allele	N. Muschalik *The Thesis*
5	w; If/CyO; Ana2 P11AR12A-GFP 1/TM6B	Ana2-GFP mutant for the Sas-4 binding domain under an endogenous promoter	(Cottee et al., 2013)
5	w; If/CyO; Ana2 R16A-GFP 3-2/TM6B	Ana2-GFP mutant as a negative control for the Sas-4 binding domain residues under an endogenous promoter	(Cottee et al., 2013)
5	w;; Ana2 ΔCC-GFP 6M/TM6C	Ana2-GFP coiled-coiled deletion (Δ195-229) under an endogenous promoter	(Cottee et al., 2015)
5	w; Ana2 CCA-GFP 2M/SM5	Ana2-GFP coiled-coiled mutation to alanine under an endogenous promoter	(Cottee et al., 2015)
5	w; Sas-6 ΔF143D-GFP/+	Sas-6-GFP head-group mutant (F143D) under an endogenous promoter	(Cottee et al., 2015)
5	w;; Ana2ΔSTAN-GFP 6M/ TM6C	Ana2-GFP STAN domain deletion (Δ316-383) under an endogenous promoter	(Cottee et al., 2015)
5	w; pUbq-Ana2-6A-GFP/SM6a	Ana2-GFP STAN domain alanine mutant S318A, S345A, S348A, S363A, S370A, S373 under a ubiquitin promoter	B.Sieber #3A-8 *This Thesis*

5	w; pUbq-Ana2-6E-GFP/SM6a	Ana2-GFP STAN domain glutamic acid mutant S318E, S345E, S348E, S363E, S370E, S373E under a ubiquitin promoter	B. Sieber #4A-9 *This Thesis*
5	w; pUbq-Ana2-2E-GFP/SM6a	Ana2-GFP STAN domain glutamic acid mutant S318E, S373E under a ubiquitin promoter	B. Sieber #50B-14 *This Thesis*
5	w; pUbq-Ana2-2A-GFP/SM6a	Ana2-GFP STAN domain alanine mutant S318A, S373A under a ubiquitin promoter	B. Sieber #49A-10 *This Thesis*
5	w; pUbq-Ana2-4A-GFP/SM6a	Ana2-GFP STAN domain alanine mutant S318A, S363A, S370A, S373A under a ubiquitin promoter	B. Sieber #19A-3 *This Thesis*
5	w; pUbq-Ana2-4E-GFP/SM6a	Ana2-GFP STAN domain glutamic acid mutant S318E, S363E, S370E, S373E under a ubiquitin promoter	B. Sieber #20A-19 *This Thesis*
5	w; $ana2^{719}$/ $ana2^{169}$; pUbq-Ana2-6A-GFP/TM6C	Ana2 STAN domain 6A mutant in a full Ana2 mutant background, do not rescue unc (uncoordinated) phenotype	*This Thesis*
5	w; $ana2^{719}$/ $ana2^{169}$; pUbq-Ana2-6E-GFP/TM6C	Ana2 STAN domain 6E mutant in a full Ana2 mutant background, rescues unc phenotype	*This Thesis*
5	w; $ana2^{719}$/ $ana2^{169}$; pUbq-Ana2-4E-GFP/TM6C	Ana2 STAN domain 4E mutant in a full Ana2 mutant background, rescues unc phenotype	*This Thesis*
5	w; $ana2^{719}$/ $ana2^{169}$; pUbq-Ana2-4A-GFP/TM6C	Ana2 STAN domain 4A mutant in a full Ana2 mutant background, do not rescue unc phenotype	*This Thesis*
5	w; $ana2^{719}$/ $ana2^{169}$; pUbq-Ana2-2A-GFP/TM6C	Ana2 STAN domain 2A mutant in a full Ana2 mutant background, rescues unc phenotype	*This Thesis*
5	w; $ana2^{719}$/ $ana2^{169}$; pUbq-Ana2-2E-GFP/TM6C	Ana2 STAN domain 2E mutant in a full Ana2 mutant background, rescues unc phenotype	*This Thesis*
5	w; elavGAL4/ pUAS+Sas4; *Df(3R)BSC221*/ $Sas4^{m}$	Sas-4 cilia rescue in a full Sas-4 mutant background ($Sas4^{m}$, *Df(3R)BSC221*)	A. Wainman *This Thesis*
5	w; elavGAL4/ pUASpAsl; *Df(3R)ED5177*/ asl^{B46}	Asl cilia rescue in a full Asl mutant background (asl^{B46}, *Df(3R)ED5177*)	A. Wainman *This Thesis*
5	w; elavGAL4/ UASpSak; $Sak^{\Delta a}$ / Sak^{aa74}	Sak cilia rescue in a full Sak ($Sak^{\Delta a}$, Sak^{aa74}) mutant background	A. Wainman & Z. Novak *This Thesis*
5	w; pUbq-Ana2-GFP#1M, pUASp-Asl/ pUbq-GFP-Sas6#89L, elavGAL4 ; $Spd2^{m}$, asl^{B46}/asl^{df},$Spd2^{df}$	Asl cilia rescue in a full Asl (asl^{B46}, *Df(3R)ED5177*) and Spd2 ($Spd2^{G0214}$, $Spd2^{df\,(Df(3L)st-j7}$) mutant background expressing GFP-Sas-6 and Ana2-GFP under a ubiquitin promoter	A. Wainman *This Thesis*
5	w; pUbq-Ana2-GFP#1M, pUASp-Asl/ pUbq-GFP-Sas6#89L, elavGAL4 ; asl^{B46}/asl^{df}	Asl cilia rescue in a full Asl (asl^{B46}, *Df(3R)ED5177*) mutant background expressing GFP-Sas-6 and Ana2-GFP under a ubiquitin promoter	A. Wainman *This Thesis*
6	w;; Jupiter-mCherry	Jupiter-mCherry homozygous	(Callan et al., 2010)
6	w;; Ana2(S284E,T301E)-GFP/+	Ana2-GFP mutant for Cdk sites S284E and T301E	*This thesis*
6	w;; Ana2(S284A,T301A)-GFP/+	Ana2-GFP mutant for Cdk sites S284A and T301A	*This Thesis*

6	w;; *ana2*^{719}/ *ana2*^{169}; Ana2(S284E,T301E)-GFP/TM6B	Ana2-GFP mutant for Cdk sites S284E and T301E in a full Ana2 mutant background (*ana2*^{719}, *ana2*^{169}), rescues unc phenotype	*This Thesis*
6	w; *ana2*^{719}/ *ana2*^{169}; Ana2(S284A,T301A)-GFP/TM6B	Ana2-GFP mutant for Cdk sites S284A and T301A in a full Ana2 mutant background (*ana2*^{719}, *ana2*^{169}), rescues unc phenotype	*This Thesis*
6	w;; *ana2*^{719}/ *ana2*^{169}; Ana2-FL-GFP/TM6B	Ana2-GFP Full length rescue in a full Ana2 mutant background (*ana2*^{719}, *ana2*^{169}), rescues unc phenotype	(Cottee et al., 2013)

2.1.3. Generation of transgenic lines

Stable transgenic fly lines were generated via random *P*-element insertion of the construct of choice, containing a w^+ gene for selection, in to a w^{1118} background. Plasmid containing constructs were generated as described (see 2.3.4). The injection, selection of transformants and the generation of transgenic stocks was performed by the Cambridge Fly Facility service at the Department of Genetics, University of Cambridge (UK) or BestGene Inc. in California (USA). The mapping of the chromosome on which the transgene inserted, was often preformed by the before mentioned facility and company. In some cases I performed the mapping and balancing myself to establish a stable stocks according to Greenspan (2004). The transgenic flies generated for this thesis are indicated in Table 2.

2.2. Bioinformatics

2.2.1. Jalview

Bioinformatic analyses were performed using the open source program Jalview (Waterhouse et al., 2009). FASTA sequences of the protein, Ana2, in different *Drosophila* species were uploaded into Jalview and the multiple sequences were aligned using the ClustalO multiple sequence alignment algorithm. Sequence similarity was visualized using the Percentage Identity colour scheme.

2.3. Molecular Biology

2.3.1. PCR reactions for DNA amplification and diagnostics

All PCR reactions preformed for DNA amplification were done using the Phusion® High Fidelity PCR Kit (NEB, #M0530S) according to the manufacturers instructions. All cloning and DNA fragment ligation was preformed via homologous recombination reactions using In-Fusion® HD EcoDry™ (ClonTech Laboratories Inc., #639812) according to the manufacturers protocol.

2.3.2. Site-directed mutagenesis on plasmids

Site-directed mutagenesis on single base pairs substitution or multiple base pair deletions was performed using the Quikchange II XL Site-directed Mutagenesis Kit (Stratagene, Agilent #200522) or the Q5 Site-directed Mutagenesis Kit (NEB, #E0554S) according to the manufactures instructions. All plasmid and primer *in silico* design and analysis was preformed in MacVector. Primers were synthesised by Invitrogen (Thermo Fisher Scientific)

2.3.3. DNA sequencing

DNA sequencing was preformed by Source BioScience and the results subsequently analysed in MacVector.

2.3.4. Constructions of plasmids for generating transgenic *Drosophila* lines

Gateway cloning (Life Technologies) was used to generate all the vectors required for *P*-element mediated transformation in flies. For all the plasmids made, the protein coding sequence was cloned into a pDONR^{TM}/Zeo vector (Gateway) that were flanked by *att*L recombination sites. For the study of proteins under endogenous promoters, the pDONR^{TM}/Zeo vector (Gateway) contained the genomic region 2 kb

upstream of the start codon through to the stop codon. For proteins under ubiquitin promoters, the pDONR™/Zeo vectors (Gateway) contain the cDNA from start to stop codon. In both cases, the stop codon was removed if required.

The all *att*R destination vectors (Gateway) were modified from existing vectors in the lab to contain a variety of different N- or C-terminal fluorescent proteins and either an ubiquitin promoter or none (for the proteins under an endogenous promoter). To attach the protein sequence of interest to the destination vector, the pDONR™/Zeo vectors were recombined to the all *attR* destination vectors via the Gateway LR reaction and performed according to the manufactures instructions. The final plasmids generated are listed in Table 3.

Table 3: List of vectors used to generate transgenic Drosophila lines

Plasmid Name	*Final Vector Description*	*Promoter*	*Resistance*
pLG01	eAsl-mKate2	Endogenous	Kanamycin
pLG02	eAsl-mRuby2	Endogenous	Kanamycin
pLG03	eSak-mNeonGreen	Endogenous	Kanamycin
pLG04	Ubq-Maple3-Cnn	Ubiquitin	Kanamycin
pLG05	Ubq-SNAPtag-Cnn	Ubiquitin	Kanamycin
pLG06	Ubq-mNeonGreen-Cnn	Ubiquitin	Kanamycin
pLG09	Ubq-Ana2-S284E,T301E-GFP	Ubiquitin	Kanamycin
pLG10	Ubq-Ana2-S284A,T301A-GFP	Ubiquitin	Kanamycin

All PCR products and plasmids were extracted using Qiagen kits and protocols (QIAprep Spin Miniprep Kit (#27106), QIAfilter Plasmid Midi Kit (#12243) and QIAquick Gel Extraction Kit (#28704)). The program MacVector was used to generate the constructs *in silico* and analyse the sequencing results.

2.3.5. Genetic screening and diagnostic PCRs for genetic recombination events

In order to establish if a genetic recombination event happened, I preformed a PCR screen for possible recombinant mutant flies. Anesthetised, possibly recombinant male flies were put into single wells of a 96-well plate and squashed in Squishing Buffer (10mM Tri-HCl, 1 mM EDTA, 25 mM NaCl, 200 µm/ml Proteinase K) on ice. Subsequently, the sealed 96 well plate was treated at 55 °C for 30 min and then at 95 °C for 10 min.

PCR reactions for the screening of genetic recombination events were performed using the OneTaq Quick-Load 2xMM (NEB, #M0486S) according to the manufacturer's protocol using the appropriate primer melting and annealing temperature. The final PCR products were run on a 1% agarose-ethidium bromide gel (1x TAE, 1% agarose, 0.005% ethidium bromide) and visualised with UV light.

2.3.6. Constructions of plasmids for *in vitro* mRNA generate for injection into *Drosophila* eggs and embryos

Gateway cloning (Life Technologies) was used to generate all the vectors required for the generation of pRNA vectors. These vectors were used to produce *in vitro* transcribed mRNA, which was injected to into live eggs and embryos. For all the plasmids made, the pDONR^{TM}/Zeo vectors (Gateway) contain the cDNA from start to stop codon. The stop codon was removed, if required. These entry clones were combined with an all *att*R site destination vector (Gateway) (kind gift of Dr. Z. Novak) containing a T3 promoter that is compatible with the mMESSAGE mMACHINE T3 Transcription Kit (Ambion, ThermoFisher). The all *att*R site destination vectors were modified from existing vectors to contain a variety of

different N- and C-terminal fluorescent tags. To attach the protein sequence of interest to the destination vector, the pDONR^{TM}/Zeo vectors were recombined to all *attR* destination vectors using the Gateway LR reaction, according to the manufacturer's protocol. The final ampicillin resistant plasmids generated are a listed in Table 4.

Table 4 List of pRNA vectors generated for mRNA injection assays

Chapter	*Gene Contained in the pRNA Vector*	*Mutation Description*	*Promoter*
3	GFP-Cnn		T3
3	mKate2-Cnn		T3
3	mRuby2-Cnn		T3
3	mNeonGreen-Cnn		T3
3	mCardinal-Cnn		T3
3	mTagRFP-Cnn		T3
3	mKO2-Cnn		T3
3	SNAP-Tag-Cnn		T3
3	CLIP-Tag-Cnn		T3
3	Halo-Tag-Cnn		T3
6	Ana2-mKate2		T3
6	Ana2-mNeonGreen		T3
6	Sas-6-mKate2		T3
6	Sas-6-mNeonGreen		T3
6	Sas-6-ΔF143D-mNeonGreen	Sas-6-GFP head-group mutant (F143D)	T3
6	Ana2-CCA-mNeonGreen	Ana2-GFP coiled-coiled mutation to alanine	T3
6	Ana2-ΔCC-mNeonGreen	Ana2-GFP coiled-coiled deletion (Δ195-229)	T3
6	Ana2-ΔSTAN-mNeonGreen	Ana2-GFP STAN domain deletion (Δ316-383)	T3
6	Ana2-P11A,R12A-mNeonGreen	Ana2-GFP mutant for the Sas-4 binding domain under an endogenous promoter	T3
6	Ana2-R16A-mNeonGreen	Ana2-GFP mutant as a negative control for the Sas-4 binding domain residues under an endogenous promoter	T3
6	Ana2-6A-mNeonGreen	Ana2-GFP STAN domain alanine mutant S318A, S345A, S348A, S363A, S370A, S373	T3

6	Ana2-6E-mNeonGreen	Ana2-GFP STAN domain glutamic acid mutant S318E, S345E, S348E, S363E, S370E, S373E	T3
6	Ana2-4A-mNeonGreen	Ana2-GFP STAN domain alanine mutant S318A, S363A, S370A, S373A	T3
6	Ana2-4E-mNeonGreen	Ana2-GFP STAN domain glutamic acid mutant S318E, S363E, S370E, S373E	T3
6	Ana2-2A-mNeonGreen	Ana2-GFP STAN domain alanine mutant S318A, S373A	T3
6	Ana2-2E-mNeonGreen	Ana2-GFP STAN domain glutamic acid mutant S318E, S373E	T3
6	Ana2-S84A-mNeonGreen	Ana2-GFP mutant for possible Cdk site S84A	T3
6	Ana2-S84E-mNeonGreen	Ana2-GFP mutant for possible Cdk site S84E	T3
6	Ana2-S284A,T301A-mNeonGreen	Ana2-GFP mutant for possible Cdk site S284A, T301A	T3
6	Ana2-S284E,T301E-mNeonGreen	Ana2-GFP mutant for possible Cdk site S84E,T301E	T3
6	Ana2-S284A-mNeonGreen	Ana2-GFP mutant for possible Cdk site S284A	T3
6	Ana2-T301A-mNeonGreen	Ana2-GFP mutant for possible Cdk site T301A	T3
6	Ana2-S284E -mNeonGreen	Ana2-GFP mutant for possible Cdk site S84E	T3
6	Ana2-T301E-mNeonGreen	Ana2-GFP mutant for possible Cdk site T301E	T3

All PCR products and plasmids were extracted using Qiagen kits and protocols (QIAprep Spin Miniprep Kit (#27106) and QIAquick Gel Extraction Kit (#28704)). The program MacVector was used to generate the constructs *in silico* and analysis the sequencing results

2.3.7. *In vitro* mRNA transcription

To generate *in vitro* transcribed mRNA for microinjection into embryos, 4 µg of DNA was linearised in 80 µl using the restriction enzyme AscI (#R0558S, NEB) for 8 hrs at 37 °C and subsequently inactivated at 8 0°C for 20 min. The linearized DNA was then precipitated in 4 µl 0.5 M EDTA, 8 µl 3 M Na-Acetate and 180 µl 100% ethanol at -20 °C for a minimum of 20 min. The DNA was then pelleted at 4° C for 15 min at 21.1 *g*, washed twice with 1 ml of -20 °C 70% ethanol, air-dried and resuspended in

10 µl of DEPC-treated ddH_2O. The transcription reaction was preformed using the mMESSAGE mMACHINE T3 Transcription Kit (Ambion, ThermoFisher) according to the manufacturer's instructions. 2 µg of linearized DNA template was used for each 150 µl reaction and incubated for 2 hrs at 37 °C. The mRNA was purified using the RNeasy Kit (Qiagen) according to the manufactures instructions and diluted to 2 µg/µl aliquots, unless otherwise stated. Aliquots were stored at -80 °C. The mRNA was injected into either Asl-mCherry, asl^{B46} or an Asl-GFP, asl^{B46} embryos or eggs and imaged as described in 2.5.1 and 2.5.2.

2.4. Biochemistry and Cell biology

2.4.1. *Drosophila* embryo and egg fixation for immunoprecipitation

For protein analysis, 0-3 hr old *Drosophila* embryos or eggs were collected and washed 3x in washing buffer (1x PBS + 0.0005% Tween-20), dechorionated in 60% bleach for 2 min and washed in 3x in washing buffer.

2.4.1.1. Conventional fixation

For conventional fixation, the embryos or eggs were then washed into a glass vial containing 2 ml of methanol + 3% 0.5 M EGTA with 2 ml of heptane and vigorously shaken for 30 sec, the embryos or eggs left to fall to the bottom of the vial. All embryos or eggs floating on the liquid-liquid interface and all the excess liquid were removed. The remaining embryos or eggs were washed 3x with a total of 6 ml of methanol. The embryos or eggs were left in methanol at 4 °C for at least 24 hrs before use. The excess embryos or eggs were stored in the methanol at 4 °C.

2.4.1.2. Formaldehyde fixation for fluorophore conservation

For better preservation of the chromophore, the embryos or eggs were then washed into a glass vial containing 1 ml of pure heptane and 1 ml of formaldehyde buffer (1

M PIPES (pH 7), 20 mM EGTA, 10 mM $MgSO_4$ in a 1:9 ratio with 16% microfiltered formaldehyde). The vial was then gently swirled for 5 min to evenly distribute the eggs or embryos on the liquid-liquid interface. Thereafter, the bottom formaldehyde buffer layer was carefully removed and 1-2 ml of methanol was added. The vial was then vigorously shaken for 30 sec. After the embryos or eggs settled on the bottom of the vial, all liquid removed and the embryos and eggs washed 3x with a total of 6 ml of methanol. The embryos or eggs were left in methanol at 4 °C for at least 24 hrs before use. Excess embryos or eggs were stored in the methanol at 4 °C for weeks.

2.4.2. SDS-PAGE and western blotting

The methanol was removed from the embryos or eggs and they were then washed 3x for 15 min with PBS/0.2% Triton X-100 at 15 rpm on a rotator (SB3 Rotator, Stuart, UK). The embryos or eggs were transferred to a clean watch glass containing fresh PBS/0.2% Triton X-100. Either 20 (for Cnn probing western blots) or 40 (for all other western blots) well-fixed, pre-cellularised embryos or eggs were selected in 20 µl of PBS/0.2% Triton X-100 and mixed with 20 µl of 2x SDS loading dye. The total 40 µl was then boiled for 10 min at >95 °C, briefly spun down and frozen at -20 °C.

Samples were run on a 3-8% NuPAGE acrylamide gels (Life Technology #EA03785BOX) with the appropriate NUPAGE tris-acetate SDS running buffer (Life Technologies #LA0041) at 150 V in a XCell SureLock Mini-Cell.

The sample was transferred from the acrylamide gel onto a nitrocellulose membrane (BIO-RAD, 0.2µm #162-0112) in a BIO-RAD Mini Trans-Blot system using a transfer buffer (25 mM Tris-base + 192 mM glycine + methanol 20% + 0.5 ml 20%, pH 7.4) with 100V for 2 hrs or at 18 V overnight. The membrane was blocked for 20-

30 min with blocking buffer (PBS + 4% milk powder + 0.1% Tween-20), incubated for 1hr with primary antibody solution (see Table 5) at room temperature and wash 3x 1 min in washing buffer (TBS + 0.1% Tween-20). For chemiluminescence analysis, either horseradish peroxidase–conjugated (GE Healthcare, ECL anti-mouse (#NA931V)) or anti-rabbit (IgG RPO-linked whole antibody (#NAV934V), or Dako, Polyclonal Swine anti-Rabbit Immunoglobulins/HRP, Ref P0399, Lot 20043737) secondary antibody was used. The membrane was incubated for 45 min in secondary antibody solution and finally washed 3x 15 min in washing buffer. The membrane was incubated in HRPO-substrate (Thermo Scientific SuperSignal West Femto Maximum Sensitivity Substrate, #34095, different dilutions deviating from manufactures instructions) for 1 min. The membranes were exposed on film and on the FujiFilm ImageQuant LAS-4000 (GE Healthcare) for a digital image.

2.4.3. In vitro kinase assay and dot blotting

2.4.3.1. Peptides production

Peptides for the *in vitro* kinase assay were synthesized by GeneScript (The Netherlands). The complete peptide sequences were either biotin-GGAIPQFP-[S/A]-PRPHPAKK (representing the S284 site) or biotin- GGAGYRAN-[T/A]-PQAKRAKK (representing the T301 site), and for a the positive control biotin-Ahx-GGAKPPKTPKKAKKL (Ahx indicates aminohexanonic acid). All peptides were resuspended and stored at -80 °C in 0.1 M phosphate buffer pH 7.4, 150 mM NaCl and 2 mM DTT.

2.4.3.2. In vitro kinase assay

The resuspended peptides, at final concentration of 50 µM, were combined with 0.36 µg of recombinant human protein CDK1/Cyclin B (Thermo Fisher, PV3292), 1x

Kinase Buffer (Cell Signaling, #9802), 100 µM cold ATPs (Cell Signaling, #9804) and 5 µCi γ-[^{32}P] ATP in a reaction volume of 20 µl. The reaction was incubated at 30 °C for 15 min, and then terminated with 10 µl of 7.5 M GuHCl. 4 µl of each reaction was spotted onto a streptavidin-coated SAM^2 Biotin Capture Membrane (Promega, #TB547). The membrane was air-dried, then washed 2x for 30 sec with 2 M NaCl, 3x 2 min with 2 M NaCl, 4x 2 min with 2 M NaCl + 1% H_3PO_4, and then 2x 30 sec with distilled water and air-dried again. The dry membrane was exposed to autoradiograph film (Carestream BioMax MR) for different lengths of time. Overnight exposures were preformed at -80 °C.

2.4.3.3. Biotin dot blot – loading control

A loading control for the kinase assay was preformed using a dot blot. 1.2 µl of the resuspended peptide was spotted on to a nitrocellulose membrane (BIO-RAD, 0.2 µm #162-0112) and left to air-dry. The dry membrane was washed in blocking buffer (PBS + 4% milk powder + 0.1% Tween-20) for 20-30 min and subsequently incubated for 45 min in Streptavidin-HRP (Thermo Scientific) diluted 1:3000 in blocking buffer. The membrane was then washed 3x 10-15 min in wash buffer (TBS + 0.1% Tween-20) followed by incubation with HRPO-substrate (Thermo Scientific SuperSignal West Femto Maximum Sensitivity Substrate, #34095) for 1 min and subsequently exposed on film.

2.4.4. *Drosophila* egg and embryo staining for immunofluorescence

Methanol was removed from the embryos or eggs before washing them 3x 15 min with PBS/0.2% Triton X-100 at 15 rpm on a rotator (SB3 Rotator, Stuart, UK). They were then blocked for 2x 30 min in PBT + 5% BSA and then incubated overnight at 4 °C with primary antibody in PBT + 5% BSA at 15 rpm on a rotator (SB3 Rotator,

Stuart, UK). The antibody was then removed and the embryos or eggs washed for 3x 20 min in PBT at room temperature. Subsequently the samples were incubated for 2 hrs at room temperature with fluorescently conjugated secondary antibodies. Finally, the samples were washed 3x 15 min in PBT, and mounted in 20µl of Vectashield (Vector Laboratories, Vectashield Antifade Mounting Medium H-1000 or H-1200 (latter contains DAPI)), on slides with 1.5H coverslips and sealed with nail polish. Slides were stored at 4 °C.

2.4.5. Primary antibodies used in this study

Table 5 Primary antibodies used for western blotting and immunofluorescence (IF)

Protein	*ID number*	*Species*	*Applications*	*Concentration*
Ana2	JR #6	Rabbit	Western blotting	1:500
Cnn	JR #37 JR #53	Rabbit Rabbit	Western blotting IF wing discs IF eggs/embryos	1:500 1:500 1:500
Actin	JR #221	Mouse	Western blotting	1:500
Asl	JR #11 JR #199 JR #200	Rabbit Guinea Pig Guinea Pig	Western blotting IF wing discs and eggs/embryos IF wing discs	1:500 1:500 1:500
Sas-4	JR #63	Rabbit	Western blotting IF wing discs	1:500 1:500
Ana1	JR #213	Guinea Pig	IF eggs/embryos	1:500
Spd-2	JR #57	Rabbit	IF eggs/embryos	1:500
PLP	JR #86	Rabbit	IF eggs/embryos	1:500
AuroraA	JR #72	Rabbit	IF eggs/embryos	1:500
DTACC	JR #135	Rabbit	IF eggs/embryos	1:500
γ-Tubulin	JR #141	Mouse	IF eggs/embryos	1:500
α-Tubulin	JR #142	Mouse	IF eggs/embryos	1:500
GFP	JR # 166	Llama	IF wing discs	1:500

2.4.6. Staining wing discs for 3D-SIM/SMLM

Wing discs were dissected in PBS from 3rd instar larvae, fixed in 3.6% formaldehyde in PBS for 20 min and placed in 10 µl PBS on a high precision #1.5H (170 ± 5 µm

thickness) coverslip (Marienfeld Superior, Germany). The coverslip was placed on a #1 thickness cover slide (VWR International) and put in between two pieces of Whatman paper, and then squashed for 10 sec. The coverslip sandwich was then placed in liquid nitrogen for 10 min. The #1 thickness coverslip was removed using a razor blade and the high precision coverslip with sample attached was placed in 100% ethanol for 15 min at -20 °C, then placed in PBS/0.1% TritonX for 10 min and washed 3x in PBS for 5 min. The coverslips were incubated in primary antibody solution overnight at 4 °C in a humid box, washed 3x in PBS for 20 min and then incubated in secondary antibody solution for 2 hrs at room temperature. The coverslips were washed in PBS 3x for 10 min. Finally, the coverslips were mounted in 8 µl of Mowiol 4-88® mounting media on a slide. The finished slides were sealed with nail polish.

2.5. Microscopy and Image analysis

Both live *Drosophila* embryos (0-30 min old) and eggs (0-1 hr old) were manually dechorinated on sticky tape, mounted on thin film of glue (Sellotape, UK) on No. 1.5H thick glass bottom MaTtek dishes (MaTtek Corperation, USA) and left to desiccate at 25 °C. For mRNA injection desiccation was 5 min or when just imaging, desiccation was 2-3 min. The embryos or eggs were then covered in Voltalef H10S PCTFE oil (ARKEMA, France).

2.5.1. Microinjection of mRNA into living *Drosophila* embryos or eggs

The injection of mRNA into living *Drosophila* embryos was performed on a Nikon TMS inverted microscope mounted with a manual injection apparatus (Micro Instruments LTD). The *in vitro* transcribed mRNA was pipetted in to 0.5 mm diameter glass needles and then injected into the live embryos or eggs. Embryos and

eggs were injected with mRNA 1-1.5 hrs prior to being imaged. For embryos, imaging normally begun during cycle 10-11 and continued until cycle 14. The injected and non-injected eggs imaged were less than 3 hrs old.

2.5.2. Live imaging of *Drosophila* embryos and eggs

2.5.2.1. Spinning Disc microscopy

2.5.2.1.1. Perkin Elmer ERS Spinning Disc microscope

Live images were acquired at room temperature using a Perkin Elmer ERS spinning disk confocal system mounted on a Zeiss Axiovert 200M microscope. All images were taken using a 63X, 1.4 NA oil objective. An immersion oil with a refractive index of 1.518 (ImmersolT 518 F, Carl Zeiss Ltd, UK) was used to minimize spherical aberration. A charged-coupled device (CCD) camera (Orca ER, Hamamatsu Photonics, 15-bit), with a gain of 200 V, was used. Full frame images (672x512 pixels) were collected with 2x2 binning (to increase the fluorescent signal without increasing the laser power or exposure time). The system was equipped with solid-state 405 nm laser, a 488 nm lasers Argon gas laser and a diode pumped solid-state 561 nm laser. All red/green images were taken in the UltraVIEW ERS 'emission discrimination' mode with these filter specifications: green emission filter: 527/55 nm band pass centre filter and blue/red emission filter: 445/60 nm band pass centre. 0.5 μm thick confocal *z*-sections were set for all images, but *z*-stack sizes depended on the experiment. In certain experiments, manual *z*-plane adjustments were done during time series acquisition as the centrosomes and centrioles move in *z* during the cell cycle. Manual re-adjustment allowed for a minimum number of *z*-slices, while still capturing all the centrosomes over the cell cycle duration. The exposure times and the

laser power settings were determined for each fluorescent fusion-protein individually. Images were analysed using Volocity (Perkin Elmer, USA).

2.5.2.1.2. UltraView Spinning Disc microscope

Dechorinated live, mRNA-injected embryos were imaged at room temperature on an Ultra-VIEW VoX Perkin Elmer spinning disc confocal microscope, mounted on a IX81 Olympus system using a 60x 1.4 NA oil objective. An immersion oil of 1.514 refractive index was used to reduce spherical aberration. The microscope was coupled to a C9100-13 electron-multiplying charged-coupled device (EMCCD) camera (Hamamatsu Photonics). The images were taken with 16-bit depth and with 1x1 binning. Due to its electron-multiplier, this camera is designed for ultra-low light imaging (i.e. dim fluorophores). Hence, I used this microscope for the imaging of mRNA injected Asl-mKate2. Argon 488 nm laser with a gain of 1 and the sensitivity set to 199 used with a band pass centre emission filter of 527/55 nm. The a solid state 561 nm laser was used with a camera gain of 1 and the sensitivity set to 190 combined with a band pass centre emission filter of 445/60 nm and 615/70 nm. GFP was image 50 msec at 100% laser power, and mKate2 was images at 500 msec at 49.9% laser power. The images were comprised of 15 *z*-slices with a 0.4 µm step size. Images were analysed using Volocity (Perkin Elmer, USA).

2.5.2.2. LSM 880 with Airyscan microscope

Live images were acquired using an inverted Axio Observer.Z1 Zeiss 880 Laser Scanning Microscope fitted with an Airyscan detector. The microscope was equipped with a Plan-Apochromat 63x/1.4 NA oil objective and immersion oil of refractive index of 1.518 (ImmersolT 518 F, Carl Zeiss Ltd, UK) was used. The microscope was additionally equipped with an Airyscan module containing a 32-channel GaAsP detector. The images were taken at 16-bit depth. The laser excitation lines used were

405 nm diode, 488 nm argon and 561 nm diode laser. All experiments were set up using the 'Smart Setup' function, which allows for an optimal imaging with respect to dichroic mirror and emission discrimination, depending on the fluorophores used. The emission discrimination settings used, where the band pass filter 495-550 nm and the long pass filters 570 for the Airyscan mode. In certain experiments, manual *z*-plane adjustments were made during a time series as the centrosomes moved up and down, in order to keep the number of *z* slices to a minimum. The exposure times, gain, zoom and the laser power settings were determined specifically for each fluorescent fusion-protein. All *z*-stacks were taken using the Piezo. The Zeiss software ZEN Black used to acquire and process Airyscan images.

2.5.2.3. OMX V3 Blaze 3D-Structured Illumination Microscope

The live images were taken at room temperature on a DeltaVision OMX V3 Blaze microscope (Applied Precision, GE Healthcare) equipped with a 60X, 1.42 NA oil objective (Olympus). A 1.514 immersion oil was used for refractive index matching to reduce spherical aberration (Demmerle et al., 2017). The microscope is fitted with four different PCO Edge 4.2 sCMOS cameras (PCO AG) for detecting different colour channels. Images were taken at 15-bit depth that resulted in a 32-bit float when SIM images were reconstructed. For excitation 488 nm diode laser and 593 nm fibre lasers were used. For 488 nm excitation, a 525/50 or 540/80 nm band pass emission filter was used (i.e. GFP and mNeonGreen). For 593 nm excitation, a 615/24 nm band pass emission filter (i.e. mCherry and 594 nm dyes) and a 642/80 nm band pass emission filter (i.e. mKate2) were used. At least 6 *z*-planes with a 0.125 µm steps size were acquired. For each plane 5 phases and 3 angles were acquired. The exposure times and laser power setting were determined individually for each fusion-protein. Images were processed with SoftWorx 6.1 software (GE Healthcare) using channel

and filter specific measured Optical Transfer Functions. For dual colour imaging, the images were aligned using 1 µm to 0.2 µm diameter TetraSpeck Microspheres (ThermoFisher) using the OMX Editor software. The images were processed further in Fiji ImageJ and their quality assessed using the SIM-Check ImageJ plugin (Ball et al., 2015) to ensure the absence of reconstruction artefacts

2.5.3. Photoconversion of fluorophores in live embryos

To assess the brightness and stability of photoconverting fluorophores, such as Maple3-Cnn and Dendra2-Cnn, I performed a variety of evaluations on different microscopes. For the quantification, data collected from the LMS 880 with Airyscan.

2.5.3.1. Photoconversion on the Perkin Elmer Spinning Disk microscope

Live Maple3-Cnn heterozygous embryos were imaged on the Perkin Elmer microscope using the same microscope settings described (2.5.2.1.1) The green and red fluorescent signals were sequentially recorded using emission discrimination filters. An region of interest (ROI) was drawn around separate centrosomes, and the Fluorescence Recovery After Photobleaching (FRAP) function used: the regions were excited with 405 nm laser, at 10% laser power with 8 iterations lasting 1 msec each. Images were acquired for every 30 msec for 37 time points, with 7 *z* slices at 0.5 µm *z*-distance.

2.5.3.2. Photoconversion on the LSM 880 with Airyscan microscope

Live Maple3-Cnn and Dendra2-Cnn heterozygous embryos were imaged on the Zeiss 880 Airyscan microscope using the same microscope settings described (2.5.2.2). Green and red fluorescent signal were recorded sequentially with emission discrimination filters. 50 time points were taken and 6 *z* slices with a *z*-distance of 0.173µm were used for quantification, in which 1 pixel was equal to 14.67 nm. The *z*-

and the *xy*-positions were manually adjusted to keep the centrosomes of interest within the field of view. For the representative image, 10 time points without a *z*-stack were taken, in which 1 pixel was equal to 23.47 nm. A ROI was drawn around separate centrosomes, and the FRAP function used exciting with 405 nm laser, at 1.5% laser power for 10 iterations. All images were processed with the Airyscan algorithm in ZEN (black edition, Zeiss).

2.5.3.3. Photoconversion on the OMX V3

Live mMaple3-Cnn heterozygous embryos were imaged on the OMX V3 Blaze microscope using the same microscope set-up used as described above (2.5.2.3). The experiments were preformed using widefield (WF) microscopy, as the SIM mode was not compatible with the mMaple3 fluorophore and the photostability of the green and red state were too low to allow for super-resolution imaging. As the system does not have a 561 nm laser ideal for the red mMaple3, 3D-SIM was not possible. The images taken in WF mode were imaged sequentially: an image was first taken of the green mMaple3, before exciting a selected ROI with 405 nm, and then imaging both red and green for 10 frames without a *z*-stack.

2.5.4. Fluorophore brightness and stability assessment on the OMX V3 Blaze

Live *Drosophila* embryos, expressing either GFP, mNeonGreen, mKate2 or mCherry, were imaged using the OMX V3 Blaze in WF mode, using the same hardware as previously described (2.5.2.3). Additional, illustrative images were taken using SIM mode, but these were not quantified due to the degree of photobleaching and the uncertainty that processing of signal is actually linear.

For the comparison of GFP and mNeonGreen, heterozygous fly embryos containing one mutant allele were excited at 488 nm for 5 msec, a *z*-stack of 8 slices at 0.4 μm was taken and signal was detected using the 525/50 nm band pass emission filter. Fluorophore brightness was assessed by imaging 10-11 different embryos with varying laser powers, specifically 100%, 50%, 31.3%, 10% and 1%. For analysis of fluorophore brightness with different excitation laser powers, from a *z*-projection the 5 brightest centrosomes were selected from each of the 10-11 embryos. To assess fluorophore stability, 9 embryos were imaged at 100% laser power for 150 frames; the 5 brightest centrosomes (identified in the first frame) were taken per embryo from a *z*-projection and their intensity measured over time.

For the comparison of mCherry and mKate2, homozygous flies in a full asl^{B46} mutant background were excited at 593 nm for 100 msec, with or without sequential exposure to 100 msec of 100% 488 nm laser. *Z*-stack of 10 slices using a 615/24 nm band pass emission filter for mCherry and 642/80 nm band pass emission filter for mKate2. These filter setting match the emission spectra of each fluorophore. The brightness was assessed by imaging 7-9 different embryos with different laser powers, specifically 100%, 50%, 31.3%, 10% and 1% and analysed a described above. Here 7 embryos were images for 500 frames with either 100% 593 nm laser power or sequential exposure at 100% 593 nm and 100% 488 nm laser power. The latter was used to assess the stability of mKate2 and mCherry during 2-colour red/green imaging. For the stability assessment, the 5 brightest centrosomes from each embryo were taken from a *z*-projection and their intensity measured over time.

2.5.5. Imaging of fixed and stained *Drosophila* samples

2.5.5.1. Imaging of fixed eggs on the Perkin Elmer ERS Spinning Disc

Previously fixed and stained eggs were imaged with the Perkin Elmer ERS spinning disc system as described above (2.5.2.1.1). The samples were image with 561 nm and 488 nm laser at a power of ~400 mW at the objective (measured with a Optical Power Meter, Thorlabs Inc.) for 7 msec. Around 30 eggs were imaged for each genotype. No *z*-stacks were taken.

2.5.5.2. Imaging fixed samples on the OMX V3 Blaze with 3D-SIM

Embryos and eggs fixed as previously described (2.4.1) and imaged with the OMX V3 Blaze system using the same hardware as previously described (2.5.2.3). The images were exposed to 488 nm laser for staining with anti-GFP antibody (Chromotek GmBH) and 593 nm laser for staining with Alexa594 (Invitrogen or Abcam). Images were acquired with variable laser power and exposure times depending on the brightness of the staining. The *z*-stack height was determined by the size of the object of interest. For the comparison of the centriole/centrosome proteins location between centrosomes and SAP, the *z*-stack was 9 slices at a *z*-distance of 0.125µm. All images were aligned using 1 µm to 0.2 µm TetraSpeck Microspheres (ThermoFisher) using the OMX Editor software. The images were processed further in Fiji ImageJ and their quality assessed using the SIM-Check ImageJ plugin (Ball et al., 2015) to ensure there was no reconstruction artefacts.

2.5.5.3. Imaging of fixed and stained samples on the OMX V2 with 3D-SIM/SMLM

3D-SIM and SMLM was performed on a DeltaVision OMX V2 microscope (Applied Precision/GE Healthcare) that has been modified with an additional light path to

increase the laser power density for SMLM, specifically direct Stochastic Optical Reconstruction Microscopy (STORM). A 100x/1.4 NA oil objective (UPlanSApo, Olympus) with 1.514 immersion oil was used and a 488 nm diode laser and 592 nm fiber laser were used for imaging. The microscope is coupled to EMCCD cameras (Evolve 512 Delta C, Photometrics), one for each channel, that were run at 10 MHz. Different emission filters were used: for 592 nm excitation, a 629/53 nm band pass emission filter, and for 488 nm excitation a 525/50 nm band pass emission filter was used. For the 3D-SIM imaging, the exposure time was set to 50 msec with an electron-multiplier gain 50. The 592 nm laser had between 20 to 200 W/cm^2 intensity at the objective. A *z*-stack of 1 μm at 0.125 μm step size was acquired (each *z*-slice consisting of 3 angles and 5 phases). Images were taken with a CCD chip size 256x256. The images were reconstructed using SoftWorx 6.1 software (Applied Precision) and quality assessed using SIMCheck (Ball et al., 2015). For the SMLM imaging, the exposure time was also set to 50 msec with an electron multiplier gain of 200. Between 2000 or 4000 frames were acquired. The 488 nm laser has an approximate intensity of 25 kW/cm^2 at the objective. Images were taken with a CCD chip size 128x128 as the laser is focused down on to an area smaller than size of a 256x256 chip. To determination of the individual positions of single fluorescent molecules, fastSPDM (Grull et al., 2011) was used that had been calibrated to the microscope camera gain.

The same area of the sample was first images in SIM mode, and subsequently in SMLM mode. Images were aligned and analysed as described in Chapter 4.

2.5.6. Image processing and presentation

All images taken on the Perkin Elmer Spinning Disc or the UltraView Spinning Disc were processed using Volocity 6.1.1 and Adobe Photoshop CS6 software version 13.0.6. These images were adjusted for contrast and brightness in each channel. These adjustments were purely visual and do not change the underlying voxel fluorescence intensity values (this information is stored unaltered in the image file). Images were exported as TIFFs and further changes to contrast and brightness were done in Adobe Photoshop.

All images taken on the OMX V3 Blaze, OMX V2 and the Zeiss 880 Airyscan system were handled in Fiji ImageJ. Contrast and brightness adjustments for each channel were preformed if required, however these changes were only for visual purposes. Images used for quantification were not altered.

Graphs were generated using Prism 6.0 for Mac OSX, GraphPad Software, Inc.

2.5.6.1. Using fastSPDM for SMLM image generation

The fastSPDM program (Grull et al., 2011) was used to visualize the SMLM data, this visualization allowed me to identify the same centriole the SIM and SMLM data and thus preform the image alignment. In summary: the fastSPDM software detects the signal of the localisation from the raw localisation data, removes the background around the spot to suppress noise and improve the accuracy of the fit, and then calculates the centre position using a Gaussian distribution. This allows the generation of an image based on the fitted localisation probability of each fluorophore. The fastSPDM is calibrated to the cameras on the OMX V2.

2.5.6.2. Radial profile analysis

For assessing the average radial distribution of PCM and centriole proteins around centrioles or SAPs, I used ImageJ (Conduit et al., 2014b). All the fixed and stained embryos and eggs, the reconstructed SIM images were assessed visually for good staining. For each protein of interest, 10 centrioles or SAPs were analysed.

For each centriole or SAP, the centre of mass was calculated by thresholding the image and running the 'analysis particle' function in ImageJ on the *z*-slice selected. The radial profile analysis was preformed by: centring concentric rings around the centre of mass spanning 1.64 μm for all centriole and centriole wall proteins, and spanning 3.28 μm for all PCM proteins, and then averaging the fluorescence in each ring. The average background intensity of the cytosol was subtracted from each centriole, SAP and protein of interest data set. As negative intensity values occur in 3D-SIM reconstructions, all data values for the centrioles, SAPs and the protein of interest were scaled so that lowest intensity was zero. For all the SAP conditions, the peak intensity value of the SAP signal was defined at distance zero (for the centriole conditions this was the centre of mass). Each individual profile was then normalized to the average peak intensity for all the centrioles or SAPs in that condition. The radii for each condition were then averaged together and the graphs plotted in using Prism 6.0 for Mac OSX, GraphPad Software, Inc.

2.5.6.3. Tracking Ana2-GFP centrioles with TrackMate

The dynamics of Ana2-GFP, Ana2-2E-Cdk-GFP, Ana2-2A-Cdk-GFP in full Ana2 mutant backgrounds was analysed through out cell cycle 12 using ImageJ as described previously (Aydogan et al., 2018). In summary: *z*-projection of the *z*-stack images were calculated and the background removed using the 'subtract background'

functions with a rolling ball radius of 1.9 pixels. Bleach corrections were applied using the exponential fit. Subsequently, the centrioles were tracked using the ImageJ plugin in TrackMate (Tinevez et al., 2017) using the following parameters: track spot size diameter of 0.9µm and initial threshold of zero. The quality was adjusted for each embryo individually and it was set so that only centrioles would be selected and tracked. Only continuous tracks that were present through out the whole time-lapse were used in the final analysis. The resulting data was plotted using Prism 6.0 for Mac OSX, GraphPad Software, Inc. to display the intensity over time.

2.5.6.4. Statistics

For statistical analysis of extracted features, Prims 6.0 was used to check for Gaussian distribution of the data and to assess statistical significance T-tests and ordinary One-Way ANOVA test were used. Significance was defined as $P < 0.05$.

3. Evaluation of fluorophores for centriole and centrosome research in the early *Drosophila* embryo

3.1. Introduction

After the first reported observation of fluorescence in 1845 (Herschel, 1845), the interest in coupling cell biology and microscopy with fluorescence was sparked. As Helmholtz postulated in 1874, microscopy images could be better contrasted, structures better differentiated and more discernable, if the specimen of interest emitted light (Helmholtz, 1874). Over the following decades, more fluorescent labelling dyes and chemicals begun to emerge, allowing for more cellular structures to be observed (Renz, 2013). In early 1940, the technology for fluorescently labelling antibodies was developed (Coons et al., 1942), leading to a dramatic expansion of cell biology knowledge. However, it was the discovery (Shimomura et al., 1962), cloning (Chalfie et al., 1994) and modification (Helm et al., 1995) of the intrinsically green fluorescent protein (GFP), that revolutionized the field of cell biology and light microscopy, as it permitted the genetic tagging of any protein with a fluorescent emitter to be followed in living cells.

GFP, originally isolated from the jellyfish *Aequorea victoria* (Shimomura et al., 1962), is a protein that is ~27kDa in size (Day and Davidson, 2009). Its crystal structure was solved in 1996 (Ormo et al., 1996) showing that the protein consists of an 11-stranded, antiparallel β-barrel encasing a single central α-helix. The chromophore itself is buried in the centre of the β-barrel and consists of three key residues: Ser^{65}, Gly^{67} and Try^{66}. The location of the chromophore in the β-barrel protects it from the surrounding environment. The tight β-barrel structure is thought to provide stability, proteolysis-resistance, resistance to moderate pH changes and to

allow for a high quantum yield (Ormo et al., 1996). A surprising feature of GFP is the ability of its chromophore to form spontaneously without the need of cofactors or additional proteins – only molecular oxygen is required (Day and Davidson, 2009). GFP appears to be minimally disruptive when fused to most proteins, can fold and fluoresce well at biological temperatures, matures quickly, is chemically inert and can fluoresce in many subcellular environments, making it an invaluable tool (Crivat and Taraska, 2012). It allows researchers to study the dynamics, localisation and function of a specific protein *in vivo* in real time in specific tissues, cells or subcellular compartments. The fluorescent protein revolution has allowed researchers to begin to unravel the complexities and regulatory mechanisms governing living cells.

Since the discovery of GFP, a plethora of related fluorescent proteins have been generated via guided or random mutagenesis of the original GFP gene, or by the discovery of novel fluorescent proteins themselves having been re-engineered by mutation (see, for example, Baird et al. (2000); Ormo et al. (1996); Shaner et al. (2004)). Many of the photophysical and photochemical properties of fluorescent proteins are influenced by the residues that surround the chromophore (Shu et al., 2006). Spontaneous and directed mutagenesis studies have led to an ever-growing list of fluorescent proteins with unique properties and features. This includes different excitation and emission wavelength, different quantum yields and brightness, varying numbers of quaternary structures (monomers, dimers or tetramer), resistance to low pH, emission of light under certain chemical environments, ability to photo-switch/activate (capability to turn on/off emission), ability to photoconvert (capacity to change the emission wavelength upon stimulation), different maturations times (fast folding versions mature, and thus fluoresce, quickly after translation) and

varying Stokes-shifts (the difference between the excitation and emission wavelengths) (Cranfill et al., 2016; Day and Davidson, 2009; Dempsey et al., 2011; Enrique Balleza et al., 2017; Hepperta et al., 2016; Shinoda et al., 2018). Even today, new fluorescent proteins are continually being generated allowing for new techniques to arise. Using fluorescent proteins, it is now possible to assess protein localisation in nanometre resolution (i.e. using SMLM), assess protein-protein associations (i.e. fluorescence resonance energy transfer), observe protein movement on a molecular scale (i.e. using FRAP and fluorescence correlation spectroscopy), identify the viscosity of a cellular environment (i.e. fluorescence lifetime microscopy) and used as biosensors that monitor cell signalling pathways (Crivat and Taraska, 2012).

However, fluorescent proteins have limitations. Their photophysical properties are outperformed by organic dyes, which are more photostable, brighter, have more colours to choose from and a wider range of chemical properties (Crivat and Taraska, 2012). As a result, new fluorescent protein labelling techniques have been developed. Most notable is the development and use of self-labelling enzymes. These innately non-fluorescent proteins can be fused to a protein of interest and can then catalyse a reaction with an exogenously supplied fluorescent ligand to result in a covalent auto-attachment between protein and ligand (Lin and Wang, 2008). There are currently three main commercial self-labelling enzymes: the 20 kDa DNA human repair protein O^6-alkylguanine-DNA alkytransferase (Juillerat et al., 2003) (marketed as SNAP-tag), a variant of the SNAP-tag that reacts specifically with O^6-benzylcytosine substrates (Gautier et al., 2008) (marketed as CLIP-tag) and the 33 kDa bacterial enzyme haloalkane dehalogenase (Los and Wood, 2007) (marketed as HaloTag). Even though these self-labelling enzymes have been reported to fold well and label efficiently

(Crivat and Taraska, 2012; Kohl et al., 2014), there are some disadvantages. First, excess and unbound dye must be washed out thoroughly in order to prevent fluorescent background. Second, particularly with the SNAP- and CLIP-tags, native mammalian proteins present in the sample may cross-react with the ligands. Finally, the size of the tags, particularly the HaloTag, may be problematic – similar to the problems that can arise with fluorescent proteins like GFP (Crivat and Taraska, 2012). Nevertheless, the fluorescent self-labelling technology is likely to play a significant part in the future of fluorescence microscopy.

One challenge in the field of fluorescence microscopy is the identification of fluorescent probes suitable for super-resolution microscopy. For most super-resolution techniques, the energy load (the laser intensity) on the sample is significantly higher compared to confocal imaging (Schermelleh et al., 2010). Therefore, in general, fluorophores used must be bright, have a high quantum yield and a low rate of photo bleaching (i.e. a high photon budget) (Fernandez-Suarez and Ting, 2008; Schermelleh et al., 2010).

It is important to note that most of these fluorescent proteins and fluorescent labels have been developed for expression and function in mammalian cells. They may therefore not be suited for use in other model organisms having different temperature requirements and protein processing machinery - both factors that can affect fluorescence and protein maturation. For this chapter, I evaluated the utility of several relatively new fluorophores for centriole and centrosome research, specifically in the early *Drosophila* embryo, as this system has many advantages for these types of

studies (Aydogan et al., 2018; Feng et al., 2017; Lattao et al., 2017; Novak et al., 2016).

3.1.1. Key findings

I initially tested the fluorescent properties of several new fluorescent proteins using an mRNA injection approach. This led to the identification of several fluorescent protein-tags that allowed new insights into the centriole biology. The fluorescent proteins that proved most useful were: (1) mKate2 (Shcherbo et al., 2009), a fast folding red protein useful for mRNA injection studies and super-resolution imaging; (2) mNeonGreen (Shaner et al., 2013), a novel green protein that is significantly brighter than GFP, allowing for imaging of low abundance proteins in super-resolution microscopy. Additionally, I performed an initial screening of self-labelling enzymes demonstrating the potential utility of this labelling approach.

My work developing mKate2 for use in mRNA injections in the early *Drosophila* embryo was published: Novak, et al., *Developmental Cell*, 2016.

My work studying the localisation of Sak-mNeonGreen in the early *Drosophila* embryo is submitted: Aydogan et al., *Nature, under review*.

3.2. Results

3.2.1. mRNA injection screening to identify potentially useful fluorescent proteins

The generation of transgenic flies is both costly and time consuming, particularly if one wishes to screen many potential proteins of interest. To circumvent this, an assay was developed in our laboratory in which *in vitro* transcribed mRNAs encoding a GFP-tagged version of a centriole/centrosome protein of interest is injected into early

fly embryos. These mRNAs are rapidly translated and within ~60 min the behaviour of the GFP-tagged protein can be detected in the living embryo on a spinning-disc confocal system (Conduit et al., 2014a) (**Figure 3.1**). This mRNA injection assay may be considered "medium throughput" as it allows the analysis of ~4-5 proteins a day.

However, this mRNA injection assay requires the fluorophore of interest to "mature" into a fluorescent form within ~60 min to allow the tagged protein to be observed during the syncytial stages of embryogenesis (the stage often most useful for centriole/centrosome studies). For a GFP-like protein to become fluorescent, for example, it must fold its β-barrel, complete torsional rearrangements, undergo cyclization, oxidation and dehydration of the chromophore (Craggs, 2009). Previous mRNA injection studies have successfully used GFP, but attempts to use mRFP or mCherry proved unsuccessful, presumably because these red proteins take too long to fold. Unfortunately, maturation time measurements for individual fluorescent proteins have often been performed under different conditions, and only recently has a study attempted to systematically characterize the maturation times of fluorescent proteins in living *E. coli* at 37 °C and 32 °C (Enrique Balleza et al., 2017). It is unclear how these maturation times translate to experiments performed in *Drosophila* (that are generally carried out at 25 °C). Thus, it is difficult to infer the potential utility of a protein from published data.

The ability to utilize a red fluorescent protein in this mRNA assay was key to my future experimental plans (see Chapter 6). Additionally, the identification of a green fluorescent protein brighter than GFP would be advantageous when studying proteins that are in low abundance such as Sak. I therefore systematically tested the

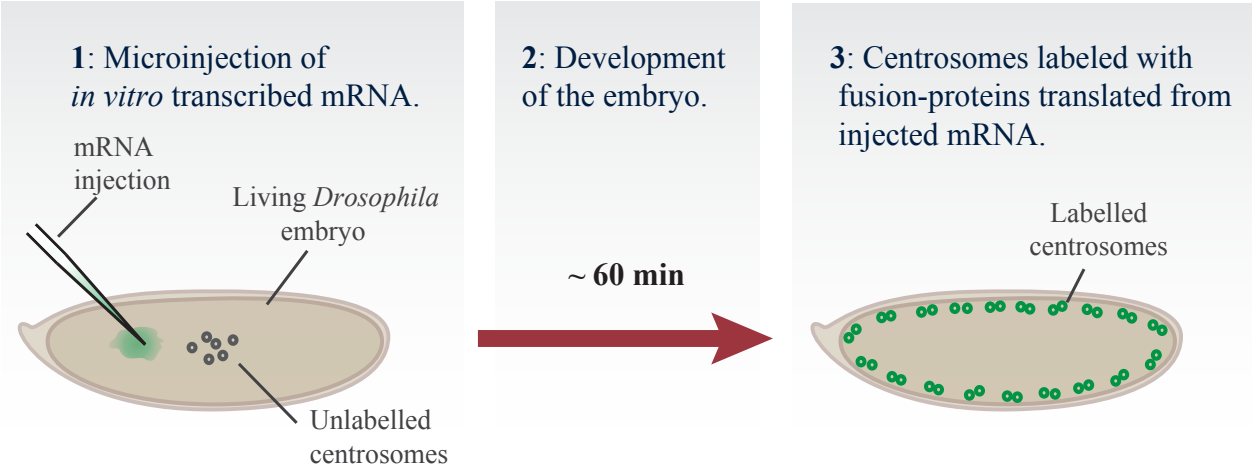


Figure 3.1: Schematic illustration of the mRNA injection procedure. The schematic illustrates how mRNA encoding a fluorescently tagged protein of interest is injected into a living early embryo. After 60 min some protein will have been translated, and hopefully will have matured into a fluorescent form, allowing to visualisation its localisation at centrosomes (as illustrated).

potential utility of several relatively new fluorescent proteins that had become available and the usefulness of the self-labelling enzyme technologies in the early *Drosophila* embryo (summarized in Table 6).

Table 6 Fluorescent proteins and self-labelling enzymes (and ligands) used in the mRNA injection screen

Fluorophore	*Excitation (nm)*	*Emission (nm)*	*Reported Brightness*	*Selection reason*	*Maturation time (min)*	*Ref*
GFP	488	507	33.54	Control	25	(Helm et al., 1995)
mNeonGreen	506	517	92.8	Brightest green FP available	10	(Shaner et al., 2013)
mKate2	588	633	25.0	Fast folding	20	(Shcherbo et al., 2009)
mRuby2	559	600	43.0	Brightest red FP available	150	(Lam et al., 2012)
mCardinal	604	659	16.53	Very photo stable	27	(Chu et al., 2014)
mKO2	551	565	39,56	Bright	108	(Sakaue-Sawano et al., 2008)
mTagRFP-T	555	584	33.21	Bright and stable	100	(Shaner et al., 2008)
Fluorophore	*Ligand used*	*Excitation (nm)*	*Emission (nm)*	*Selection Reason*		*Purchased from*
SNAP-tag	TMR-Star 647-SiR	554 645	580 661	Bright organic dyes, SiR increases fluorescence upon binding		New England BioLabs, Inc.
HaloTag	TMR Star	554	580	Bright organic dye		Promega Corp.

In these experiments, all fluorescent proteins and self-labelling enzymes were genetically fused to the N-terminus of the centrosomal protein Cnn. Vector construction and the *in vitro* mRNA transcription details are described 2.3.6-2.3.7. All embryos were imaged on the Perkin Elmer ERS Spinning Disc (2.5.2.1.1) or, in the case of mKate2 on the Perkin Elmer UltraView Spinning Disc (2.5.2.1.2).

I first compared the new green fluorophore mNeonGreen (Shaner et al., 2013) to GFP; mNeonGreen has ben characterised to be one of the brightest green fluorescent proteins to date (Rodriguez et al., 2016). I injected mRNAs encoding each protein into WT embryos expressing Asl-mCherry as a centrosomal marker (**Figure 3.2**). mNeonGreen was able to mature in the *Drosophila* embryo, making it a promising candidate for a brighter green fluorophore in fly embryos. Hence, seemed worthwhile to follow this up more quantitatively in transgenic lines (see Section 3.2.2.1).

Next, I tested the various red fluorophores, injecting mRNA encoding fusions to Cnn into WT embryos expressing Asl-GFP as a centrosomal marker. Of the 5 proteins I tested, only mKate2 and mCardinal were detectably fluorescent within the given time frame of my assay (**Figure 3.3**). Both proteins were qualitatively much dimmer than GFP or mNeonGreen, with mKate2 being brighter than mCardinal. I suspect that these red proteins were poorly fluorescent in this assay as they generally take longer to fold than green proteins (this is well documented *in vitro*, but has not been rigorously tested *in vivo*). Thus, I tried shorter collections of 15 min and a longer incubation time of 20-30 min for mKate2 injections, which greatly enhanced the fluorescent signal (data not shown). From these initial studies, I concluded that mKate2 could be used as a red fluorophore in the mRNA injection assay.

Next, I tested the various self-labelling enzymes, co-injecting mRNA encoding Cnn-fusions into embryos expressing Asl-mCherry (in an *asl* mutant background), with appropriate tagging dyes (Table 6). This strategy worked well for the SNAP-tag and HaloTag (**Figure 3.4A**).

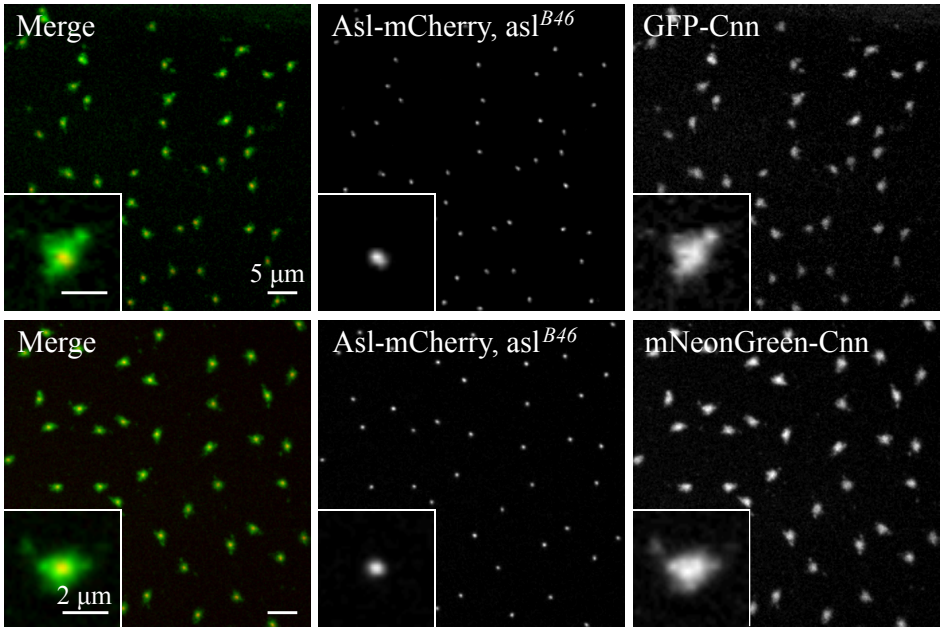


Figure 3.2: mNeonGreen seems brighter than GFP in the mRNA injection assay. mRNAs encoding either GFP-Cnn or mNeonGreen-Cnn were injected into wild type (WT) embryos expressing Asl-mCherry as a centrosomal marker. The samples were imaged on a spinning discs under 561 nm and 488 nm laser exictation. It is not clear from these single images, though, that mNeonGreen-Cnn reproducibly appeared to be brighter than GFP-Cnn. This was confirmed in various semi-quantitative assays but, because the mRNA injection assay is inevitably somewhat variable, I decided that mNeonGreen looked promising enough to generate transgenic lines allowing me to more accurately compare it to GFP in a more quantitative manner.

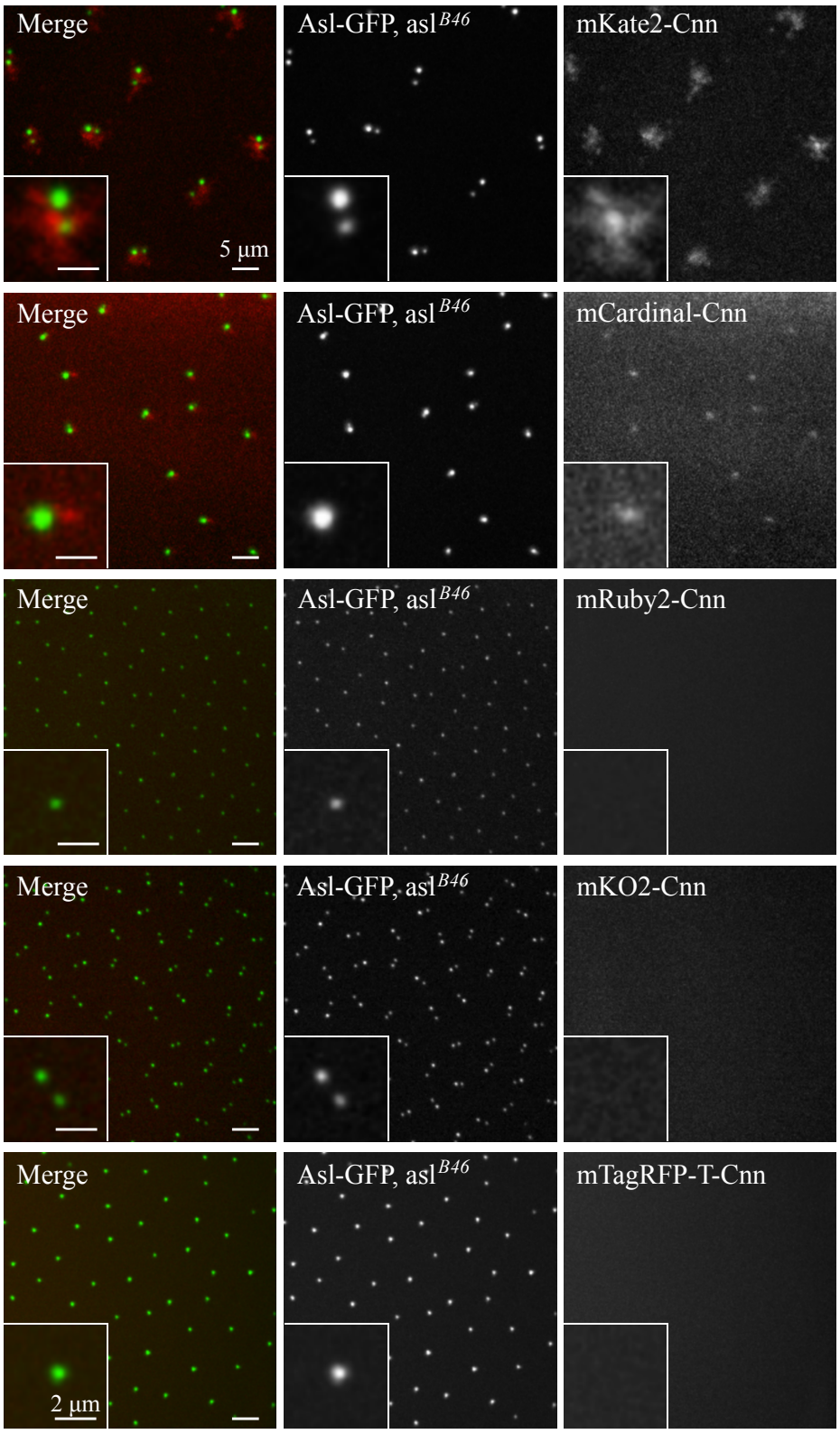


Figure 3.3: mKate2 and mCardinal can fluoresce in the mRNA injection assay. mRNA encoding Cnn-fusions to mKate2-, mCardinal-, mRuby2-, mKO2- and mTag-RFP-T were injected into the WT embryos expressing Asl-GFP as a centrosomal marker. The samples were imaged on a spinning discs under 488 nm 561 nm laser excitation. mKate2 and mCardinal are the only two red/orange fluorescent proteins that detectably fluoresce in the mRNA injection assay. mKate2 is significantly brighter than mCardinal. In order to further assess the properties of mKate2 and test its suitability for 3D-SIM, transgenic fly lines were generated.

However, the application of self-labelling enzymes and their fluorescent ligands in this assay was problematic: as the latter have to be co-injected with the mRNA and the excess, unbound ligand cannot be removed or washed out. This problem was particularly apparent in a pilot test to evaluate the potential use of these self-labelling enzymes on the OMX V3 3D-SIM system. Here, I injected SNAP-tag-Cnn mRNA and TMR-Star ligand into an Asl-GFP fly in a mutant asl^{B46} background. As can be seen (**Figure 3.4B**), the inability to remove the unbound fluorescent ligand leads to a poor signal-to-noise ratio resulting in the appearance of high frequency noise ('hammerstroke' artefact) making the background highly textured (**Figure 3.4B, right panel**) (Demmerle et al., 2017). This inability to remove the dye is due to the waxy layer that encompasses the vitelline membrane of the *Drosophila* embryo. This ~5 nm thick layer acts as a barrier to the entry of small molecules (Margaritis et al., 1980; Rand et al., 2010). Nevertheless, the dye-tagged Cnn molecules seem qualitatively brighter and more photostable than GFP-Cnn molecules imaged previously (Conduit et al., 2014b). I concluded that SNAP-tag and the HaloTag labelling is potentially promising if the amount of injected ligand is carefully optimised to avoid background problems.

3.2.2. Evaluation of new fluorophores using transgenic lines

Although the mRNA injection screen provided valuable insight into potentially useful fluorophores (and identified mKate2 as a red-fluorophore that could work in the mRNA injection assay), transgenic flies that stably express the fusion-protein are essential for a systematic comparison. The mRNA injection assay relies on manual injection of mRNA, therefore the volume injected may vary between embryos, which could have a direct effect on the amount of fluorescence measured. In flies that stably

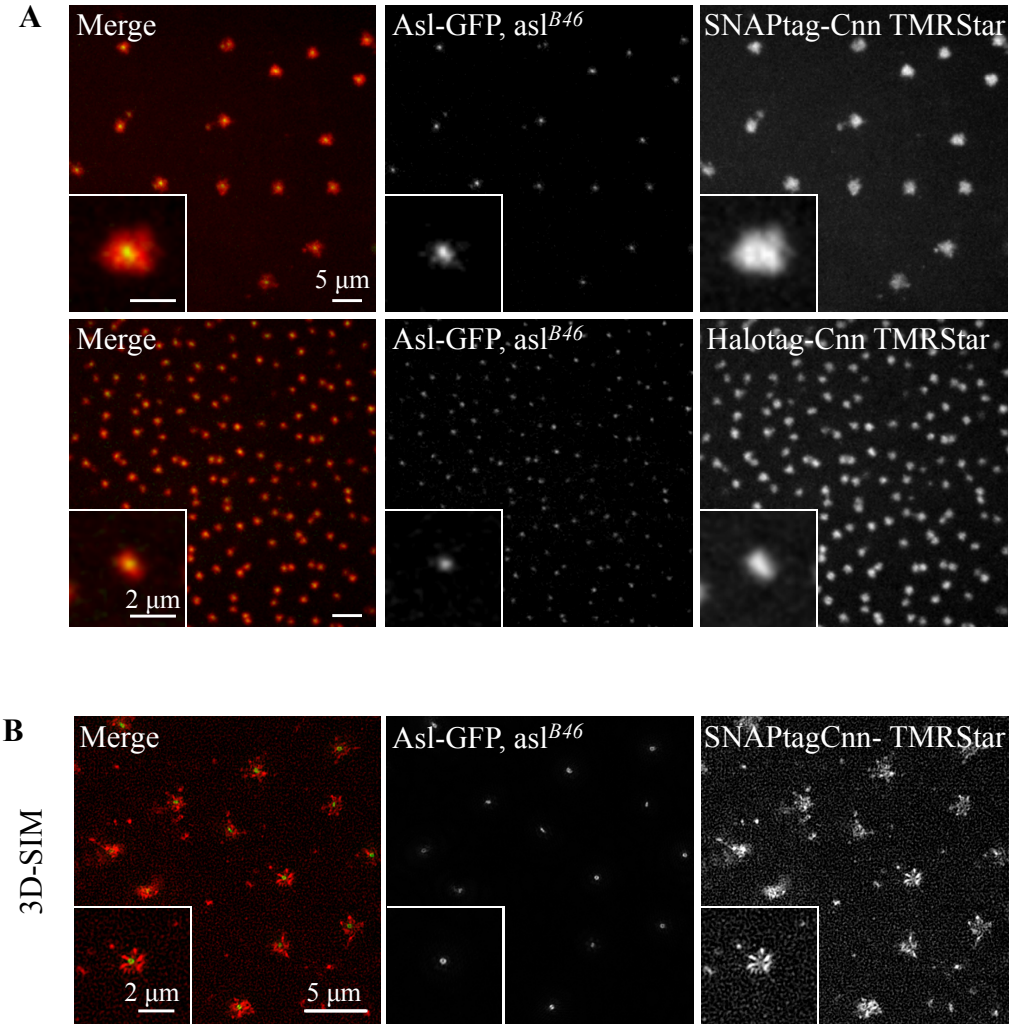


Figure 3.4: Self-labelling enzymes exhibit high levels of background. A) mRNA encoding SNAP-tag and Halo-tag were co-injected with TMR Star, into WT embryos expressing Asl-mCherry or Asl-GFP as a centrosomal marker. The samples were imaged on a spinning discs under 488 nm and 561 nm laser excitation. Fluorescence can be seen in the SNAP-tag and Halo-tag injections. Both the SNAP-tag and Halo-tag injections have relatively high background levels due to the presence of unbound dye. **B**) A *z*-projected 3D-SIM image taken from embryos expressing Asl-GFP injected with SNAP-tag-Cnn mRNA and TMRStar dye under 488 nm and 593 nm excitation. The inability to remove the unbound TMR-Star dye leads to a poor signal to noise ratio (high frequency noise clearly visible, right panel). Transgenic SNAP-tag flies were generated in order to test protocols and methods to reduce the amount of background.

express the genetic construct, it is possible to accurately compare expression levels. Similar expression level can be ensured by assessing different transgenic lines and selecting those with comparable expression. Therefore, based on the result of the mRNA injection screen the following transgenic *Drosophila* lines were generated using random *P*-element insertion (Table 7) (2.1.2-2.1.3).

Table 7 List of transgenic flies generated for further fluorophore evaluation

Line Name	*Final Vector Description*	*Promoter*
LG01	eAsl-mKate2	Endogenous
LG02	eAsl-mRuby2	Endogenous
LG03	eSak-mNeonGreen	Endogenous
LG04	Ubq-mMaple3-Cnn	Ubiquitin
LG05	Ubq-SNAP-tag-Cnn	Ubiquitin
LG06	Ubq-mNeonGreen-Cnn	Ubiquitin

Although mRuby2 did not fluoresce in the mRNA injection screen, it is still, according to the literature, one of the brightest red fluorescent proteins (Table 6). I assumed that in transgenic flies it might be possible that mRuby2 has enough time to mature – similar to the way in which mCherry and mRFP are fluorescent in transgenic embryos, but not in the mRNA injection assay. Additionally, I generated flies with Cnn tagged to the photoconvertible fluorescent protein mMaple3 (Wang et al., 2014); mMaple3 is one of the best and brightest photoconvertible fluorescent proteins – it photoconverts from green (max emission 506 nm) to red (max emission 583 nm) (Wang et al., 2014) and has been shown to function well in *C. elegans* (Dr. G. Ou, personal communication). As the maturation time of mMaple3 was reported to be 49 min, I decided not to perform the mRNA injection assay with it. My results for mMaple3 and a brief discussion of their implications can be found in Appendix 1.1.

3.2.2.1. Evaluation of green fluorescent protein mNeonGreen

The fluorescent protein mNeonGreen, originally found in *Branchiostoma lanceolatum*, has been described as the brightest yellow-green fluorescent protein available to date (Shaner et al., 2013). This fluorescent protein has a high quantum yield (~0.80) (Shaner et al., 2013); for comparison, the quantum yield of GFP is 0.60. According to the original publication, mNeonGreen is 1.5-3x brighter than GFP (Shaner et al., 2013); my mRNA injection screen confirmed that this was likely to be true for mNeonGreen in *Drosophila* embryos.

In order to assay the differences between GFP and mNeonGreen, I compared the fluorescence in transgenic flies containing one copy of the transgene that was recombined with a mutant allele of Cnn (Cnn^f) (Lucas and Raff, 2007) in an otherwise WT background (FP denotes the fluorescent protein).

$$w; \frac{+}{+}; \frac{\text{FP-Cnn, } Cnn^f}{+}$$

To test whether these transgenic flies expressed similar levels of tagged Cnn, I performed a western blot (**Figure 3.5A**). The expression levels were similar, although not identical, suggesting that any differences in my subsequent comparison are most likely due to intrinsic properties of the fluorophore and not due to the amount of fluorescent protein present.

One of my key aims was to assess if mNeonGreen would outperform GFP on the OMX V3 Blaze 3D-SIM system (2.5.2.3) as many of the Raff laboratory's live-cell super-resolution studies are performed on this system due to its high spatial and

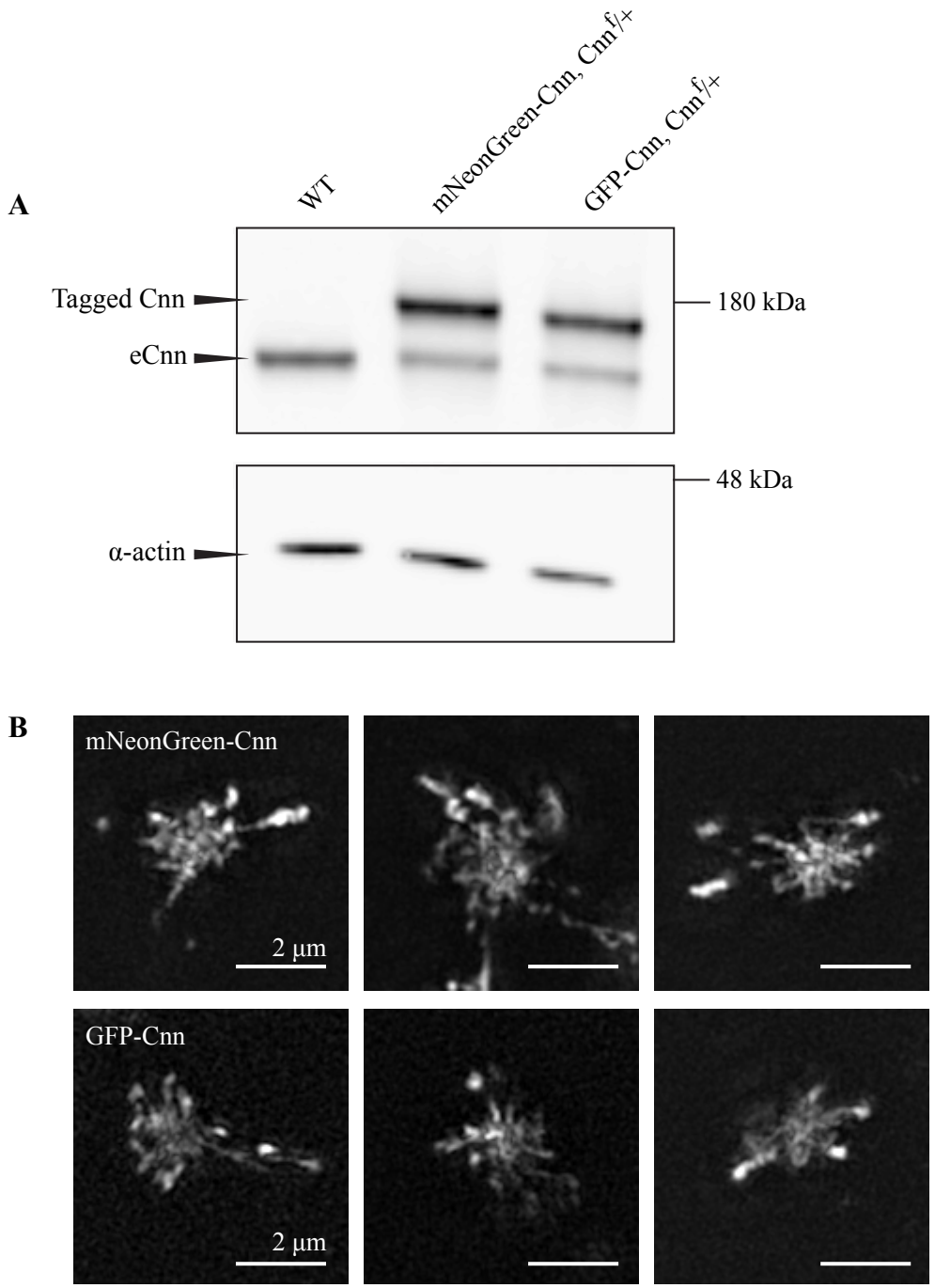


Figure 3.5: mNeonGreen-Cnn performs well in our OMX V3 3D-SIM system.
A) A western blot shows the expression levels of the fusion proteins mNeonGreen-Cnn and GFP-Cnn in transgenic flies; each lane contains 5 early embryos. These early *Drosophila* embryos express one copy of the transgene in the presence of one copy of the endogenous WT gene. The expression levels of the fusion proteins appear to be comparable between the two transgenic flies, when compared to the actin loading control. Endogenous Cnn (eCnn), tagged Cnn and α-actin (loading control) are indicated by the arrowheads. **B**) Images show *z*-projected 3D-SIM reconstructions from embryos expressing mNeonGreen-Cnn, $Cnn^{f}/+$ (top row) and GFP-Cnn, $Cnn^{f}/+$ (bottom row) under 100% 488 nm excitation (5 msec/frame). The 3D-SIM images were not quantified, but serve as a representative image.

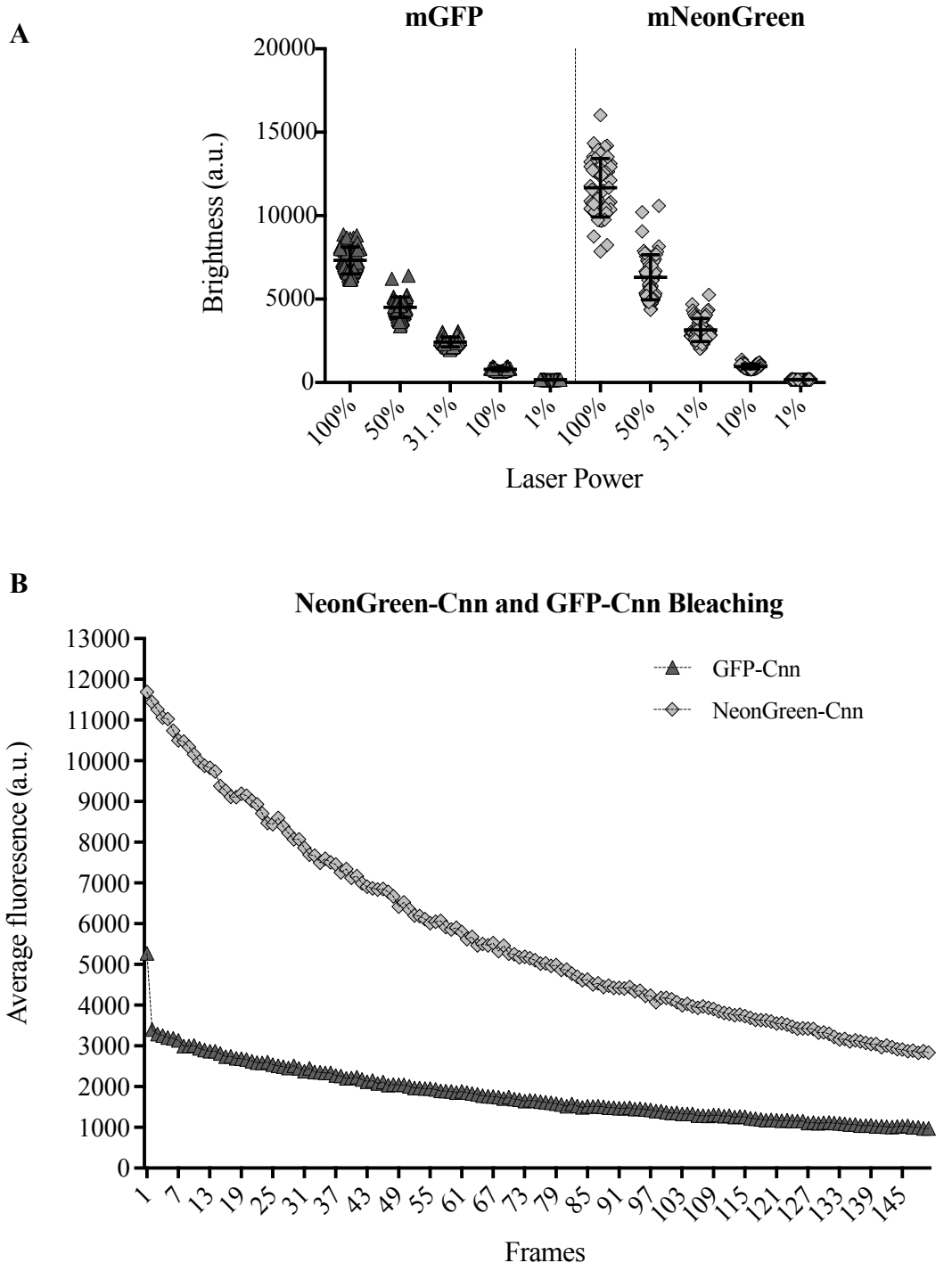


Figure 3.6: Brightness and stability quantification of mNeonGreen and GFP. A) Graph displays the signal intensity – brightness – at different 488 nm laser powers (100%, 50%, 31.3% 10% and 1% with 5 msec exposure) in embryos expressing GFP or mNeonGreen in WF mode on the OMX V3 system. The brightest 5 centrosomes in each of the 10-11 embryos were measured (50-55 centrosomes in total) for each laser intensity tested. mNeonGreen is ~1.6x brighter than GFP at 100% laser power. **B**) A graph charts the photo-stability of mNeonGreen and GFP measured over 150 continuous frames (5 msec/frame) at 100% laser power. The brightest 5 centrosomes in each of 8-9 embryos were measured (40-45 centrosomes in total). mNeonGreen remains brighter than GFP over 150 frames of continuous imaging.

temporal resolution. Illustrative images of mNeonGreen- and GFP-Cnn were taken using the 3D-SIM mode (**Figure 3.5B**) showing that both fluorescent proteins allow for reliable and high-quality 3D-SIM imaging. The 3D-SIM images were not quantified due to uncertainty about the processing of the signal being linear (Dr. A. Wainman, personal communication). Instead, I quantified the brightness and stability of mNeonGreen and GFP on this system using WF mode (see 2.5.4). To assess the brightness of the fluorescent proteins, embryos were exposed to different levels of laser power (**Figure 3.6A**). At 100% laser power, mNeonGreen is 1.59x brighter than GFP, but is less photostable when compared over 150 frames of imaging (**Figure 3.6.B**); it appears that mNeonGreen is initially more stable than GFP, but GFP seems more stable in later frames. These findings are consistent with previously published comparisons (Shaner et al., 2013).

I concluded that mNeonGreen might be useful for the study of low abundance proteins as it is generally brighter and it remains brighter than GFP during continuous imaging over 150 frames. Taken together, my data suggests that mNeonGreen would lend itself to long time-lapse or the study of low abundance proteins with 3D-SIM due to its brightness and bleaching characteristics. I show below that this improvement over GFP was crucial for the analysis of the subcellular localisation of Sak (3.2.3).

3.2.2.2. Evaluation of red fluorophores mRuby2 and mKate2

The fluorescent protein mRuby2 (Lam et al., 2012) is derived from mRuby, which was originally discovered in the anemone *Entacmaea quadricolor* (Kredel et al., 2009). mRuby2 is reported to be one of the brightest red fluorescent proteins with a reported brightness of 43 – calculated from the quantum yield and the extinction coefficient and with a quantum yield of 0.38 (Lam et al., 2012). As noted above in

Table 6, mRuby2 has a long maturation time of 150 min, probably explaining why it failed to work in the mRNA injection assay.

I generated transgenic flies that expressed Asl-mRuby2 under the control of the endogenous *asl* promoter and recombined 3 different lines with the asl^{B46} mutant allele (Novak et al., 2014); for comparison, I used an Asl-mCherry, asl^{B46} recombinant line:

$$w;\ \frac{+}{+};\ \frac{\text{Asl-FP}, asl^{B46}}{\text{TM6C}}$$

A western blot to examine protein expression levels revealed the presence of an Asl-mRuby2 fusion-protein of the expected size expressed at similar levels to the Asl-mCherry fusion-protein (**Figure 3.7A**). However, I was not able to detect any fluorescence in early embryos (data not shown). I therefore examined the testes of 3rd instar larvae in these lines and detected Asl-mRuby2 at the large, V-shaped centrioles present in these cells (Stevens et al., 2010b; Varmark et al., 2007) (**Figure 3.7B**). I concluded that the long maturation time of mRuby2, possibly compounded by the lower ambient temperature of studies in *Drosophila* (typically at 25 °C rather than the 37 °C used pervious studies), makes mRuby2 unsuitable for imaging in the early *Drosophila* syncytial embryo.

mKate2 is an engineered variant of mKate, also derived from the anemone *Entacmaea quadricolor* (Shcherbo et al., 2007). mKate2, although not as bright as mRuby2, is still brighter than mCherry by 1.57x according to the original publication (Shcherbo et al., 2009). I generated transgenic flies that expressed Asl-mKate2 under the control of

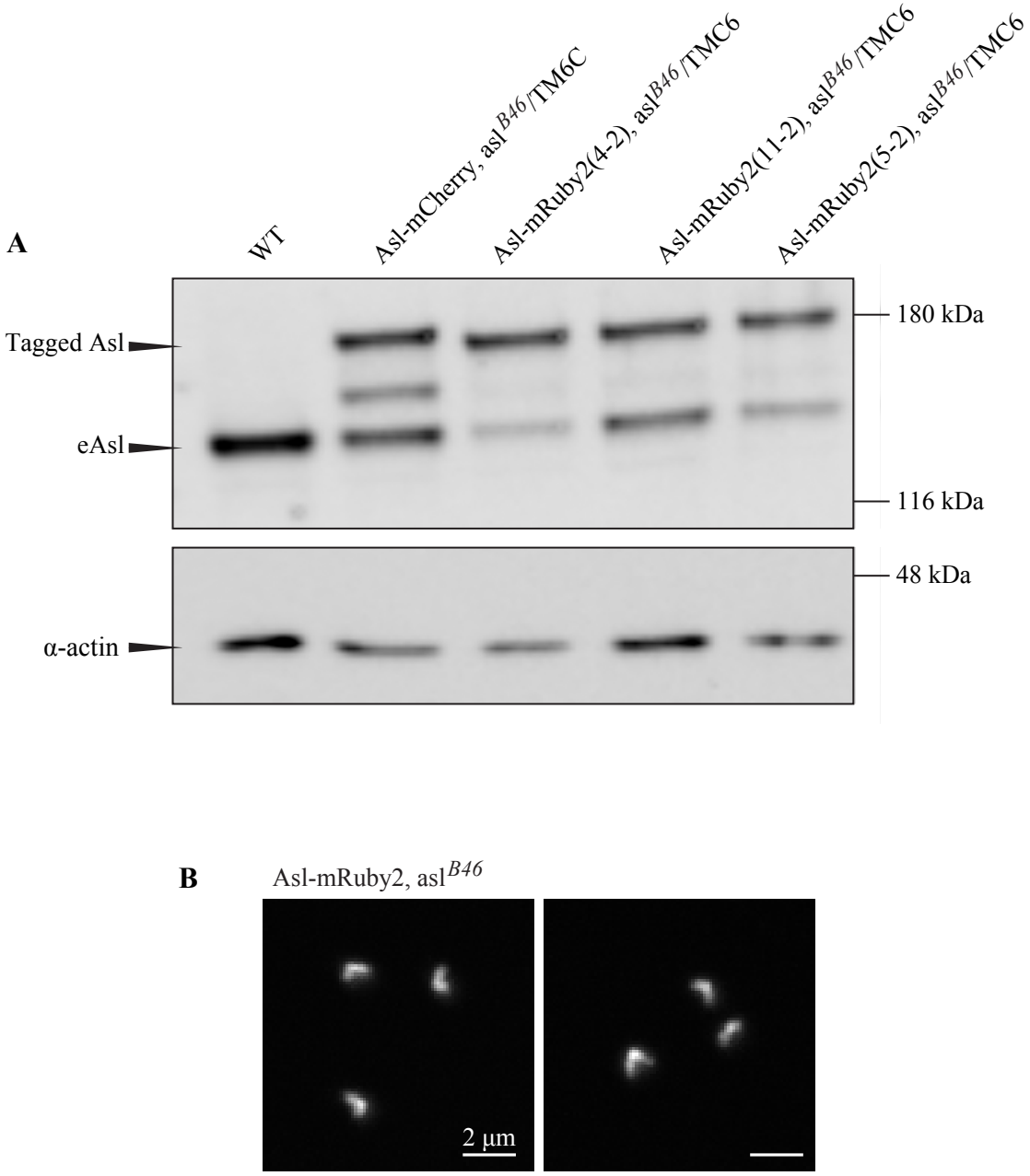


Figure 3.7: mRuby2 does not mature quickly enough to allow imaging in the early *Drosophila* embryo. A) A western blot shows the expression levels of the fusion proteins Asl-mRuby2 and Asl-mCherry in transgenic flies; each lane contains 10 early embryos. These early *Drosophila* embryos express one copy of the transgene in the presence of one copy of the endogenous WT gene. The expression levels of the fusion proteins are comparable between the different transgenic flies. Endogenous Asl (eAsl), tagged Asl and α-actin (loading control) are indicated by the arrowheads. **B**) Images show how Asl-mRuby2 signal is detectable at the large centrioles in 3rd instar larval spermatocytes on a spinning discs under 561 nm excitation. In the early Drosophila embryo no mRuby2 signal was seen (data not shown). This demonstrates that Asl-mRuby2 is functional in *Drosophila*, however does not have time to fold properly in embryos.

the endogenous *asl* promoter and recombined 3 different lines with the asl^{B46} mutant allele (Novak et al., 2014):

$$w; \frac{w^+}{w^+}; \frac{\text{Asl-FP}, asl^{B46}}{\text{Asl-FP}, asl^{B46}}$$

Western blotting revealed that all lines expressed Asl-mKate2 at levels broadly comparable to the control line expressing Asl-mCherry, asl^{B46} (**Figure 3.8A**). The transgenic line Asl-mKate2(14-10), asl^{B46} was selected for the further analysis.

As a key aim of this work was to identify a red fluorescent protein that functions on the OMX V3 Blaze 3D-SIM system, I used the same approach as described in 3.2.2.1, to compare the Asl-mCherry and Asl-mKate2 fusions on this system. Due to the larger Stokes-shift of mKate2, the peak emission is shifted towards far-red and therefore a different emission filter set had to be used. Thus, a truly direct comparison of the fluorophores was not possible.

While I could not image the ring of Asl around the mother centriole in embryos expressing Asl-mCherry using SIM (the images did not reconstruct and failed SIMCheck (data not shown)), I could image the Asl ring in embryos expressing Asl-mKate2 (**Figure 3.8B**). This suggests that mKate2 may be a useful tool allowing for two-colour 3D-SIM imaging on the OMX system.

Furthermore, when quantifying the widefield images, the mKate2-fusion was significantly brighter (~1.75x brighter) than the mCherry-fusion under these conditions (**Figure 3.9**) and it was also more stable than mCherry over time (**Figure**

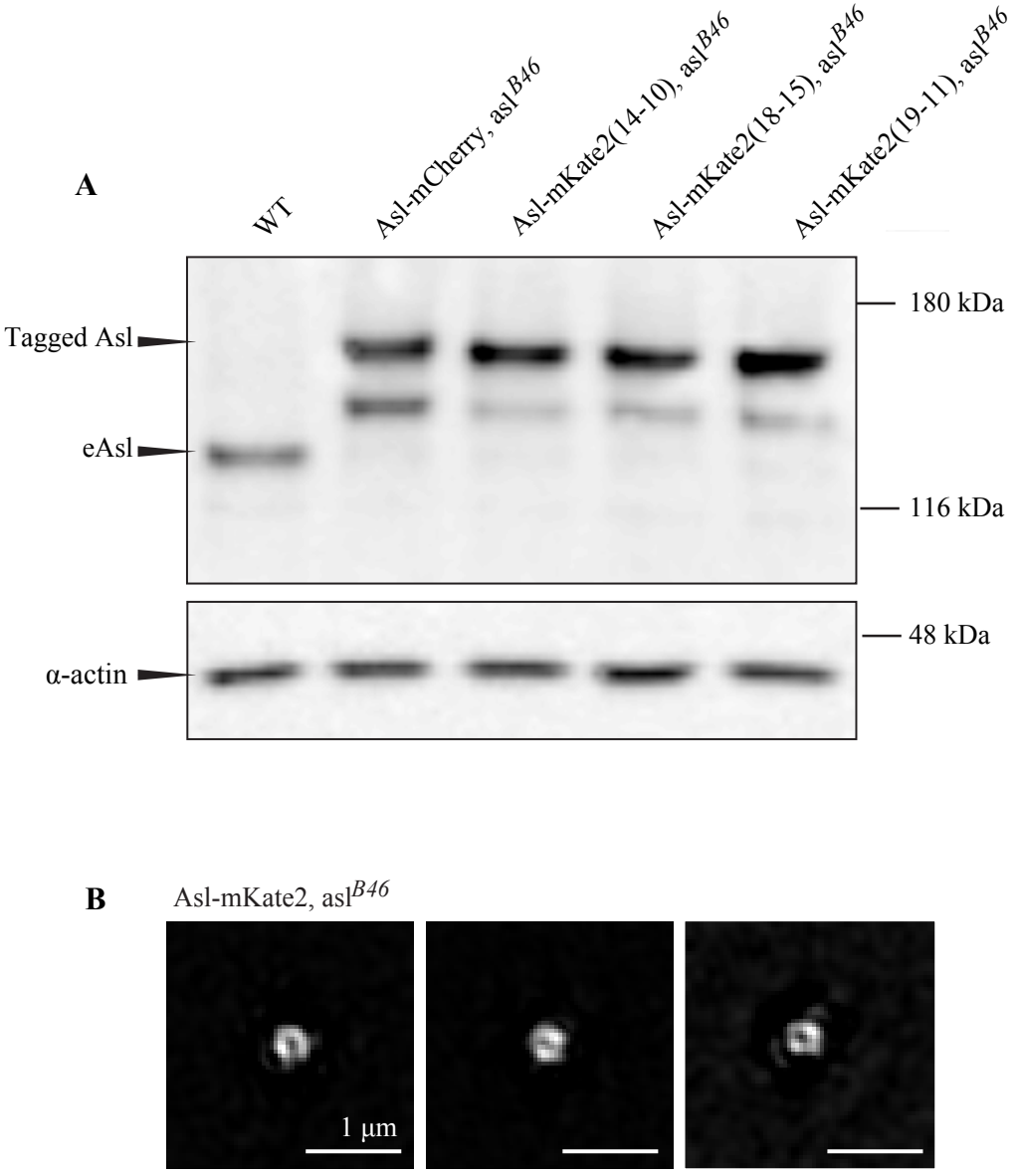


Figure 3.8: Asl-mKate2 can be imaged using 3D-SIM. A) A western blot shows the expression levels of the fusion proteins Asl-mKate2 and Asl-mCherry in transgenic flies; each lane contains 10 early embryos. These early *Drosophila* embryos express two copies of the transgene in the absence of the endogenous WT gene (they are homozygous for the chromosome). The expression levels of Asl-mCherry and Asl-mKate2 (14-10) fusion proteins are most comparable. Endogenous Asl (eAsl), tagged Asl and α-actin (loading control) are indicated by the arrowheads. **B**) Images show representative *z*-projected 3D-SIM images taken from embryos expressing Asl-mKate2 under 593 nm excitation.

3.10A). One of the problems with using mCherry in two-colour red-green imaging is that mCherry quickly gets bleached by the 488 nm light (Dr. A. Wainman, personal communication). Therefore, I examined the rate of Asl-mKate2 and Asl-mCherry photobleaching upon sequential exposure of 593 nm and 488 nm light (**Figure 3.10B**). Like mCherry, mKate2 is bleached by 488 nm light, but seems to be more photostable than mCherry. This again suggests that mKate2 may be more suitable for two-colour live 3D-SIM imaging.

In conclusion, mKate2 exhibits significantly improved brightness and photostability compared to mCherry and can be used in 3D-SIM experiments, potentially in combination with another protein labelled with a green-fluorophore.

3.2.2.3. Evaluation of the self-labelling enzyme SNAP-tag

The SNAP-tag is a commercially available self-labelling enzyme that can be labelled with a fluorescent ligand. Being able to utilize self-labelling enzymes and their fluorescent organic labelling dyes would be useful when imaging low abundance proteins with super-resolution microscopy.

As mentioned above, the removal of the unbound, excess fluorescent ligand is important for the success of the SIM when using the SNAP-tag system. Therefore, I generated transgenic flies expressing SNAP-tag-Cnn under an ubiquitin promoter, and tried to permeabilize the embryos according to a protocol outlined previously (Rand et al., 2010). This permeabilization method allows the entry of small molecules, such as Rodamine B, in to the early *Drosophila* embryo while still maintaining the embryos viability and health, allowing it to continue development. However, this protocol was unsuccessful in my hands.

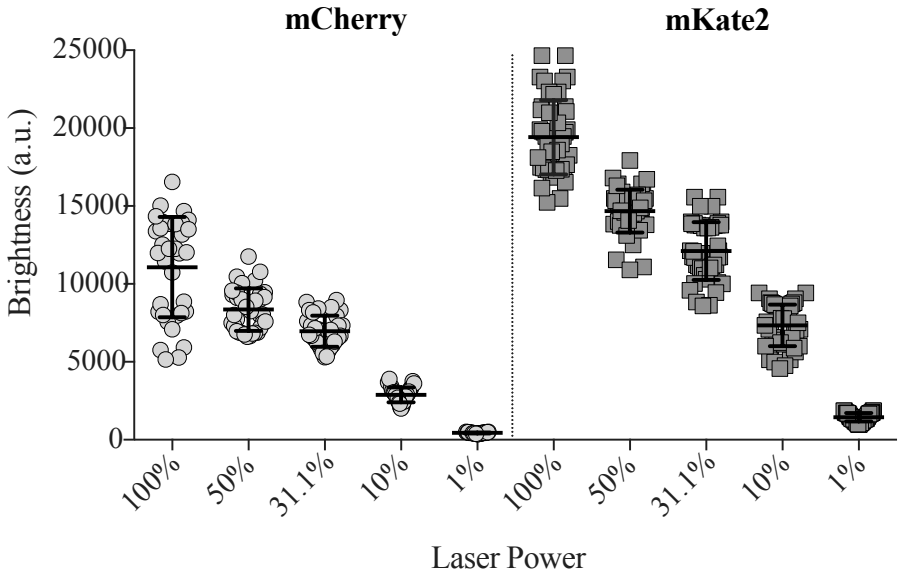


Figure 3.9: mKate2 is brighter than mCherry. Graphs display the signal intensity – brightness – at different 593 nm laser powers (100%, 50%, 31.3% 10% and 1% with 30 msec exposure) in embryos expressing mCherry or mKate2 fused to Asl in WF mode on the OMX V3 system. The brightest 5 centrosomes in each of the 7-9 embryos were measured (35-45 centrosome in total) for each laser intensity tested. mKate2 is ~1.75x brighter than mCherry at 100% laser power.

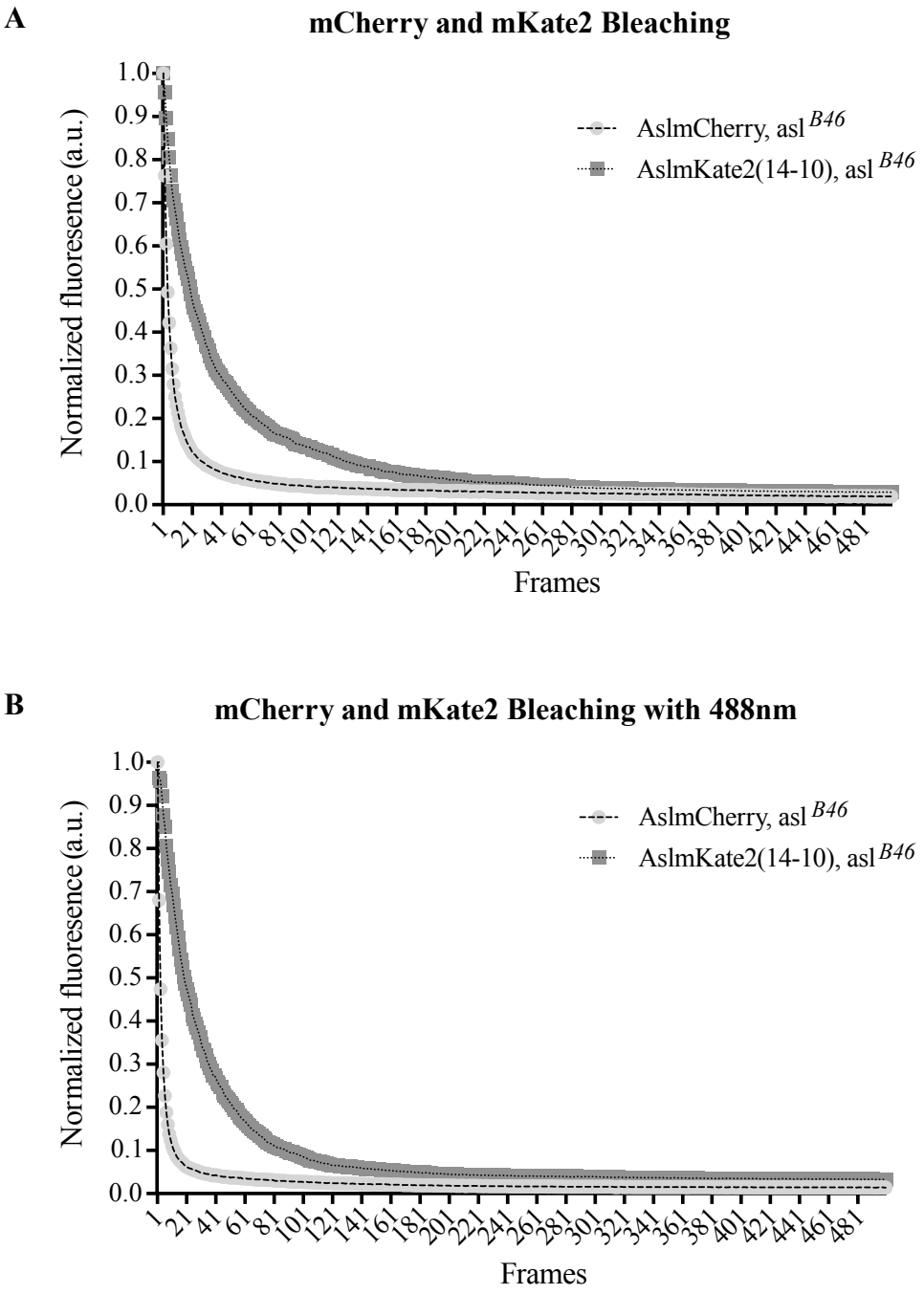


Figure 3.10: mKate2 is more stable than mCherry. A) Graphs display the stability of mKate2 and mCherry over 500 continuous frames (30 msec/frame) at 100% 593 nm laser power in WF mode on the OMX V3 system. The brightest 5 centrosomes in each of 7 embryos were measured (35 centrosomes in total). mKate2 is more stable than mCherry and thus lends itself for longer time-lapse imaging. **B**) Graph charts the photo-stability of mKate2 and mCherry measured over 500 continuous frames (30 msec/frame) at 100% 593 nm laser power in WF mode on the OMX V3 system. The brightest 5 centrosomes in each of 7 embryos were measured (35 centrosomes in total). The stability of both mKate2 and mCherry is decreased in the presence of 488 nm light. However mKate2 is also more stable than mCherry in these conditions.

I have not tested this self-labelling technology any further, but there are plans in the laboratory to use the SNAP-tag-Cnn flies. Possible experiments could include labelling SNAP-tag-Cnn with very low concentrations of dye (reducing the excess unbound dye) and then test whether the behaviour of single SNAP-tag-Cnn molecules can be followed at the centrosome.

3.2.3. Using mNeonGreen: Protein dynamics of Sak in the early *Drosophila* embryo

One of the aims of this fluorescent protein screen was to identify a fluorescent probe that would allow the imaging of the protein Sak in living embryos over the cell cycle in the early *Drosophila* embryo. This kinase is responsible for the initiation of the centriole duplication and defines the position of daughter centriole formation (Habedanck et al., 2005); its precise localisation has previously only been imaged by 3D-SIM in fixed human or *Drosophila* cell lines (Dzhindzhev et al., 2017; Ohta et al., 2014; Sonnen et al., 2012).

With the identification of mNeonGreen as a bright and stable fluorescent protein functioning well in the *Drosophila* embryo, I generated transgenic flies that express Sak-mNeonGreen under the control of its endogenous promoter. I subsequently generated a recombinant line allowing me to express two copies of the Sak-mNeonGreen transgene in a *Sak* mutant background. These flies are still slightly uncoordinated, but can be maintained as a stable line indicating that the transgene significantly rescues the *Sak* mutant phenotype. I then generated lines that also expressed Asl-mKate2 to use as marker to stage the embryos during the nuclear cycle:

$$w;\ \frac{\text{Asl-mKate2(1-2)}}{CyO};\ \frac{\text{eSak-mNeonGreen}, sak^{aa74}}{\text{eSak-mNeonGreen}, sak^{aa74}}$$

It has previously been shown that Sak/Plk4 is initially recruited to centrioles in a ring, later resolving into a single "dot" marking the site of the daughter centriole assembly. These studies were all performed on fixed cells, so it was unclear exactly when or how the Sak/Plk4 ring is converted to a dot (Kim et al., 2013; Ohta et al., 2014; Ohta et al., 2018).

Using 3D-SIM, I imaged the early *Drosophila* embryos over the different stages of the cell cycle, that in the early embryo consist only of an S- and M-phase (see 2.5.2.3 and 2.5.2). Individual Sak localisations were examined and selected based on their Modulation Contrast Noise Ratio (MCNR: the ratio of the SIM illumination pattern strength to the noise strength. This functions as a measure of reconstruction reliability and identification of artefact) values using SIMCheck (Ball et al., 2015). I observed that in the beginning of S-phase, just after centriole separation, Sak already localises as a dot (**Figure 3.11A**). Sak continues to localise as a dot in mid S-phase (**Figure 3.11B**) and all through the beginning of M-phase (**Figure 3.11C**). However, in late M-phase, Sak localises as a ring that also usually contained a prominent dot (**Figure 3.12**). These data shows that Sak is localised primarily as a dot throughout the cell cycle, except for in late M-phase where it localises again as a ring. This finding is important, as it has recently been shown in our laboratory that Sak levels at the centriole oscillate during these early embryonic cycles, with levels being lowest in early mitosis, and highest in mid-S-phase (Aydogan et al., Nature, under review). My findings demonstrate that Sak is localised as a dot through almost all of these embryonic cycles, with only a brief period as a ring in late mitosis (presumably when Sak is first being recruited to the mother centriole in preparation for the next round of

centriole duplication). Thus, centriolar Sak levels oscillate primarily at the dot that defines the site of daughter centriole assembly.

3.3. Discussion

In this Chapter I described the systematic evaluation several fluorescent proteins and self-labelling enzymes for their utilization for centriole/centrosome research in the early *Drosophila* embryo. This evaluation had a particular focus on the fluorophores used in super-resolution SIM imaging. I used an mRNA injection assay as a first screen to identify potentially useful tags. From this initial screen I identified mKate2, mNeonGreen and the self-labelling enzymes (SNAP- and Halo-Tag) as interesting candidates for further analysis. Flies containing these fluorescent tags coupled to various proteins of interest were generated. This allowed a systematic comparison under conditions of stable expression of the fusion-proteins.

mKate2 was the only fluorescent protein emitting in red that was suitable for the mRNA injection assay and it performed better on the SIM system than mCherry the other commonly used red fluorescent protein used in the laboratory. The ability to co-inject 2 mRNA species, each encoding a different coloured fluorescent protein, was important for the work I describe in Chapter 6. Moreover, the identification of mKate2's functionality in the mRNA injection screen allowed Dr. Z. Novak, a post-doctoral researcher in the laboratory, to perform crucial mRNA injection experiments to dissect the process of daughter-to-mother centriole conversion (Novak et al., 2016). Finally, Asl-mKate2's improved stability and brightness allowed me to image the cell cycle stage of *Drosophila* embryos when assessing the localisation of Sak-mNeonGreen on our 3D-SIM system – this had not been possible with flies expressing Asl-mCherry due to rapid photobleaching (data not shown). The ability to

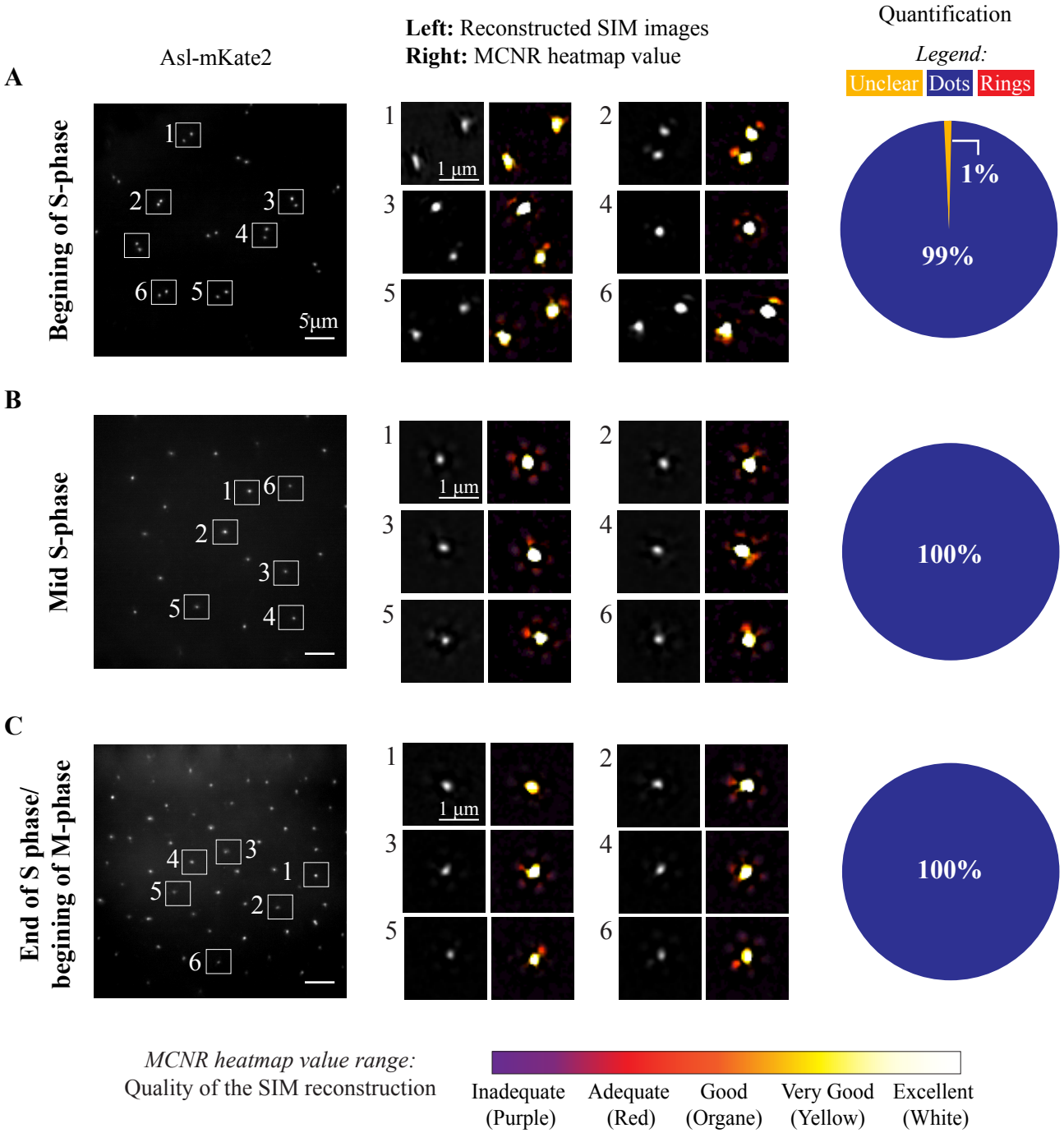


Figure 3.11: Sak-mNeonGreen is present as a dot at centrioles from early S-phase to early M-phase. 3D-SIM images taken under 488 nm exictation from embryos in early S-phase (**A**), mid S-phase (**B**) and late S-phase/early M-phase (**C**) show Asl-mKate2 (left panels) imaged in SIM mode and then reconstructed as a pseudo-widefield image, and higher magnification views of Sak-mNeonGreen (right panels, numbers correspond to boxes in the Asl-mKate2 image) reconstructed from SIM data. Individual Sak localizations were examined and their Modulation Contrast Noise Ratio (MCNR) heatmaps displayed. Pie charts (right panels), quantify the percentage of centrioles classified as “rings”, “dots” or “unclear”; the 10 best centrioles (defined by MCNR) from six embryos for each cell cycle stage were scored blind (so a total of 60 centrioles at each stage). Sak predominantly localises as a dot in early S- to early M-phase.

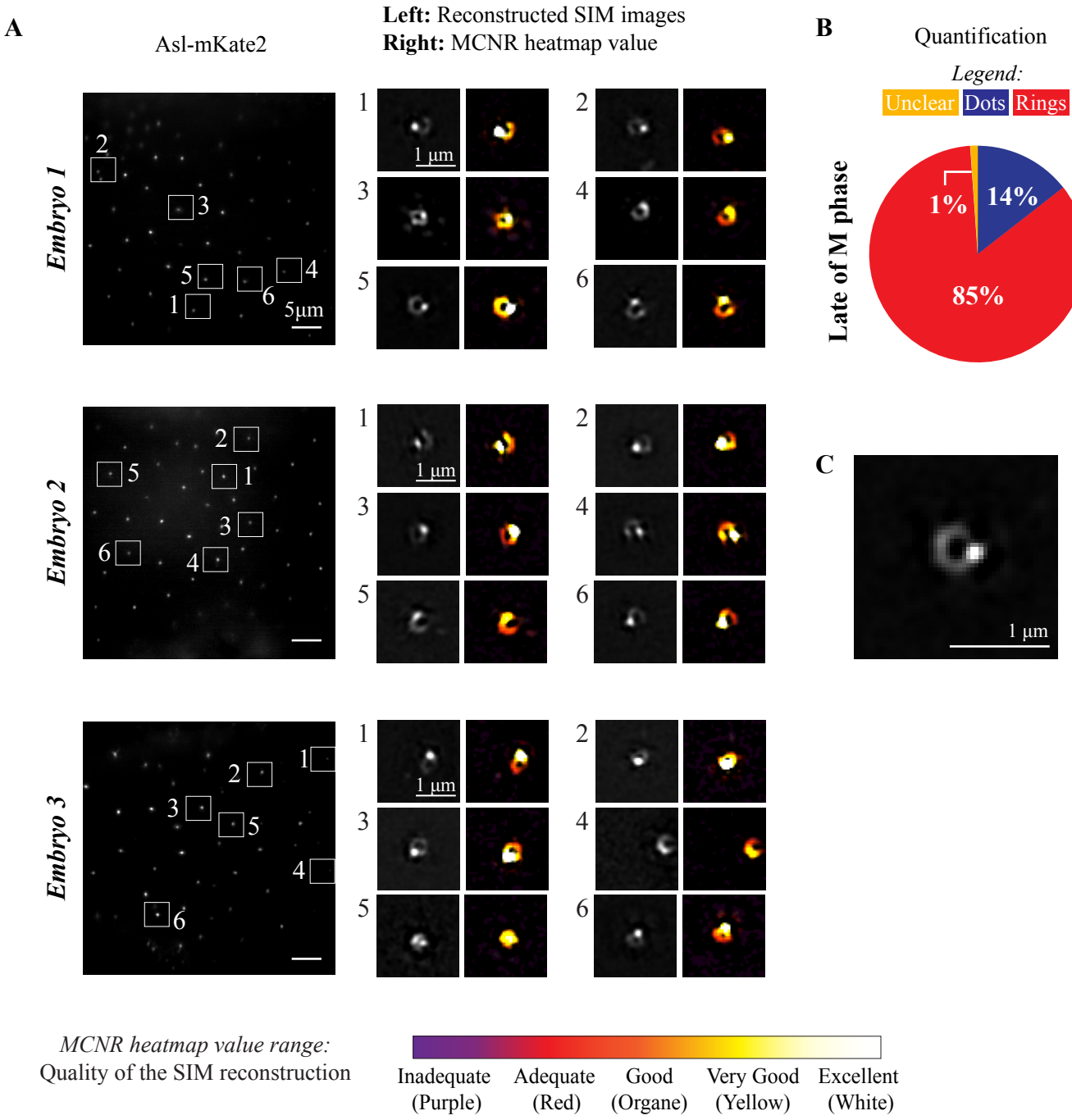


Figure 3.12: Sak-mNeonGreen is present as a ring at centrioles in late M-phase. 3D-SIM images taken under 488 nm exictation taken from 3 embryos in late M-phase show Asl-mKate2 (left panels) imaged in SIM mode and then reconstructed as a pseudo-widefield image, and higher magnification views of Sak-mNeonGreen (right panels, numbers correspond to boxes in the Asl-mKate2 image) reconstructed from SIM data. Individual Sak localizations were examined and their Modulation Contrast Noise Ratio (MCNR) heatmaps displayed. **B**) Pie chart,quantifies the percentage of centrioles classified as "rings", "dots" or "unclear"; the 10 best centrioles (defined by MCNR) from twelve embryos in late M-phase were scored blind (a total of 120 centrioles). Sak predominantly localises as a ring in late M-phase. **C**) Enlarged image of Sak-mNeonGreen localising as a ring.

image mKate2 reliably with SIM will allow more super-resolution studies using both red and green fluorescent protein tags.

mNeonGreen was found to perform well in the mRNA injection assay and for SIM imaging. The fast folding time and brightness, making it ideal for the mRNA injection screen, allowed me to detect signal soon after injection (data not shown) and provided more sensitivity. I used mNeonGreen in mRNA injection assays to assess protein-protein interactions in Chapter 6. These features of mNeonGreen make it a superb fluorescent protein to use for 3D-SIM. I was able, to my knowledge for the first time, to image the localisation of a Sak-fusion protein in a living cell.

Two key advantages of my approach using live embryos were that I was able to precisely assess the cell cycle stage (early, mid and late S-phase, and early and late M-phase) due to the presence of Asl, and to identify the changes in localisation of centriolar Sak-mNeonGreen. Additionally, I was able to image embryos at two different time points and was able to note the change in Sak-mNeonGreen localisation over the cell cycle (data not shown); this indicated that Sak-mNeonGreen localisation is dynamic. It is important to note that even though the use of Sak-mNeonGreen allowed for live imaging, technical challenges still limit this investigation. Improved fluorescent tags would permit better temporal resolution and thus better insight into the dynamics of Sak localisation.

It appears that Sak remains localised to a dot over the whole cell cycle, except for a brief period in late M-phase, were it localises to a ring. This is important, as it means that the Sak oscillations recently identified in our laboratory occur primarily at the

single “dot” of Sak that marks the site of daughter centriole assembly (Aydogan et al., Nature, under review).

The self-labelling enzymes evaluated in this study do have potential for use in microscopy studies. They have been shown to function well in fixed tissues (Kohl et al., 2014), however the presence of the waxy layer surrounding the early *Drosophila* embryo, prevents the washing out of unbound fluorescent ligand. This was seen both in the mRNA injection assay and, more pronounced, in the SIM images. Therefore, to use this system in the *Drosophila* embryo is not straightforward. However, it may be possible to use this system successfully by titrating the amount of injected fluorescent label to maximise specific labelling and minimize the amount of unbound fluorophore. Interestingly, one of the major future applications for this technology might be in single molecule studies—following the behaviour of single molecules at the centriole or centrosome. If this was the case, then a good strategy might be to inject very low levels of fluorophore so that only a small subset of the total tagged-protein of interest becomes labelled.

It will be important in the future to evaluate new and interesting fluorescent proteins and labelling systems that are developed as they can be transformative for research and allow insight into biological processes that have not been able to be studied before.

4. A correlative SIM/SMLM pipeline to examine the localisation of proteins within centrioles with nanometre precision

4.1. Introduction

Centrioles are structurally complicated organelles. The many proteins that comprise the centriole have been characterized and localised to varying extents. Although there have been many insightful electron microscopy (EM) studies of centrioles (Gonczy, 2012; Paintrand et al., 1992), and more recently some impressive cryo-ET studies (Greenan et al., 2018; Guichard et al., 2012; Guichard et al., 2013), these analyses provide no direct information about the localisation of specific components. Immuno-gold labelling has been used successfully to localise several proteins within the centriole, see for example Kleylein-Sohn et al. (2007), but this technique is challenging, often gives sparse data (as most molecules within a structure are not labelled), and the resolution is often compromised by the treatments necessary for antibody labelling (Ellisman et al., 2012; Hurbain and Sachse, 2011)

Light microscopy, on the other hand, allows for precise labelling of specific proteins via fluorescent tags and is therefore advantageous when trying to localise proteins. Historically, however, the precise localisation of centrosome and centriole proteins by light microscopy has been severely limited by the small size of centrioles, which are significantly smaller than the diffraction limit of light. Only recently have research groups begun to localise PCM and centriole proteins with super-resolution light microscopy, mainly SIM was used (Fu and Glover, 2012; Lawo et al., 2012; Mennella et al., 2012; Sonnen et al., 2012). Several centriole proteins exhibit a defined orientation at the centriole – usually with one protein terminus located more closely to

the centriole cartwheel and the other radiating outwards, giving a toroidal organisation of these proteins around the cartwheel (Fu and Glover, 2012; Lawo et al., 2012; Mennella et al., 2012; Saurya et al., 2016; Sonnen et al., 2012) (**Figure 4.1A,B**). On average, the radii of these toroids are ~100-300 nm with a standard deviation (s.d.) of ± ~3-45 nm.

However, the centriole cartwheel proteins Sas-6 and Ana2 have been poorly studied with light microscopy, as they localise to a region smaller than the diffraction limit of SIM (see **Figure 4.2** for a comparison of the localisation of Asl at centrioles using different microscopy techniques). The diffraction limit of SIM depends on the excitation wavelength: the theoretical resolution in *x* and *y* are 100 nm, 110 nm and 130 nm for blue, green and red light, respectively (Schermelleh et al., 2019; Schermelleh et al., 2010). From EM studies in *Chlamydomonas reinhardtii*, the central hub of the cartwheel (which is widely accepted to comprise the N-terminal region of Sas-6) has been estimated to have a radius of ~12 nm (Guichard et al., 2017); this is in line with previous crystal studies performed with *Leishmania major, C. reinhardtii, C. elegans, Dani rerio* and *Drosophila* Sas-6 (Cottee et al., 2015; Kitagawa et al., 2011; van Breugel et al., 2011; van Breugel et al., 2014). The outer region of the cartwheel (which is thought to be positioned by the C-terminal region of Sas-6) has been estimated to have a radius of ~50-60 nm (Guichard et al., 2017). Elegant cryo-ET reconstructions of the *Trichonympha* cartwheel (see Figure 1.3) have led to similar conclusions of cartwheel size (Guichard et al., 2013).

To date, very few studies have attempted to image the Sas-6 termini with light microscopy. Using STED microscopy, the C-terminus of human Sas-6 has been

A

	Protein	Species	Tissue	Mean radius (nm)	s.d. (nm)	ref.
Sas-4/CPAP	Sas-4 NT	*Drosphila*	S2 cells	101	10	Mennella et al., 2012
	Sas-4 NT	*Drosphila*	S2 cells	100	30	Fu & Glover, 2012
	CPAP	*Human*	Hela, REP-1 cells	97.0	13.0	Lawo et al., 2012
	CPAP CT	*Human*	U2OS, REP-1 cells	249.35	19.1	Sonnen et al., 2012
Cep135	Cep135 CT	*Drosophila*	Testes	66.9	4.9	Saurya et al., 2016
	Cep135 CT	*Drosphila*	S2 cells	61	11	Fu et al, 2016
	Cep135	*Human*	U2OS, REP-1 cells	85.0	20	Sonnen et al., 2012
	Cep135 NT	*Drosophila*	Testes	93.6	8.3	Saurya et al., 2016
Asl/Cep152	Asl CT	*Drosphila*	Testes	177	28.7	Saurya et al., 2016
	Asl CT	*Drosphila*	S2 cells	97	21	Mennella et al., 2012
	Asl CT	*Drosphila*	S2 cells	117	12	Fu et al, 2016
	Asl	*Drosphila*	S2 cells	170	20	Fu & Glover, 2012
	Asl NT	*Drosphila*	S2 cells	182	16	Fu et al, 2016
	Asl NT	*Drosphila*	S2 cells	138	15	Mennella et al., 2012
	Asl NT	*Drosphila*	Testes	176.5	2.8	Wegel et al., 2016
	Asl NT	*Drosphila*	Testes	266	66.2	Saurya et al., 2016
	CEP152 CT	*Human*	U2OS, REP-1 cells	156.65	3.5	Sonnen et al., 2012
	CEP152 NT	*Human*	Hela, REP-1 cells	217.5	21.4	Lawo et al., 2012
	CEP152 NT	*Human*	U2OS, REP-1 cells	207.2	2.9	Sonnen et al., 2012
Plp/Pericentrin	Plp	*Drosphila*	S2 cells	170	20	Fu & Glover, 2012
	Pericentrin CT	*Human*	U2OS, REP-1 cells	249.5	46.5	Sonnen et al., 2012
	Plp CT	*Drosphila*	S2 cells	86	9	Mennella et al., 2012
	Plp Mid	*Drosphila*	S2 cells	126	11	Mennella et al., 2012
	Plp NT	*Drosphila*	S2 cells	146	11	Mennella et al., 2012

B

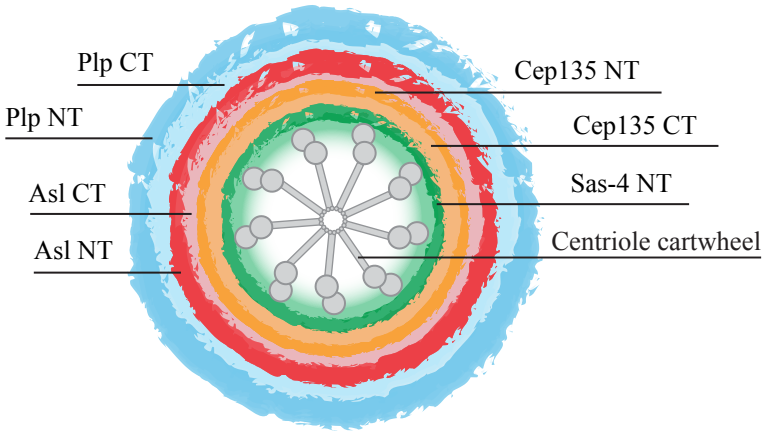


Figure 4.1: Summary of localisation data of centriole and centriole wall proteins. A) A table summarizing the known radii of the toroids of different centriole and centrosome proteins observed by SIM in humans and Drosophila. **B**) A schematic of the relative positions of various previously described centriole and centrosome proteins. The centriole cartwheel is viewed end-on and has a ~150 nm diameter**.**

visualised as a toroid with a diameter of 107 nm and its N-terminus was calculated to have a diameter of 57 nm (Fong et al., 2014). The inconsistency between this study's calculated radius of the N-terminus of Sas-6 and those derived from the previous EM and crystal studies (mentioned above) is, however, not commented upon. Additionally, the logic of the methodology used was difficult to understand. The only other study which utilized a correlative 3D-SIM and 3D-dSTORM approach to visualize the N-terminus of Sas-6 (CrBld12p) in *Chlamydomonas* used purified basal bodies (Hamel et al., 2014). The CrBld12p was imaged using 3D-STORM, which has a higher resolving power then SIM, allowing greater precision in the nanometre range in biological samples (Huang et al., 2008; Schermelleh et al., 2019; Schermelleh et al., 2010). Hamel and colleagues measured a diameter of ~41 and ~55 nm for the N-terminus of CrBld12p in 2 basal bodies. The limited sample size and the discrepancy between the measured radii and the EM and crystal structure estimations suggests room for further improvement.

While the crystal structures and EM studies of the Sas-6 molecule have provided considerable insight into how Sas-6 is likely to be organised within the cartwheel, there is essentially no information on how Ana2/STIL, the other protein that appears to be essential for cartwheel assembly (Cottee et al., 2015; Dobbelaere et al., 2008; Goshima et al., 2007; Stevens et al., 2010a; Tang et al., 2011), is organised within the cartwheel. This question is particularly important as, although an interaction between Sas-6 and Ana2/STIL appears to be a conserved feature of the centriole assembly pathway, it remains unclear and controversial exactly how Sas-6 proteins interact with Ana2/STIL proteins (Leidel et al., 2005; Moyer et al., 2015; Stevens et al., 2010b; Tang et al., 2011). Moreover, in flies, Ana2 can form a tetramer through its conserved

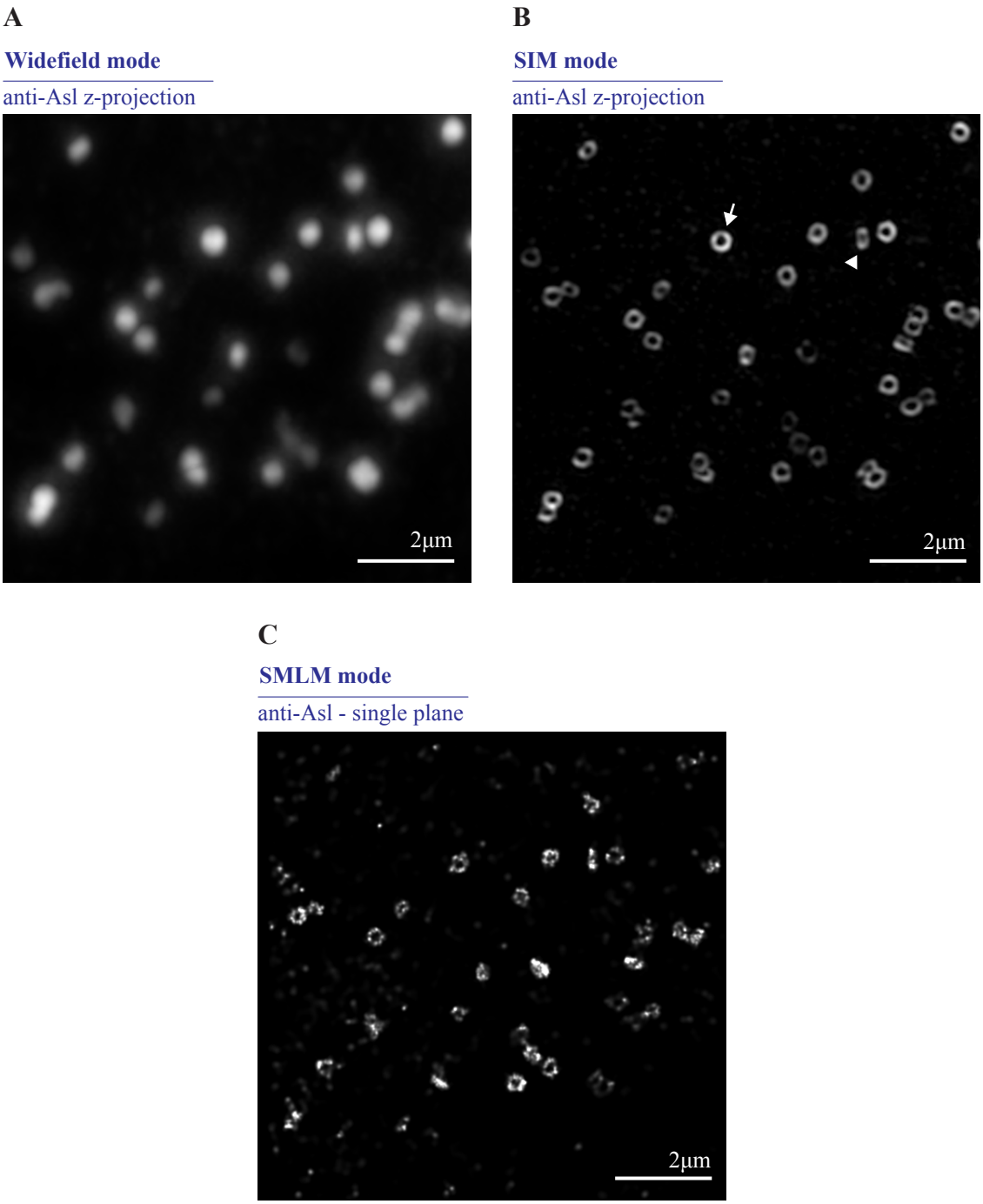


Figure 4.2: Images of wing disc centrioles taken with different microscopy modes. The same field of view of a wing disc was imaged with different microscopy modes. The centrioles are stained with antibodies against the N-terminal region of Asl. **A**) A widefield, *z*-projected image of wing discs centrioles. **B**) A 3D-SIM, *z*-projected image of wing discs centrioles. A well-orientated centriole (white arrow) and a poorly orientated centriole (white arrowhead) are shown. **C**) A SMLM, image of wing discs centrioles (single *z*-plane).

central coiled-coil region and it has been proposed that such a tetramer could function to bridge two Sas-6 dimers in several ways (**Figure 4.3**). In other species, the ability of the central coiled-coil domain to oligomerise also appears to be crucial to Ana2/STIL function, but this region can also interact with Plk4, another essential component of the centriole assembly pathway (Arquint et al., 2015; Cottee et al., 2017). Thus, determining how Ana2 is arranged within the cartwheel structure is an important goal.

In this chapter, I describe my attempts to combine 3D-SIM and SMLM to more precisely localise the position of proteins within the centriole. This work was collaborative: the project was conceived from some initial feasibility studies performed by Dr Alan Wainman, a postdoctoral fellow in the Raff laboratory; Dr. Ian M. Dobbie and Dr. Maryam Qurashi wrote the custom image processing and analysis python code Centriole Origin Optimising Localiser (COOL) (available at: https://github.com/MicronOxford/cool); I received help from Dr. Rainer Kaufmann with the setting up of fastSPDM software and amending it; Dr. Sebastian Schubert provided expert advice in setting up the OMX V2 system for correlative 3D-SIM/SMLM; I prepared and imaged the wing disc samples and then processed and analysed the data from all the experiments.

4.1.1. Key findings

Development of a correlative 3D-SIM and SMLM processing approach which allows for the assessment of centriole orientation, precise centre of mass definition and weighted radius measurements. Utilization of this custom code and data collection from different transgenic flies lead to the localisation of the C- and N-termini of Sas-6

and Ana2, and the C-termini of Sas-4 with nanometre precision. This was the first time the termini of Ana2 were localised.

This work was recently published: Gartenmann, et al., *Current Biology*, 2017.

4.2. Results

4.2.1. Selection of *Drosophila* fly lines, sample tissue and staining methods

The following *Drosophila* fly lines were used in this project (see 2.1.2): eSas-4-GFP (Novak et al., 2014), eAna2-GFP, eSas-6-GFP (Aydogan et al., 2018) (all of these transgenes are expressed from their own promotors at levels that are comparable to the endogenous proteins), Ubq-GFP-Ana2 (Stevens et al., 2010a), Ubq-GFP-Sas-6 (Peel et al., 2007), Ubq-Sas-4-GFP (Cottee et al., 2013) and YFP-Asl (Varmark et al., 2007) (all of these transgenes are expressed from the ubiquitin (Ubq) promoter (Lee et al., 1988), usually resulting in a moderate overexpression of 3-5x compared to the endogenous protein). These fusion-proteins have been shown to rescue the centriole defects in their respective mutant backgrounds, indicating that they are functional (Aydogan et al., 2018; Cottee et al., 2015; Cottee et al., 2013; Peel et al., 2007) (Dr. Z. Novak, personal communication).

I used fixed 3rd instar *Drosophila* larval wing discs for these experiments as this tissue offers several advantages. First, the centrioles in this tissue tend to be clustered at the apical surface (Franz et al., 2013; Saurya et al., 2016) (**Figure 4.2B**). This allowed me to image many centrioles in a relatively thin volume of tissue (9 *z*-slices at a 0.125µm step size), and having the fluorescently labelled protein of interest located close to the tissue surface, and hence close to the coverslip, is particularly important for SMLM as

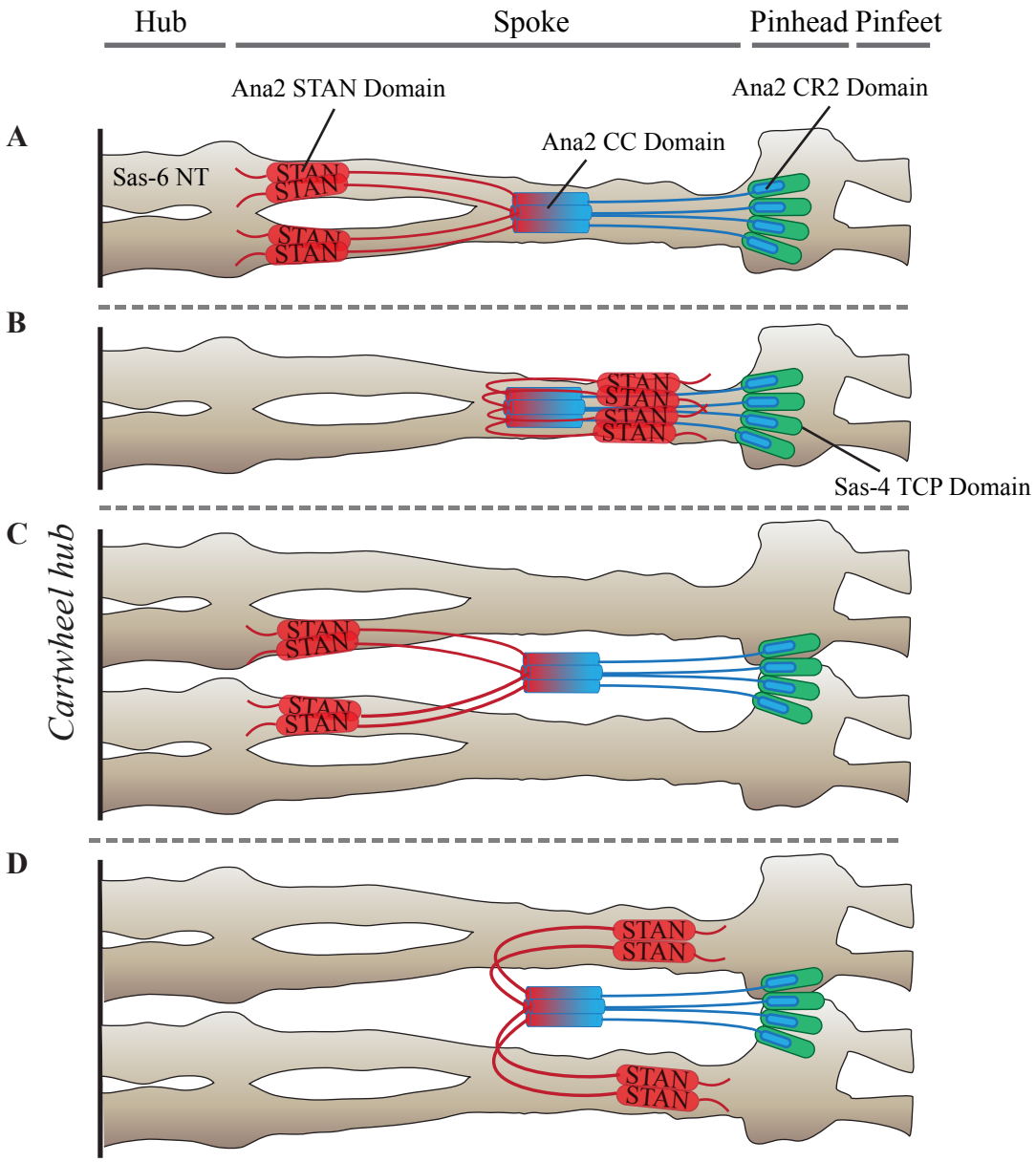


Figure 4.3: A schematic model of different possible modes of interaction between the Ana2 tetramer and the Sas-6 cartwheel. The brown area is the electron density map of the Trichonympha cartwheel; the hub (on the left) is thought to contain the Sas-6 N-terminus. The Ana2 STAN domains ares indicated in red, the Ana2 CC domain tetramer is coloured in red/blue and the N-terminal Ana2 CR2 domain (blue) which binds to the Sas-4 C-terminal TCP domain is indicated (green) (adapted from Cottee et al., 2015). Four ways in which Ana2 molecules might fit into the density map are illustrated (in all cases the CR2 domain is depicted as interacting with the Sas-4-TCP domain at the periphery of the cartwheel): **A**) The Ana2 STAN domain extends to the hub of the cartwheel. **B**) The STAN domain binds close to the C-terminus of Sas-6. **C**) The Ana2 STAN domain interacts with Sas-6 close to the hub. **D**) The Ana2 tetramer spans two Sas-6 cartwheel pairs with its STAN domain binding near the outer region of the Sas-6 spokes.

the deeper the labelled proteins are in the tissue, the more emitted photons are absorbed or lost due to scattering. Second, the mother centrioles in this tissue are usually oriented orthogonally to the apical surface; it is not clear why this is the case, but it means that mother centrioles are almost always in approximately the correct orientation for accurately measuring the radial distance of any protein of interest from the centre of the centriole **(Figure 4.2B**).

In order to study the localisation of the cartwheel protein termini with high precision using SMLM (**Figure 4.2C**), it was essential to label the proteins of interest with as small a fluorescent tag as possible. This is because the signal detected from the fluorophore does not represent the true position of the terminus of the protein, but rather the position of a fluorescent protein attached to the protein terminus, or of a fluorophore attached to an antibody that binds to the terminus of a protein. Additionally, I had to ensure that the fluorescent tag would undergo sufficient on/off cycles of photon emission to perform well for SMLM. I decided to utilize the existing *Drosophila* flies available in the Raff laboratory in which individual centriole proteins had been tagged with GFP at either their N- or C-terminus (see paragraph above or 2.1.2). The GFP tag is approximately 5 nm in size, but GFP itself is a poor fluorophore for this type of experiment, particularly in fixed tissues (Joosen et al., 2014; Schnell et al., 2012). I therefore stained fixed tissue from the lines expressing the GFP-fusions with a fluorophore conjugated Nanobody, a single domain Alpaca antibody fragment which is coupled to an Atto488 dye (Chromotek GmbH, Raff Stock #166). The Atto488 fluorophore has excellent properties for these studies (Dempsey et al., 2011) and Nanobodies are only about 2 nm in size, significantly

smaller than a conventional IgG complex containing both primary and secondary antibodies, which are usually on the order of 20-30 nm in size (Ewers, 2018).

In the experiments described below, the orientation of the centrioles was initially visualized using 3D-SIM by co-staining the wing discs with Guinea-Pig anti-Asl antibody (Raff Stock: #199 and #200) and a Goat anti-Guinea Pig IgG Alexa Fluor 594 (Invitrogen) (**Figure 4.2B**). Asl surrounds only mature, mother centrioles (Novak et al., 2014), thus ensuring that I only analysed centrioles that had a fully assembled cartwheel. Importantly, it has recently been shown that the key cartwheel component Sas-6 does not turnover at centrioles once it has been incorporated into the cartwheel (Aydogan et al., 2018), strongly suggesting that the *Drosophila* centriole cartwheel does not significantly change its structure or shape once it is assembled. Sample preparation, microscope set up and imaging parameters are described in the 2.4.6 and 2.5.5.3. For each GFP-fusion studied, two to three technical repeats were performed and data were collected from at least five different larval wing discs.

4.2.2. Developing a new analysis method to image the relative position of centriole proteins with 3D-SIM/SMLM

SMLM methods have the potential to calculate the position of a fluorophore with great precision (~10-30 nm) (Schermelleh et al., 2010). However, by their nature, these methods rely on the relatively sparse labelling of the molecules within any structure, so it can be difficult to accurately measure the exact shape of an object and to determine the average distribution of all the specific molecules of interest within that structure. We hoped, therefore, that we might be able to use 3D-SIM imaging to select centrioles that were well oriented, and then extract the SMLM data for proteins of interest from these centrioles to accurately calculate the average radial distance of

these proteins from the centre of the centriole. To this end, and through several iterations with data that I provided, Dr. Ian M. Dobbie and Dr. Maryam Qurashi wrote a custom image processing and analysis python 2 script, COOL. This script tackled three separate issues: (1) assessment of centriole orientation; (2) alignment of the relevant regions of interest from the SIM and SMLM data; (3) calculating the average radii of the SMLM data from the centre of the centriole. Each step is described in detail below.

The reconstructed 3D-SIM *z*-stack images, revealing the Asl staining, were viewed as maximum intensity projections, and the coordinates of the well-oriented centrioles (initially assessed by eye) were noted (**Figure 4.4A**). Using the COOL script, a 0.6μm square region around these coordinates was cropped, resulting in a series of cropped images that each contained a seemingly well-oriented centriole (**Figure 4.4B, raw data panels**). Subsequently, the position of the centre of each Asl ring was fitted using an elliptical annular Gaussian profile that generated fitted parameters for the centre coordinates, the major and minor axes, and the angle of the ellipse. The fitted ellipses were then filtered using an arbitrary eccentricity of <1.2 (major:minor axis ratio) to only retain those centrioles that were not tilted (**Figure 4.4B, fitted ellipse panels**). In general, approximately half of the hand-selected centrioles were filtered out in this way. This filtering minimized errors but did not change the overall results: tests without an eccentricity filter of <1.2 generated similar final radii averages, but with a standard deviation that was approximately 2-3x larger.

One challenge with this project was the alignment of the data taken on two different cameras in different imaging modes. As the image generated from SMLM data is in

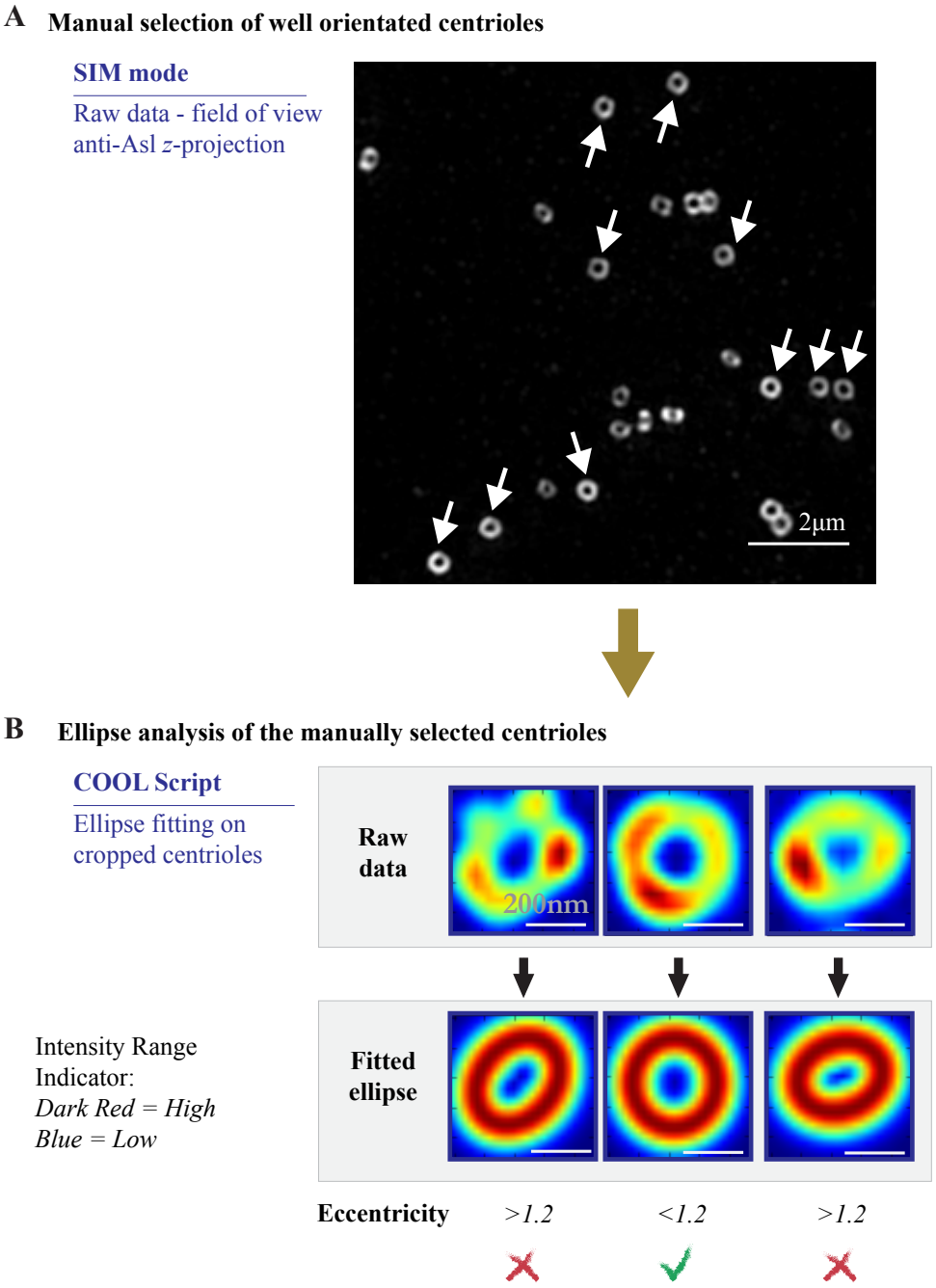


Figure 4.4: Schematic summary of the initial selection of well-oriented centrioles. A) Isolated centrioles that appeared well-orientated (white arrows) were initially selected manually and their position noted. **B**) The selected centrioles were cropped to 30 x 30 pixel image and an ellipse was fitted to each. The eccentricity of the fitted ellipse was calculated and those with an eccentricity of <1.2 were retained and used for further analysis.

fact a localisation probability map, not an proper image, it is not possible to align it to its corresponding SIM image in the conventional fashion, where images of fluorescent beads are taken in the appropriate channels to account for shifts in *x*, *y*, *z*, scale and rotation. However, we assumed that the SMLM signal was contained within the SIM signal, and that both shared the same centriole centre, and we used this assumption to iteratively align one image to the other (**Figure 4.5**). The SIM images were first scaled to the same 20 nm pixel size as the SMLM image. The centres of the coordinates of the well-oriented centrioles (initially assessed by eye) were noted in SMLM images (generated using fastSPDM generated images (Grull et al., 2011), see 2.5.6.1). The COOL script then performed a least square rigid body fitting (which includes, *x* and *y* shift, rotation and scale) on the SIM image, initially using a centroid position of the SMLM data that I had defined manually and the fitted SIM centroid locations (**Figure 4.5Ai**). As there were usually multiple centrioles in the 128x128 pixel field of view, the errors made during manual selection were evened out. The centroids of the fitted SIM centrioles were plotted (**Figure 4.5.Aii**) and initial round of SMLM centroid calculation was performed: an 80 nm radius (except for the Asl calculation which used 300 nm) from the SIM centroid defined the area in which the SMLM centroid could be calculated (**Figure 4.5Aiii**). This constraint radius ensured that the SMLM localisation points measured were those of the correct centriole and not background. The centroid calculation was weighted – the weights were defined by the precision of each localisation (**Figure 4.5Aiv**). The calculated centroid served as the starting point for the next round of centroid optimization calculations with the 80 nm constraint radius (**Figure 4.5.Av**). Multiple rounds (typically 3-7) of centroid optimization using the raw SMLM localisation positions were performed and accuracies gradually refined the manually defined centres of the SMLM centrioles

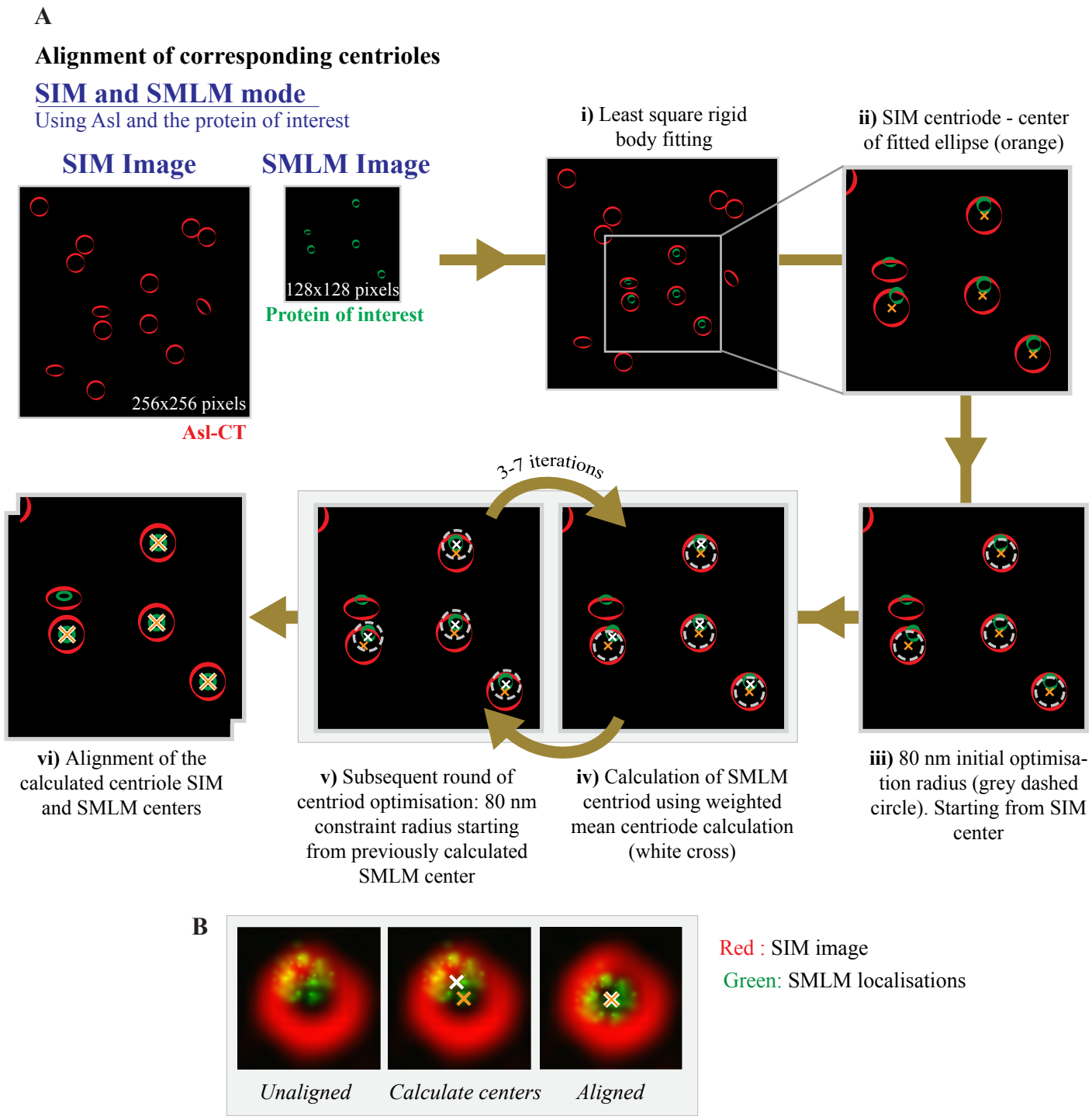


Figure 4.5: Summary of the procedure for the alignment of the SIM and SMLM data. A) Schematic of the alignment and centroid calculation process: **i**) Images are aligned using least square rigid body fitting based on the center of the fitted SIM ellipses and the manually defined centers for SMLM; **ii**) Plotting of the SIM centroids, calculated using the ellipse analysis. **iii**) The initial round of SMLM centroid optimisation occur in an 80 nm radius (grey dashed circle) starting from the SIM centroid. **iv**) Calculations of the SMLM centroid (white cross) in the given 80 nm constraint radius determined by a weighted mean centroid calculation (weights determined by the inverse localisation probability of each localisation). **v**) Further centroid optimization for SMLM data, 80 nm constraint radius starting from most recently calculated centroid. **vi**) Alignment of the SIM and SMLM data based on the calculated centroids. **B**) An example of the alignment using a single centriole of the eSas-4 CT data set.

(**Figure 4.5Avi**). This process ensured that the centroid of the SMLM localisations was calculated and that the SMLM localisation data and SIM image of each centriole could be aligned (**Figure 4.5B**).

Once the "optimized centroid" for the SMLM data for each protein terminus of interest had been calculated in this way, a histogram of the radii of the anti-GFP Nanobody localisations from this centre was examined (see Sas-4 CT example shown in **Figure 4.6A**). Localisations that were within a distance of two times the radius of the most frequent observation on the histogram were then selected for further analysis: this was done to reduce the contribution of diffuse background signal, yet was likely to include all the localisations stemming from the specific signal from the Nanobodies bound to the protein at the centriole. Further refinement was performed to improve the radial distance measurement by selecting only the localisations that had a precision greater (more precise) than 30 nm; centrioles that had less than 10 localisations were discarded from the analysis – as having less than 10 localisations meant the weighted centroid optimization was likely not reliable (**Figure 4.6B**). The highest frequency radius of this histogram varied depending on the protein termini. It was usually between 50-120 nm, except for Asl, which was 280 nm. The refinement results in the final histogram from which the weighted radius was calculated (**Figure 4.6C**). The number of centrioles and final localisations used to analyse each protein terminus was in the range of 40-100 and 1200-12000, respectively (**Figure 4.7A**).

Finally for each data set, an average radial distance of each protein terminus was calculated using the selected localisations using a weighted mean approach, in which the weights were defined by localisation precision. A mean-of-means then combined

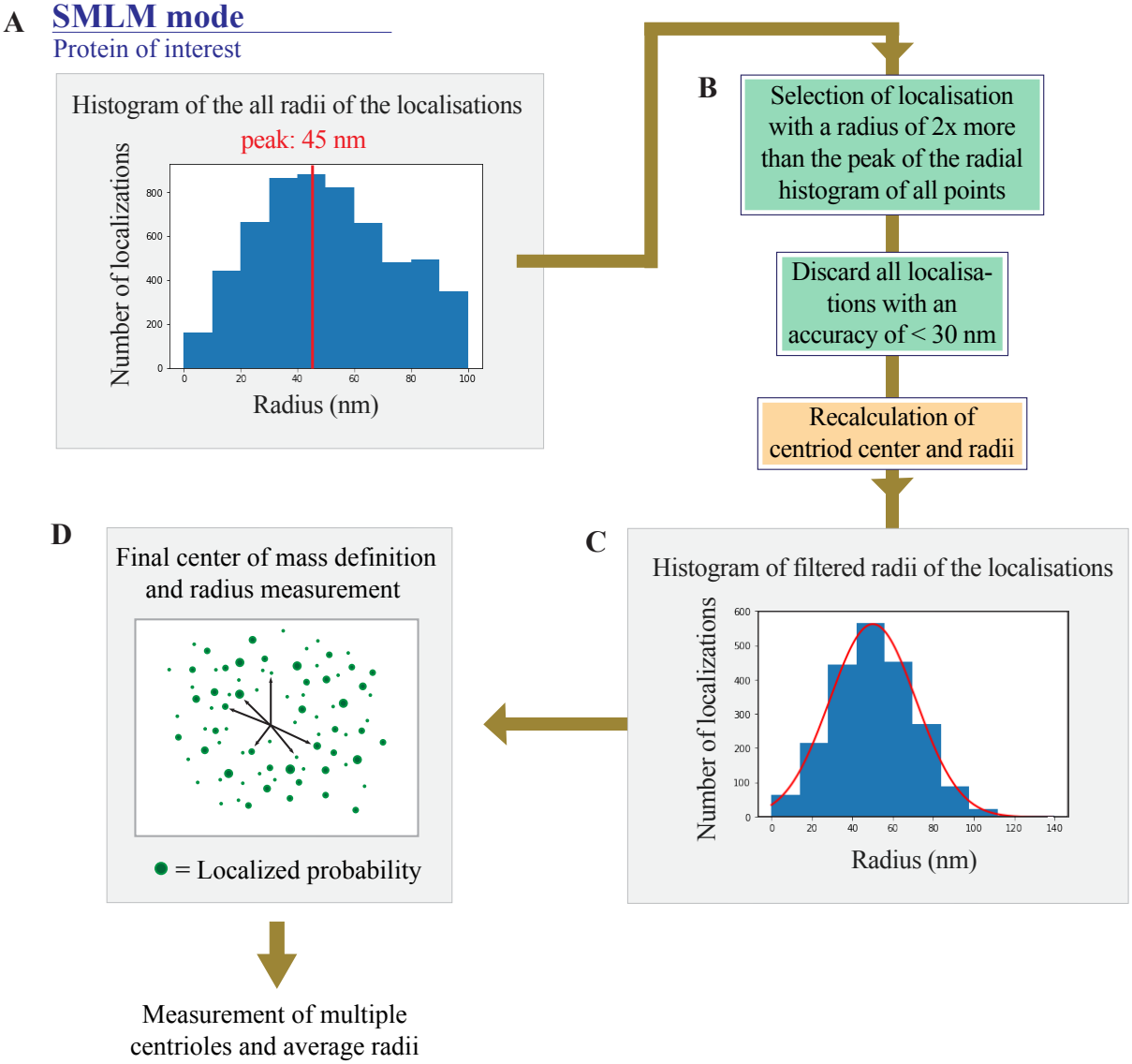


Figure 4.6: Summary of the data processing and the calculation of the radii of the SMLM data. A) The initial histogram displaying the number of localisations present at different distances (radii) from the SMLM centroid. The peak of the radii is indicated with a red line. **B**) Data quality control was performed: only localisations that lie with in the 2x the peak radii were used, that had a localisation precision of <30 nm; centrioles had to have more than 10 localisations meeting these criteria to be included in the analysis. **C**) The resulting, final histogram containing only the refined localisations after the final centroid calculation. **D**) Schematic representation of the weighted radius calculation using the refined localisation points (the size of each individual dot illustrates its relative weighting).

all the data sets for each protein terminus (**Figure 4.6D**). Heat maps were generated for each protein examined by aligning the centres of all the centroids measured and plotting all the localisations on one image, shown alongside a manually aligned images showing a representative SIM/SMLM centriole for each protein terminal of interest (**Figure 4.7B**).

4.2.2.1. 3D-SIM/SMLM proof of principle using Asl

To assess the potential accuracy of this analysis pipeline, I analysed data collected from flies expressing YFP-Asl that I analysed by 3D-SIM with antibodies specific for the N-terminal region of Asl (Conduit et al., 2010; Roque et al., 2012) and then with SMLM using the anti-GFP Nanobodies (which also works well with YFP) (**Figure 4.8A**). Previous 3D-SIM measurements of Asl NT have shown a wide variation in the reported radii (**Figure 4.8B**); this could be due to the particular tissue studied, the number of microtubules present on centrioles (testes centrioles have microtubule triplets, whereas wing discs and S2 cells, derived from the early *Drosophila* embryo, have doublets) (Franz et al., 2013; Gottardo et al., 2017; Roque et al., 2018; Schneider, 1972), and the type of fixation processed used (Schnell et al., 2012).

My 3D-SIM measurements are most comparable with *Drosophila* S2 cells (Fu and Glover, 2012; Fu et al., 2016; Mennella et al., 2012): centrioles have microtubule doublets in both tissues. My measurements, taken from 278 individual well-oriented centrioles, appeared to be about 3-4 fold more accurate by (as judged by the standard deviation of the data) (**Figure 4.8B**). Encouragingly, the radius calculated from the SIM and SMLM data is nearly identical (0.8 nm difference, s.d. differing by 3.3 nm), and, interestingly, the accuracy of the SIM data is higher than the SMLM data. This is

A

Protein	Centrioles selected	Centrioles measured	Total number of localisations	Number of localisations used
GFP-Sas-6	94	49	4170	1237
Ana2-GFP	136	66	11750	4744
Sas-6-GFP	102	46	11113	4091
GFP-Ana2	98	37	8525	2651
eSas-4-GFP	198	102	18332	8811
UbqSas-4-GFP	47	19	2796	1170
YFP-Asl	127	91	22023	12245

B

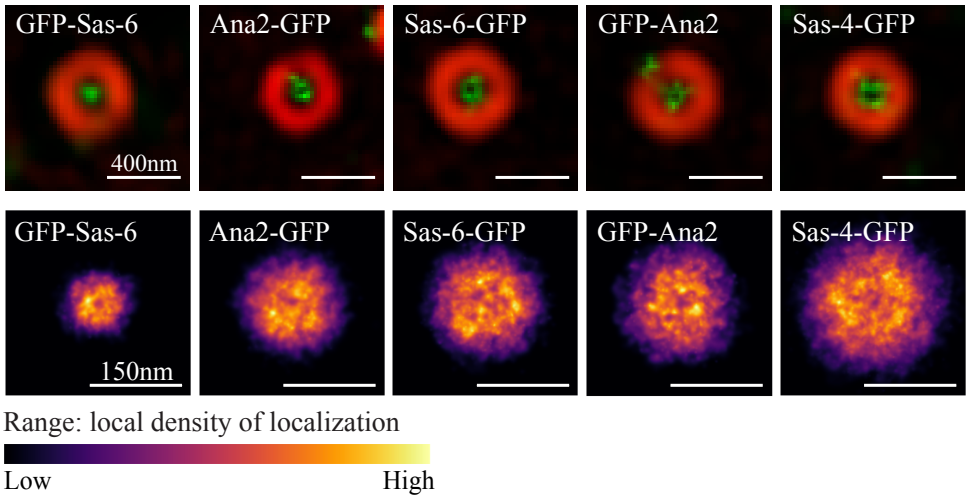


Figure 4.7: Calculations of the radial distribution of several centriole proteins. A) A table summarizes the number of centrioles and localisations initially obtained and then finally used for the calculation of radial distance for each fusion-protein. **B**) Panels show examples of aligned Asl 3D-SIM (red) and the corresponding SMLM (green) images of the various protein termini (upper panels). Merged heatmaps of all the SMLM localisations analysed for each GFP fusion are also shown (lower panels).

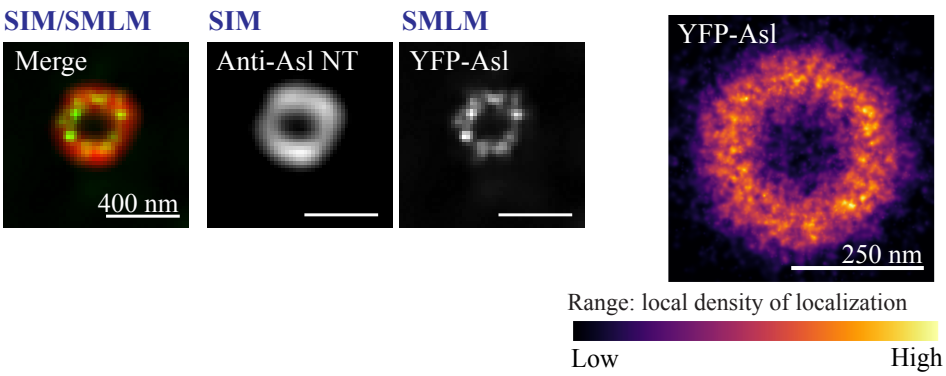
likely to be due to the fact that when imaging with SIM, all fluorophores are sampled, giving a more accurate estimation of fluorophore distribution, whereas only a subset of fluorophores are sampled in the SMLM imaging. However the accuracy of my SIM measurement of the Asl NT radius is not as precise as a previous measurement taken in primary spermatocytes (Wegel et al., 2016) (**Figure 4.8B**). This is probably because the centrioles in primary spermatocytes are much longer than the centrioles in wing disc cells, allowing one to measure the radius at multiple points along the length of a single centriole.

4.2.3. Precise localisation of the centriole cartwheel proteins

Using the pipeline described above, I was able to calculate the average radii of the SMLM localisations for each GFP-fusion. Representative images (**Figure 4.7B, upper panels**), show how different protein termini localise to differently sized toroids, and this is further supported by the size of the heat maps generated by the localisations used to generate the final average radii (**Figure 4.7B, lower panels**). I confirmed that all the localisation data for each protein termini were normally distributed by using a Gaussian fit. The final average radial distance (± the s.d.) of each GFP-fused protein terminus is shown in **Figure 4.9A**. The toroids measured range from 26.7 nm for GFP-Sas-6 to 64.1 nm for Sas-4-GFP with a high precision of ±3.78 nm-5.18 nm. These radii were superimposed on an outline of the cryo-ET generated *Trichonympha* cartwheel (Guichard et al., 2013) (**Figure 4.9B**). The approximate size of the GFP and the Nanobody were indicated with a light colour box, indicating the range in which the true protein termini are likely to lie.

Several aspects of these data suggest that they are likely to give an accurate representation of the relative radial positions of the protein termini examined (with

A



B

	Protein	Tissue	n	Mean radius (nm)	s.d. (nm)	ref.
SIM	anti-Asl NT	Wing discs	278	145.4	5.5	*This work*
	anti-Asl NT	S2 cells	21	138	15	Mennella et al., 2012
	anti-Asl	D.Mel-2 cells		170	20	Fu & Glover, 2012
	anti-Asl NT	S2 cells	15	182	16	Fu et al, 2016
	anti-Asl NT	Testes	30	266	66.2	Saurya et al., 2016
	anti-Asl NT	Testes		176.5	2.8	Wegel et al., 2016
SMLM	Asl NT	Wing discs	91	144.7	8.8	*This work*
	anti-Asl NT	Testes	30	172	2.7	Wegel et al., 2016

Figure 4.8: Precise localisation of the N-terminus of Asl using SIM and SMLM. A) Panels show the aligned 3D-SIM (red) and SMLM data (green) of Asl (left three panels) and a merged heatmap of all the localisation measured in the SMLM radii calculation (right panel). **B**) A table comparing the Asl SIM measurements obtained in my studies to those obtained in previous publications. This table also shows the radius of the N-terminal Asl protein calculated separately from the 3D-SIM and SMLM data in this work, which only differ by 3.3 nm (judged by the standard deviation (s.d.)).

some caveats, see discussion below). These data strongly suggest, therefore, that both the N- and C-terminal regions of Ana2 are located towards the outer region of the cartwheel (close to where the C-terminal region of Sas-6 is located), with the N-terminal region of Ana2 being slightly more displaced towards the inner cartwheel hub than the C-terminal region. This has some interesting consequences in thinking about how Ana2 might function in cartwheel assembly (see discussion below).

A possible criticism of my analysis is that some proteins were analysed using lines that expressed an GFP-fusion from its endogenous promoter, while others were analysed using lines that expressed the GFP-fusion from the Ubq-promoter — that tends to lead to the overexpression of these proteins by ~3-5x compared to the endogenous protein (Lee et al., 1988). Western blots performed previously demonstrated that Ubq-Sas-4-GFP is moderately overexpressed when compared to the eSas-4-GFP line used in this study (Cottee et al., 2013; Novak et al., 2014). I suspected that this was unlikely to be a major problem because the centriole and cartwheel are highly structured, and so the relative position of the proteins within the structure was unlikely to be significantly affected by the overexpression of any individual protein in the cytoplasm. However, to test whether this was the case, I compared the localisation of Sas-4-GFP expressed either from its endogenous promoter or from the Ubq-promoter (as these lines were already available in the laboratory). The average radial distance of Sas-4-GFP calculated from both lines was only ~2.3 nm different, and this difference was not statistically significant (**Figure 4.10**). Thus, at least for Sas-4, the centriolar localisation of the C-terminal region of the protein does not appear to be affected by its overexpression in the cytoplasm.

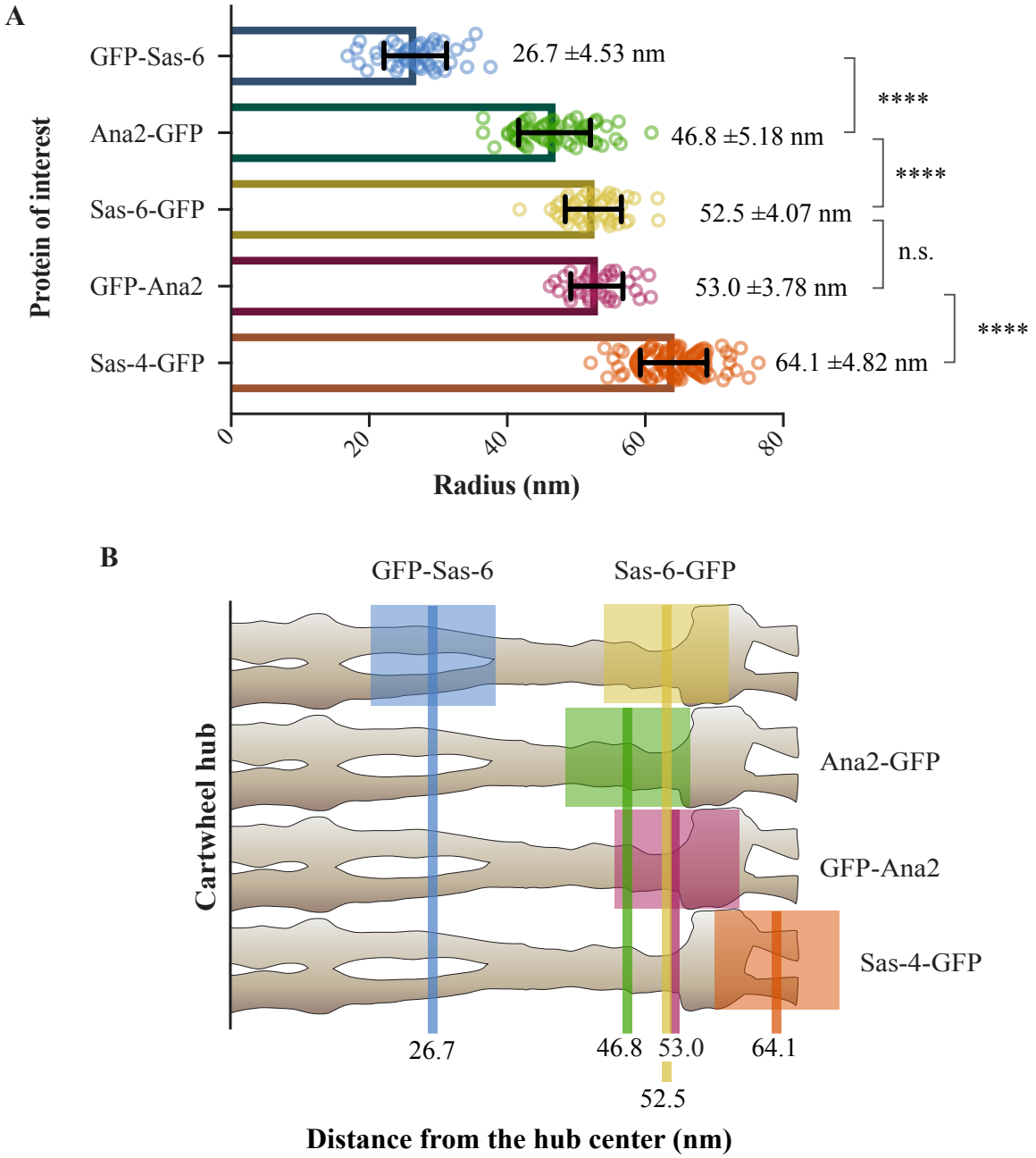


Figure 4.9: The N- and C-termini of Ana2 are located towards the periphery of the cartwheel. A) The bar chart indicates the mean radii (± s.d.) of the SMLM localisation data analysed for each GFP-fusion protein. The differences are statistically significant (unpaired T-test) for all proteins, except for Sas-6-GFP and GFP-Ana2 which differ by only 0.5 nm. The indicated error bars represent the s.d.. **B**) Schematic shows the mean radial distribution of each protein (solid vertical lines) superimposed on a cartoon of the EM-density calculated from the Trichonympha cartwheel structure (brown); the cartwheel hub is to the left. The possible range of locations of the true protein termini is indicated by the lighter coloured boxes around each line.

4.3. Discussion

In this Chapter, my collaborators and I set out to establish methods to combine the power of 3D-SIM and SMLM to measure the precise position of tagged proteins within the highly structured centriole. We used 3D-SIM to identify mother centrioles that were appropriately oriented for our analysis, and to accurately calculate the centroid position of these centrioles. We then used this information to iteratively calculate the centroid of the much sparser SMLM data for individually tagged centriole proteins, and then calculated the average distance of each protein from the centroid. This allowed us to position proteins within the centriole with a precision (standard deviation) of just ± ~4-5 nm. These methods allowed us to confirm with light microscopy that Sas-6 is organized with its N-terminus towards the central hub and its C-terminus towards the periphery of the cartwheel. More importantly, they allowed us to position the N- and C-terminal regions of Ana2 within the cartwheel, indicating that both termini of Ana2 are located close to the C-terminal region of Sas-6 at the periphery of the cartwheel.

Before I discuss the implications of these findings, it is important to point out that this analysis pipeline is likely to inherently overestimate the average radial distance. This is because non-specific "background" localisations are increasingly likely to be encountered as one moves outward from the centre of the centroid—simply because the area in which background is present increases as the radius increases. This means that the non-specific background is not evenly distributed, and this will skew the radial distance measurements to more distant measurements. This problem becomes more pronounced as the radial distance of the protein becomes smaller; thus, this problem is more acute for the GFP-Sas-6 measurements (that have the smallest

average radii) than for the Sas-4-GFP measurements (that have the largest average radii). This may help explain why our radial distance measurement of the N-terminally-tagged GFP-Sas-6 protein appears to be too large and is not congruent with other measurements. EM and cryo-ET data (Guichard et al., 2013; Guichard et al., 2017; van Breugel et al., 2011) and crystallography studies (Cottee et al., 2015; Kitagawa et al., 2011; van Breugel et al., 2011), for example, strongly suggests that the radius of the inner cartwheel, which is almost certainly formed by the N-terminal region of Sas-6, is ~12 nm whereas my measurements suggest that the N-terminal domain of Sas-6 resides at a radius of ~27 nm ±4.53 nm. Nevertheless, my measurements are similar to those Hamel and colleagues calculated using a 3D-SIM/STORM approach in *Chlamydomonas* basal bodies (Hamel et al., 2014). Even if I allow for the size of the GFP and the anti-GFP Nanobody (about ~7.5 nm in total), I would get a radius of ~19.5 nm. It will be necessary to perform a similar analysis with other proteins that have a very small radius to test if this overestimation of the size of small objects is indeed a general problem associated with our methodology.

My data reveal, for the first time, the location and orientation of Ana2 within the centriole. Ana2 appears to be located on the outer region of the cartwheel, with its C-terminus slightly further towards the centre of the cartwheel than the N-terminus. Although the average distance between the N- and C-termini is small (~6 nm), it is highly significant (P<0.0001), illustrating the potential power of our method. This localisation is consistent with the N-terminus of Ana2 interacting with the C-terminus of Sas-4 at the cartwheel periphery (Cottee et al., 2013), and also with data indicating that in worms, the C-terminal region of *C. elegans* SAS-5 interacts with the central coiled-coil region of SAS-6 (although the interacting regions of Sas-6 and Ana2/STIL

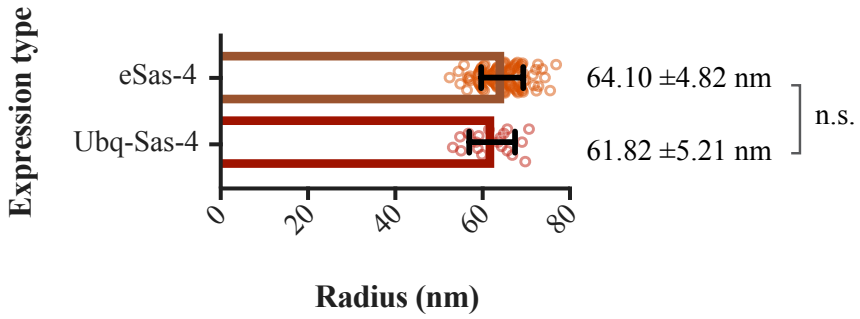


Figure 4.10: Fusion-protein expression levels do not affect the localisation of Sas-4-mGFP. Comparison of the calculated mean radii (± s.d.) of Sas-4-GFP expressed at endogenous levels (eSas-4-GFP) and moderately overexpressed (Ubq-Sas-4-GFP). There is no statistical difference between the two measurements (unpaired T-test; *P*=0.0641). The indicated error bars represent the s.d..

homologues generally remain poorly characterized)(Leidel et al., 2005). These findings suggest that it is unlikely that Ana2 is responsible for the Cartwheel Inner Density observed in *Trichonympha* using cryo-ET (Guichard et al., 2012).

My findings suggest that Ana2 is likely to promote cartwheel assembly with Sas-6 through interaction at the cartwheel spokes, not the hub. This would suggest a likely model for the Ana2-Sas-6 interaction as shown in **Figure 4.3B**, in which both the C-terminal STAN domain — that promotes the interaction with Sas-6 (Dzhindzhev et al., 2014; Moyer et al., 2015; Ohta et al., 2014)— and the N-terminal CR2 domain — that promotes the interaction with Sas-4/CPAP (Cottee et al., 2013)— are located towards the periphery of the Sas-6 cartwheel. As Ana2 appears to be a tetramer (Cottee et al., 2015), these data would suggest that four Ana2 molecules could bridge and fix two of the Sas-6 cartwheels rings together, and thus stabilize the cartwheel. In the EM tomograms of the cartwheel, there is some additional density within the central cartwheel hub (Guichard et al., 2013); my data suggest that this additional density is unlikely to come from Ana2. More density is seen around the spokes of the cartwheel, making the presence of other proteins, such as Ana2, more likely (Guichard et al., 2013). My data suggest that the models A and C (**Figure 4.3A,C**) are unlikely, as the C-terminus of Ana2 appears to be only 6.2 nm more proximal to the Sas-6 hub than the N-terminus. Even with the true protein termini possibly being ~7.5 nm away from the calculated radius, the C-terminus of Ana2 would not be able to span to the cartwheel hub. Model D (**Figure 4.3D**), on the other hand, cannot be ruled out. To date, however, no EM or cryo-ET data (Guichard et al., 2013; Guichard et al., 2017) have shown densities in the space between two Sas-6 cartwheel units. If Ana2 is flexible and dynamic, its density and, thus, location, may not be detected. It will be

important to perform similarly detailed EM and ET images of centrioles in other organisms, as to date they have only been performed in *Trichonympha* and *Chlamydomonas*. It is possible that the organisation of Ana2 may differ in other organisms.

With certain modifications to the microscope set up, this correlative 3D-SIM/SMLM imaging and processing pipeline could provide more insight in to centriole biology. First, the addition of a new hardware component, such as a cylindrical lens, could allow one to collect SMLM data in the *z* dimension as well; the axial resolution of 3D-SMLM that one can achieve has been reported to be 20-50 nm (Huang et al., 2008). This would allow one to identify the position that proteins occupy along the length of the centriole. For example, it would be possible to establish if centrioles always have the same proximal-distal orientation with respect to the apical and basal surface of the tissue, such as wing discs and the early *Drosophila* embryo. Establishing centriole orientation within a tissue may streamline the investigation into proteins likely to influence and/or define the orientation. Additionally, 3D-SMLM would allow insight into the localisation of distal end proteins CP110, Klp10A, Cep104 and Cep97. These proteins have been found to be critical for controlling the centriole cartwheel length and microtubule length (Delgehyr et al., 2012; Franz et al., 2013; Jiang et al., 2012; Satish Tammana et al., 2013; Spektor et al., 2007). The precise relative localisation of distal appendage proteins has been established using 3D-dSTORM in human basal bodies at the cilium (Yang et al., 2018); this study has refined the structure of basal body appendages and also provided insight into their function. It would be interesting and insightful to apply a similar approach to distal end proteins located on the centrioles in *Drosophila*.

Second, being able to perform two-coloured SMLM could be advantageous by allowing one to directly assess the relationship between two different proteins at the same time. Finally, using new protein labelling technology, such as the SNAP-tag system, one would be able to detect fluorescent signals closer to the actual protein termini; however this improvement would only be ~2 nm (which is the size of the Nanobody). Therefore, it is probably not worth pursuing, as it would require the generation of new transgenic flies.

4.3.1. Future Directions

One of the drawbacks of fluorescence microscopy is the lack of cellular context; this method only provides information related to the specific subset of labelled proteins. In contrast, EM provides cellular context by providing ultra structural information that is not limited to a specific protein tag (Ellisman et al., 2012). Therefore, either a combined light microscopy and EM (CLEM) approach or an EM approach that relies on genetic tags for protein labelling might provide more insight into the localisation of proteins within the centriole, as it would allow one to precisely map the proteins (or their termini) on to the EM centriole cartwheel structure.

For a CLEM approach, it is now possible to perform the imaging with proteins tagged with standard fluorescent proteins (such as GFP) (Johnson et al., 2015). The average single molecule localisation accuracy reported was ~17 nm, which is comparable to my 3D-SIM/SMLM precision. Additionally, this approach would allow the use of GFP tagged flies use in my 3D-SIM/SMLM study and eliminate the need to generate new transgenic flies. However, using genetic protein tags that generate contrast during EM sample preparation can be advantageous. These tags include: miniSOG (Shu et al., 2011), a small fluorescent protein which generates mass densities when exposed

to light and diaminobenzidine, thus generating clear and precise localisation information; APEX (Martell et al., 2012), a peroxidase which withstands strong EM fixation and generates mass density upon addition of daminobenzidine and peroxide, and which also generates very precise labelling in tissues when viewed with EM. The recent advances in the genetic labelling technology for CLEM or EM would allow deeper and higher resolution insight into the localisation of the centriole cartwheel proteins in the context of the centriole.

5. SAPs as a model for centriole and centrosome biogenesis

5.1. Introduction

Mass-spectrometry-based proteomic studies of purified centrosomes have revealed that these organelles consist of hundreds of unique proteins (Andersen et al., 2003; Keller et al., 2005; Muller et al., 2010). In a series of elegant experiments, just a few of these proteins were shown to be essential for centriole assembly in *C. elegans* (Delattre et al., 2006; Pelletier et al., 2006). This led to the identification of homologs and orthologous of the *C. elegans* proteins that were found to also be essential for centriole assembly in other organisms; to date there are five essential proteins, named Sak, Sas-4, Sas-6, Ana2 and Asl, that have been shown to be essential for centriole assembly in *Drosophila* (Basto et al., 2006; Bettencourt-Dias et al., 2005; Blachon et al., 2008; Dobbelaere et al., 2008; Goshima et al., 2007; Leidel et al., 2005; Peel et al., 2007; Stevens et al., 2010a). However, the detailed study of the centriole assembly pathway requires one to study the centriole biogenesis in the absence of key proteins or protein domains. As mutations in the essential centriole assembly genes leads to the complete absence of centrioles, the study of the assembly pathway is problematic. Furthermore, the *Drosophila* embryo is a powerful system with which to study centriole and centrosome assembly, but key players in the centrosome assembly pathway—such as Spd-2 and Asl (Conduit et al., 2015b)—cannot easily be studied in embryos because mutations in their genes lead to a failure in embryonic development (Bonaccorsi et al., 1998; Dix and Raff, 2007; Giansanti et al., 2008). Thus, new methods are required to allow one to study these assembly pathways in the powerful fly embryo model.

It has previously been shown that moderate co-overexpression of two key centriole cartwheel proteins—GFP-Ana2 and GFP-Sas-6—leads to the formation of large macromolecular structures named Sas-6-Ana2-Particles (SAPs) (Stevens et al., 2010b). In spermatocytes, SAPs form large round structures that are composed of many tubules (SAS-tubules) that have a highly ordered ultrastructure that resembles the central cartwheel. These SAPs recruit several other centriole proteins, but they do not detectably recruit any PCM components (Stevens et al., 2010b).

In unfertilized *Drosophila* eggs (where there are no centrioles naturally present—(Mahowald and J.M., 1970; Riparbelli and Callaini, 2003; Rodrigues-Martins et al., 2007b)), large SAPs are formed, and, although these do not appear to have the highly ordered ultrastructure visible in spermatocyte SAPs (Vicente, 2013), they can recruit several PCM proteins. Previous work by a former PhD student in the laboratory, Dr. C. Vicente, showed that SAPs are surprisingly similar to centrioles and centrosomes. Specifically, they are able to recruit other centriole and centrosome proteins, their PCM seems functional and is able to respond to cell cycle cues. Thus, although these SAPs cannot divide or duplicate like centrioles, they form independently of any pre-existing centriole, and so they may be useful tools with which to study the centriole and centrosome assembly pathways (Vicente, 2013). In this Chapter, I further characterize these SAPs, and I use them to address several important questions about the centriole and centrosome assembly pathways.

5.1.1. Key findings

I show that SAPs recruit and organize several centriole and centrosome proteins in a very similar way to how these proteins are organized at *bona fide* centrosomes. I show that SAP assembly requires all the known protein-protein interactions that are

required for centriole assembly. I show that in the absence of Asl, the proteins Spd-2 and Cnn can still be recruited to SAPs, although at lower levels, indicating the presence of an alternative PCM recruitment pathway that does not require Asl. Finally, I examine the contribution of the key centriole assembly proteins, Sak, Sas-4 and Asl, to SAP assembly. Surprisingly, I find that Sak is dispensable in SAP assembly, while Sas-4 is essential; Asl is not essential for SAP assembly, but the process is less efficient in its absence. These observations potentially have important implications for our understanding of centriole and centrosome assembly.

5.2. Results

5.2.1. Centriole and centrosome proteins display a strikingly similar organization at SAPs and at bona fide centrioles/centrosomes

Previous work using standard confocal fluorescence microscopy has shown that SAPs in eggs recruit several centriole and centrosome proteins (Stevens et al., 2010a; Vicente, 2013). However, the precise localisation of these proteins had not been studied, as super-resolution microscopy was not available at the time of these earlier studies. It has previously been shown that several centriole and centrosome proteins are organised in concentric toroids around the centriole cartwheel (Fu and Glover, 2012; Lawo et al., 2012; Mennella et al., 2014; Mennella et al., 2012; Sonnen et al., 2012). Such a super-resolution investigation on SAPs would provide insight into whether the organization of these proteins at SAPs and centrioles/centrosomes was similar.

In order to address this question, I used previously described Ubq-GFP-Ana2 (Stevens et al., 2010a), Ubq-GFP-Sas-6 (Peel et al., 2007) lines to generate SAPs.

These fusion-proteins can rescue the centriole defect in their respective mutant phenotypes (Cottee et al., 2013; Peel et al., 2007). The relatively moderate overexpression (~5-10X) of these two proteins (**Figure 5.1**) in flies leads to the formation of SAPs. I used unfertilized *Drosophila* eggs for all the studies regarding SAPs as eggs contain no naturally occurring centrioles (Riparbelli and Callaini, 2003; Rodrigues-Martins et al., 2007b; Vicente, 2013). I confirmed that the co-expression of GFP-Ana2 and GFP-Sas-6 is required for the formation of SAPs in eggs (**Figure 5.2A,B**). As these eggs contain no endogenous centrioles, I can be sure that all the signal or staining in eggs is due to SAPs.

I imaged SAPs in eggs on the OMX V3 3D-SIM system (see 2.5.2.3). I used only eggs that were 0-2hrs old, as I observed that the SAPs seemed to change shape and become less round over time (presumably because the unfertilized eggs are starting to deteriorate). They appear to be spherical and hollow when very young (0-2 hrs old) (**Figure 5.2C**) and begin to deform into misshaped blobs as the SAPs age (3+ hrs old) (**Figure 5.2D**).

To investigate the distribution of centriole and centrosome proteins, I fixed and stained the SAP eggs with various antibodies (see 2.4.1.1 and 2.4.4). As a control I also monitored the distribution of these proteins at *bona fide* centrioles in fixed embryos expressing just Sas-6-GFP (as these embryos form centrioles labelled with Sas-6-GFP, but they do not form SAPs because Ana2-GFP is not overexpressed). All eggs and embryos were stained with a fluorophore conjugated Nanobody coupled to an Atto488 dye (Chromotek GmbH, Raff Stock #166). All other centriole and centrosome proteins were probed using primary antibodies listed in Table 5. Eggs and

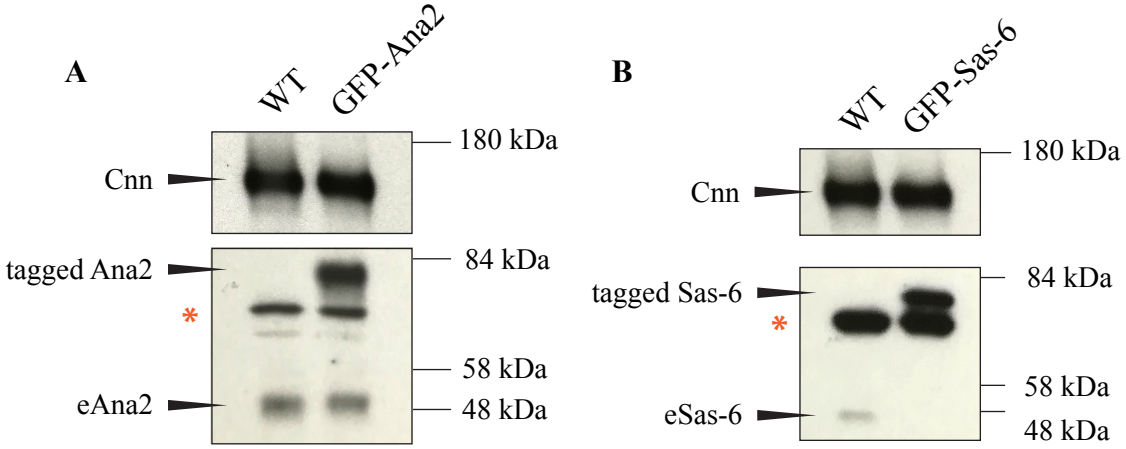


Figure 5.1: The co-overexpression of Sas-6 and Ana2 leads to SAP formation. A) A western blot showing the expression levels of the fusion-protein GFP-Ana2 in transgenic flies; each lane contains 10 early embryos. The embryos express one copy of the transgene in the presence of two copies of the endogenous WT gene. Endogenous Ana2 (eAna2), tagged Ana2 and Cnn (loading control) are indicated by the arrowheads. The red star indicates notable non-specific bands. **B**) A western blot showing the expression levels of the fusion-protein GFP-Sas-6 in transgenic flies; each lane contains 10 early embryos. These embryos express two copies of the transgene in the presence of one copy of the endogenous WT gene. Endogenous Sas-6 (eSas-6), tagged Sas-6 and Cnn are indicated by the arrowheads. The red star indicates notable non-specific bands. It is interesting to note that eSas-6 appears to be down-regulated in the presence of GFP-Sas-6.

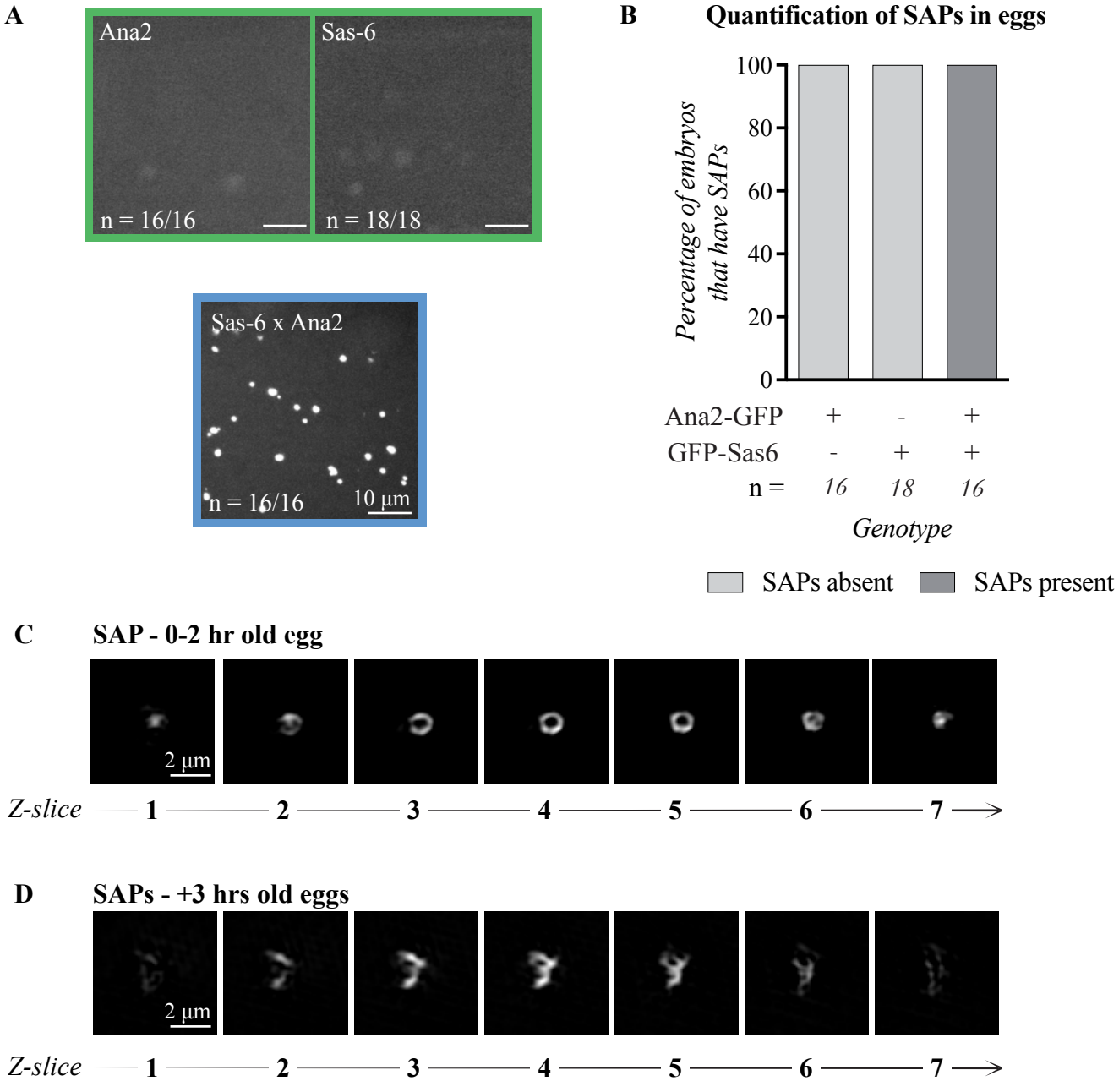


Figure 5.2: SAPs in Drosophila eggs. A) Confocal images taken in 0-3 hour old eggs expressing either GFP-Ana2 or GFP-Sas-6 (top) or both (bottom). SAPs only form upon the co-overexpression of mGFP-Ana2 and mGFP-Sas-6. The fraction of eggs exhibiting the phenotype shown is indicated in the bottom left hand corner of each image. **B**) Quantification of presence of SAPs in eggs that express either mGFP-Ana2, GFP-Sas-6 or both (quantification of data shown in (**A**)). **C**) A representative stack (0.125 µm/slice) of 3D-SIM images were taken under 488 nm excitation of a SAP in a 0-2 hrs old egg. These images demonstrate that these SAPs appear hollow in eggs. **D**) A representative stack (0.125 µm/slice) of 3D-SIM images were taken under 488 nm excitation of a SAP in a +3 hr old egg. The SAP appears to deform as the eggs age.

embryos were subsequently stained with appropriated secondary antibodies (see 2.4.4). 3D-SIM images were obtained from eggs or embryos for each protein, and these images were analysed as outlined in **Figure 5.3**.

To calculate the protein distribution as a function of the radial distance from the centre of the centriole or SAP, I used the Radial Profile analysis plugin in ImageJ (see 2.5.6.2 for more details). This analysis method measures the intensity of the signal in concentric rings around a defined centre (schematically illustrated in **Figure 5.3C)**. First, the centre of the centriole and the SAP were measured by centre of mass calculation. Second, for centrioles, the peak intensity value of the centriole dot was taken as position zero; for SAPs the centre of the hollow sphere was calculated, and the middle of the outer ring of GFP signal was taken as position zero. This generated radial profiles as illustrated in **Figure 5.3D, E**. Using these methods, I showed that SAPs and centrioles recruit similar proteins, (**Figure 5.3A,B**; **Figure 5.4**), and appear to organize them in a broadly similar manner (**Figure 5.3.D,E** and **Figure 5.5**). The protein localise to the highly similar toroids in SAPs and in centrioles.

5.2.2. SAP assembly requires the same molecular interactions required for centriole assembly

Although SAPs are able to recruit and organize a similar set of proteins as *bona fide* centrioles, this does not prove that SAPs are a good model for studying the pathway of centriole and centrosome assembly. The size and topology of centrioles and SAPs in eggs are very different, and the SAPs in eggs do not obviously have a well-organized cartwheel-like structure as is seen in the SAPs in spermatocytes (Stevens et al., 2010b; Vicente, 2013), raising the possibility that these SAPs may be

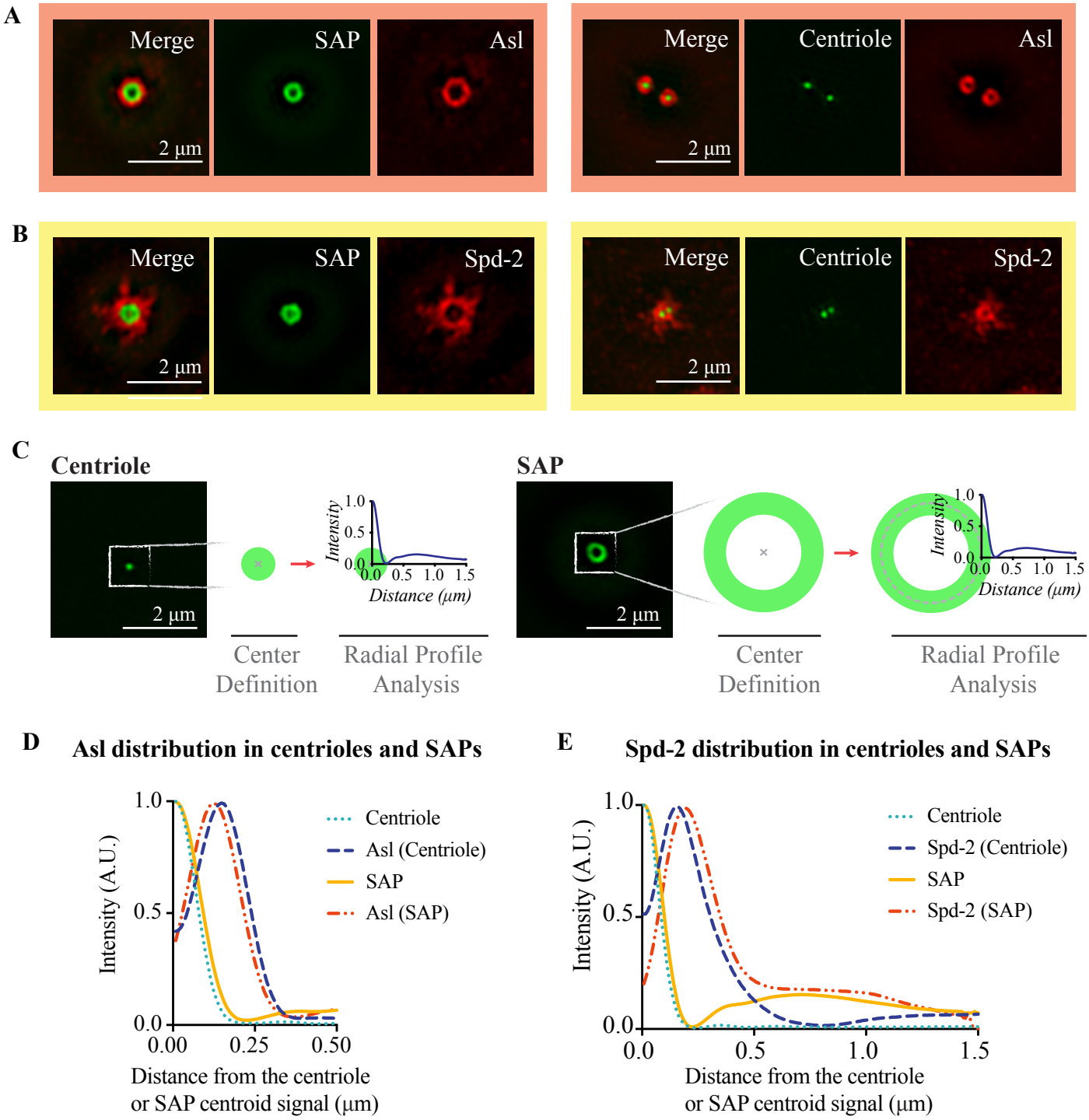


Figure 5.3: Centriole and centrosome protein organization at SAPs and centrioles. A) Representative 3D-SIM image of Asl localization (red, 593 nm excitation) around a SAP in eggs (left, green, 488 nm excitation, n=4) and around a *bona fide* centriole in embryos (right, green 593 nm excitation, n=4). Note how Asl surrounds the green signal in both samples. **B**) Representative SIM image of Spd-2 localization (red, 593 nm excitation) around a SAP in eggs (left, green, 488 nm excitation, n=5) and around a *bona fide* centriole in embryos (right, green, n=5). Note how Spd-2 surrounds the green signal in both samples and flares. **C**) Schematic of radial profile analysis. The center of mass (grey cross) is defined for both centriole and SAP and the zero position of the radial profile is the peak intensity value: for *bona fide* centrioles this is the center of mass (grey cross), for SAPs this is the middle of the toroid ring signal (grey dashed line). **D**) Radial profile of Asl in SAPs and *bona fide* centrioles. A total of 10 centrioles or SAPs were measured from at least 3 different eggs or embryos. **E**) Radial profile of Spd-2 in SAPs and *bona fide* centrioles. Note the similarity between the radial profiles between SAPs and centrioles. A total of 10 centrioles or SAPs were measured from at least 3 different eggs or embryos.

disorganized aggregates of protein that simply have some residual ability to recruit centriole and centrosome proteins in a way that is not closely related to the normal pathways of centriole and centrosome assembly.

To address this issue, I tested whether any of the previously published interactions between the key centriole proteins that have been shown to be important for centriole assembly are also important for SAP assembly. In particular, I focused on the interactions between Ana2, Sas-6 and Sas-4, as several mutations and deletions in the genes encoding these proteins have been identified that lead to a failure in centriole duplication *in vivo* (summarized in **Figure 5.6**). The mutations I used were: (1) Sas-6 N-terminal head group mutation, which prevents Sas-6 dimerization and thus centriole formation (Cottee et al., 2015; Kitagawa et al., 2011; van Breugel et al., 2011); (2) the Ana2 STAN domain deletion which is thought to prevent Ana2 and Sas-6 interaction preventing centriole formation (Cottee et al., 2015); (3) the Ana2 coiled–coil deletion (ΔCC) and the coiled-coil alanine substitution (CCA), which prevent Ana2 homo-tertramerization, preventing centriole formation (Cottee et al., 2013); (4) Ana2 proline11, arginine 12 (P11,R12) substitutions to alanine, which disrupts the interaction between Ana2 and Sas-4, preventing centriole assembly (Cottee et al., 2013); (5) an R16A mutation which should not affect the Ana2/Sas-4 interaction and serves as a negative control (Dr. Matthew Cottee, personal communication); (6) several alanine or glutamic acid substitutions of either 2, 3 or 6 amino acids in the Ana2 STAN domain that are phosphorylated to promote the interaction with Sas-6—the alanine substitutions prevent phosphorylation and hinder centriole assembly, while the glutamic acid substitutions mimic phosphorylation and lead to centriole overduplication (Dzhindzhev et al., 2014).

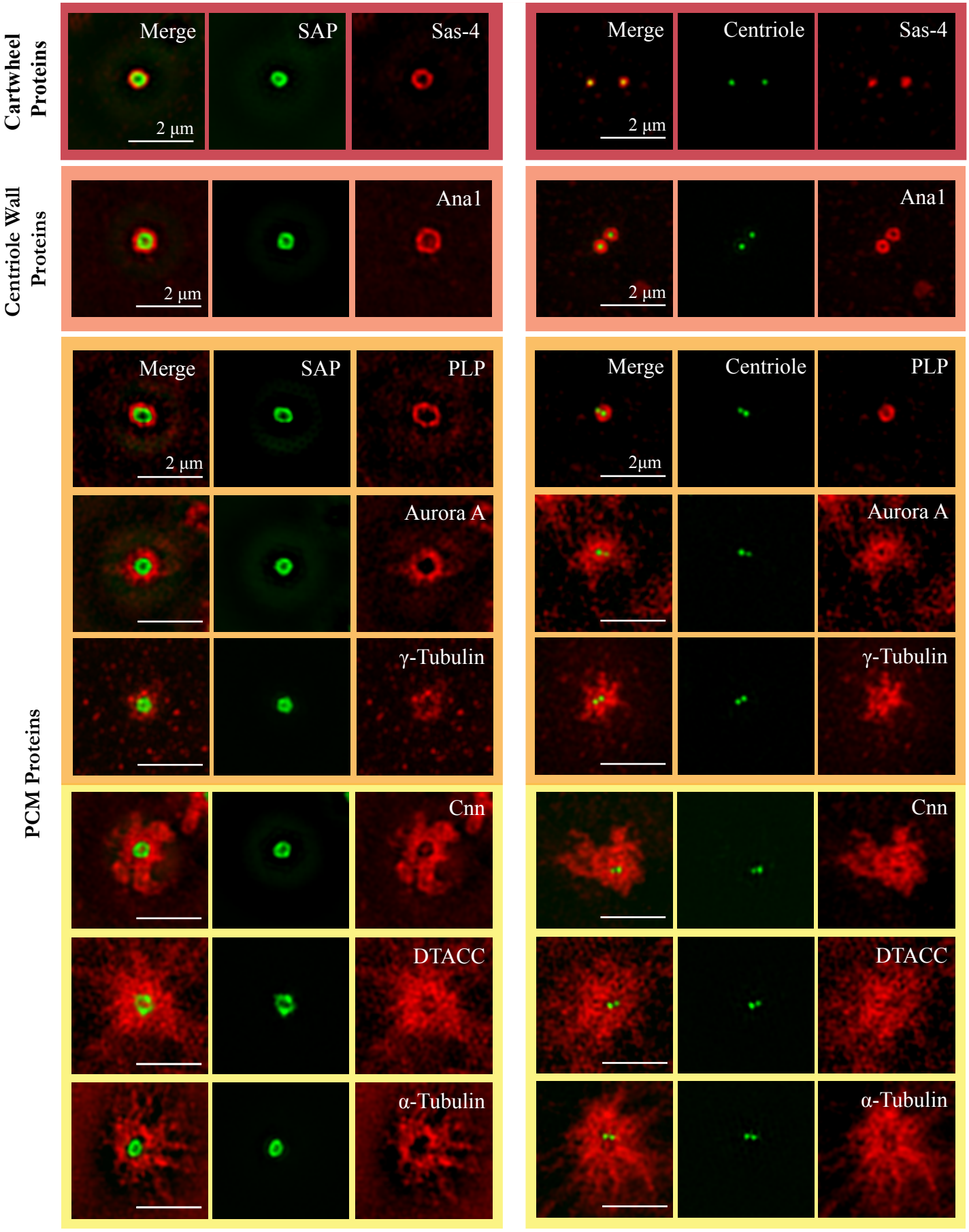


Figure 5.4: The organization of centriole and centrosome proteins is similar at centrioles and SAPs. Representative 3D-SIM images (red = 593 nm excitation, green = 488 nm excitation) of various centriole and centrosome proteins localized around SAPs (left column) and bona fide centrioles (right column), as indicated. The proteins include: cartwheel proteins: Sas-4, centriole wall protein: Ana1, and PCM proteins: PLP, Aurora A, γ-Tubulin, Cnn, DTACC and α-Tubulin. For each staining condition 4-5 eggs or embryos were imaged.

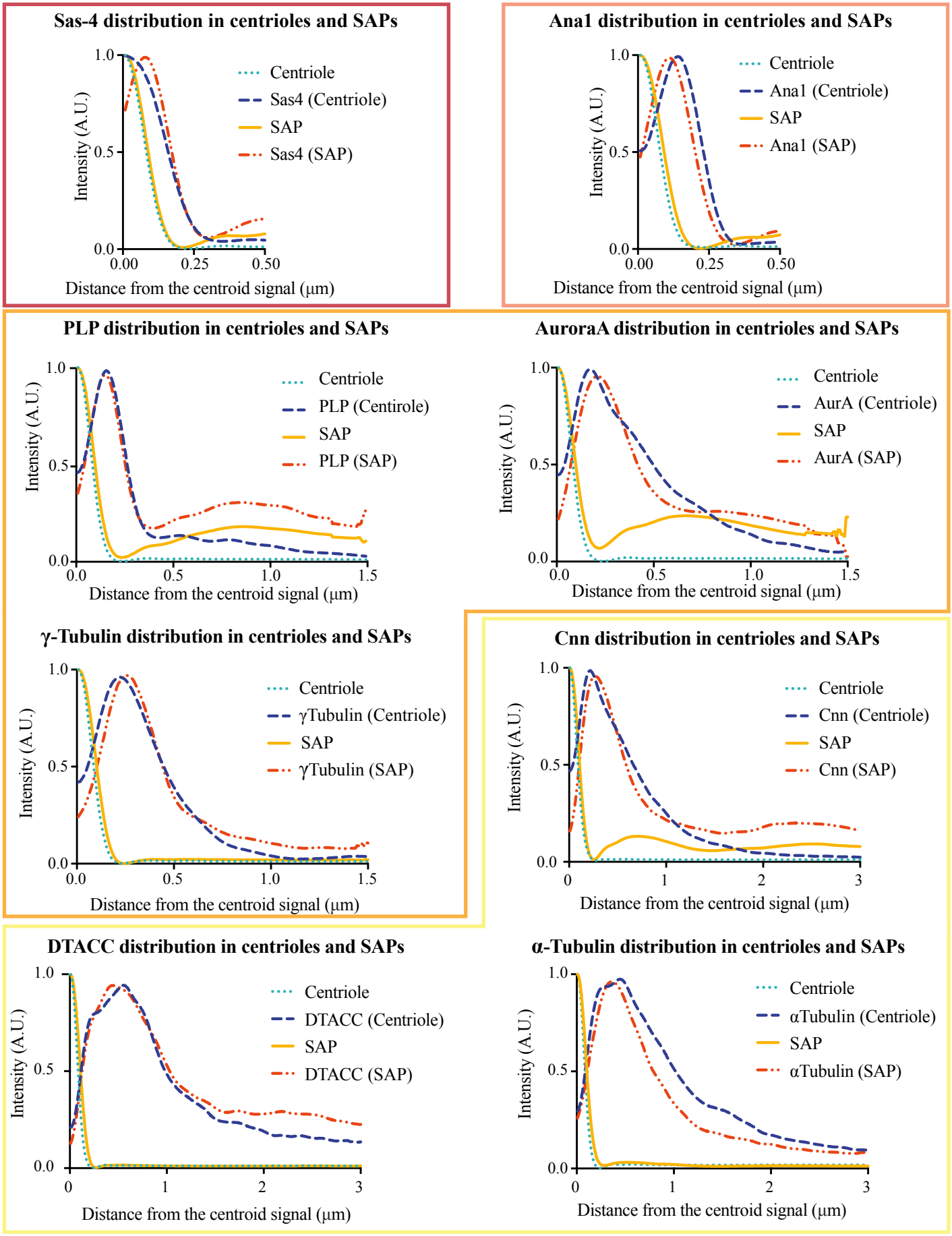


Figure 5.5: The distribution of centriole and centrosome proteins is similar between SAPs and centrioles. The radial profiles of various centriole and centrosome proteins (data taken from the analysis shown in **Figure 5.4**) in SAPs and bona fide centrioles. 10 SAPs or centrioles from at least 3 different eggs or embryos were measured for the radial profile analysis. The distribution of the proteins of interest is, in most cases, similar in SAPs and centrioles.

Therefore flies of the following genotype were use (see Table 2): Ubq-Sas-6-ΔF143D-GFP (Cottee et al., 2015), Ubq-Ana2-ΔCC-GFP (Cottee et al., 2015), Ubq-Ana2-CCA-GFP (Cottee et al., 2015), Ubq-Ana2-P11AR12A-GFP (Cottee et al., 2013), Ubq-Ana2-R16A-GFP (kind gift from Dr. Matthew Cottee), and the STAN phosphorylation substitutions: Ubq-Ana2-6A-GFP, Ubq-Ana2-6E-GFP, Ubq-Ana2-4A-GFP, Ubq-Ana2-4E-GFP, Ubq-Ana2-2A-GFP and Ubq-Ana2-2E-GFP (kind gift from Boris Sieber). These flies were then either crossed to Ubq-GFP-Ana2 (Stevens et al., 2010a) or Ubq-GFP-Sas-6 (Peel et al., 2007), as appropriate, to test if SAPs could be formed. I performed western blots to confirm the appropriate expression of the Ana2-GFP or GFP-Sas-6 mutants in eggs (**Figure 5.7** and **5.10A**). The imaging was done as described in 2.5.2 and 2.5.1.1.

I found that all mutations that interfered with Sas-6 or Ana2 self-interactions, or the deletion of the STAN domain that prevents the interaction between Sas-6 and Ana2, strongly blocked SAP assembly (**Figure 5.8**). These observations strongly suggest that SAPs are not simply random aggregates of protein, and that their assembly relies on interactions between Sas-6 and Ana2 that are also required for centriole assembly.

Interestingly, however, SAPs could still form when the interaction between Ana2 and Sas-4 was perturbed (**Figure 5.9A,B**). The Ana2 P11A,R12A mutant still formed SAPs, but these were relatively sparse and were much smaller than normal SAPs; in contrast the control R16A mutation produced SAPs that were more similar to WT (**Figure 5.9C**). These findings indicate that the interaction between Ana2 and Sas-4 can influence the efficiency of SAP assembly, but it may not be essential.

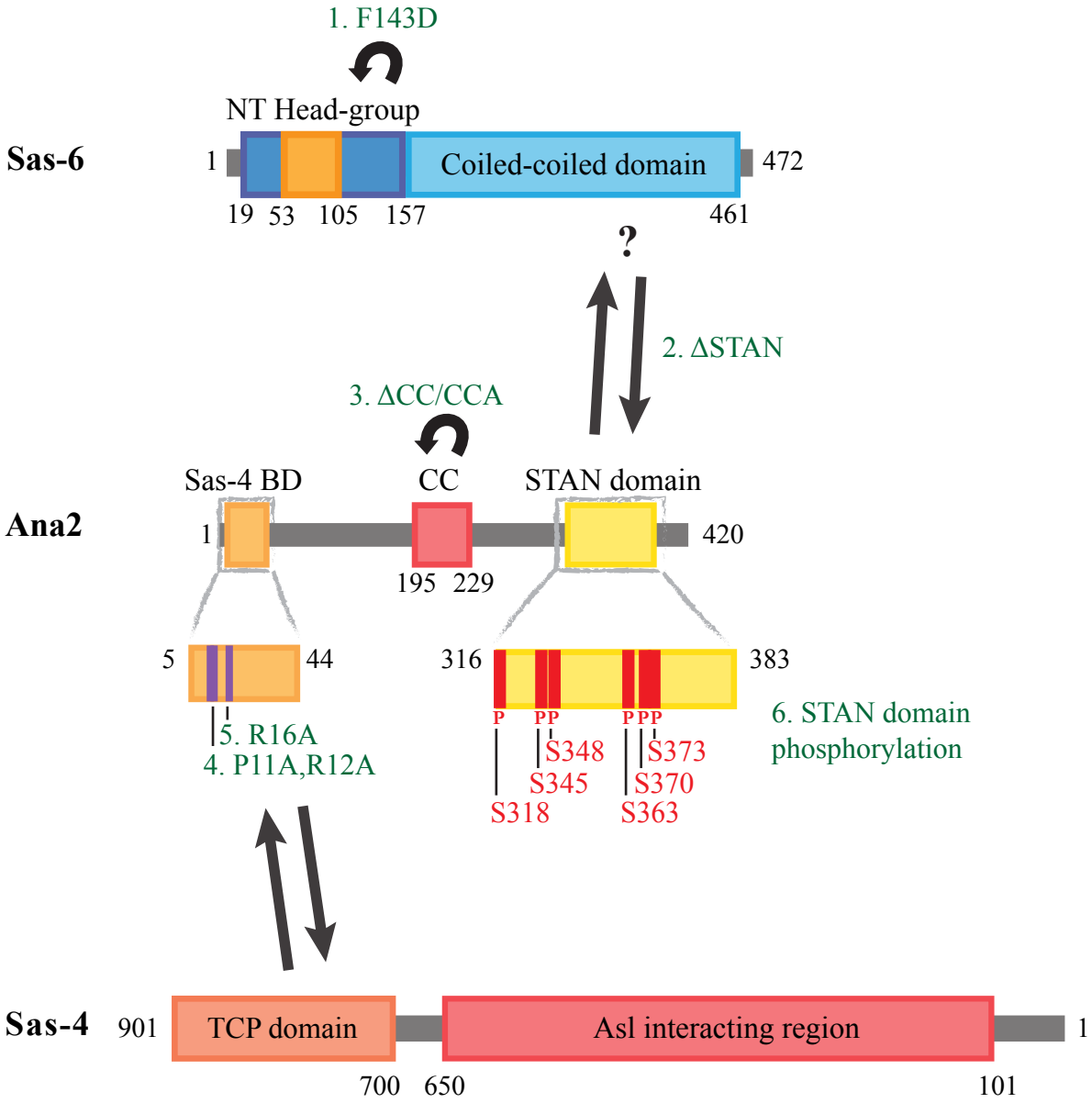


Figure 5.6: Schematic illustration of the key centriole interaction residues and domains analyzed in this study. Schematic of the proteins Sas-6, Ana2 and Sas-4 with key residues and mutations marked (labeled 1-6, as described in the main text) that lead to centriole assembly failures or centriole overduplication. For the STAN domain phosphorylation mutants: either 2 serine residues (S318, S373), 4 serine residues (S318, S363, S370, S373), or all 6 serine residues are substituted with an alanine or glutamic acid residue. The black curly arrows indicate that the residues or domains are important for self-interactions. The black straight arrows indicate that this domain is required for the interaction with another protein. Black numbers indicate amino acid number.

Alternatively, it may be that the Ana2 P11A, R12A mutation does not completely abolish the interaction with Sas-4 (see discussion below).

Most interestingly, STAN domain mutations that either blocked or mimicked phosphorylation had similar effects on SAP assembly: mutations that mimicked phosphorylation (and that promote centriole overduplication in cultured cells (Dzhindzhev et al., 2014)) led to the robust assembly of SAPs that were much bigger than normal, while mutations that blocked phosphorylation (and that inhibit centriole duplication in cultured cells (Dzhindzhev et al., 2014)) led to a dramatic reduction in the number and size of the SAPs, although SAP assembly was not completely abolished (**Figure 5.10B** and **5.11**). Thus, the assembly of SAPs seems to be promoted or inhibited by the same phosphorylation events in the STAN domain that promote or inhibit centriole assembly.

Taken together these data strongly suggest that the centriole and SAP assembly pathways rely on similar molecular mechanisms. I therefore decided to use SAPs as an assay to probe in more detail aspects of the centrosome and centriole assembly pathways.

5.2.3. Using SAPs to probe the centriole assembly pathway

Centrioles assemble upon a Sas-6/Ana2 cartwheel, while SAPs assemble around a much larger structure that is presumably formed by Sas-6 and Ana2. Therefore, I investigated what the contribution of the other core duplication proteins, Sak, Sas-4 and Asl, are in terms of facilitating the interaction of Ana2 and Sas-6 that drives SAP, and so potentially centriole, assembly.

For this analysis, I generated transgenic flies which were mutant for the gene encoding a protein of interest but expressed this gene from a neural promoter, *elav* (Campos et al., 1987; Yao and White, 1994). This allows the flies to form centrioles and cilia in their sensory neurons, so they are not uncoordinated and can feed and mate, but the rest of the fly is genetically mutant for this gene; these flies are referred to as 'cilia rescued' (Richens et al., 2015). The mutations I used for this analysis result appear to be genetic nulls or very strong hypomorphs—$sas\text{-}4^{m}$ (Basto et al., 2006), sak^{aa74} (Aydogan et al., 2018) and asl^{B46} (Baumbach et al., 2015; Novak et al., 2014). For more detail on the flies used, see section 1.1.2. I was able to confirm the absence of Asl and Sas-4 protein in these eggs by western blotting (**Figure 5.12**) (unfortunately, Sak cannot be detected in eggs or embryos by western blotting—M. Aydogan, personal communication). To examine the effect of the absence of the protein of interest on the ability of Ana2 and Sas-6 to interact and form SAPs, I utilized an mRNA injection approach (see Chapter 6 for more details and see 2.5.1, 2.3.6 and 2.5.1.1). Upon co-injection of Ana2-mNeonGreen and mNeonGreen-Sas-6 mRNA I was able to induce the formation of SAPs in >80% of WT eggs, and I confirmed that SAPs only formed efficiently when both Ana2 and Sas-6 mRNA were co-injected (**Figure 5.13**). Importantly, in this assay I found there was always a low background of SAP-like structures that were formed in ~10% of eggs injected with either mRNA alone.

I injected either *Sak*, *Sas-4* or *asl* mutant eggs, with Ana2-mNeonGreen and mNeonGreen-Sas-6 mRNA and scored the eggs for the presence of SAPs (**Figure 5.14**). As shown, SAPs form readily in *Sak* mutant eggs, but not in *Sas-4* mutant eggs (although ~10% of eggs still exhibited some SAP-like structures, potentially similar

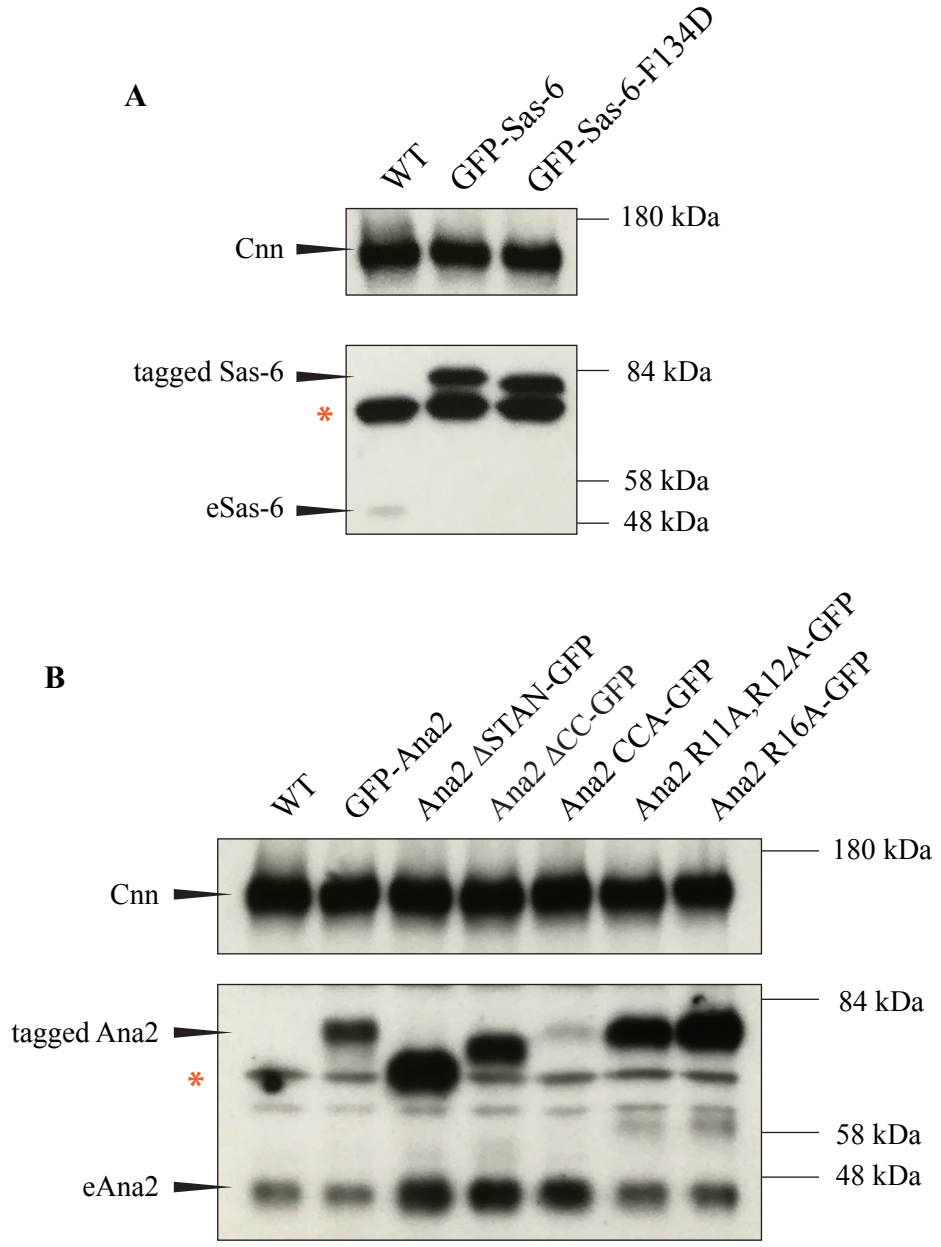


Figure 5.7: Analysis of the expression levels of mutant protein in transgenic flies. A) A western blot showing the expression levels of the fusion-protein GFP-Sas-6 in transgenic flies; each lane contains 10 early embryos. These embryos express two copies of the transgene in the presence of one copy of the endogenous WT gene. Endogenous Sas-6 (eSas-6), tagged Sas-6 and Cnn (loading control) are indicated by the arrowheads. The red star indicates notable non-specific bands. It is interesting to note that eSas-6 appears to be down-regulated in the presence of GFP-Sas-6 and GFP-Sas-6-F143D. **B**) A western blot showing the expression levels of the fusion-proteins GFP-Ana2 in transgenic flies; each lane contains 10 early embryos. These embryos express one copy of the transgene in the presence of two copies of the endogenous WT gene. Endogenous Ana2 (eAna2), tagged Ana2 and Cnn (loading control) are indicated by the arrowheads. The red star indicated notable non-specific bands. It is interesting to note that eAna2 expression appears to be upregulated in the transgenic lines that express forms of Ana2 that should not interact with Sas-6 or should not tetramerise.

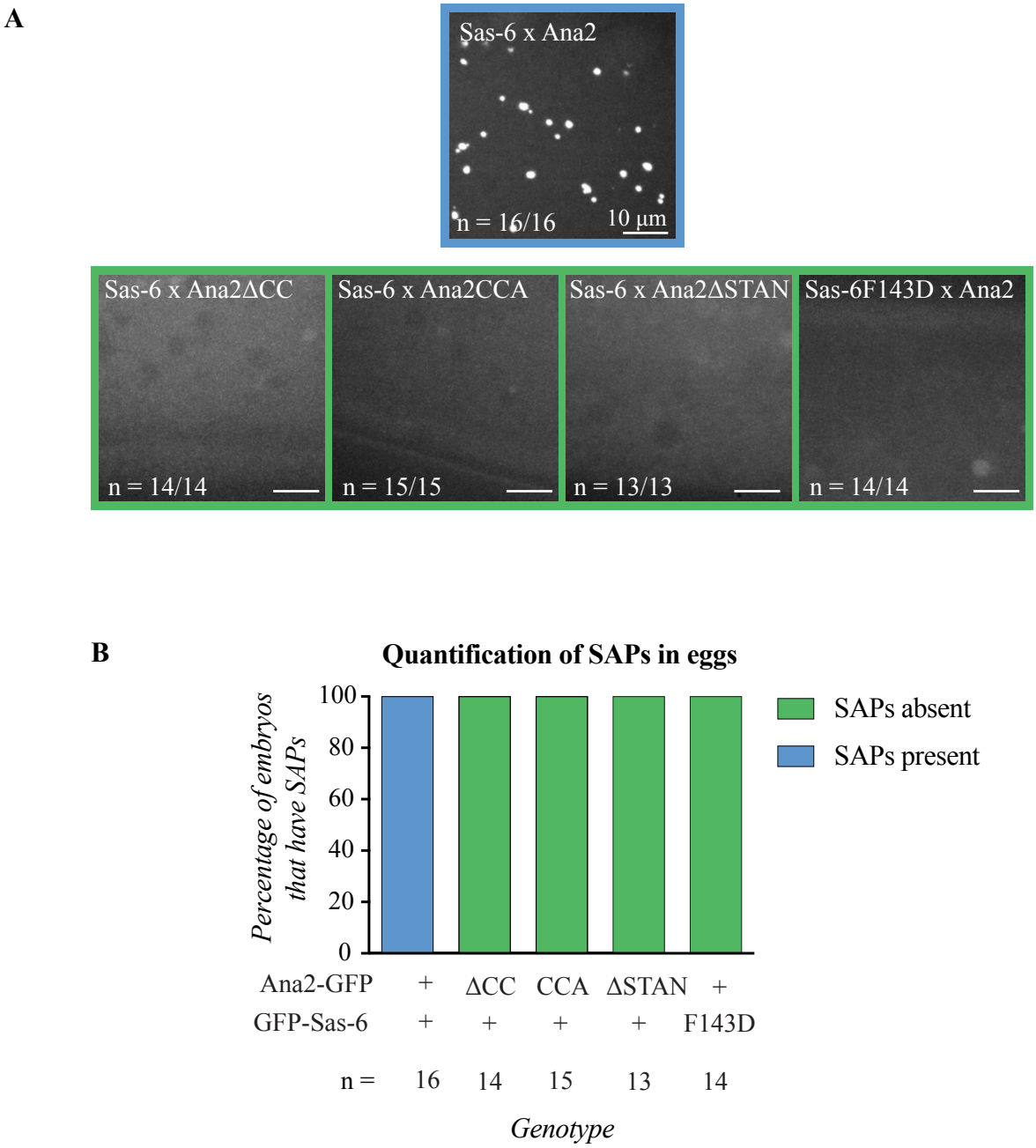


Figure 5.8: SAP assembly appears to require the same Ana2 and Sas-6 domains and residues as centriole assembly. A) Confocal images under 488 nm excitation were taken in 0-3 hr old live eggs expressing either a SAP control (GFP-Sas-6 x GFP-Ana2, top) or mGFP-Ana2 or GFP-Sas-6 with a Sas-6 or Ana2 mutant (bottom). SAPs only form upon the co-overexpression of GFP-Ana2 and GFP-Sas-6 and require the same domains and residues as are required for centriole formation. The fraction of eggs exhibiting the phenotype shown is indicated in the bottom left hand corner of each image. **B**) Quantification of the presence of SAPs in eggs laid by females of the indicated genotype (quantification of (**A**)).

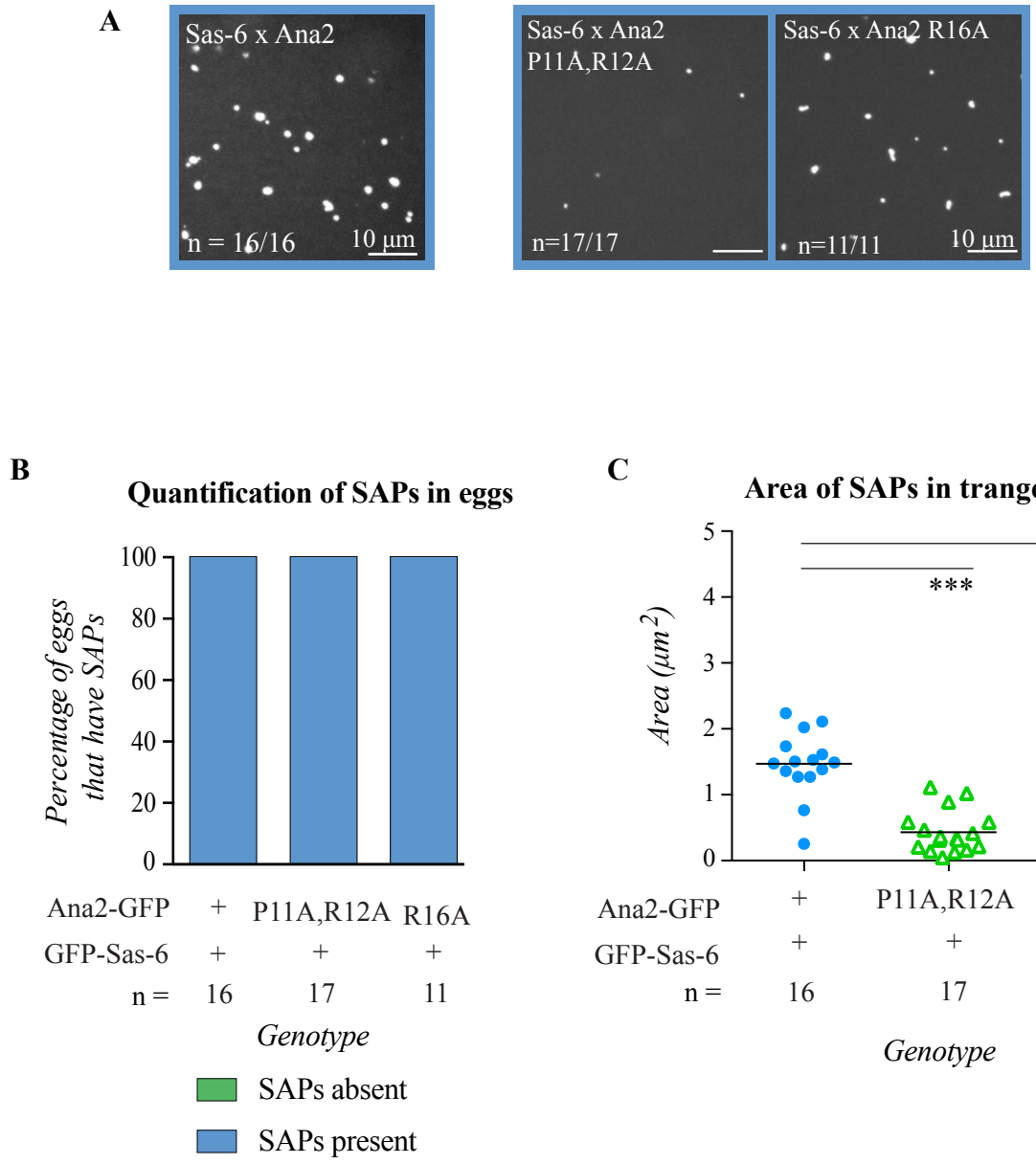


Figure 5.9: The interaction between Ana2 and Sas-4 is required for efficient SAP assembly. A) Confocal images under 488 nm excitation were taken in 0-3 hr old live eggs expressing either a SAP control (GFP-Sas-6 x GFP-Ana2, left) or GFP-Sas-6 with Ana2 P11A,R12A and R16A mutants (right). It appears that SAPs can form in the presence of both Ana2 mutants, however SAP size appears to vary. The fraction of eggs exhibiting the phenotype shown is indicated in the bottom left hand corner of each image. **B**) Quantification of the presence of SAPs in eggs of flies with the described genotype (quantification of (**A**)). **C**) Quantification of SAP size in the eggs of the described genotype. For each image, the area of each SAP in the field of view was measured and the average area was calculated and plotted. This demonstrates that even though all genoptypes form SAPs, there are significant differences in SAP size. Sas-6 x Ana2 P11A,R12A SAP are much smaller than Sas-6 x Ana2 SAPs, suggesting that these SAP from less efficiently. All data set were normally distributed according to the D'Agostino & Pearson or Shapiro-Wilk normality test and a one-way ANOVA test was used to assess statistical significance (P<0.05).

to the controls injected with either mRNA alone), while *asl* mutant eggs exhibited an intermediate phenotype.

I conclude that, perhaps surprisingly, Sak, the key kinase that initiates centriole assembly, is not actually required for Ana2 and Sas-6 to assemble into structures (SAPs) that, as discussed above, have many features in common with *bona fide* centrioles. These findings are in line with my investigation of the Ana2 STAN domain phosphorylations that also do not appear to be essential, but are important for efficient interaction (**Figure 5.10B** and **5.11**). Taken together is it likely that Sak is not required for Ana2 and Sas-6 to interact, but it has a major effect on efficiency in a centriole context. Sak may normally lower the activation energy required for this interaction, allowing temporal control over when centrioles duplicate.

Strikingly, Sas-4 seems to be essential for SAP assembly. This suggests that Ana2 and Sas-6 are unable to form higher order assemblies without Sas-4. This is consistent with data from human cells, in which Sas-6 and Ana-2 have only been found to interact when they are in the presence of Sas-4 (Tang et al., 2011). This observation may explain why it has been so hard to characterize the precise interaction between Ana2 and Sas-6, as this interaction may be unstable without Sas-4.

Interestingly, Asl, which is thought to be important for both PCM recruitment (see below) and centriole duplication (Cizmecioglu et al., 2010; Dzhindzhev et al., 2010), does seem to have strong effect on SAP assembly (**Figure 5.14**). Whatever function Asl performs in this context appears to be independent of Sak, as Sak is not required for SAP assembly. Asl interacts with Sas-4, and it was originally postulated that Asl

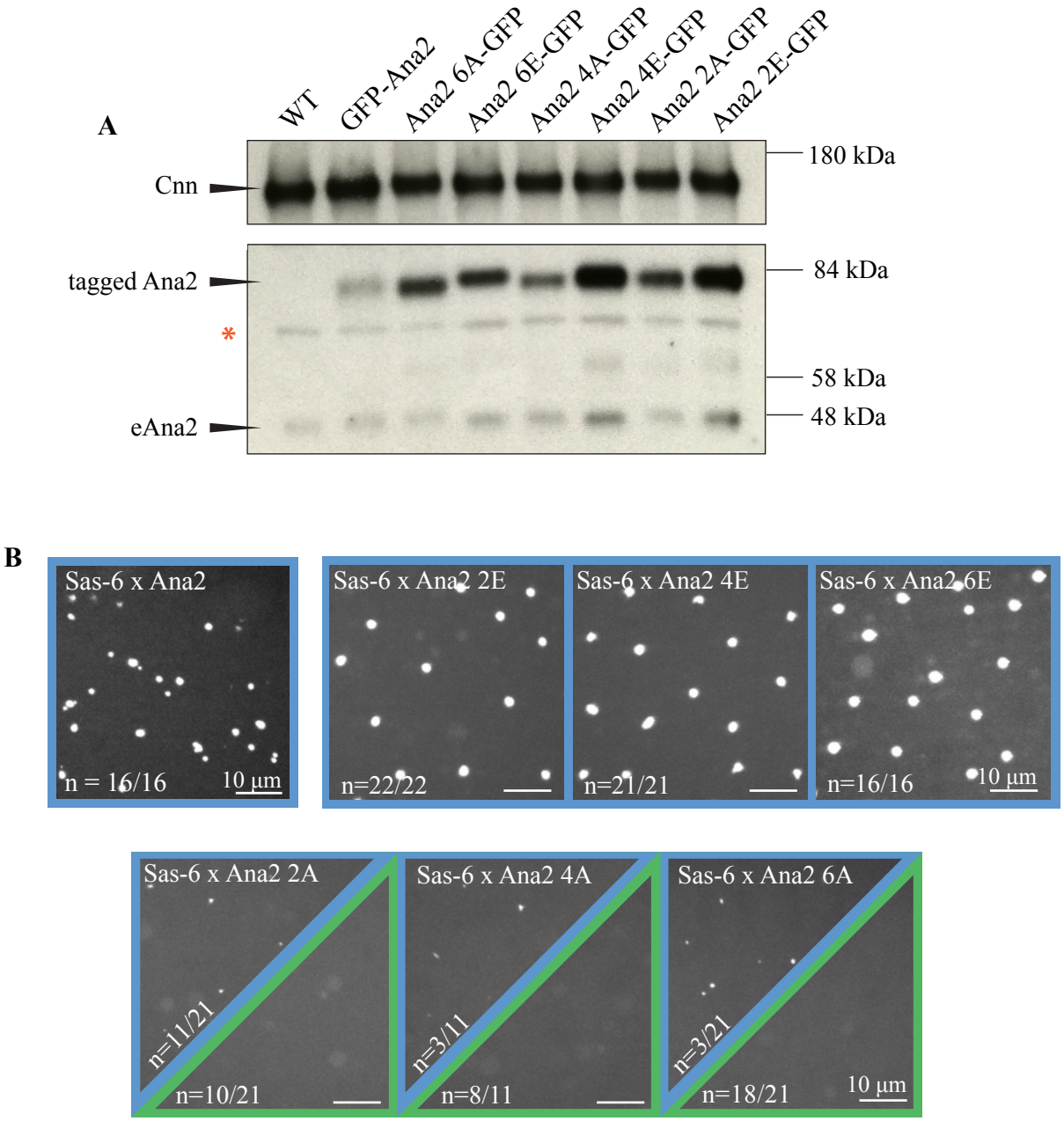


Figure 5.10: Phosphorylation of the Ana2 STAN domain is required for efficient SAP assembly. A) A western blot showing the expression levels of the fusion-proteins GFP-Ana2 in transgenic flies; each lane contains 10 early embryos. These early *Drosophila* embryos express one copy of the transgene in the presence of two copies of the endogenous WT gene. Endogenous Ana2 (eAna2), tagged Ana2 and Cnn are indicated by the arrowheads. E= glutamic acid, A= alanine. The red star indicated strong non-specific bands. **B**) Confocal images under 488 nm excitation were taken in 0-3 hr old live eggs expressing either a SAP control (GFP-Sas-6 x GFP-Ana2, top left), GFP-Sas-6 with Ana2 STAN phosphomimetic mutation (top right), GFP-Sas-6 with Ana2 STAN phosphonull mutation (bottom). As can been seen, the phosphonull containing genotypes form very small or no SAPs, whereas the phosphomimetic containing genotypes all form large SAPs. This suggests that these amino acid substitutions strongly affect the ability of SAPs to form. The egg genotype is indicated at the top of each image and the number of eggs exhibiting the phenotype shown is seen in the bottom left hand corner of each image.

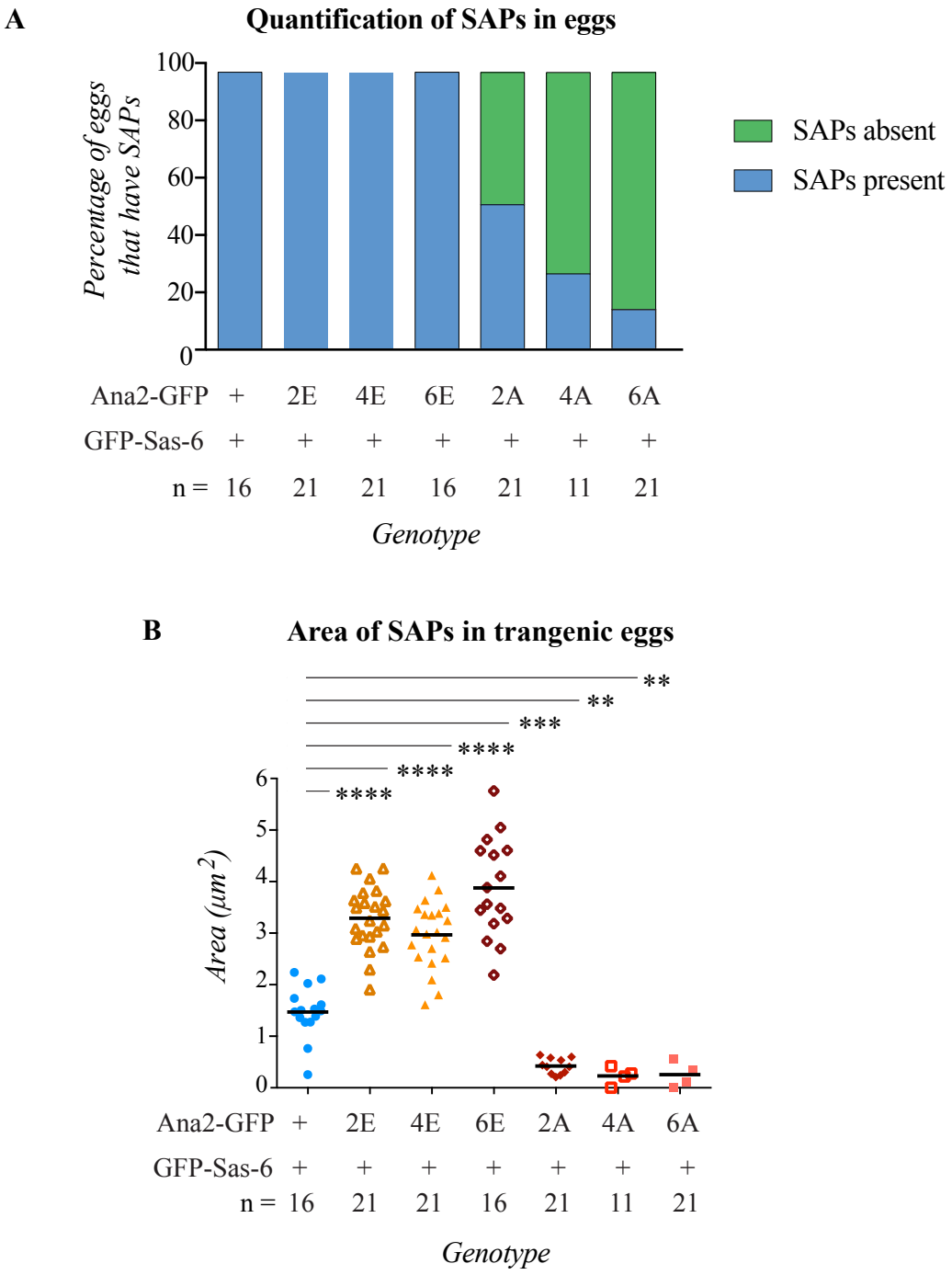


Figure 5.11: Quantification of SAP assembly when the Ana2 STAN domain is mutated. **A**) Quantification of the presence of SAPs in eggs of flies with the described genotype (quantification of **Figure 5.10B**). **B**) Quantification of SAP size in the eggs of the described genotype as shown in **5.10A**. For each image, the area of each SAP in the field of view was measured and the average area was calculated and plotted. This quantification demonstrates that phosphomimetic and phosphonull mutants facilitate or impede, respectively, the ability of Ana2 and Sas-6 to interact and form SAPs. This is reminiscent of the function of these residues in centriole assembly: phosphomimetic substitutions lead to centriole over-duplication whereas the phosphonull substitutions hinder centriole duplication (see main text for more details). All data set were normally distributed according to the D'Agostino & Pearson or Shapiro-Wilk normality test and a one-way ANOVA test was used to assess statistical significance (P<0.05).

helps recruit Sas-4 to centrioles (Cizmecioglu et al., 2010; Dzhindzhev et al., 2010). However, recent data suggests that Sas-4 may recruit Asl to centrioles in embryos (Novak et al., 2014; Novak et al., 2016). This is further supported by findings that show that Sas-4 can still be recruited to SAPs in at the absence of Asl (Vicente, 2013). My results suggest that Asl is recruited by Sas-4 and has a role in stabilizing the centriole structure.

In conclusion, I have shown that Sas-4 and Asl play a role in allowing Ana2 and Sas-6 to interact to drive SAP assembly. Sas-4 seems to be vital for this interaction in an *in vivo* setting, whereas Asl seems to have a role in stabilizing the interaction. Sak, on the other hand, does not seem to be crucial for the interaction between the two proteins, but is likely to be critical for the interaction efficiency, particularly in the context of centrioles.

5.2.4. Using SAPs to probe the pathway of centrosome assembly

The pathway of mitotic centrosome assembly in fly embryos has been extensively studied in the Raff laboratory (Conduit et al., 2010; Conduit et al., 2014a; Conduit et al., 2014b; Dix and Raff, 2007; Feng et al., 2017; Lucas and Raff, 2007). These studies have led to a model where a ring of Asl around the mother centriole initially recruits Spd-2 to the centriole, Spd-2 then recruits Cnn, and these two proteins form a scaffold around the mother centriole that recruits the other PCM proteins. Cnn cannot recruit Spd-2, but it helps to maintain Spd-2 at the centrosome, creating a positive feedback loop that drives the expansion of the mitotic PCM (Alvarez Rodrigo et al., 2018; Conduit et al., 2014b; Conduit et al., 2015b). This pathway, however, is largely derived from antibody injection studies, because *asl* and *Spd-2* mutant females do not produce developing embryos: strong *asl* mutant alleles like asl^{mecD} lack centrioles and

so flies are uncoordinated and produce no embryos (Basto et al., 2006), while weaker *asl* alleles, like asl^{1} (Varmark et al., 2007), and strong *Spd-2* alleles (Dix and Raff, 2007; Giansanti et al., 2008), have centrioles and so are viable, but they lay embryos that fail in pronuclear fusion as they cannot assemble a centrosome around the fertilizing sperm centriole. Thus, the pathway of centrosome assembly in embryos remains poorly explored genetically.

This is not a trivial problem, as several observations suggest that the pathway described may be oversimplified, and may differ in different cell types. In *Drosophila* brain cells, for example, some Cnn can be recruited to centrosomes in the absence of Spd-2, suggesting that there must be an alternative pathway of Cnn recruitment (Vicente, 2013). Moreover, the role of Asl in PCM assembly has also been disputed. Early reports suggested that *asl* has a key role in PCM assembly (Bonaccorsi et al., 1998), as asl^{1} mutants fail to recruit PCM in spermatocytes and brain cells (Bonaccorsi et al., 1998; Varmark et al., 2007). This mutant allele appears to make centrioles, but has strong PCM assembly defects (Blachon et al., 2008; Bonaccorsi et al., 1998; Varmark et al., 2007). The asl^{1} mutant was later shown to be a hypomorphic allele in which the last 140aa are missing due to a nonsense mutation (Vicente, 2013) (**Figure 5.15**). Interestingly, a stronger hypomorphic *asl* allele, asl^{mecD}, leads to failure in centriole duplication and thus mutant flies lack centrioles and cilia; asl^{mecD} contains only the first 483aa of Asl (Blachon et al., 2008) (**Figure 5.15**). However, it was observed that the stem cells located at the testes tip still contain centrioles (which are thought to be centrioles formed during early embryogenesis from the maternal contribution of Asl mRNA) and these still organized substantial amounts of PCM (Blachon et al., 2008; Galletta et al., 2016).

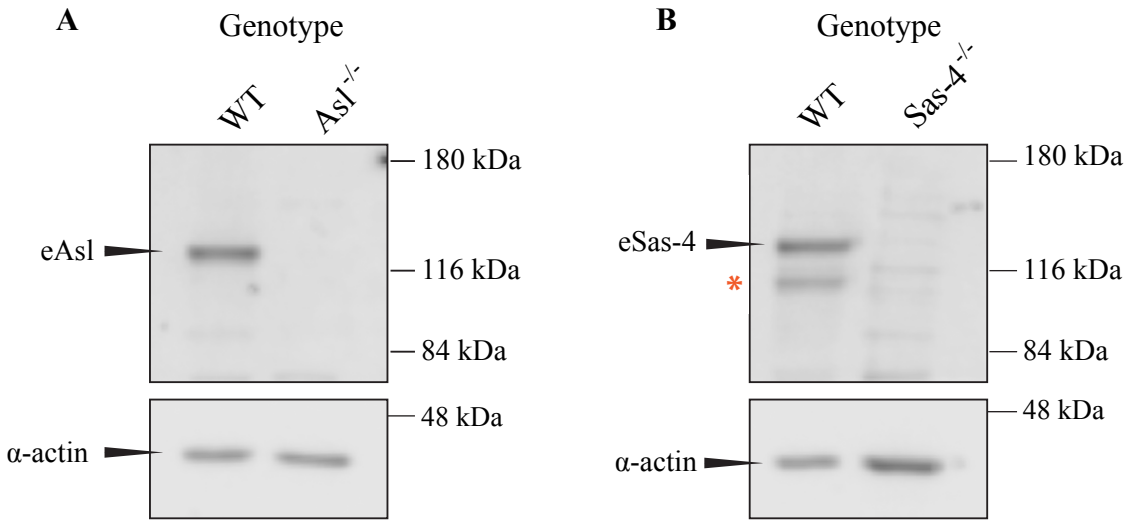


Figure 5.12: The generation of 'cilia rescue' eggs that lack Asl and Sas-4. A) A western blot of WT eggs and Asl cilia rescued eggs (denoted Asl $^{-/-}$); 10 eggs in each lane. The eggs from Asl cilia rescued flies do not contain any endogenous Asl protein. Endogenous Asl (eAsl) and α–actin (loading control) are indicated by the arrowheads. **B**) A western blot, of WT eggs and Sas-4 cilia rescued eggs (denoted Sas-4 $^{-/-}$); 10 eggs in each lane. The eggs from Sas-4 cilia rescued flies do not contain any endogenous Sas-4 protein. Endogenous Sas-4 (eSas-4) and α–actin (loading control) are indicated by the arrows**.**

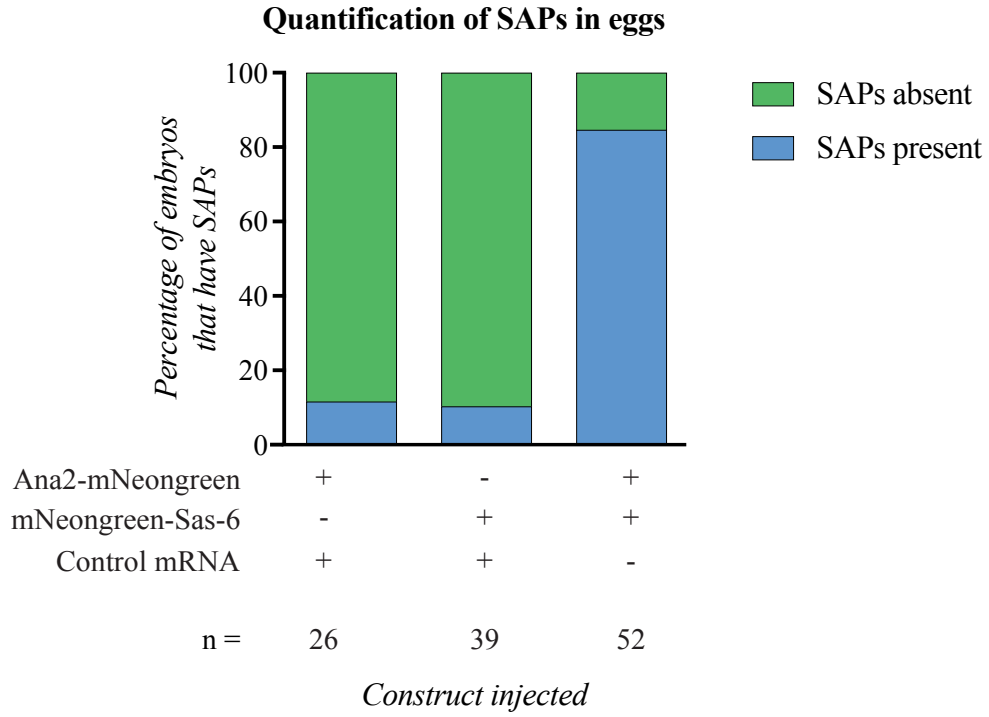


Figure 5.13: mRNA injections assay to generate SAPs. A graph showing the ability to form SAPs in eggs upon the injection of Ana2-mNeongreen or mNeongreen-Sas-6, or both. SAPs seems to form exclusively in the eggs inject with both Ana2 and Sas-6 mRNA. The percentage of eggs in which SAPs form is indicated. The number of eggs injected for each condition is shown on the bottom.

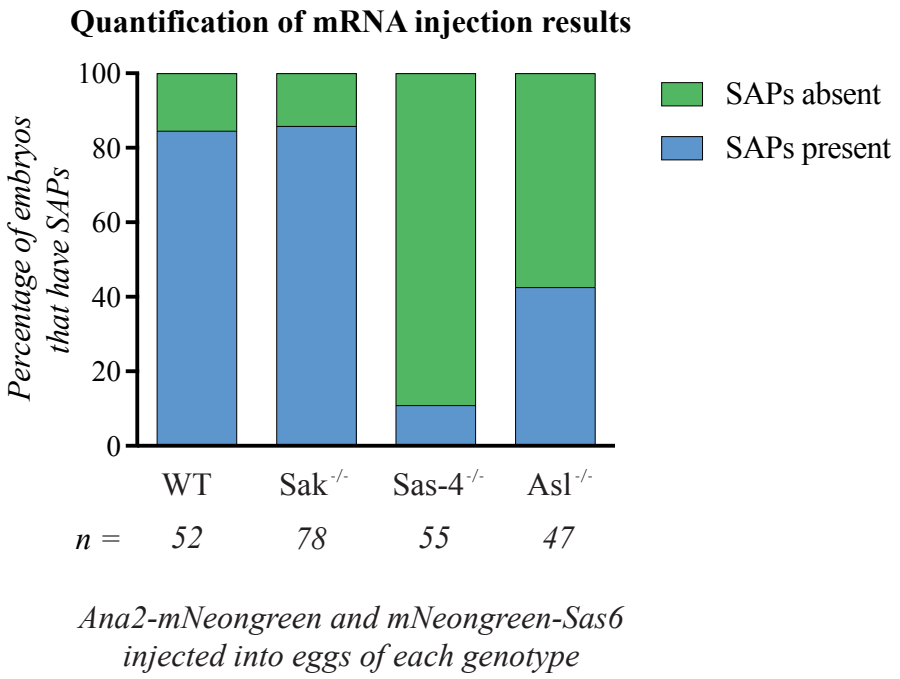


Figure 5.14: Efficient SAP assembly requires Sas-4 and Asl, but not Sak. A graph showing the percent of eggs that develop SAPs after co-injection of Ana2-mNoengreen and Sas-6-mNeongreen mRNA into eggs laid by WT females, or females mutant for *sak*, *sas-4* or *asl*, as indicated. Sak is not required for the interaction between Ana2 and Sas-6 (~86% of eggs can form SAPs, similar to WT controls), whereas Sas-4 appears to be crucial (~89% of eggs can not form SAPs). Asl seems to be important for interaction efficiency (~57% of eggs don't form SAPs). The number of eggs scored for each genotype is indicated below the chart.

SAPs provide an ideal model to examine the role of Asl in PCM recruitment as one can use Asl mutations that lead to an absence of centrioles in the fly. Using unfertilized eggs that express SAPs and the *asl*^{1} allele, it was shown that the SAPs essentially failed to recruit Spd-2 or Cnn (Vicente, 2013) (**Figure 5.16A**). This strongly supports the idea that Asl plays a major role in recruiting Spd-2 and Cnn to centrosomes, as concluded from the antibody injection experiments (Conduit et al., 2014b).

Surprisingly, however, I found that the recruitment of Spd-2 and Cnn to SAPs was perturbed, but not abolished, in eggs laid by female mutants for the stronger, null *asl*^{B46} allele (**Figure 5.16B**). Indeed, approximately half of these mutant eggs had all SAPs recruit relatively normal levels of Spd-2 and Cnn. This suggests that, in the absence of Asl, there is a relatively robust alternative pathway that can recruit Spd-2 and Cnn, but, in the presence of the truncated 854aa form of Asl produced in the *asl*^{1} allele, this pathway is suppressed. This result is discussed in more detail below

To test whether the Cnn recruited in the *asl*^{B46} eggs required Spd-2 for its recruitment to SAPs, I analysed the recruitment of Cnn in eggs laid by *asl*^{B46} and *Spd-2* double mutant females. As expected, essentially no Spd-2 was detectable at the SAPs in these eggs (data not shown), but a few eggs exhibited some residual Cnn recruitment (**Figure 5.16C**), perhaps indicating that eggs/embryos might have a relatively weak alternative pathway that can recruit some Cnn in the absence of Spd-2.

The data presented in **Figure 5.16** is preliminary, but supports previous work (Vicente, 2013). I am in the process for repeating these experiments to include all

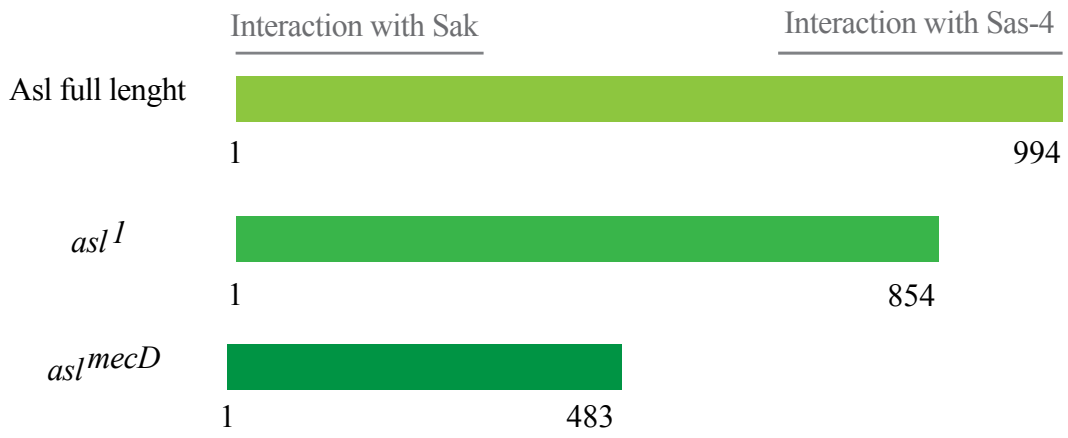


Figure 5.15: Schematic of the different Asl proteins produced by different asl mutations. Schematic illustration of the different proteins produced by WT *asl*, *asl* ^{1} and *asl* ^{mecD}. The two regions that interact with Sak and Sas-4 are indicated (grey) (adapted from Dzhindzhev et al. (2010)).

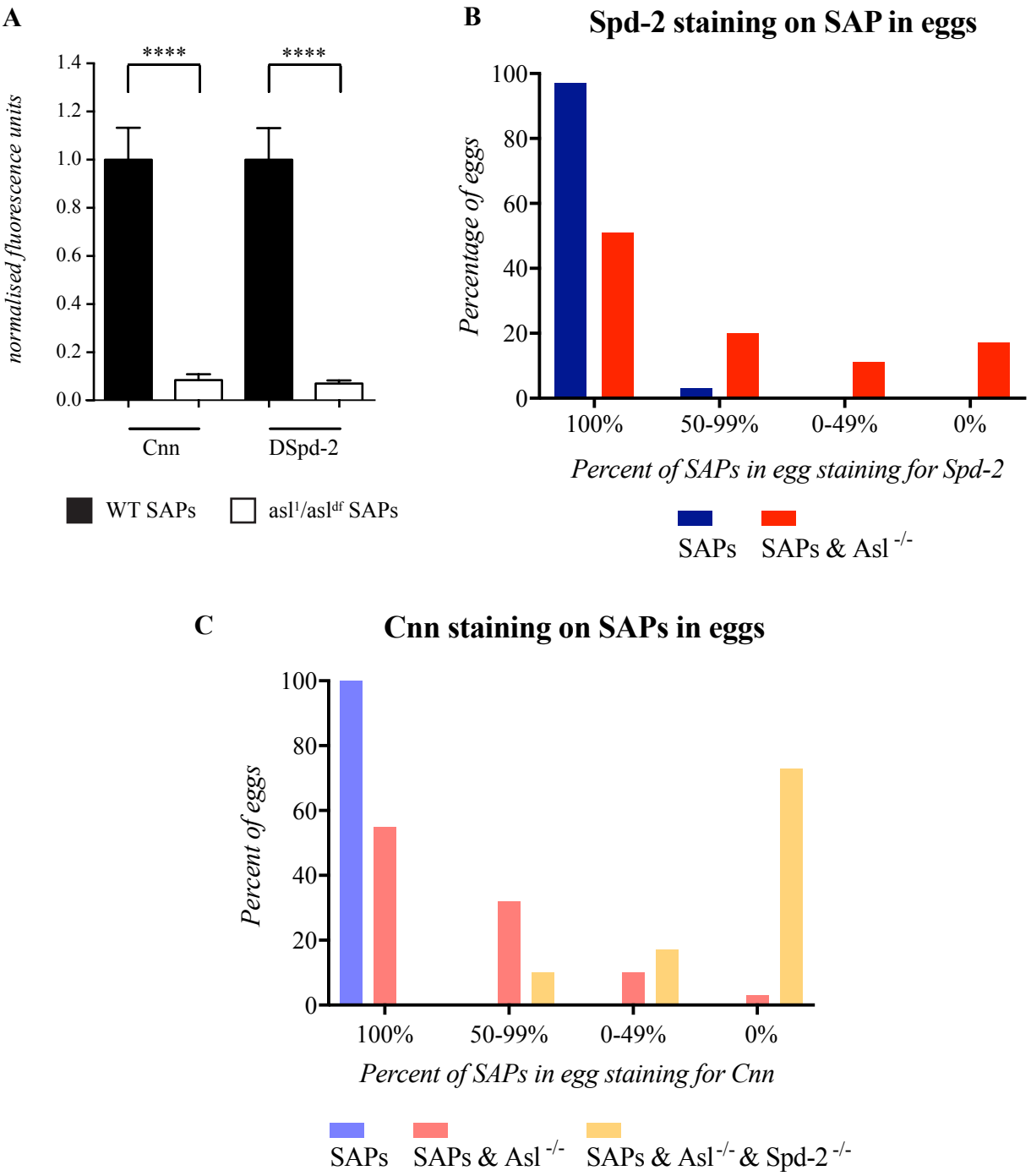


Figure 5.16: The requirement of Asl and Spd-2 in PCM recruitment. A) The degrees of Cnn and Spd-2 recruitment in *asl*^{1} mutant fly. Barely any Cnn or Spd-2 is recruited in, indicating that this *asl*^{1} mutation prevents the activation of the alternative PCM recruitment pathway. Quantification relies on SAPs measured from at least 14 different eggs. **B**) The degree of Spd-2 recruitment in SAP expression eggs (blue) and in SAP expressing eggs null for Asl (red). In each egg expressing SAPs, the amount of SAPs that recruited Spd-2 was noted. 30 eggs were analyzed for each condition. Asl does not appear to be essential for Spd-2 recruitment. **C**) The degree of Cnn recruitment by SAPs in SAP expressing eggs (purple), and in SAP expressing eggs null for Asl (pink), or null for both Asl and Spd-2 (yellow). In each egg expressing SAPs, the amount of SAPs that recruited Cnn was noted. 30 eggs were analyzed for each condition. Note that Asl is not essential for Cnn recruitment, but Spd-2 is.

genotypes of interest (the asl^{1}/asl^{df} SAP mutant I used initially was not correct and needed to be remade). Additionally, I will quantify the amount of Spd-2 and Cnn recruited to the SAPs in each genotype to establish if there are differences in recruitment.

Nevertheless, from this preliminary data I concluded that Asl is not essential to recruit Spd-2, and thus Cnn, to the PCM, and that an alternative, non-canonical PCM assembly pathway exists in *Drosophila*. However, the failure of the asl^{1} mutant to recruit Spd-2 would indicate that if certain regions of are Asl still present, the alternative assembly pathways is not activated. This suggests a model in which the known recruiters of Asl, such as Sas-4 and Cep135 (Fu et al., 2016; Novak et al., 2014), are able to inefficiently recruit Spd-2 in the absence of Asl. However, it appears that the C-terminus seems crucial: a small deletion of the C-terminus will lead to these alternative recruiters possibly being bound and stopped from recruiting Spd-2 (i.e. asl^{1}), whereas if all of Asl is deleted, Asl can no longer bind these alternative recruiters and they can then circumvent Asl in Spd-2 recruitment (i.e. asl^{B46}).

Additionally, the use of SAPs in studying PCM assembly has provided insight into the requirements of the PCM protein, Cnn. Studies preformed in *Drosophila* suggest Spd-2 is essential for Cnn recruitment (Conduit et al., 2010; Conduit et al., 2014b). It appears that Cnn recruitment is not dependent on Asl, as Cnn is recruited to some degree in 97% of eggs expressing SAP that are devoid of Asl, (**Figure 5.16C**). However, Cnn recruitment seems severely impaired in eggs expressing SAPs that are devoid of Asl and Spd-2 (**Figure 5.16C**), with only 27% of eggs showing some degree of Cnn staining. It is currently unclear what protein is responsible for this

residual recruitment. These results suggest that Cnn requires only Spd-2 for efficient recruitment.

5.3. Discussion

In this chapter I have confirmed that SAPs are very similar to centrioles and can be used to gain insight into centriole and PCM assembly. I have shown the centriole and centrosome proteins localise to strikingly similar toroids in SAPs and in centrioles and centrosomes. This super-resolution study, combined with previous data from the Raff laboratory, which showed correct Spd-2 and Cnn post-translational processing and that a SAP's PCM can respond to cell cycle cues and form mitotic spindles (Vicente, 2013), suggests that SAP PCM is genuinely functional and a valid model system.

Additionally, I have shown that SAPs require the same protein-protein interactions that are essential for centriole duplication and assembly to form. The key Ana2 and Sas-6 residues and domains that are essential for centrioles are also essential for centrioles to form. However, mutations in the Ana2/Sas-4 binding domain do not seem to be essential: P11A,R12A mutation generates small and sparse SAPs whereas the R16 control mutation produces SAPs of comparable size to normal SAPs. The two residues P11 and R12 are important for centriole duplication and are key for the interaction between the C-terminus of Sas-4 and the Ana2 Sas-4 binding domain as seen by the crystal structure (Cottee et al., 2013). Therefore there are a few possible explanations as to why SAPs still form when the P11A,R12A mutations are present. First, it is possible that the endogenous Ana2 present in the eggs is enough to help form these small SAPs. Second, other regions of Ana2 and Sas-4 may be able to bind each other, but at lower efficiency. Finally, and most likely in my opinion, it may be

that these residues are important for the efficient interaction between Ana2 and Sas-4, but are not absolutely essential, so that, when overexpressed, Ana2 can still interact with Sas-4 sufficiently to promote some residual SAP assembly. In support of this possibility, the P11A,R12A mutation can partially rescue the centriole assembly defect in *ana2* mutant brain cells, whereas deletion of the N-terminal interaction domain cannot (Cottee et al., 2013).

Similarly, my studies show that mutation of Ana2 STAN domain phosphorylation residues that would disrupt centriole formation are not essential for SAP formation. Here, the SAPs can again provide insight, as these sites seem important for Ana2 and Sas-6 interaction efficiency—as SAPs are smaller and more sparse when these sites cannot be phosphorylated, but much larger when these sites have been mutated to phospho-mimicking residues. This suggests that SAPs can provide insight into true function of certain protein domains. The conserved requirement for correct protein-protein interactions between centrioles and SAPs, suggests that SAP could be used as a model to study the role of key centriole assembly proteins.

SAPs have provided useful insights into the role of Sak, Sas-4 and Asl in facilitating Sas-6 and Ana2 assembly. In line with my previous finding on the role of the STAN domain phosphorylations, Sak is not essential for allowing Ana2 and Sas-6 to interact, but is likely to be central to controlling when Ana2 and Sas-6 interact by increasing the interaction efficiency. Therefore, Sak could function as a controller linking the centriole duplication cycle to the cell cycle. Sas-4 on the other hand, is critical to allow Sas-6 and Ana2 to stably interact. Without Sas-4, Sas-6 and Ana2 cannot assemble into SAPs. This suggests that Sas-4 may be essential for even the earliest

stages of centriole cartwheel assembly even at high concentrations. Finally, Asl seems to facilitate Ana2 and Sas-6 assembly, but it is not essential, suggesting it may be important for stabilizing the cartwheel, rather than for cartwheel assembly. Indeed, this seems almost certain to be the case as Asl protein is only incorporated into the daughter centriole as it matures into a mother centriole (Novak et al., 2014). Nevertheless, the precise roles of these proteins in the context of centriole duplication is still unclear. As SAPs do not duplicate, they are not able to shed light on this issue.

Finally, using SAPs as a model for PCM assembly, I investigated the role of Asl in the recruitment of Spd-2 and Cnn. I was able to show that in the absence of Asl, Spd-2 and Cnn are still recruited by a non-canonical PCM recruitment pathway. However, the activation of this pathway relies on the absence of the C-terminal part of Asl, as in the *asl*^{1} mutant, Spd2 and Cnn are no longer recruited. Perhaps the simplest interpretation of this finding is that the Asl^{1} protein (comprising aa1-854) is still recruited to centrioles but, because it is missing the C-terminal domain (aa854-994), it cannot recruit Spd-2 (and so Cnn), and so PCM assembly is strongly inhibited. Perhaps the *asl*^{B46} allele (which does not generate any detectable protein) can no longer be recruited to centrioles at all; this allows the protein that would normally recruit Asl to now recruit Spd-2 instead (and so Cnn). Such a scenario may sound far-fetched, but it fits the data well. Importantly, this hypothesis makes several testable predictions: (1) The C-terminal region of Asl (aa854-994) will be essential for recruiting Spd-2; (2) The middle region of Asl (aa483-854) will be essential for recruiting Asl to centrioles; (3) Whatever protein recruits Asl to centrioles—Sas-4 (Novak et al., 2014; Novak et al., 2016) and Ana1 (Fu et al., 2016; Saurya et al., 2016) are strong candidates—can also recruit Spd-2, but only in a mutually exclusive

manner. Using SAPs and a variety of transgenic mutants (of Asl, for example), it would be possible to find answers to these questions.

Additionally, I observed that Cnn requires Spd-2 for efficient recruitment, however, in the absence of Spd-2 some residual Cnn can still localise to the PCM. This is in agreement with previous reports that reduced amounts of Cnn can be recruited to centrioles in the absence of Spd-2 (Conduit et al., 2015a). The molecule(s) responsible for this residual recruitment remain to be identified, but SAPs may provide a powerful model with which to investigate this alternative pathway. For example, SAPs can still form in *Cep135* and *ana1* mutant embryos/eggs (Roque et al., 2012) (S. Saurya, personal communication) so it would be interesting to see if Cnn can still be recruited to SAPs in backgrounds in which *Spd-2* is also mutated.

In conclusion, I have shown that SAPs are a good model for studying centriole and centrosome assembly. In the next chapter, I use SAPs to screen for previously unknown protein-protein interaction and regulatory sites.

6. SAPs: a model for identifying interaction required for centriole assembly

6.1. Introduction

As outlined in Chapter 5, the study of the key centrioles proteins Sak, Asl, Ana2, Sas-6 and Sas-4 is problematic due to the absence of centrioles when the genes encoding these proteins are mutated. Even though flies without centrioles can develop and eclose, they are uncoordinated due to the lack of functioning Type I sensory neurons that rely on the presence of cilia (Jana et al., 2016), thus centrioles (Basto et al., 2006). These mutant flies are difficult to maintain as they have to be hand-fed to be kept alive, and they are unable to mate so females produce oocytes but no developing embryos (Stevens et al., 2007; Vicente, 2013). However, the selective expression of the relevant protein in just the nervous system using the *elav* promoter (Campos et al., 1987; Yao and White, 1994) can rescue the uncoordinated phenotype of the relevant mutant, making fly handling easier and allowing females to lay fertilized embryos that lack the protein of interest (Richens et al., 2015). Although these "cilia-rescued" flies can lay fertilized embryos, these fail to develop significantly as they cannot assemble centrioles (Stevens et al., 2007).

In the previous chapter, I showed that SAPs are a useful model system with which to study centriole assembly, as they require the same protein-protein interactions, and can lend insight into questions of protein-protein interaction efficiency. This makes them an interesting *in vivo* model. I showed that SAP formation could be induced by the co-injection of mRNA encoding tagged versions of Ana2 and Sas-6 into *Drosophila* eggs, so I suspected that this would also be the case in developing *Drosophila* embryos. Such an approach would potentially allow me to probe how the

SAP assembly pathway (and so by extension the centriole assembly pathway) is regulated in these rapidly dividing embryos.

The interactions that govern centriole (thus SAP) assembly appear to be highly conserved; yet, several of them are poorly understood. For example, the STAN domain of Ana2 is required for centriole assembly (Stevens et al., 2010a), but it is unclear where it interacts with Sas-6. Evidence from *C. elegans* suggests the STAN domain interacts with coiled-coil region of SAS6 (Leidel et al., 2005; Qiao et al., 2012), but it is not clear if this is conserved in other species. Additionally, phosphorylations are major players in regulating duplication. For example, Sak/Plk4 phosphorylates the Ana2 STAN domain, promoting Ana2's interaction with Sas-6 (Dzhindzhev et al., 2014; Kratz et al., 2015; McLamarrah et al., 2018). However, the precise consequence of this *in vivo*, are not fully understood. Therefore, more research is required to further understand centriole assembly *in vivo*.

In this chapter I establish and validate a SAP mRNA injection assay as a powerful, fast and efficient method to screen for protein domains and regulatory regions required for the interaction between Sas-6 and Ana2. I use this assay to identify highly conserved, but previously uncharacterised, potential Cdk1/Cyclin B phosphorylation sites in Ana2 that seem to influence the efficiency of SAP assembly. I validate these sites by generating transgenic lines and characterizing centriole assembly in these lines.

6.1.1. Key findings

I establish and validate a SAP mRNA injection assay as useful and efficient tool for identifying key, previously unknown protein domains and regulatory sites that appear

to influence centriole assembly and duplication. Using this assay I identified two-such conserved Cdk1/Cyclin B sites in Ana2. These findings provide novel insight into the relationship between the centriole duplication cycle and the cell cycle.

6.2. Results

6.2.1. Generating SAPs by mRNA injections

In order to establish an SAP mRNA injection assay, I first had to establish that I can generate SAPs in embryos using injected mRNA and that the SAPs generated are similar to those formed in eggs.

The following *Drosophila* fly lines were use for this study: Oregon R flies were used as wild type flies, and Jupiter-mCherry flies (Callan et al., 2010) were used as a marker for microtubules (see 2.1.2); Jupiter is a microtubule associated protein that is often used to follow microtubule behaviour in flies (Callan et al., 2010). Embryos from these flies were injected with different *in vitro* transcribed mRNA. For more details on the cloning, constructs generated, *in vitro* mRNA transcription see 2.3.2, 2.3.6, 2.3.7, respectively

First, I wanted to assess whether I could make SAPs in embryos by mRNA injection. I took advantage of my previous demonstration that mKate2 folded quickly enough to become fluorescent in this mRNA injection assay (see Chapter 3) and injected mRNA encoding Ana2-mKate2 and mNeonGreen-Sas-6 at a concentration of 2 µg/µl into early wild type *Drosophila* embryos. As shown in **Figure 6.1A**, SAPs formed ~1 hr after injection, and these contained both Ana2-mKate2 and mNeonGreen-Sas-6. It is

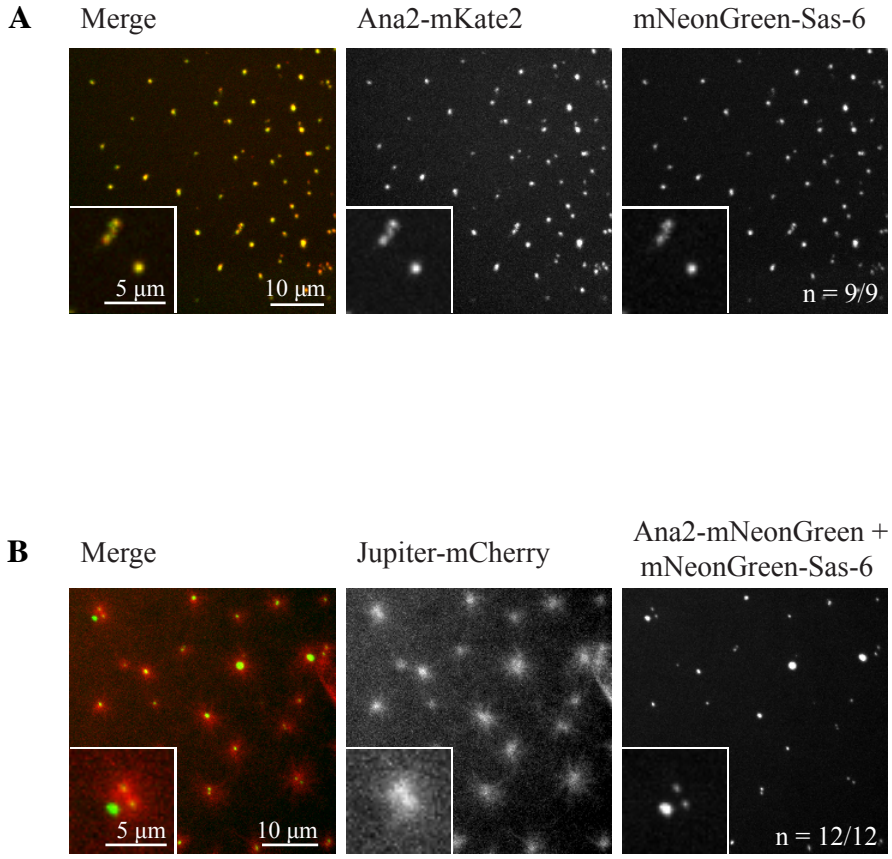


Figure 6.1: SAPs can be formed by mRNA injection. A) Panels show how the injection of mRNA encoding Ana2-mKate2 (red) and mNeonGreen-Sas-6 (green) into WT embryos leads to the formation of SAPs. The SAPs contain both fusion proteins and exhibit a variety of shapes and sizes. The fraction of embryos exhibiting the phenotype shown is indicated in the bottom left hand corner of the merge image. **B**) Panels show how the SAPs formed by mRNA injection are able to nucleate microtubules (Jupiter-mCherry). All the SAPs present nucleate microtubules regardless of size and shape. The fraction of embryos exhibiting the phenotype shown is indicated in the bottom left hand corner of the merge image. The presence of the microtubules indicates that all the necessary components of the PCM are recruited to the SAPs.

clear that the aggregates that form in injected embryos are SAPs and not centrioles as they exhibit a range of shapes and sizes (**Figure 6.1A**). Moreover, these structures did not divide and in embryos where a lot of SAPs formed during early nuclear cycles (before the nuclei had migrated to the embryo cortex) the embryo cell cycle appeared to be arrested and the embryos did not develop (data not shown). I also injected Ana2 and Sas-6 mRNA in to embryos expressing Jupiter-mCherry. All the aggregates that formed were able to nucleate microtubules (**Figure 6.1B**), indicating that the aggregates recruit functional PCM. Taken together, these results suggest that the aggregates formed upon co-injection of Ana2 and Sas-6 are indeed SAPs.

Second, I wanted to identify conditions in which SAPs only form upon co-injection of Ana2 and Sas-6 mRNA. I titrated the mRNA concentration of both Ana2-mNegonreen and mNeonGreen-Sas-6 to identify the correct concentration (**Figure 6.2A, left panel**). To ensure that total concentration of mRNA injected was similar when titrating the Ana2 and Sas-6 mRNA individually, I co-injected a 'control' mRNA (mRuby2-Cnn) with the individual Ana2 and Sas-6 mRNAs. I knew from my previous work that mRuby2 does not fluoresce in an mRNA injection assay (Chapter 3), and no direction interaction between Ana2/Sas-6 and Cnn has been reported. I found that at a final concentration of 0.3µg/µl of each mRNA species (Ana2-mNeonGreen and mNeonGreen-Sas-6) SAPs reliably form upon co-injection, but not upon individual injection (**Figure 6.2A,B**). The presence of SAPs was determined by the presence of green fluorescent foci; these foci are able to nucleate microtubules and compete with the endogenous centrosomes to form spindle poles (**Figure 6.2.A, right panel**), but they do not duplicate.

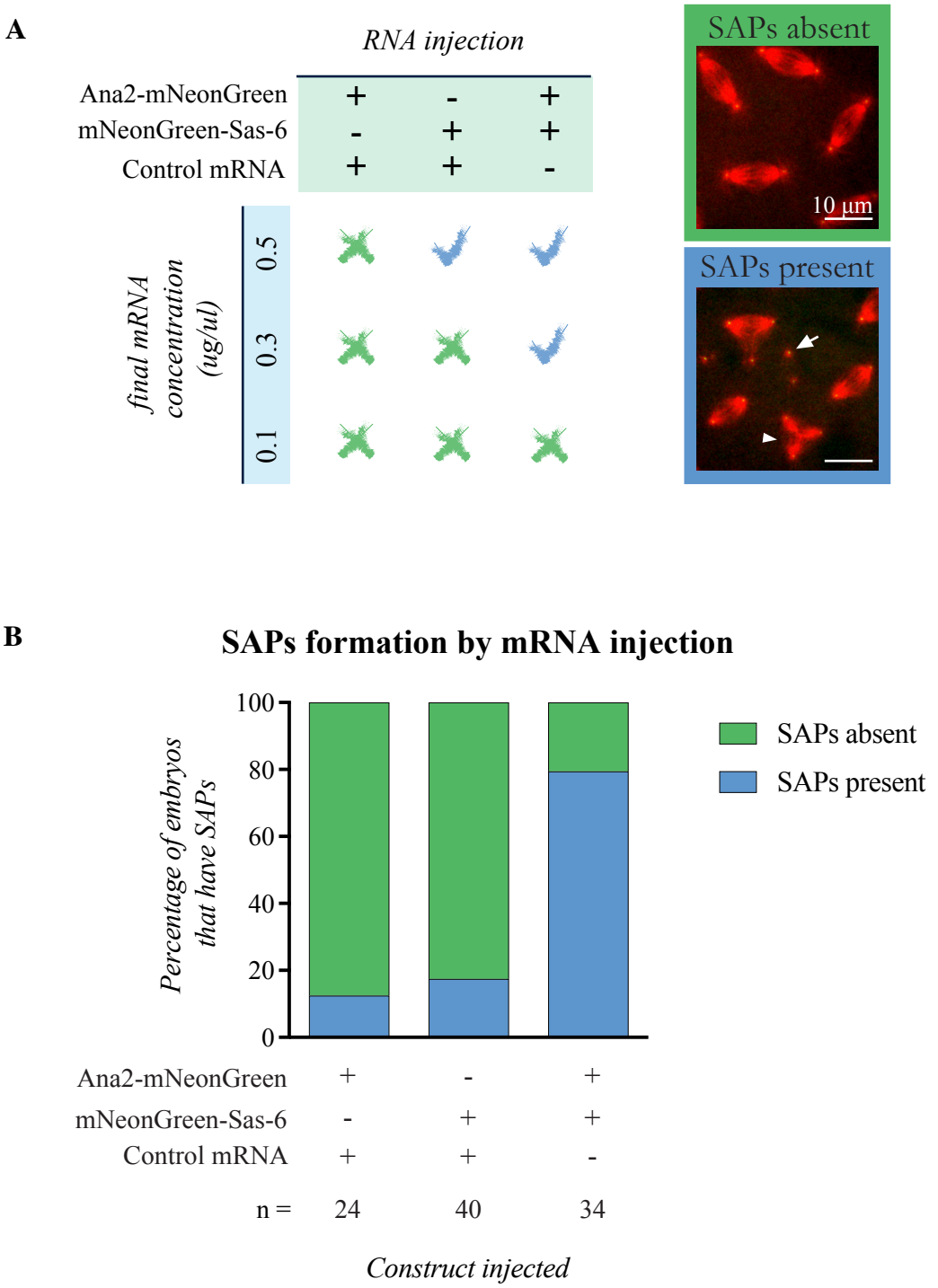


Figure 6.2: Titration of the concentration of mRNA needed to generate SAPs only when both mRNA species are present. A) Left: a table summarises the conditions required to generate SAPs by mRNA injection only when both Ana2-mNeonGreen and mNeonGreen-Sas-6 are present. Embryos were injected with mRNA at the indicated concentrations and scored for the presence of SAPs. For each condition 9-34 embryos were injected and scored. Right: representative images the absence of SAPs (top) and the presence of SAPs (bottom) in developing embryos. The white arrow indicates a SAP, which has nucleated microtubules, and the white arrowhead indicates a tripolar spindle formed by a SAP interacting with a spindle. **B**) Quantification of the percentage of injected embryos that form SAPs when 0.3 µg/µl of mRNA of Ana2-mNeongreen and mNeonGreen-Sas-6 either on their own or together (quantification of 0.3 µg/µl mRNA concentration condition in (**A**)). Only when both Aan2 and Sas-6 mRNA is present, do ~80% of the eggs develop SAPs.

SAPs require the same protein-protein interactions as centrioles do to form in eggs (Chapter 5). To confirm that this was also the case in embryos, I injected mRNAs encoding the same mutant forms of either Ana2-mNeonGreen or mNeonGreen-Sas-6 as I tested in eggs: Sas-6 ΔF143D (Cottee et al., 2015), Ana2 ΔCC (Cottee et al., 2015), Ana2 CCA (Cottee et al., 2015), Ana2 P11AR12A (Cottee et al., 2013), Ana2 R16A (Dr. M. Cottee, personal communication), and the STAN phosphorylation substitutions: Ana2-6A, Ana2-6E, Ana2-4A Ana2-4E, Ana2-2A and Ana2-2E (B. Sieber, personal communication).

I was able to show that SAPs only from when Ana2 and Sas-6 are able to interact with themselves and when the STAN domain is present, SAPs can form (**Figure 6.3A**). Furthermore, I was able to show that the STAN phosphorylation site are critical for SAP formation. Mutations to alanine, prevent SAP formation, whereas the mutations to glutamic acid, seems to influence the how efficiently Ana2 and Sas-6 can interact (**Figure 6.3B**). I attribute the differences seen in the mRNA injection screen and the transgenic eggs (**Figure 5.10B**), due to the timing. In the mRNA injection screen, the time frame for SAPs to form in 1 hr, whereas in the transgenic eggs, it is unclear if the SAPs are present before being laid by the female – meaning the SAP have more than 1 hr to form. Additionally, it must be noted that the injections are preformed manually, as oppose to a constant expression via a transgene. Finally, the SAP mRNA injection results confirm the transgenic egg findings (**Figure 5.9B**) for the importance of the Ana2 P11, R12 residues (**Figure 6.3C**) – SAPs are still able to form in embryos in the Ana2 P11A, R12A mutant but less efficiently. The Ana2 R16A mutant forms SAPs as expected.

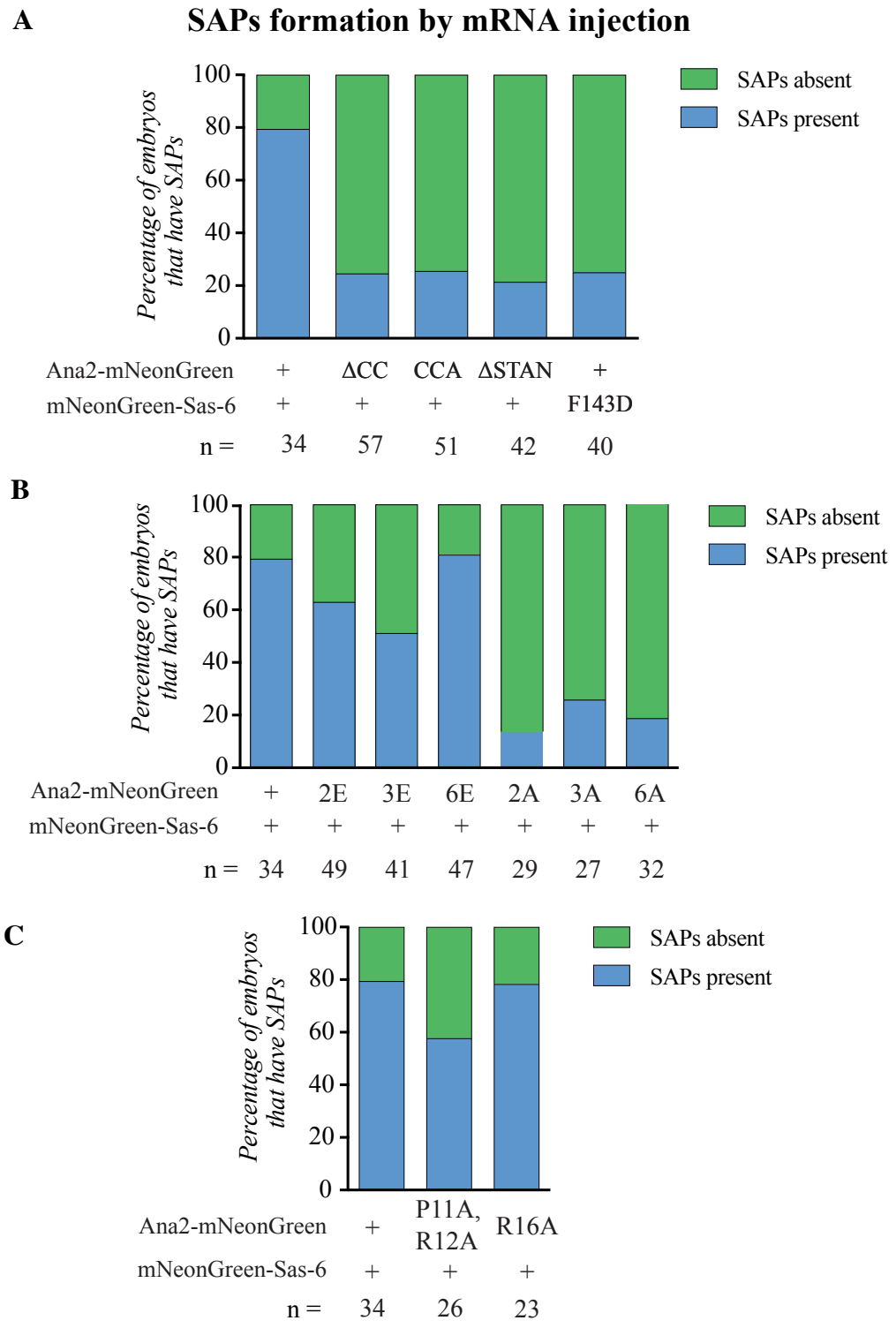


Figure 6.3: SAPs generated by mRNA injection require the same protein-protein interaction domains and regulatory residues to form as in transgenic eggs. A) Quantification of the percentage of embryos that develop SAPs when key Ana2 and Sas-6 residues and domains are mutated. These results are similar to results from **Figure 5.8**. **B**) Quantification of the percentage embryos that form SAPs when key Ana2 STAN domain phosphorylation sites are substituted. It appears that the STAN domain phosphorylations are important for efficient interaction, similar to results in **Figure 5.10B** and **5.11A. C**) Quantification of the percentage embryos that form SAPs when key Ana2 and Sas-4 interaction residues are mutated. These findings are similar to the results in Figure 5.9. All n-numbers are shown below each bar. Overall, it appears that SAPs require the same interaction domains and regulatory residues as centrioles do to form.

It is important to note that the cloning, generation of mRNA, injection of mRNA and analysis of the results took between 2-3 weeks for this study. This is opposed to the ~6+ months it would take to generate the transgenic lines and perform the appropriate crosses for this analysis. The mRNA injection screen cost effective and comparatively cheap, and it allows one to screen many mutants in a very short time frame. This streamlines the process of identifying potentially interesting mutations.

6.2.2. Identification of potential Cdk phosphorylation sites in Ana2

As the SAP mRNA injection assay is performed in fly embryos, it lends itself to the identification of protein domains and residues that are involved in centriole duplication regulation. One particularly interesting topic is the regulatory connection between the centriole duplication cycle and the cell cycle. Centrioles duplicate only in S-phase (Khodjakov et al., 2002) and centrioles require Sak/Plk4 to duplicate (Bettencourt-Dias et al., 2005; Habedanck et al., 2005). Sak/Plk4 determines the place of daughter centriole biogenesis (Kim et al., 2013; Ohta et al., 2018), and it binds and phosphorylates Ana2, allowing Ana2 to bring Sas-6 to the site of centriole biogenesis (Arquint et al., 2015; Dzhindzhev et al., 2014; McLamarrah et al., 2018; Moyer et al., 2015; Ohta et al., 2014). It was shown recently that in human cells and in *Xenopus* egg extracts that the major cell cycle regulator Cdk1/Cyclin B directly binds to STIL and phosphorylates it (Zitouni et al., 2016). This direct binding seems to prevent the premature binding of Plk4 to STIL and so the phosphorylation of STIL by Plk4. In human cells, Cdk1/Cyclin B can phosphorylate STIL at the N-terminus and can bind STIL at the CC region (Cottee et al., 2017; Zitouni et al., 2016). This interaction seems to prevent the STIL CC region from interacting with Plk4's conserved PB3 domain (Arquint et al., 2015). Upon mitotic exit, when Cdk1/Cyclin B is degraded, Plk4 can then bind and phosphorylate Ana2 (Zitouni et al., 2016). However, the CC

of Ana2 is not closely related to the CC region of STIL (Cottee et al., 2017). Furthermore, the binding of the STIL CC domain to PB3 of Plk4 does not appear to be conserved in flies (Cottee et al., 2017). I wondered, therefore, whether Cdk1/Cyclin B might regulate Ana2 by phosphorylation in flies as opposed to direct binding.

I performed a multi sequence alignment (see 2.2.1) of the protein Ana2 in 12 different *Drosophila* species and I was able to identify three conserved potential Cdk sites—S84, S284 and T301 (**Figure 6.4A**). These sites are defined by a serine or threonine, followed by a proline. The S84 site was located close to the Sas-4 binding domain, while S284 and T301 are located close to the STAN domain (**Figure 6.4B**). Moreover, a recent study showed that the S84 and S284 sites are phosphorylated on endogenous Ana2 *in vivo* (McLamarrah et al., 2018).

I mutated these residues to either alanine (phosphonull) or glutamic acid (phosphomimetic) and then tested the ability of these mutant proteins to form SAPs in the embryo mRNA injection assay (**Figure 6.5A**). Disappointingly, individually mutating any of these residues did not have a strong or consistent effect on SAP assembly: the S284A and T301E perhaps slightly promoted SAP assembly (as judged by the percentage of embryos in which SAPs were formed), while the other mutants had little effect. As the S284 and T301 sites are close to each other, I also tested the effect of mutating both sites at the same time. Strikingly, the phosphomimetic S284E,T301E mutations strongly suppressed SAP assembly, while the phosphonull S284A,T301A mutant appeared to promote SAP assembly. These observations suggest that during M-phase, the Cdk1-dependent phosphorylation of Ana2 at S284

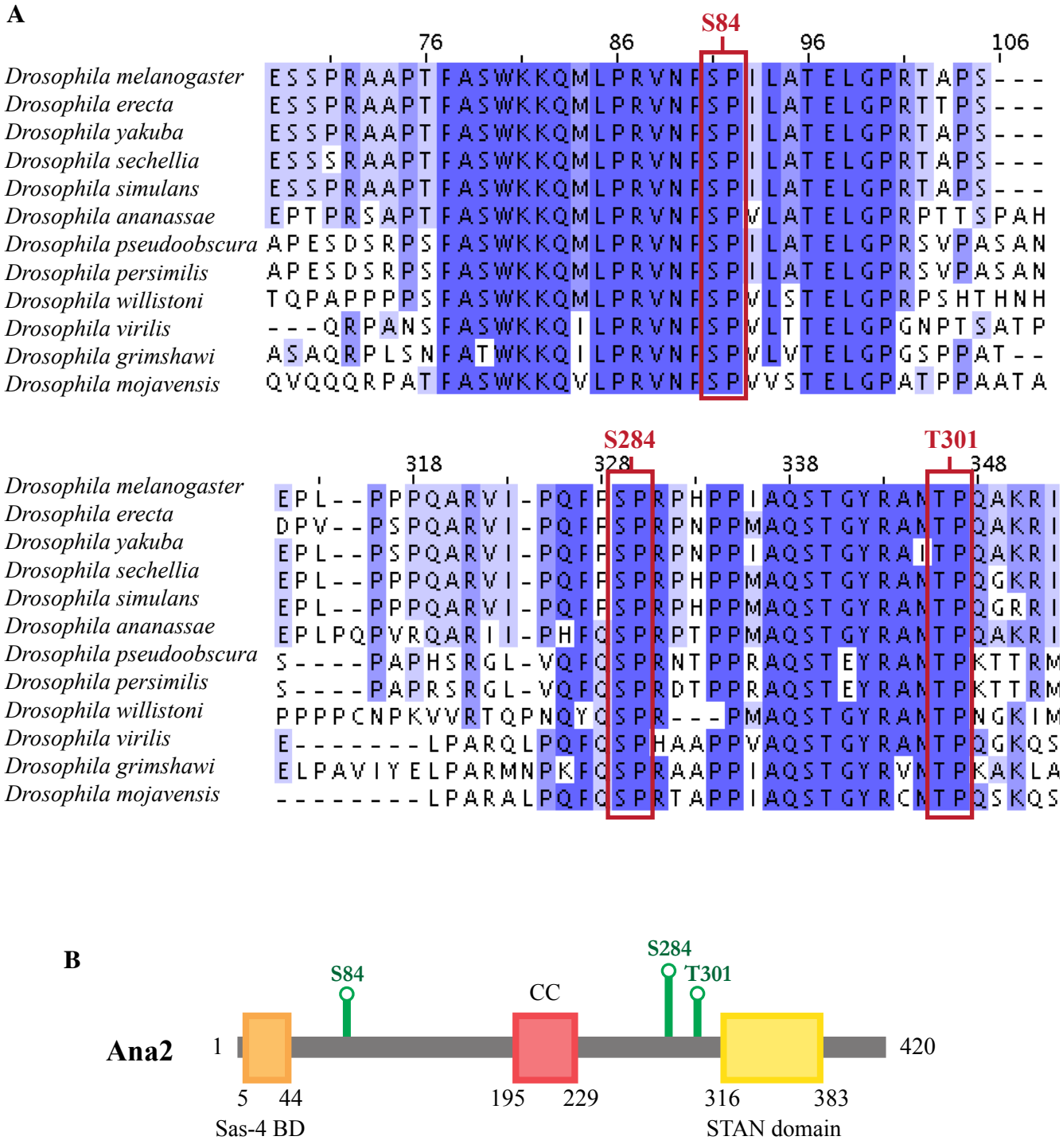


Figure 6.4: The identification of conserved putative Cdk sites in Ana2. A) Multi-sequence alignment of 12 different *Drosophila* species led to the identification of 3 conserved Cdk sites (Cdk site motif is Serine/Threonine, followed by a Proline, red boxes). Three Cdk sites are conserved in all of these Drosophila species: S84, S284 and T301 (in *Drosophila melanogaster*). **B**) Schematic of the location of these Cdk sites on the Ana2 protein. Note the S84 is located close to the Sas-4 BD and that both S284 and T301 are adjacent to the STAN domain.

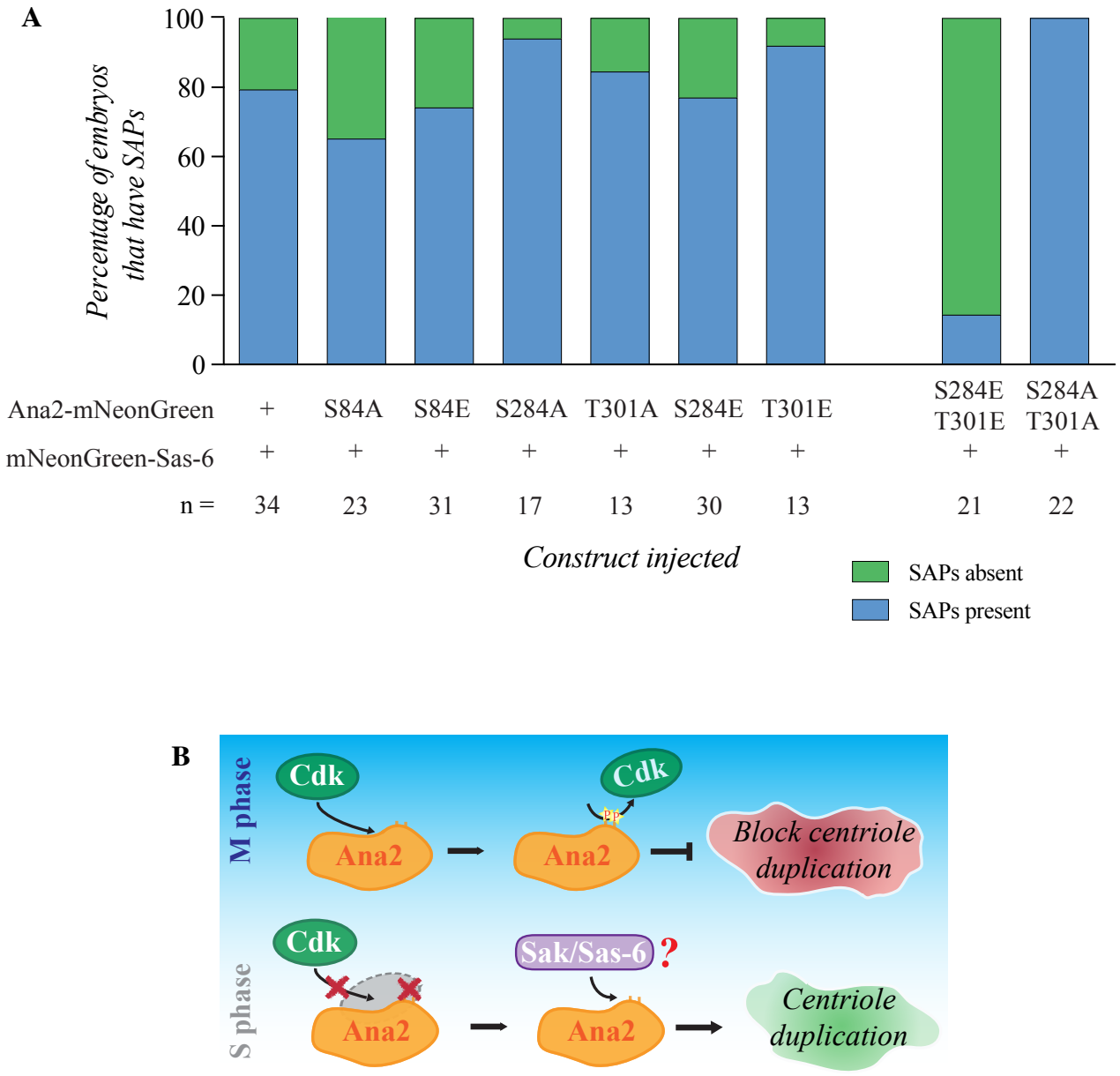


Figure 6.5: The conserved putative Cdk sites S284 and T301 could have a role in preventing centriole duplication in M-phase. A) Quantification of the percentage of embryos that form SAPs upon mRNA co-injection of Sas-6 and various Ana2 Cdk site mutants, as indicated. The double S284,T301 mutation has the strongest affect, however when mutated individually, the sites do not produce a strong effect. The number of embryos injected is shown below each bar. **B**) Schematic of the proposed Ana2 centriole duplication control by Cdk1 in M phase and Sak (or possibly Sas-6) in S phase. The model would suggest that the phosphorylations placed on Ana2 by Cdk1 in M phase, block centriole duplication. As Cdk1 levels decrease, the phosphorylations on Ana2 are removed. This now allows Sak to phosphorylate or allow Sas-6 to interact with Ana2 to drive a new round of centriole duplication. A control mechanism restricts centriole duplication to S-phase.

and T301 could function to inhibit the ability of Ana2 to promote centriole assembly (**Figure 6.5B**). This might help to explain why centriole assembly does not normally occur during mitosis, when Cdk1 is active.

To test this possibility, I generated transgenic flies with a transgene expressing GFP-Ana2 with either the S284A, T301A mutations (GFP-Ana2-2A-Cdk) or the S284E, T301E mutations (GFP-Ana2-2E-Cdk) under the control of the ubiquitin promoter (**Figure 6.6A**) (see 2.1.2). Examination of unfertilized eggs expressing Sas-6-GFP and Ana2-2A-Cdk-GFP or Ana2-2E-Cdk-GFP, revealed that SAPs are formed in 100% of the eggs examined (**Figure 6.6B,C**); showing that interaction between Ana2 and Sas-6 is not prevented. However, the SAPs formed by the Ana2-2A-Cdk protein seemed slightly larger (although this difference was not significant) (**Figure 6.6D**). These results are preliminary. I am in the process of repeating this experiment to increase the sample size and include a SAP (Sas-6xAna2) control.

I next wanted to test whether the S284 and T301 residues could be phosphorylated by Cdk1/Cyclin B *in vitro* (see 2.4.3). I had peptides synthesized containing either the wild type sequence around the S284 or T301 sites, or a mutant version in which these residues were mutated to alanine (**Figure 6.7**). The positive control was a peptide containing the optimal Cdk1/Cyclin B binding sequence (Holt et al., 2009). As can be seen, Cdk1/Cyclin B phosphorylates both wild type peptides with a similar efficiency to the optimal control, but it did not detectably phosphorylate the S284A or T301A mutant peptides (**Figure 6.7**). This strengthens the possibility (but does not prove) that S284 and T301 may be phosphorylated by Cdk1/Cyclin B *in vivo*.

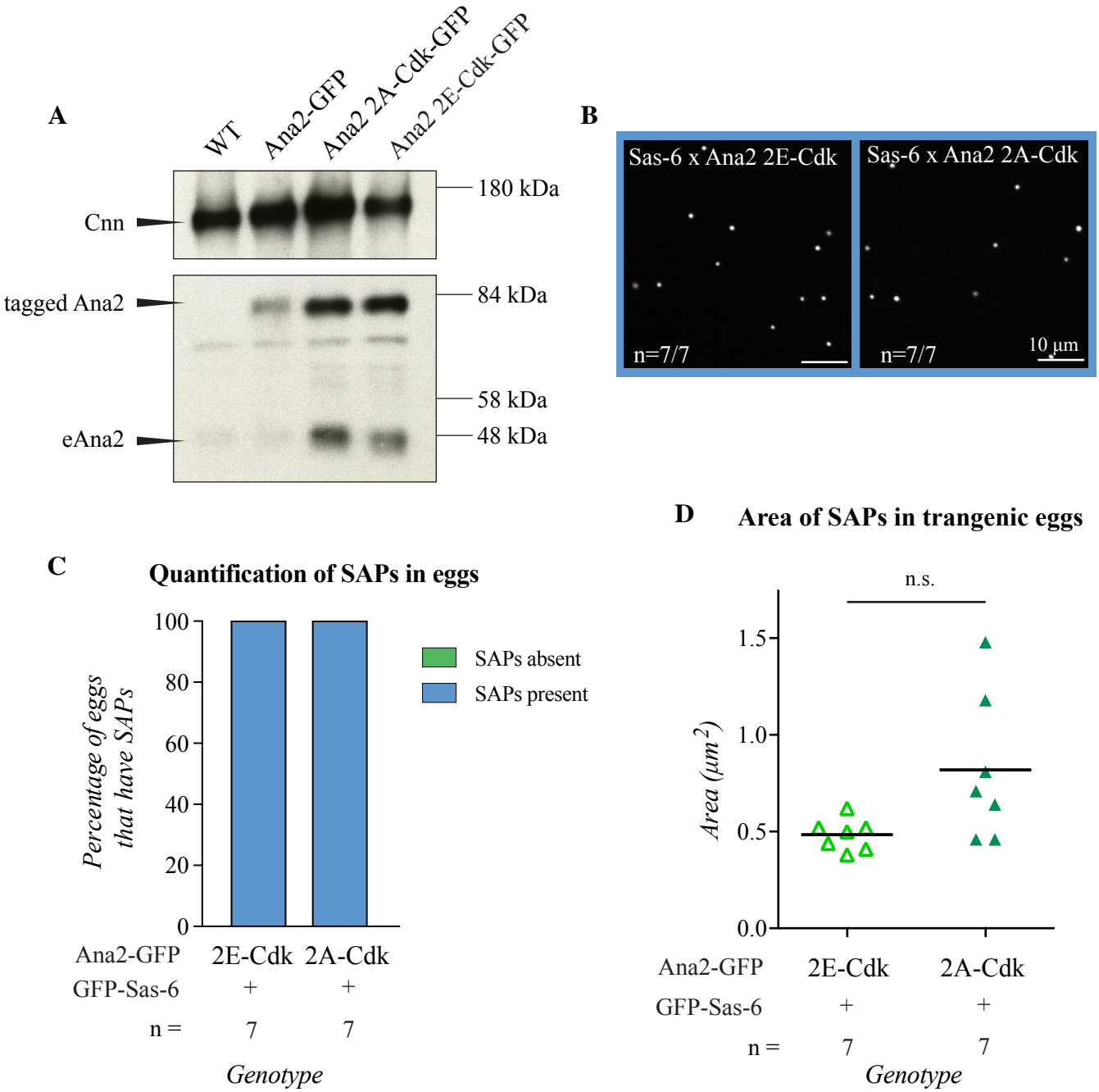


Figure 6.6: Transgenic Ana2-2E-Cdk and Ana2-2A-Cdk mutants can form SAPs. A) A western blot shows the expression levels of the fusion proteins Ana2-GFP, Ana2-2E-Cdk-GFP and Ana2-2A-Cdk-GFP in transgenic flies; each lane contains 10 early embryos. These embryos express one copy of the transgene in the presence of two copies of the endogenous WT gene. Endogenous Ana2 (eAna2), tagged Ana2 and Cnn (loading control) are indicated by the arrowheads. It is interesting to note, that the expression level of eAna2 differs between the different fly lines. **B**) Panels show confocal images of 0-3 hr eggs expressing either Sas-6 and Ana2-2E-Cdk or Ana2-2A-Cdk. SAPs form in the eggs of both genotypes suggesting that the mutations do not affect the ability of Ana2 and Sas-6 to interact. The fraction of embryos exhibiting the phenotype shown is indicated in the bottom left hand corner of each image**. C**) Quantification of the percent of eggs that contains SAPs upon co-expression of Sas-6 and Ana2-2E-Cdk or Ana2-2A-Cdk (quantification of **(B)**). **D**) Quantification of SAP size in the eggs of different genotypes, as indicated. For each image, the area of each SAP in the field of view was measured and the average area was calculated and plotted.

To assess whether these mutations effect the centriole duplication cycle, I expressed one copy of the Ubq-GFP-Ana2-2A-Cdk or Ubq-GFP-Ana2-2E-Cdk mutant transgenes in an *ana2* mutant background (see 2.1.2 for details) and compared to a Ubq-GFP-Ana2-WT (Cottee et al., 2013). Both transgenes rescued the uncoordinated phenotype of the *ana2* mutation indicating that the ability of these residues to be phosphorylated by Cdk1/Cyclin B is not essential for centriole duplication (data not shown). This is perhaps not surprising, however, as the data from my SAP experiments suggests that phosphorylation on these sites may normally function to inhibit the efficiency of Ana2's interaction with Sas-6 and so help to prevent centriole assembly during mitosis. Presumably several mechanisms cooperate to ensure that centriole duplication is normally restricted to S-phase, so the mutation of these sites may have only a subtle phenotype.

Methods have recently been developed in the laboratory that allow one to very accurately monitor the incorporation dynamics of centriole proteins in the syncytial embryo (Aydogan et al., 2018). I therefore decided to use these methods to see if these mutations led to any subtle differences in Ana2 incorporation dynamics in the embryo. I imaged the behaviour of wild type and mutant Ana2 proteins expressed in an *ana2* mutant background over cell cycle 12 in the early *Drosophila* embryo, analysing 5 to 6 embryos per condition. I measured the intensity of the Ana2 signal at multiple centrioles using the ImageJ plugin TrackMate (see 2.5.6.3) (**Figure 6.8, Figure 6.9, and Figure 6.10**). Several parameters can be derived from these graphs, and are shown for comparison in **Figure 6.11**.

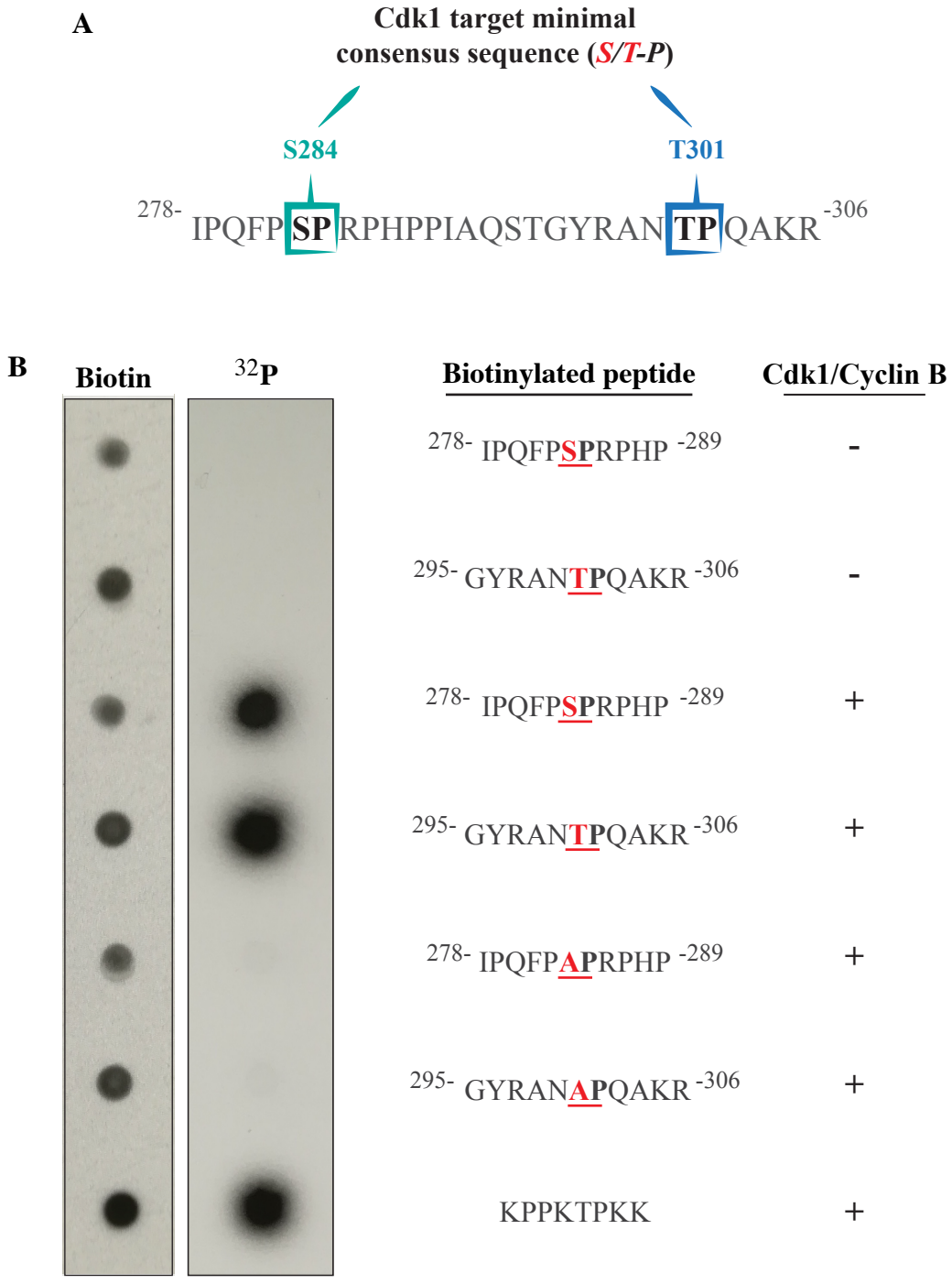


Figure 6.7: *In vitro* kinase assay to assess the ability of Cdk1/Cyclin B to phosphorylate peptides containing the putative Ana2 Cdk sites. A) Schematic of the sequences that contain the conserved Cdk sites, S284 marked in green and T301 marked in blue. **B**) Result of the *in vitro* kinase assay shows that only S284 and T301 can be phosphorylated by Cdk1/Cyclin B (seen by ^{32}P signal) *in vitro*. Left: a biotin dot blot to demonstrate similar loading for all peptides. The peptide KPPKTPKK serves as a positive control for Cdk1/Cyclin B phosphorylation. Typical data are shown from 3 technical repeats.

The length of S- and M-phase did not seem to vary significantly in embryos expressing Ana2 WT or either of the mutant forms (**Figure 6.11A,B**); however, it was very noticeable that the timing of both S-phase and M-phase was more variable than previously seen when this assay was used to monitor the behaviour of other centriole and centrosome proteins (M. Aydogan, personal communication). The reason for this variability is uncertain but is worthy of further investigation, as it suggests overexpressed Ana2 could influence cell cycle timing in these embryos in some way. Strikingly, however, the peak-amount of Ana2 incorporated into the centrioles during S-phase was significantly lower for GFP-Ana2-2E-Cdk than for GFP-Ana2-2A-Cdk or wild type GFP-Ana2. This is consistent with the idea that the phosphorylation of these resides decreases the efficiency of the Ana2/Sas-6 interaction, and so less Ana2 is incorporated into the growing daughter centrioles. Moreover, the observation that the GFP-Ana2-2A-Cdk mutant is incorporated to normal levels supports the idea that it is the phosphorylation of these residues, rather than the residues themselves, that is important for this regulation: preventing the phosphorylation of these residues should not perturb the incorporation of Ana2 during S-phase—as these residues would not normally be expected to be phosphorylated during S-phase.

Overall, my findings provide a proof of concept that the SAP mRNA injection assay can be a useful tool for identifying previously unknown regulatory residues and domains. Through this assay I was able to identify two conserved Cdk sites that appear to play a subtle role in centriole assembly: the Cdk site phosphorylations seem to partially inhibit the ability of Ana2 to promote centriole assembly, but not completely. Additionally, these findings provide evidence that the regulation of the interaction between Ana2 and Sak by Cdk1/Cyclin B may be different in *Drosophila*

Ana2 full length, full mutant background
- GFP intensity over cell cycle 12

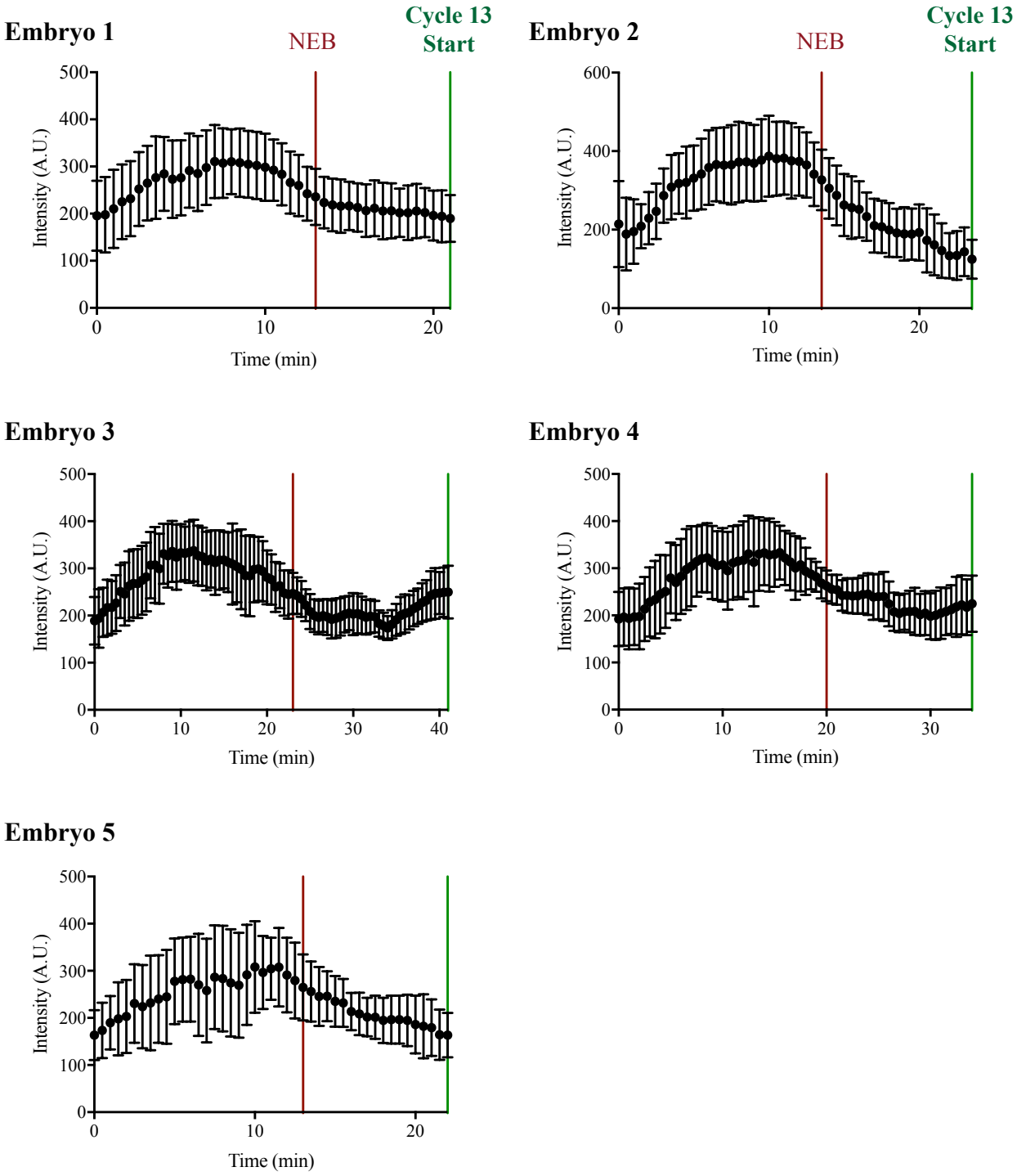


Figure 6.8: Ana2-GFP incorporation dynamics during nuclear cycle 12. All 5 embryos were imaged from the start of cycle 12 (t=0; scored as the time centriole separation was first detected at the end of cycle 11) until the end of cycle 12 (scored as the time centriole separation was first detected at the end of cycle 12; indicated by the green line). The start of M-phase was scored as the time of nuclear envelope breakdown (NEB) and is indicated with a red line.

Ana2 S284E T301E, full mutant background
- GFP intensity over cell cycle 12

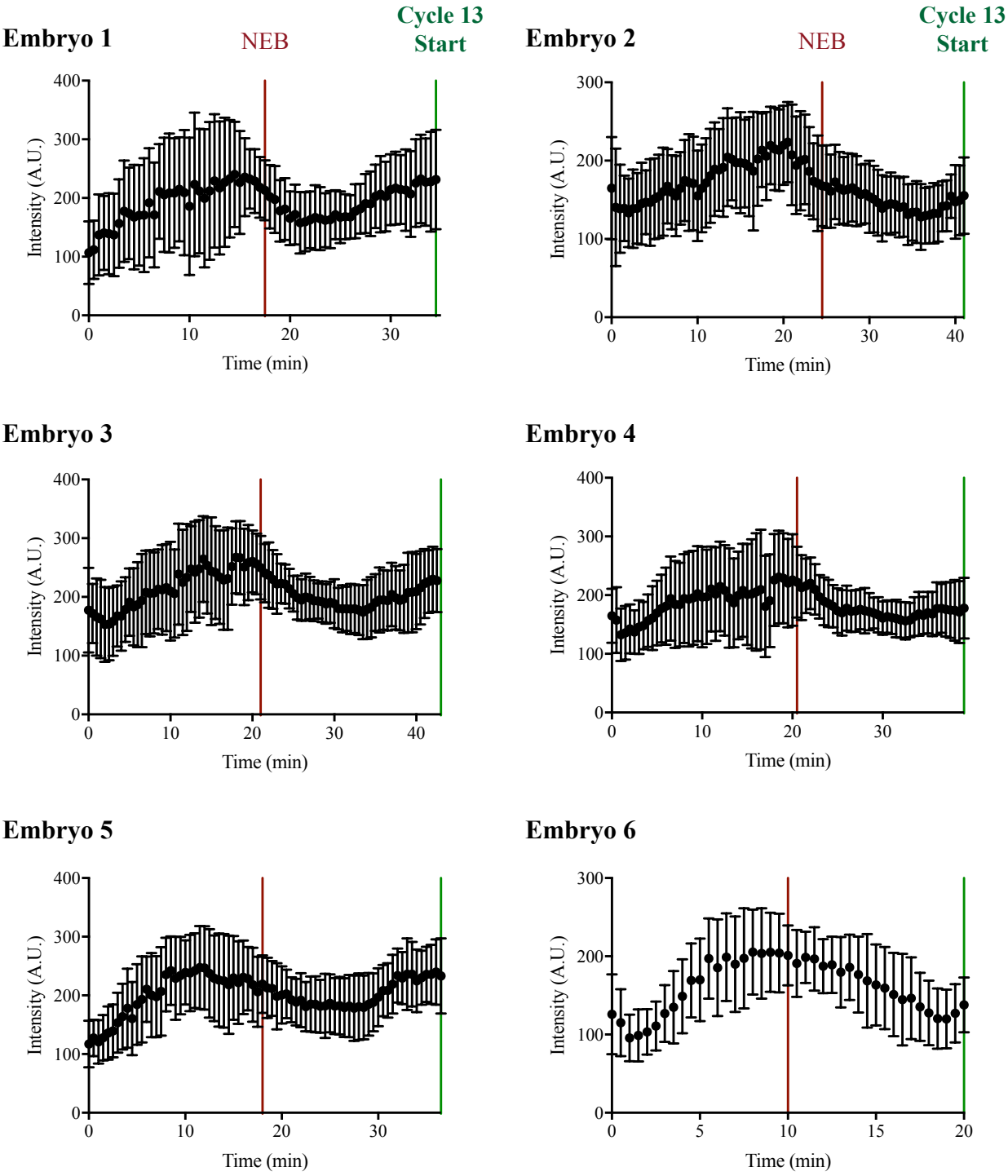


Figure 6.9: Ana2-S284E,T301E-GFP incorporation dynamics during nuclear cycle 12. All 6 embryos were imaged from the start of cycle 12 (t=0; scored as the time centriole separation was first detected at the end of cycle 11) until the end of cycle 12 (scored as the time centriole separation was first detected at the end of cycle 12; indicated by the green line). The start of M-phase was scored as the time of nuclear envelope breakdown (NEB) and is indicated with a red line.

Ana2 S284A T301A, full mutant background
- GFP intensity over cell cycle 12

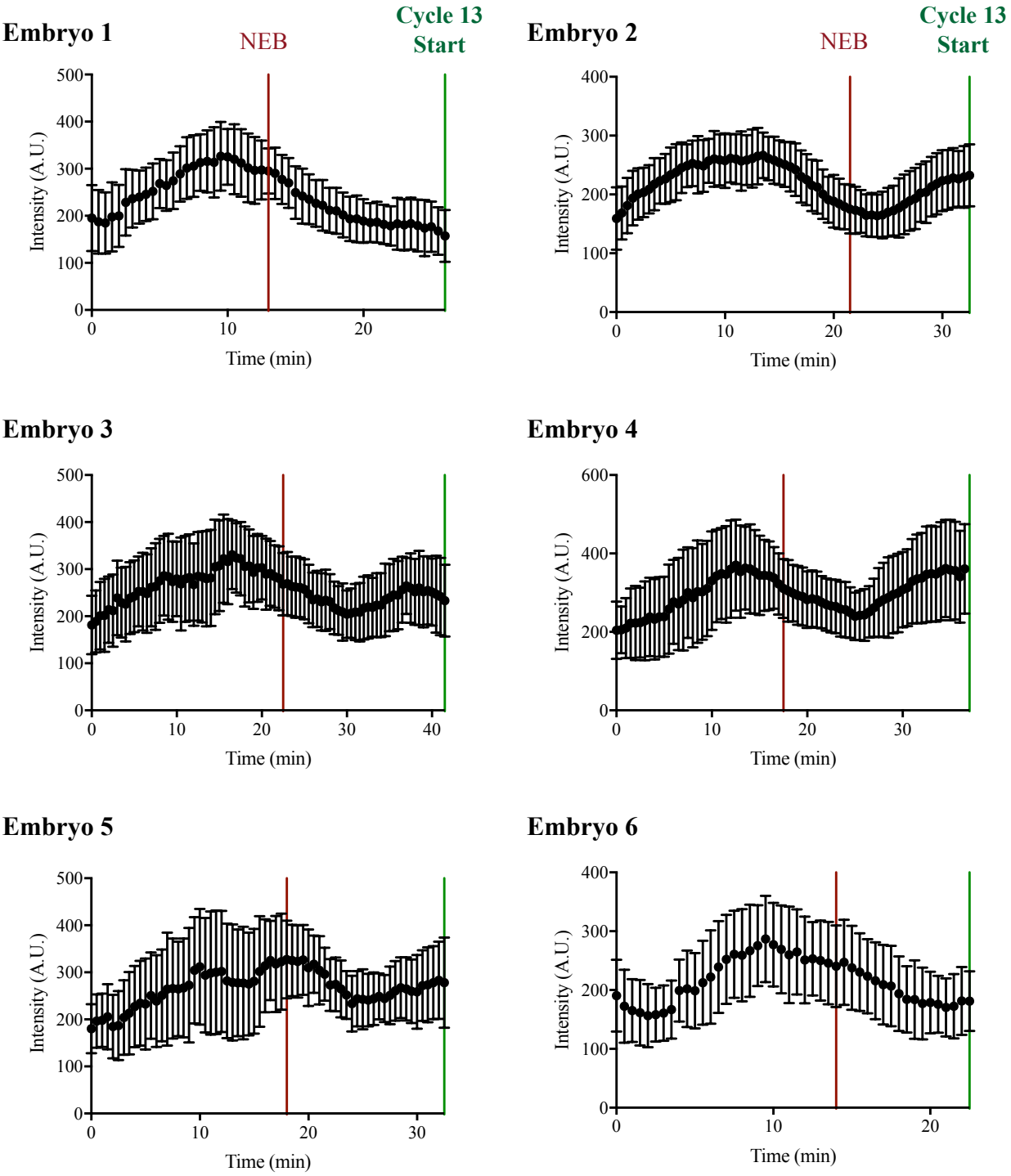


Figure 6.10: Ana2-S284A,T301A-GFP incorporation dynamics during nuclear cycle 12. All 6 embryos were imaged from the start of cycle 12 (t=0; scored as the time centriole separation was first detected at the end of cycle 11) until the end of cycle 12 (scored as the time centriole separation was first detected at the end of cycle 12; indicated by the green line). The start of M-phase was scored as the time of nuclear envelope breakdown (NEB) and is indicated with a red line.

than in vertebrates. Further characterization and more extensive studies on these mutants is required to fully assess the role of these Cdk sites on Ana2 function and identify how they link the centriole duplication cycle and the cell cycle. Additionally, the finding that even moderate over expression of full length Ana2 affect the cell cycle would be an area worth of further study.

6.3. Discussion

In this chapter, I have shown that SAPs can be generated in embryos by the co-injection of fluorescently tagged Ana2 and Sas-6. These SAPs behave as transgenically generated SAPs do in eggs: they are of varying sizes and shape, they are not able to divide, but they are able to nucleate microtubules, their PCM is able to respond to cell cycle cues, and they require the same protein-protein interactions needed for *bona fide* centriole assembly. The ability to form SAP in embryos has allowed me to set up a SAP mRNA injection assay, which allows for the quick and cost-effective testing of potentially interesting protein-protein interaction regions and/or regulatory domains or residues potentially involved in centriole assembly.

I validated my SAP mRNA injection assay by examining the role of three conserved Cdk sites in Ana2. I identified 2 sites that, when mutated together, generate a strong effect: phosphomimetic mutations seem to inhibit SAP formation, whereas phosphonull mutations promote SAP formation. I generated transgenic flies to corroborate these findings, and showed that both putative phosphorylation sites can be phosphorylated by Cdk1/Cyclin B *in vitro*. Most importantly, the phosphomimetic mutation seems to partially inhibit the recruitment of Ana2-2E-Cdk to the growing daughter centriole during S-phase. Taken together, these finding suggest that Ana2 interaction with Sak (or possibly Sas-6) is regulated by Cdk1 phosphorylation in M-

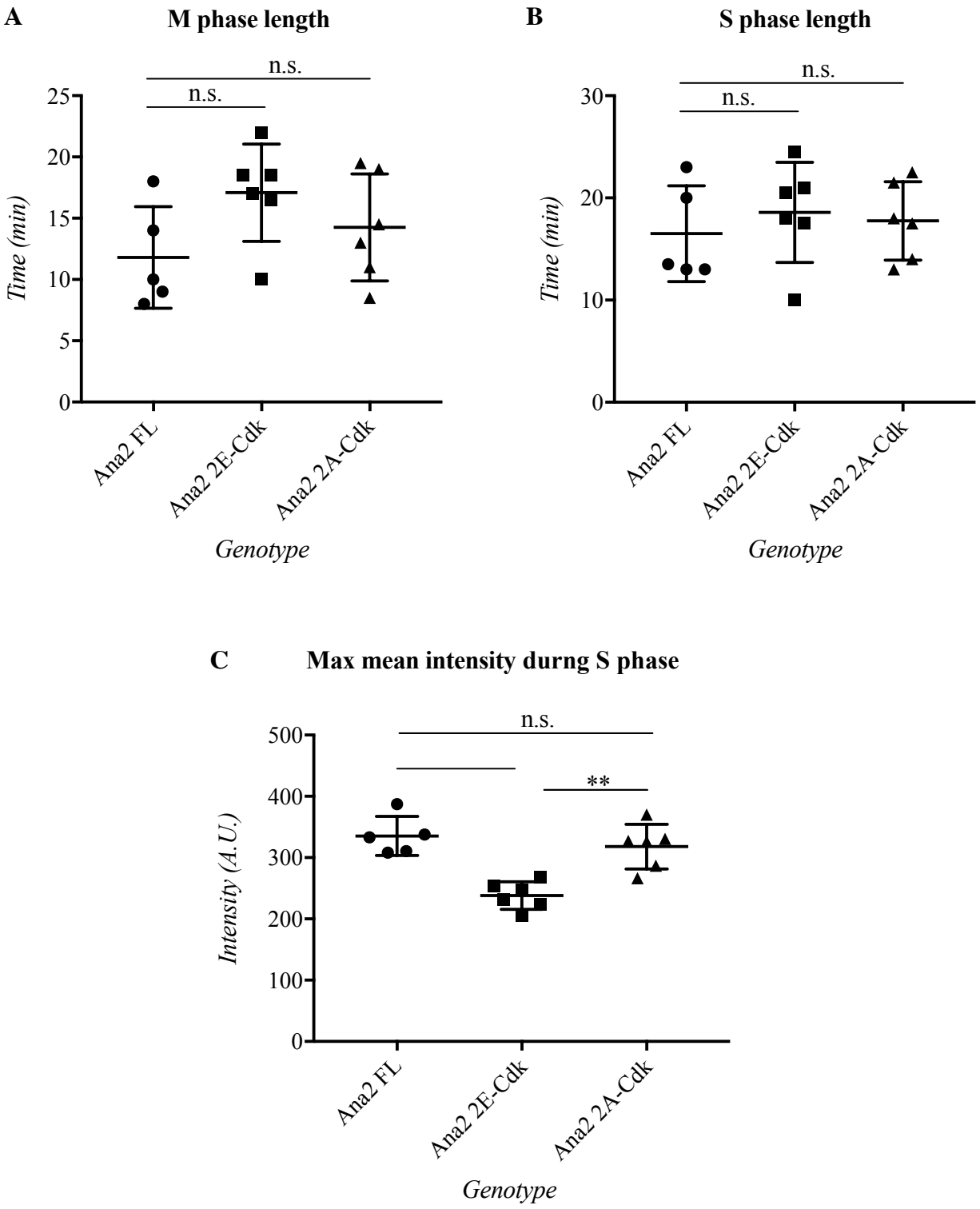


Figure 6.11: Analysis of cell cycle and centriole assembly parameters during nuclear cycle 12. A,B) The average length of S-phase and M-phase is not significantly different in any of the genotypes. Each data point plotted represents 1 embryo. **C**) A graph showing the maximum mean intensity of the GFP signal over S-phase of nuclear cycle 12 in the different genotypes, as indicated. The Ana2-2E-Cdk mutation significantly inhibits the amount of Ana2 that is recruited to the centriole in S-phase.

phase, similar to the regulation of the STIL/Plk4 interaction in vertebrates (Zitouni et al., 2016). However, the site of phosphorylation seems different: in vertebrates, Cdk1/Cyclin B phosphorylates Ana2 at the N-terminus (and the function of this phosphorylation is unknown) (Zitouni et al., 2016), whereas in *Drosophila*, Cdk1/Cyclin B seems to phosphorylate Ana2 in the C-terminus, near the STAN domain. It is known that the STAN domain is key for Ana2-Sas-6 interactions (Cottee et al., 2015) and that it is the region phosphorylated by Sak/Plk4 (Dzhindzhev et al., 2014; Kratz et al., 2015; McLamarrah et al., 2018; Moyer et al., 2015; Ohta et al., 2014; Zitouni et al., 2016). Therefore, phosphorylations by Cdk1 close to the STAN domain could directly affect the accessibility of Sak to this critical region of Ana2.

Further examination of the roles of these two Cdk site is required to fully understand their importance and role in controlling the centriole duplication in *Drosophila*. In order to gain deeper insight, it is critical to show that these conserved Cdk1 sites are phosphorylated *in vivo*: it has been shown that the residue S284 is phosphorylated *in vivo* by mass-spectrometry (McLamarrah et al., 2018). It is possible that the residue T301 was not identified in that study due to insufficient coverage. An alternative method to confirm and demonstrate that the S284 and T301 site are phosphorylated is to raise specific phospho-antibodies against the site and probing for the phosphorylation via western blot. If such antibodies work, an interesting prediction would be that they might not stain centrioles in immunofluorescence experiments, as the phosphorylated form of Ana2 may not be efficiently recruited to centrioles. Second, it will be important to image more mutants and wild type embryos in cell cycle 12; as the cell cycle appears rather variable, imaging more embryos would help identify clear trends such as increased M-phase length. Third, generating transgenic

flies that express the Cdk site mutations under an endogenous promoter may reduce the variability in the cell cycle, providing a clearer phenotype. Finally, it will be important to investigate why the moderate overexpression of Ana2 appears to lead to cell cycle length variation. Such investigation may provide insight into the possible role of Ana2 as a cell cycle regulator.

7. General discussion and conclusion

7.1. Summary

My thesis work has focused on trying to tackle several hurdles, both technical and biological, restraining the centriole and centrosome field so far. The technical challenges involved testing whether several recently developed fluorescent probes are useful for our research into centriole and centrosome function in *Drosophila*. In collaboration with researchers at Micron Oxford, I also developed a 3D-SIM/SMLM imaging pipeline to gain insight into centriole structure with nanometre precision. Finally, I characterized SAPs as a model system for dissecting the centriole and centrosome assembly pathways and discovered a novel mechanism whereby Cdk1/Cyclin B kinase activity might regulate centriole assembly via the phosphorylation of Ana2.

In this discussion, I will briefly outline my major findings and discuss their significance in a wider context, highlighting areas for future work.

7.2. Fluorescent probes - technical limitations for centriole research in Drosophila

Evaluating new tools can open many new research avenues, even though the evaluation is potentially tedious. The first chapter of this thesis, although largely technical, highlights the importance of this approach. With evermore questions aimed at understanding increasingly detailed and complicated molecular mechanisms, more powerful tools and novel approaches are required. These new tools are critical to allow research to continue to advance when the existing tools no longer provide the

answers. In particular, I focused on testing recently developed fluorescent probes and evaluating their utility for light microscopy studies in living *Drosophila* embryos.

Since the discovery of GFP, an ever-growing list of fluorescent proteins with a variety of chemical- and photophysical properties have been developed. More fluorescent proteins are continually being added to the list. Additionally, recent developments in the field of self-labelling enzyme technology have opened up new and exciting avenues. My identification of mKate2 as a red-fluorescent protein that folds quickly enough in flies to function in an mRNA injection assay, has allowed experiments that have contributed to a deeper understanding of centriole maturation (Novak et al., 2016), PCM recruitment (Alvarez Rodrigo et al., 2018) and to the generation of a SAP-based assay system for testing protein-protein interactions in the centriole assembly pathway (Chapter 5). The ability to reliably image mKate2-fusion proteins using 3D-SIM in transgenic flies demonstrates, that it is likely to be important in future studies by allowing more two-coloured super-resolution live cell imaging. To date, certain super-resolution studies have not been possible or been limited by the red fluorescent protein used, for examples mCherry, due to their low brightness, poor photostability or long maturation times.

My finding that mNeonGreen is significantly brighter than GFP in the fly system (at least over short imaging periods) proved to be crucial for gaining a deeper understanding Plk4/Sak localisation during the cell cycle (**Figure 7.1A**). Recent studies performed in our laboratory using my transgenic Sak-mNeonGreen flies revealed how oscillating levels of Sak/Plk4 at the centriole are central to the control

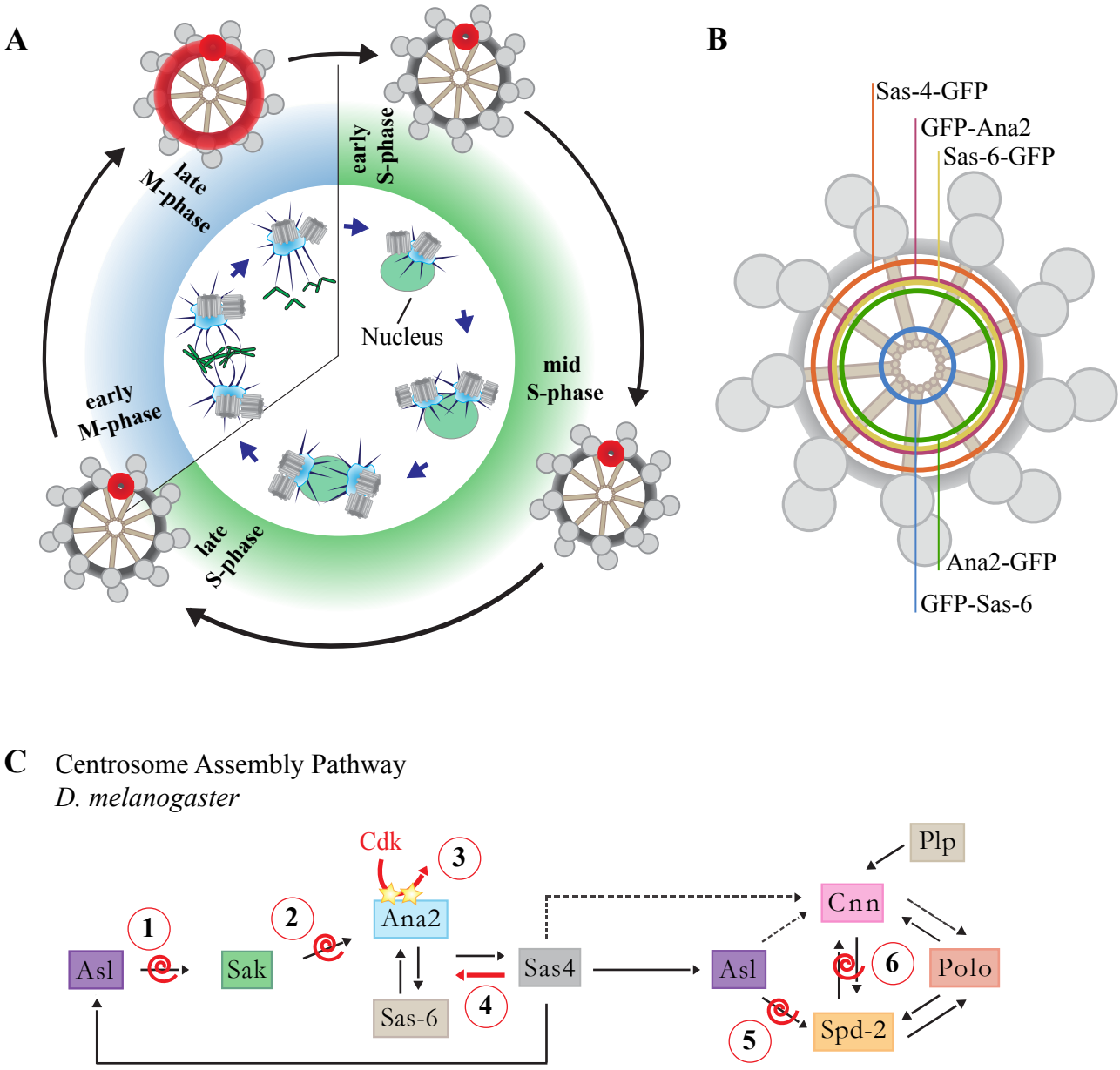


Figure 7.1: Schematics of thesis findings in context. A) The observed ring-to-dot transition on the early Drosophila embryo. Sak localises as a dot through most of the cell cycle, except in late M-phase where it localises as a ring. **B**) The position of the Sas-6, Ana2 and Sas 4 protein termini shown on a cross section of the cartwheel as calculated from the SIM/SMLM data. **C**) The proposed centriole and mitotic PCM assembly pathway in Drosophila with the findings from SAP studies indicated. **1** and **2**) Asl and Sak are not required for Ana2 and Sas-6 interaction and thus not likely to be essential for cartwheel formation. **3**) Ana2 appears to be phosphorylated by Cdk1 to ensure appropriate centriole duplication. **4**) Sas-4 is essential for Ana2 and Sas-6 interaction, and hence likely to be required for cartwheel formation. **5**) Asl is not essential for Spd-2 and Cnn recruitment. This confirms the presence of an alternative PCM recruitment pathway. **6**) Cnn can be recruited at a low level to a SAP in the absence of Spd-2.

of centriole growth (Aydogan et al., Nature, under review). In conjunction with this project, my work, utilizing both mNeonGreen and mKate2, showed for the first time Sak's localisation over the cell cycle in living embryos at super-resolution. In line with previous studies, (Dzhindzhev et al., 2017; Ohta et al., 2014; Ohta et al., 2018; Sonnen et al., 2012), I found that the ring-to-dot transition, which defines the position of the daughter centriole assembly, is a rapid process that occurs during a very brief period in late M-phase. Interestingly, in human cells STIL was found to play a key role in this process and Plk4 degradation is critical for the formation of a single dot (Ohta et al., 2018). It remains to be seen if this process is conserved in *Drosophila*. In order to address this question, I have generated various transgenic Sak-mNeonGreen mutants (with reduced, or no, kinase activity, for example). It will be interesting to determine the localisation of these mutant Sak proteins using 3D-SIM.

The development of self-labelling enzymes has enormous potential for fluorescence microscopy. These tools have previously been shown to function well in fixed fly tissues (Kohl et al., 2014), but I found their application in the *Drosophila* embryo not to be straightforward, as unbound ligand cannot be washed out. However, it may be possible to use this system successfully by titrating the amount of injected fluorescent label to maximise specific labelling and minimize the amount of unbound fluorophore. Otherwise, using photogenic ligands, ligands that only fluoresce upon binding, or photoconvertible ligands may be of alternative methods to minimize the high background. Alternatively, one of the major future applications for this technology in *Drosophila* embryos might be in single molecule studies—trying to follow the behaviour of single molecules at the centriole or centrosome. Injection of very small amounts of dye should generate sparse enough labelling to allow for single

molecule tracking in structures like the PCM. Such an application could provide insight into the behaviour of individual molecules, rather than bulk populations (as, for example, in FRAP experiments). This technology should be explored further as it could provide a valuable research tool in early *Drosophila* embryos.

7.3. Correlative 3D super-resolution microscopy – new perspectives on centriole biology

Collaborators and I developed a correlative microscopy approach to tackle a long-standing question in the centriole field regarding the organization of the centriole cartwheel. Correlating, assessing and analysing each centriole taken in the two imaging modes (SMLM and SIM) required us to develop a new image analysis method, COOL. It assesses the orientation of a centriole imaged with SIM and correlates it with high precision SMLM data. The average radius of the SMLM data is then calculated (**Figure 7.1B**). Using this two correlative 2-coloured approach, I was able to marry the advantages of both microscopy techniques: the sparse, but high precision of SMLM with the 3D structural information provided by SIM.

As COOL is an open source code it is possible to apply the same rational (using SIM to define the orientation of an object and correlating this data with SMLM data) to other cellular structures and organelles. Currently the code is written to analyse circular structures and could therefore be used to study other biological structures that are circular, such as nuclear pore complexes, the bacterial Type 3 secretion system or the cilium. With simple modifications to the code, it is possible to study highly ordered structures that are not circular, such as the kinetochore or membrane bound protein complexes. This could also extend to organelles that have an approximately regular shape, such as peroxisomes, mitochondria or even bacteria. With more

extensive modifications to the code, it would also be possible to correlate SIM/SMLM images in 3D (3D SMLM images would be required). This would allow even more precise analysis of a protein's 3D distribution that could reveal new insight into a variety of different cellular structures in the context of macromolecules structures.

On the other hand, other researchers may find it difficult to use the COOL code that we have developed here, as it is very much tailored to answering our specific questions. Unfortunately, we have not had the resources to properly annotate the code and make it easy to understand and adapt. Additionally, modifying the code to answer other biological questions requires coding knowledge. I highlight these as general problems with bespoke coding, and one that is not easy to solve.

7.4. SAPs – a protein-protein interaction assay and a model for centriole and PCM assembly

The further characterisation of SAPs and their use to generate a protein-protein interaction assay demonstrated they could be used to generate deeper insight into centriole assembly (**Figure 7.1C**).

One interesting recurring theme that I noticed while working with SAPs is that the expression levels of the endogenous Ana2 and Sas-6 seem to be downregulated in transgenic flies that moderately overexpression GFP fusions of the respective protein (see **Figure 6.6A** or **Figure 5.8A,B**). It is unclear how this expression modulation occurs. The generation of CRISPR mutants would allow me to assess if the mutations themselves affect the expression level of the proteins. The expression modulation strongly suggests that the expression levels of Sas-6 and Ana2 are tightly regulated, presumably to prevent centriole overduplication (Arquint et al., 2012; Peel et al.,

2007; Strnad et al., 2007). Tight control of Ana2 may be critical for proper cell cycle progression: when full length Ana2 was moderately overexpressed it surprisingly influenced the length of the cell cycle (**Figure 6.11**). Although this experiment needs to be repeated, it suggests that Ana2 may function as an important link between the centriole duplication cycle and the cell cycle. Further studies should provide more insight into this possible additional level of centriole duplication control.

The identification of putatively conserved Cdk1 sites on Ana2 using the SAPs in a protein-protein interaction assay, suggests a novel centriole duplication control mechanism. In vertebrate cells, Cdk1/Cyclin B and the PB3 region of Plk4 seem to compete for binding to the central CC region of STIL, hinting to a mechanism by which active Cdk1/Cyclin B prevents centriole duplication during mitosis (Zitouni et al., 2016). Phosphorylation of STIL by Cdk1/Cyclin B was found to also occur in the N-terminal region, however this phosphorylation was not implicated in the process of controlling the STIL/Plk4 interaction (Zitouni et al., 2016). It seems unlikely, however, that this mechanism is conserved in flies, as here the fly central CC region forms a tight tetramer that cannot be displaced by the PB3 domain (Cottee et al., 2017). I found that the phosphorylation of *Drosophila* Ana2 near the STAN domain by Cdk1/Cyclin B may provide an alternative mechanism for Cdk activity to regulate centriole assembly. The mutation of these two sites to phospho-mimicking residues seems to strongly suppress SAP formation in my mRNA injection assay, and to partially suppress the recruitment of Ana2 to the centriole *in vivo* (**Figure 6.11**). It is possible that these Cdk1/Cyclin B phosphorylation sites near the C-terminal region provide a control mechanism to prevent Plk4 interacting with and phosphorylating the STAN domain (thus allowing the Ana2/Sas-6 interaction). Intriguingly, one of these

mutations also seem to affect the length of M-phase, providing another hint that Ana2 might regulate the cell cycle (**Figure 6.11**). Further research is required to investigate the role of Cdk1/Cycling B phosphorylations on Ana2 and its affect on centriole assembly.

The SAP-based protein-protein interaction assay allows for a rapid and efficient identification of potentially interesting mutants. Using this screen it will be possible to probe for the domains required for Ana2 and Sas-6 interaction, possibly via Sas-4. This interaction interface has been elusive to date and conflicting reports show the presence or absence of a direct interaction between Ana2 and Sas-6 (Arquint et al., 2012; Stevens et al., 2010b; Tang et al., 2011). The SAPs protein-protein interaction assay could rapidly identify key interaction interfaces that could then be confirmed using transgenic flies. Thus, the SAPs could resolve several critical questions regarding centriole and centrosome assembly.

The work described in this thesis will hopefully help to further the study into centrioles, towards completing our understanding of this ancient and important cellular structure.

8. Appendix

8.1. Evaluation of the fluorophore mMaple3

mMaple3 is an improved variant of the photoconvertible fluorescent protein mMaple, derived from *Clavularia* coral (McEvoy et al., 2012; Wang et al., 2014). This fluorescent protein converts from green to red upon activation with 405 nm light. This newly developed fluorescent protein was designed to have a high-photon yield (defined as the average number of photons emitted when photoconverted), a low rate of spontaneous photoconversion in the absence of activating 405 nm light, folds efficiently and has a low tendency to dimerise (Wang et al., 2014). The ability of a fluorescent protein to photoconvert would make for an interesting tool to use to study protein dynamics in living *Drosophila* embryos. The fluorophore mDendra2 has previously been used to study Cnn dynamics at centrosomes (Conduit et al., 2014a). However, its a high rate of photobleaching and spontaneous photoconversion, made it unsuitable for time-lapse studies (Dr. A. Caballe and Dr. A. Wainman, personal communication). Thus, I chose evaluate this photoconvertible fluorescent protein mMaple3 as its photostability would render it more suitable for longer time-lapse imaging.

First, I generated transgenic flies that expressed mMaple3-Cnn under the control of the ubiquitin promoter; for comparison against I used a previously generated Dendra2-Cnn fusion-protein controlled by the same promoter:

$$w; \frac{+}{+}; \frac{\text{FP-Cnn}}{+}$$

It must be noted that due to time constraints, these flies were not recombined with a mutant Cnn^{f} allele. Comparing fusion-protein expression by western blot revealed

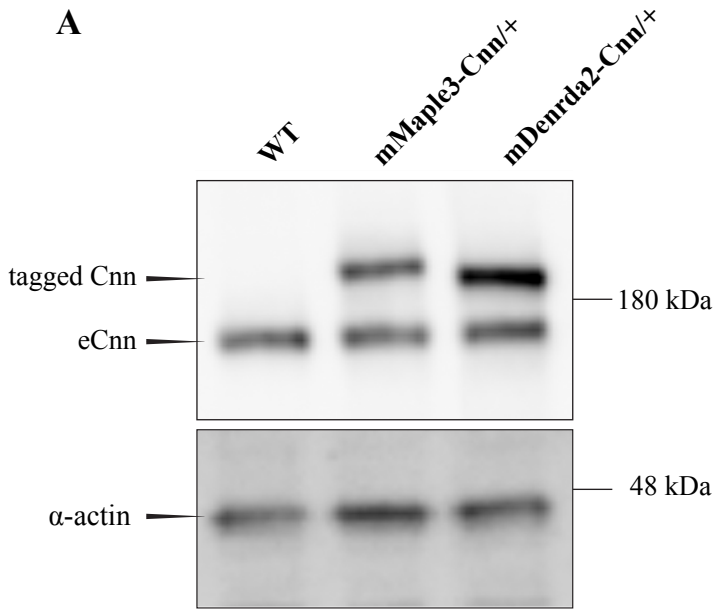


Figure 7.1: Assessment of fusion protein expression levels in mMaple3-Cnn and mDendra2-Cnn lines. The western blot shows the expression levels of the fusion proteins mNeongreen-Cnn and GFP-Cnn in transgenic flies. Each lane contains 5 early embryos. These early *Drosophila* embryos express one copy of the transgene in the presence of one copy of the endogenous WT gene (therefore endogenous, wild type Cnn is still expressed). The expression levels of the fusion proteins appear to be comparable between the two transgenic flies, when compared to the α-actin loading control. Endogenous Cnn (eCnn), tagged Cnn and α-actin are indicated by the arrows.

overall comparable expression levels, with mDendra2 expression slightly higher than that of the selected mMaple3 fly line (**Figure 8.1**).

Time-lapse studies were performed on three different microscopes (Perkin Elmer Spinning Disc, OMX V3 3D-SIM, Zeiss LSM880 Airyscan systems to assess the compatibility of mMaple3 with these systems commonly used for early *Drosophila* embryo imaging in the lab. Detail on the microscopes and the imaging procedures can be found in section 2.5.2 and 2.5.3, respectively. Briefly, the mMaple3 embryos were imaged for one time point (T=0) and ROIs selected. These ROIs were subsequently exposed to 405 nm light which induces the photoconversion from green to red emitting fluorescence. When using the Perkin Elmer spinning disc system, the photoconversion of mMaple3 seems efficient and surprisingly stable over ~18 min of imaging (**Figure 3.12A**). Imaging mMaple3 on the OMX V3 system proved unsuccessful in 3D-SIM mode. Even after 5 time points, a signification portion of the green signal had been photobleached (**Figure 3.12B**). Furthermore, the 593 nm excitation laser on the OMX V3 was not ideal for the excitation of mMaple3, which is more optimally by a 561 nm laser excitation. Hence, the red signal of the photoconverted mMaple3 was very dim. While it was possible to take an image of green mMaple3-Cnn with 3D-SIM, this was not possible with red mMaple3-Cnn (**Figure 8.2B, top right**) rendering this variant unsuitable for use on the OMX V3 system. In order to image mMaple3 in super-resolution, I used the Zeiss LSM880 Airyscan laser scanning microscope that is able to image in super-resolution. The photoconversion worked well on the Zeiss LSM880 (**Figure 8.2C**), however, even after 10 time points, there was significant photobleaching for both green and red

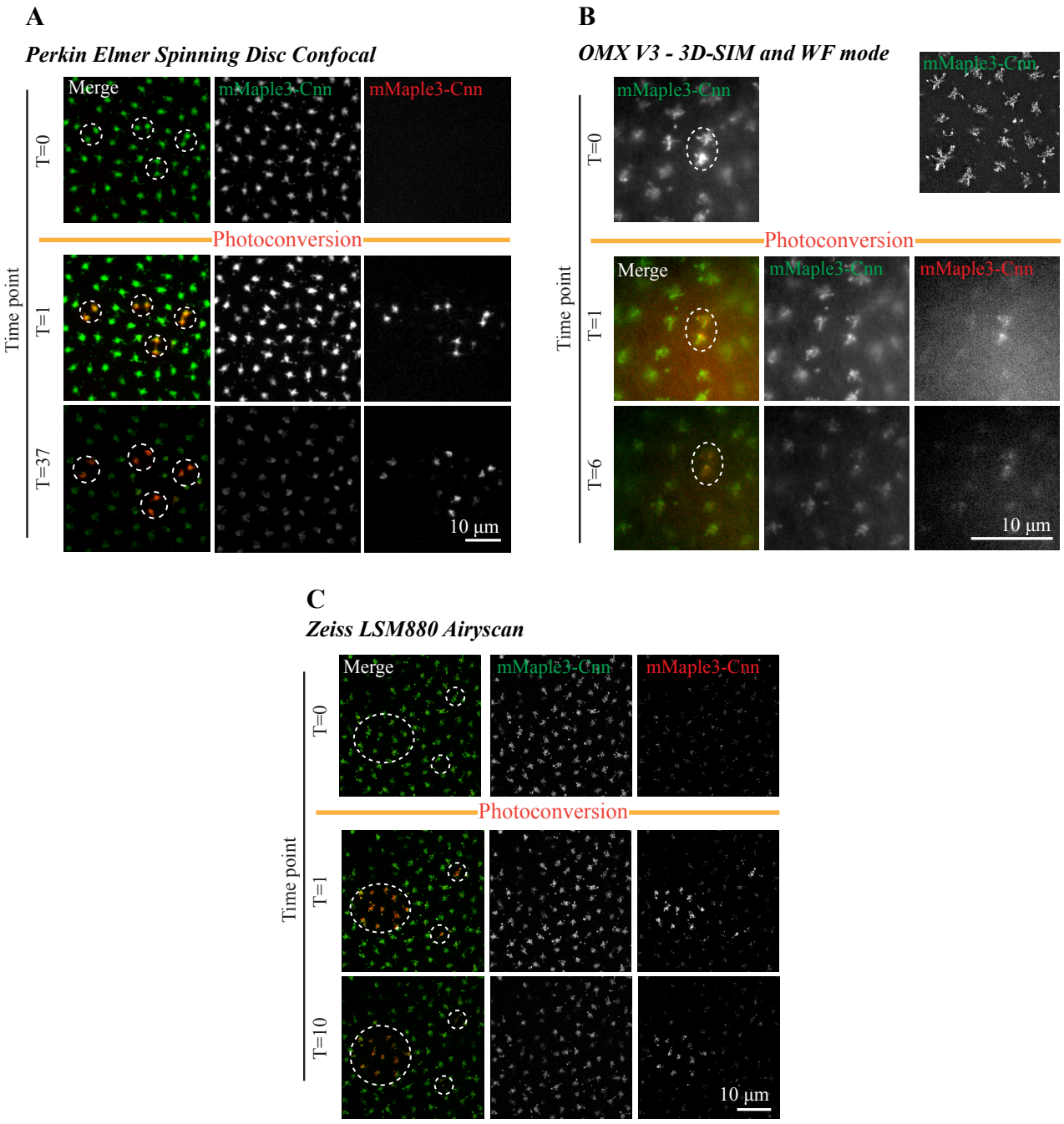


Figure 7.2: Photoconversion of mMaple3 on different microscopes. The white dashed circles indicate the ROI illuminated with 405 nm light to induce the photoconversion from green to red. Representative images from the following microscope are shown: **A**) a Perkin Elmer spinning disc (37 time points imaged, 561 nm excitation). Note the clarity and apparent stability of the signal in both green and red channels. **B**) OMX V3 in widefield mode (6 time points were images, 594 nm excitation). Note poorly the red emitting mMaple3 is being excited and how quickly the green and red signal photobleaches. The small right hand panel shows a 3D-SIM image of green emitting mMaple3. **C**) A Zeiss LSM880 lasers scanning microscope (10 time points imaged, 561 nm excitation). As shown the photo conversion from green to red is efficient, however, the sensitive detector is able to detect the low levels of spontaneous photoconversion from green to red (see T=0, red channel).

mMaple3. Additionally, with the more efficient excitation with 561 nm and increased detector sensitivity, I was able to detect the low level of photoconversion from green to red that mMaple3 undergoes without activation with 405 nm light (see **Figure 8.2C**, T=0, red channel).

In the following I used the Zeiss LSM880 Airyscan to compare the brightness and stability of mMaple3 and mDendra2. Analysing the signal intensity of the first 2 time points, pre-and post- photoconversion for both green and red emissions, it can be seen that mDendra2 is many fold brighter than mMaple3 in the green channel, whereas similar in the red channel (**Figure 8.3A**). However, the photostability over time revealed that mMaple3 is more stable in green and in red (**Figure 3.13B**), than mDendra2. The red signals form both fluorescent proteins exhibit comparable stability.

Taken together, it appears that mMaple3 is not brighter than mDendra2, but its green signal is more stable indicating that mMaple3 may be better suited for longer time-lapse imaging. However, the low level of photoconversion without photoactivation may become problematic when trying to convert very small amounts of labelled protein.

8.1.1. Discussion

The photoconvertible fluorescent protein mMaple3 in its green form was found to be more stable than mDendra2 currently used in the laboratory, while mDendra2 is still brighter in both green and red compared to mMaple3. Furthermore, mMaple3 is not compatible with the 594 nm laser of our 3D-SIM system. Additionally, its low level of photoconversion occurring without 405 nm activation, may make photoconversion

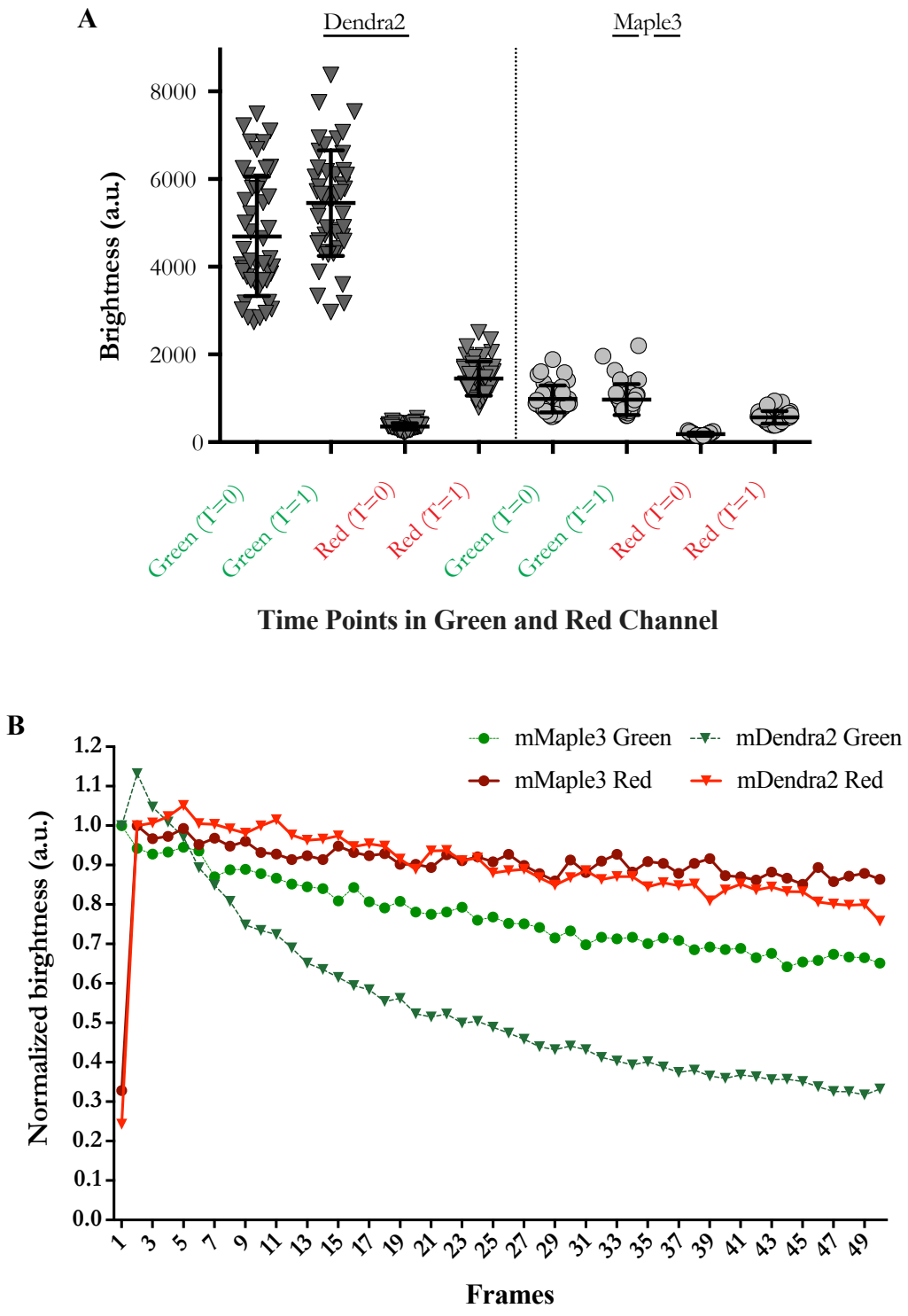


Figure 7.3: Brightness and stability comparison of mMaple3 and mDendra2 A) Graph displaying the signal intensity at different laser powers for the two different fluorophores under 561 nm excitation on the Zeiss LSM880 Airyscan. The brightest 5 centrosomes from 5 embryos were measured (a total of 25 centrosomes). As shown, the green and red signal in mDendra2 is brighter than mMaple3. **B**) The stability of the fluorophores over 60 continuous frames with exposure to both 488 nm and 561 nm laser. The brightest 5 centrosomes from 5 embryos were measured (a total of 25 centrosomes). The data for each fluorophore was normalized to itself. As shown, the green signal of mMaple3 is more stable than the mDendra2 green signal, whereas the red signal's stability is similar**.**

studies difficult as it may become difficult to identify ROIs, particularly if these are very small.

It must be noted that transgenic flies were not placed into a full mutant background. Endogenous un-tagged protein will be preferentially be recruited over fusion-proteins and the fluorescent protein signal may become dimmer in flies which are not in full mutant backgrounds (data not shown). It is unclear, if the level of fusion-protein recruitment in flies still expressing endogenous protein is the same for different fluorescent proteins. Therefore, it will be important to place the mMaple3-Cnn in a full Cnn mutant background, to properly assess its usefulness for time-lapse, super-resolution photoconversion experiments.

9. References

Alvarez Rodrigo, I., Conduit, P.T., Baumbach, J., Novak, Z.A., Aydogan, M.G., Wainman, A., and Raff, J. (2018). A positive feedback loop drives centrosome maturation in flies. bioRxiv 380907 https://doi.org/10.1101/380907.

Alves-Cruzeiro, J.M., Nogales-Cadenas, R., and Pascual-Montano, A.D. (2014). CentrosomeDB: a new generation of the centrosomal proteins database for Human and Drosophila melanogaster. Nucleic acids research *42*, D430-436.

Andersen, J., Wilkinson, C., Mayor, T., Mortensen, P., Nigg, E., and Mann, M. (2003). Proteomic characterization of the human centrosome by protein correlation profiling. Nature *426*, 570-574.

Arquint, C., Gabryjonczyk, A.M., Imseng, S., Bohm, R., Sauer, E., Hiller, S., Nigg, E.A., and Maier, T. (2015). STIL binding to Polo-box 3 of PLK4 regulates centriole duplication. eLife *4*.

Arquint, C., Gabryjonczyk, A.M., and Nigg, E.A. (2014). Centrosomes as signalling centres. Philos Trans R Soc Lond B Biol Sci *369*.

Arquint, C., and Nigg, E.A. (2014). STIL microcephaly mutations interfere with APC/C-mediated degradation and cause centriole amplification. Current biology : CB *24*, 351-360.

Arquint, C., Sonnen, K.F., Stierhof, Y.D., and Nigg, E.A. (2012). Cell-cycle-regulated expression of STIL controls centriole number in human cells. J Cell Sci *125*, 1342-1352.

Aydogan, M.G., Steinacker, T.L., Gartenmann, L., Wainman, A., Saurya, S., Conduit, P.T., Boemo, M.A., and Raff, J. (Nature, under review). A free-running oscillator times and executes centriole biogenesis.

Aydogan, M.G., Wainman, A., Saurya, S., Steinacker, T.L., Caballe, A., Novak, Z.A., Baumbach, J., Muschalik, N., and Raff, J.W. (2018). A homeostatic clock sets daughter centriole size in flies. J Cell Biol *217*, 1233-1248.

Azimzadeh, J. (2014). Exploring the evolutionary history of centrosomes. Philosophical Transactions of the Royal Society B: Biological Sciences *369*, 20130453-20130453.

Azimzadeh, J., Wong, M.L., Downhour, D.M., Sánchez Alvarado, A., and Marshall, F.D. (2012). Centrosome Loss in the Evolution of Planarians. Science *335*, 461-463.

Baird, G.S., Zacharia, D.A., and Tsien, R.Y. (2000). Biochemistry, mutagenesis, and oligomerization of DsRed, a red fluorescent protein from coral. Proceedings of the National Academy of Sciences *97*, 11984-11989.

Ball, G., Demmerle, J., Kaufmann, R., Davis, I., Dobbie, I.M., and Schermelleh, L. (2015). SIMcheck: a Toolbox for Successful Super-resolution Structured Illumination Microscopy. Sci Rep *5*, 15915.

Basto, R., Brunk, K., Vinadogrova, T., Peel, N., Franz, A., Khodjakov, A., and Raff, J.W. (2008). Centrosome amplification can initiate tumorigenesis in flies. Cell *133*, 1032-1042.

Basto, R., Lau, J., Vinogradova, T., Gardiol, A., Woods, C.G., Khodjakov, A., and Raff, J.W. (2006). Flies without centrioles. Cell *125*, 1375-1386.

Baumbach, J., Novak, Z.A., Raff, J.W., and Wainman, A. (2015). Dissecting the function and assembly of acentriolar microtubule organizing centers in Drosophila cells in vivo. PLoS Genet *11*, e1005261.

Bazzi, H., and Anderson, K.V. (2014). Acentriolar mitosis activates a p53-dependent apoptosis pathway in the mouse embryo. Proceedings of the National Academy of Sciences of the United States of America *111*, E1491-1500.

Bettencourt-Dias, M., Rodrigues-Martins, A., Carpenter, L., Riparbelli, M., Lehmann, L., Gatt, M.K., Carmo, N., Balloux, F., Callaini, G., and Glover, D.M. (2005). SAK/PLK4 is required for centriole duplication and flagella development. Current biology : CB *15*, 2199-2207.

Blachon, S., Gopalakrishnan, J., Omori, Y., Polyanovsky, A., Church, A., Nicastro, D., Malicki, J., and Avidor-Reiss, T. (2008). Drosophila asterless and vertebrate Cep152 Are orthologs essential for centriole duplication. Genetics *180*, 2081-2094.

Bonaccorsi, S., Giansanti, M.G., and Gatti, M. (1998). Spindle Self-organization and Cytokinesis During Male Meiosis in asterless Mutants of Drosophila melanogaster. The Journal of Cell Biology *142*, 751-761.

Brooks, E.R., and Wallingford, J.B. (2014). Multiciliated cells. Current biology : CB *24*, R973-982.

Brownlee, C.W., Klebba, J.E., Buster, D.W., and Rogers, G.C. (2011). The Protein Phosphatase 2A regulatory subunit Twins stabilizes Plk4 to induce centriole amplification. J Cell Biol *195*, 231-243.

Callaini, G., Whitefield, W.G.F., and Riparbelli, M. (1997). Centriole and Centrosome Dynamics during the Embryonic Cell Cycles That Follow the Formation of the Cellular Blastoderm in Drosophila. Experimental Cell Research *234*, 183-190.

Callan, M.A., Cabernard, C., Heck, J., Luois, S., Doe, C.Q., and Zarnescu, D.C. (2010). Fragile X protein controls neural stem cell proliferation in the Drosophila brain. Hum Mol Genet *19*, 3068-3079.

Campos, A.R., Rosen, D.R., Robinow, S.N., and White, K. (1987). Molecular analysis of the locus elav in Drosophila melanogaster: a gene whose embryonic expression is neural specific. EMBO J *6*, 425-431.

Carvalho-Santos, Z., Azimzadeh, J., Pereira-Leal, J.B., and Bettencourt-Dias, M. (2011). Tracing the origins of centrioles, cilia, and flagella. The Journal of Cell Biology *194*, 165-175.

Carvalho-Santos, Z., Machado, P., Branco, P., Tavares-Cadete, F., Rodrigues-Martins, A., Pereira-Leal, J.B., and Bettencourt-Dias, M. (2010). Stepwise evolution of the centriole-assembly pathway. J Cell Sci *123*, 1414-1426.

Cavalier-Smith, T. (2002). The phagotrophic origin of eukaryotes and phylogenetic classification of Protozoa. International Journal of Systematic and Evolutionary Microbiology *52*, 297-354.

Chalfie, M., Tu, Y., Euskirchen, G., Ward, W.W., and D.C., P. (1994). Green fluorescent protein as a marker for gene expression. Science *263*, 802-805.

Chan, J.Y. (2011). A Clinical Overview of Centrosome Amplification in Human Cancers. International Journal of Biological Sciences *7*, 1122-1144.

Chavali, P.L., Putz, M., and Gergely, F. (2014). Small organelle, big responsibility: the role of centrosomes in development and disease. Philos Trans R Soc Lond B Biol Sci *369*.

Chu, J., Haynes, R.D., Corbel, S.Y., Li, P., Gonzalez-Gonzalez, E., Burg, J.S., Ataie, N.J., Lam, A.J., Cranfill, P.J., Baird, M.A.*, et al.* (2014). Non-invasive intravital imaging of cellular differentiation with a bright red-excitable fluorescent protein. Nat Methods *11*, 572-578.

Cizmecioglu, O., Arnold, M., Bahtz, R., Settele, F., Ehret, L., Haselmann-Weiss, U., Antony, C., and Hoffmann, I. (2010). Cep152 acts as a scaffold for recruitment of Plk4 and CPAP to the centrosome. J Cell Biol *191*, 731-739.

Conduit, P.T. (2013). The dominant force of Centrobin in centrosome asymmetry. Nature cell biology *15*, 235-237.

Conduit, P.T., Brunk, K., Dobbelaere, J., Dix, C.I., Lucas, E.P., and Raff, J.W. (2010). Centrioles regulate centrosome size by controlling the rate of Cnn incorporation into the PCM. Current biology : CB *20*, 2178-2186.

Conduit, P.T., Feng, Z., Richens, J.H., Baumbach, J., Wainman, A., Bakshi, S.D., Dobbelaere, J., Johnson, S., Lea, S.M., and Raff, J.W. (2014a). The centrosome-specific phosphorylation of Cnn by Polo/Plk1 drives Cnn scaffold assembly and centrosome maturation. Developmental cell *28*, 659-669.

Conduit, P.T., Richens, J.H., Wainman, A., Holder, J., Vicente, C.C., Pratt, M.B., Dix, C.I., Novak, Z.A., Dobbie, I.M., Schermelleh, L.*, et al.* (2014b). A molecular mechanism of mitotic centrosome assembly in Drosophila. eLife *3*, e03399.

Conduit, P.T., Wainman, A., Novak, Z.A., Weil, T.T., and Raff, J.W. (2015a). Re-examining the role of Drosophila Sas-4 in centrosome assembly using two-colour-3D-SIM FRAP. eLife *4*.

Conduit, P.T., Wainman, A., and Raff, J.W. (2015b). Centrosome function and assembly in animal cells. Nat Rev Mol Cell Biol *16*, 611-624.

Coons, A.H., Creech, H.J., Jones, R.N., and Berliner, E. (1942). The demonstration of pneumococcal antigen in tissues by the use of fluorescent antibody. Journal of Immunology *45*, 159-170.

Corbit, K.C., Aanstad, P., Singla, V., Norman, A.R., Stainier, D.Y., and Reiter, J.F. (2005). Vertebrate Smoothened functions at the primary cilium. Nature *437*, 1018-1021.

Corbit, K.C., Shyer, A.E., Dowdle, W.E., Gaulden, J., Singla, V., Chen, M.H., Chuang, P.T., and Reiter, J.F. (2008). Kif3a constrains beta-catenin-dependent Wnt signalling through dual ciliary and non-ciliary mechanisms. Nature cell biology *10*, 70-76.

Cottee, M.A., Johnson, S., Raff, J.W., and Lea, S.M. (2017). A key centriole assembly interaction interface between human Plk4 and STIL appears to not be conserved in flies. Biology Open.

Cottee, M.A., Muschalik, N., Johnson, S., Leveson, J., Raff, J.W., and Lea, S.M. (2015). The homo-oligomerisation of both Sas-6 and Ana2 is required for efficient centriole assembly in flies. eLife *4*, e07236.

Cottee, M.A., Muschalik, N., Wong, Y.L., Johnson, C.M., Johnson, S., Andreeva, A., Oegema, K., Lea, S.M., Raff, J.W., and van Breugel, M. (2013). Crystal structures of the CPAP/STIL complex reveal its role in centriole assembly and human microcephaly. eLife *2*, e01071.

Cottee, M.A., Raff, J.W., Lea, S.M., and Roque, H. (2011). SAS-6 oligomerization: the key to the centriole? Nat Chem Biol *7*, 650-653.

Craggs, T.D. (2009). Green fluorescent protein: structure, folding and chromophore maturation. Chemical Society Reviews *38*, 2865.

Cranfill, P.J., Sell, B.R., Baird, M.A., Allen, J.R., Lavagnino, Z., de Gruiter, H.M., Kremers, G.J., Davidson, M.W., Ustione, A., and Piston, D.W. (2016). Quantitative assessment of fluorescent proteins. Nat Methods *13*, 557-562.

Crivat, G., and Taraska, J.W. (2012). Imaging proteins inside cells with fluorescent tags. Trends in biotechnology *30*, 8-16.

Cunha-Ferreira, I., Bento, I., Pimenta-Marques, A., Jana, S.C., Lince-Faria, M., Duarte, P., Borrego-Pinto, J., Gilberto, S., Amado, T., Brito, D.*, et al.* (2013). Regulation of autophosphorylation controls PLK4 self-destruction and centriole number. Current biology : CB *23*, 2245-2254.

Cunha-Ferreira, I., Rodrigues-Martins, A., Bento, I., Riparbelli, M., Zhang, W., Laue, E., Callaini, G., Glover, D.M., and Bettencourt-Dias, M. (2009). The SCF/Slimb ubiquitin ligase limits centrosome amplification through degradation of SAK/PLK4. Current biology : CB *19*, 43-49.

Dammermann, A., Muller-Reichert, T., Pelletier, L., Habermann, B., Desai, A., and Oegema, K. (2004). Centriole assembly requires both centriolar and pericentriolar material proteins. Developmental cell *7*, 815-829.

David, A., Liu, F., Tibelius, A., Vulprecht, J., Wald, D., Rothermel, U., Ohana, R., Seitel, A., Metzger, J., Ashery-Padan, R.*, et al.* (2014). Lack of centrioles and primary cilia in STIL(-/-) mouse embryos. Cell Cycle *13*, 2859-2868.

Day, R.N., and Davidson, M.W. (2009). The fluorescent protein palette: tools for cellular imaging. Chem Soc Rev *38*, 2887-2921.

Delattre, M., Canard, C., and Gonczy, P. (2006). Sequential protein recruitment in C. elegans centriole formation. Current biology : CB *16*, 1844-1849.

Delattre, M., Leidel, S., Wani, K., Baumer, K., Bamat, J., Schnabel, H., Feichtinger, R., Schnabel, R., and Gonczy, P. (2004). Centriolar SAS-5 is required for centrosome duplication in C. elegans. Nature cell biology *6*, 656-664.

Delgehyr, N., Rangone, H., Fu, J., Mao, G., Tom, B., Riparbelli, M.G., Callaini, G., and Glover, D.M. (2012). Klp10A, a microtubule-depolymerizing kinesin-13, cooperates with CP110 to control Drosophila centriole length. Current biology : CB *22*, 502-509.

Demmerle, J., Innocent, C., North, A.J., Ball, G., Müller, M., Miron, E., Matsuda, A., Dobbie, I.M., Markaki, Y., and Schermelleh, L. (2017). Strategic and practical guidelines for successful structured illumination microscopy. Nature Protocols *12*, 988-1010.

Dempsey, G.T., Vaughan, J.C., Chen, K.H., Bates, M., and Zhuang, X. (2011). Evaluation of fluorophores for optimal performance in localization-based super-resolution imaging. Nat Methods *8*, 1027-1036.

Dix, C.I., and Raff, J.W. (2007). Drosophila Spd-2 recruits PCM to the sperm centriole, but is dispensable for centriole duplication. Current biology : CB *17*, 1759-1764.

Dobbelaere, J., Josue, F., Suijkerbuijk, S., Baum, B., Tapon, N., and Raff, J. (2008). A genome-wide RNAi screen to dissect centriole duplication and centrosome maturation in Drosophila. PLoS Biol *6*, e224.

Dumont, J., and Desai, A. (2012). Acentrosomal spindle assembly and chromosome segregation during oocyte meiosis. Trends Cell Biol *22*, 241-249.

Dzhindzhev, N.S., Tzolovsky, G., Lipinszki, Z., Abdelaziz, M., Debski, J., Dadlez, M., and Glover, D.M. (2017). Two-step phosphorylation of Ana2 by Plk4 is required for the sequential loading of Ana2 and Sas6 to initiate procentriole formation. Open Biol *7*.

Dzhindzhev, N.S., Tzolovsky, G., Lipinszki, Z., Schneider, S., Lattao, R., Fu, J., Debski, J., Dadlez, M., and Glover, D.M. (2014). Plk4 phosphorylates Ana2 to trigger Sas6 recruitment and procentriole formation. Current biology : CB *24*, 2526-2532.

Dzhindzhev, N.S., Yu, Q.D., Weiskopf, K., Tzolovsky, G., Cunha-Ferreira, I., Riparbelli, M., Rodrigues-Martins, A., Bettencourt-Dias, M., Callaini, G., and Glover, D.M. (2010). Asterless is a scaffold for the onset of centriole assembly. Nature *467*, 714-718.

Eila, A.E.H., Cantley, L.C., and Yaffe, M.B. (2003). Proteomic Screen Finds pSer/pThr-Binding Domain Localizing Plk1 to Mitotic Substrates. Science *299*, 1228-1231.

Ellisman, M.H., Deerinck, T.J., Shu, X., and Sosinsky, G.E. (2012). Picking faces out of a crowd: genetic labels for identification of proteins in correlated light and electron microscopy imaging. Methods Cell Biol *111*, 139-155.

Enrique Balleza, E., Kim, J.M., and Cluze, P. (2017). Systematic characterization of maturation time of fluorescent proteins in living cells. Nature Methods.

Ewers, H. (2018). Open-source recombinant monoclonal secondary nanobodies. J Cell Biol *217*, 809-811.

Feng, Z., Caballe, A., Wainman, A., Johnson, S., Haensele, A.F.M., Cottee, M.A., Conduit, P.T., Lea, S.M., and Raff, J.W. (2017). Structural Basis for Mitotic Centrosome Assembly in Flies. Cell *169*, 1078-1089 e1013.

Fernandez-Suarez, M., and Ting, A.Y. (2008). Fluorescent probes for super-resolution imaging in living cells. Nat Rev Mol Cell Biol *9*, 929-943.

Foe, E.V., and Alberts, B.M. (1983). Studies of nuclear and cytoplasmic behaviour during the five mitotic cycles that precede gastrulation in Drosophila embryogenesis. Journal of Cell Science *61*, 31-70.

Fong, C.S., Kim, M., Yang, T.T., Liao, J.C., and Tsou, M.F. (2014). SAS-6 assembly templated by the lumen of cartwheel-less centrioles precedes centriole duplication. Developmental cell *30*, 238-245.

Franz, A., Roque, H., Saurya, S., Dobbelaere, J., and Raff, J.W. (2013). CP110 exhibits novel regulatory activities during centriole assembly in Drosophila. J Cell Biol *203*, 785-799.

Fu, J., and Glover, D.M. (2012). Structured illumination of the interface between centriole and peri-centriolar material. Open Biol *2*, 120104.

Fu, J., Lipinszki, Z., Rangone, H., Min, M., Mykura, C., Chao-Chu, J., Schneider, S., Dzhindzhev, N.S., Gottardo, M., Riparbelli, M.G.*, et al.* (2016). Conserved molecular interactions in centriole-to-centrosome conversion. Nature cell biology *18*, 87-99.

Galletta, B.J., Jacobs, K.C., Fagerstrom, C.J., and Rusan, N.M. (2016). Asterless is required for centriole length control and sperm development. J Cell Biol *213*, 435-450.

Ganem, N.J., Godinho, S.A., and Pellman, D. (2009). A mechanism linking extra centrosomes to chromosomal instability. Nature *460*, 278-282.

Gautier, A., Juillerat, A., Heinis, C., Correa, I.R., Jr., Kindermann, M., Beaufils, F., and Johnsson, K. (2008). An engineered protein tag for multiprotein labeling in living cells. Chem Biol *15*, 128-136.

Giansanti, M.G., Bucciarelli, E., Bonaccorsi, S., and Gatti, M. (2008). Drosophila SPD-2 is an essential centriole component required for PCM recruitment and astral-microtubule nucleation. Current biology : CB *18*, 303-309.

Gilmore, E.C., and Walsh, C.A. (2013). Genetic causes of microcephaly and lessons for neuronal development. Wiley Interdiscip Rev Dev Biol *2*, 461-478.

Godinho, S.A., Picone, R., Burute, M., Dagher, R., Su, Y., Leung, C.T., Polyak, K., Brugge, J.S., Thery, M., and Pellman, D. (2014). Oncogene-like induction of cellular invasion from centrosome amplification. Nature *510*, 167-171.

Gonczy, P. (2012). Towards a molecular architecture of centriole assembly. Nat Rev Mol Cell Biol *13*, 425-435.

Gonzalez, C., Saunders, R.D.C., Casal, J., Molina, I., Carmena, M., Ripoll, R., and Glover, D.M. (1990). Mutations at the asp locus of Drosophila lead to multiple free centrosomes in syncytial embryos, but restrict centrosome duplication in larval neuroblasts. Journal of Cell Science *96*, 605-616.

Gopalakrishnan, J., Mennella, V., Blachon, S., Zhai, B., Smith, A.H., Megraw, T.L., Nicastro, D., Gygi, S.P., Agard, D.A., and Avidor-Reiss, T. (2011). Sas-4 provides a scaffold for cytoplasmic complexes and tethers them in a centrosome. Nat Commun *2*, 359.

Goshima, G., Wollman, R., Goodwin, S.S., Zhang, N., Scholey, J.M., Vale, R.D., and Stuurman, N. (2007). Genes required for mitotic spindle assembly in Drosophila S2 cells. Science *316*, 417-421.

Gottardo, M., Callaini, G., and Riparbelli, M.G. (2017). Correction: The Drosophila centriole - conversion of doublets into triplets within the stem cell niche (doi: 10.1242/jcs.172627). J Cell Sci *130*, 4225.

Gottardo, M., Pollarolo, G., Llamazares, S., Reina, J., Riparbelli, M.G., Callaini, G., and Gonzalez, C. (2015). Loss of Centrobin Enables Daughter Centrioles to Form Sensory Cilia in Drosophila. Current biology : CB *25*, 2319-2324.

Greenan, G.A., Keszthelyi, B., Vale, R.D., and Agard, D.A. (2018). Insights into centriole geometry revealed by cryotomography of doublet and triplet centrioles. eLife *7*.

Greenspan, R.J. (2004). Fly pushing: The theory and practice of Drosophila genetics (New York: Cold Spring Harbour Laboratory Press).

Grull, F., Kirchgessner, M., Kaufmann, R., Hausmann, M., and Kebschull, U. (2011). Accelerating Image Analysis for Localization Microscopy with FPGAs. IEEE *Field Programmable Logic and Applications (FPL), 2011 International Conference* 1-5.

Guderian, G., Westendorf, J., Uldschmid, A., and Nigg, E.A. (2010). Plk4 trans-autophosphorylation regulates centriole number by controlling betaTrCP-mediated degradation. J Cell Sci *123*, 2163-2169.

Guichard, P., Desfosses, A., Maheshwari, A., Hachet, V., Dietrich, C., Brune, A., Ishikawa, T., Sachse, C., and Gonczy, P. (2012). Cartwheel architecture of Trichonympha basal body. Science *337*, 553.

Guichard, P., Hachet, V., Majubu, N., Neves, A., Demurtas, D., Olieric, N., Fluckiger, I., Yamada, A., Kihara, K., Nishida, Y*., et al.* (2013). Native architecture of the centriole proximal region reveals features underlying its 9-fold radial symmetry. Current Biology *23*, 1620-1628.

Guichard, P., Hamel, V., Le Guennec, M., Banterle, N., Iacovache, I., Nemcikova, V., Fluckiger, I., Goldie, K.N., Stahlberg, H., Levy, D*., et al.* (2017). Cell-free reconstitution reveals centriole cartwheel assembly mechanisms. Nat Commun *8*, 14813.

Habedanck, R., Stierhof, Y.D., Wilkinson, C.J., and Nigg, E.A. (2005). The Polo kinase Plk4 functions in centriole duplication. Nature cell biology *7*, 1140-1146.

Hamel, V., Guichard, P., Fournier, M., Guiet, R., Fluckiger, I., Seitz, A., and Gonczy, P. (2014). Correlative multicolor 3D SIM and STORM microscopy. Biomed Opt Express *5*, 3326-3336.

Haren, L., Stearns, T., and Luders, J. (2009). Plk1-dependent recruitment of gamma-tubulin complexes to mitotic centrosomes involves multiple PCM components. PLoS One *4*, e5976.

Hatch, E.M., Kulukian, A., Holland, A.J., Cleveland, D.W., and Stearns, T. (2010). Cep152 interacts with Plk4 and is required for centriole duplication. J Cell Biol *191*, 721-729.

Heald, R., Tournebize, R., Habermann, A., Karsenti, E., and Hyman, A. (1997). Spindle Assembly in Xenopus Egg Extracts: Respective Roles of Centrosomes and Microtubule Self-Organization. The Journal of Cell Biology *138*, 615-628.

Helm, R., Cubitt, A.B., and Tsien, R.Y. (1995). Improved green fluorescence. Nature *373*, 663-664.

Helmholtz, H. (1874). Die theoretischen Grenzen fu¨r die Leistungsfa¨higkeit der Mikroskope. Ann Phys.

Hepperta, J.K., Dickinson, D.J., Pani, A.M., Higginsa, C.D., Steward, A., Ahringer, J., Kuhnd, J.R., and Goldstein, B. (2016). Comparative assessment of flourescent proteins for in vivo imaging in an animal model system. Molecular Biology of the Cell *27*, 3385-3394.

Herschel, J.F.W. (1845). On a case of superficial colour presented by a homogeneous liquid internally colourless. . Philosophical Transactions Royal Society of London *135*, 143-145.

Hilbert, M., Erat, M.C., Hachet, V., Guichard, P., Blank, I.D., Fluckiger, I., Slater, L., Lowe, E.D., Hatzopoulos, G.N., Steinmetz, M.O.*, et al.* (2013). Caenorhabditis elegans centriolar protein SAS-6 forms a spiral that is consistent with imparting a ninefold symmetry. Proceedings of the National Academy of Sciences of the United States of America *110*, 11373-11378.

Hilbert, M., Noga, A., Frey, D., Hamel, V., Guichard, P., Kraatz, S.H., Pfreundschuh, M., Hosner, S., Fluckiger, I., Jaussi, R.*, et al.* (2016). SAS-6 engineering reveals interdependence between cartwheel and microtubules in determining centriole architecture. Nature cell biology *18*, 393-403.

Hinchcliffe, E.H., Li, C., Thompson, E.A., Maller, J.L., and Sluder, G. (1999). Requirement of Cdk2–Cyclin E Activity for Repeated Centrosome Reproduction in Xenopus Egg Extracts. Science *283*, 851-854.

Holland, A.J., Fachinetti, D., Zhu, Q., Bauer, M., Verma, I.M., Nigg, E.A., and Cleveland, D.W. (2012). The autoregulated instability of Polo-like kinase 4 limits centrosome duplication to once per cell cycle. Genes Dev *26*, 2684-2689.

Holland, A.J., Lan, W., Niessen, S., Hoover, H., and Cleveland, D.W. (2010). Polo-like kinase 4 kinase activity limits centrosome overduplication by autoregulating its own stability. J Cell Biol *188*, 191-198.

Holt, L.J., Tuch, B.B., Villen, J., Johnson, A.D., Gygi, S.P., and Morgan, D.O. (2009). Global analysis of Cdk1 substrate phosphorylation sites provides insights into evolution. Science *325*, 1682-1686.

Huang, B., Wang, W., Bates, M., and Zhuang, X. (2008). Three-Dimensional Super-Resolution Imaging by Stochastic Optical Reconstruction Microscopy. Science *319*, 810-813.

Huang, J., and Raff, J.W. (1999). The disappearance of cyclin B at the end of mitosis is regulated spatially in Drosophila cells. EMBO J *18*, 2184-2195.

Huangfu, D., Liu, A., Rakeman, A.S., Murcia, N.S., Niswander, L., and Anderson, K.V. (2003). Hedgehog signalling in the mouse requires intraflagellar transport proteins. Nature *426*, 83-87.

Hung, L., Chen, H.C., Chang, C., Li, B., and Tang, T.K. (2004). Identification of a Novel Microtubule-destabilizing Motif in CPAP That Binds to Tubulin Heterodimers and Inhibits Microtubule Assembly. Molecular Biology of the Cell, 6.

Hung, L., Tang, C.C., and Tang, T.K. (2000). Protein 4.1 R-135 Interacts with a Novel Centrosomal Protein (CPAP) Which Is Associated with the gamma-Tubulin Complex. Molecular & Cellular Biology *20*, 7813-7825.

Hurbain, I., and Sachse, M. (2011). The future is cold: cryo-preparation methods for transmission electron microscopy of cells. Biol Cell *103*, 405-420.

Insolera, R., Bazzi, H., Shao, W., Anderson, K.V., and Shi, S.H. (2014). Cortical neurogenesis in the absence of centrioles. Nat Neurosci *17*, 1528-1535.

Jana, S.C., Bettencourt-Dias, M., Durand, B., and Megraw, T.L. (2016). Drosophila melanogaster as a model for basal body research. Cilia *5*, 22.

Jiang, K., Toedt, G., Montenegro Gouveia, S., Davey, N.E., Hua, S., van der Vaart, B., Grigoriev, I., Larsen, J., Pedersen, L.B., Bezstarosti, K.*, et al.* (2012). A Proteome-wide screen for mammalian SxIP motif-containing microtubule plus-end tracking proteins. Current biology : CB *22*, 1800-1807.

Johnson, E., Seiradake, E., Jones, E.Y., Davis, I., Grunewald, K., and Kaufmann, R. (2015). Correlative in-resin super-resolution and electron microscopy using standard fluorescent proteins. Sci Rep *5*, 9583.

Joosen, L., Hink, M.A., Gadella, T.W., Jr., and Goedhart, J. (2014). Effect of fixation procedures on the fluorescence lifetimes of Aequorea victoria derived fluorescent proteins. J Microsc *256*, 166-176.

Joseph, N., Al-Jassar, C., Johnson, C.M., Andreeva, A., Barnabas, D.D., Freund, S.M.V., Gergely, F., and van Breugel, M. (2018). Disease-Associated Mutations in CEP120 Destabilize the Protein and Impair Ciliogenesis. Cell Rep *23*, 2805-2818.

Juillerat, A., Gronemeyer, T., Keppler, A., Gendreizig, S., Pick, H., Vogel, H., and Johnsson, K. (2003). Directed Evolution of O6-Alkylguanine-DNA Alkyltransferase for Efficient Labeling of Fusion Proteins with Small Molecules In Vivo. Chemistry & Biology *10*, 313-317.

Keller, L.C., Romijn, E.P., Zamora, I., Yates, J.R., and Marshall, W.F. (2005). Proteomic Analysis of Isolated Chlamydomonas Centrioles Reveals Orthologs of Ciliary-Disease Genes. Current Biology *15*, 1090-1098.

Khodjakov, A., Cole, R.W., Oakley, B.R., and Reider, C.L. (1999). Centrosome-independent mitotic spindle formation in vertebrates. Current Biology *10*, 59-67.

Khodjakov, A., Rieder, C.L., Sluder, G., Cassels, G., Sibon, O., and Wang, C.-L. (2002). De novo formation of centrosomes in vertebrate cells arrested during S phase. The Journal of Cell Biology *158*, 1171-1181.

Kim, T.S., Park, J.E., Shukla, A., Choi, S., Murugan, R.N., Lee, J.H., Ahn, M., Rhee, K., Bang, J.K., Kim, B.Y.*, et al.* (2013). Hierarchical recruitment of Plk4 and regulation of centriole biogenesis by two centrosomal scaffolds, Cep192 and Cep152. Proceedings of the National Academy of Sciences of the United States of America *110*, E4849-4857.

Kirkham, M., Müller-Reichert, T., Oegema, K., Grill, S., and Hyman, A.A. (2003). SAS-4 is a C. elegans centriolar protein that controls centrosome size. Cell *112*, 575-587.

Kitagawa, D., Vakonakis, I., Olieric, N., Hilbert, M., Keller, D., Olieric, V., Bortfeld, M., Erat, M.C., Fluckiger, I., Gonczy, P.*, et al.* (2011). Structural basis of the 9-fold symmetry of centrioles. Cell *144*, 364-375.

Klebba, J.E., Buster, D.W., McLamarrah, T.A., Rusan, N.M., and Rogers, G.C. (2015). Autoinhibition and relief mechanism for Polo-like kinase 4. Proceedings of the National Academy of Sciences of the United States of America *112*, E657-666.

Klebba, J.E., Buster, D.W., Nguyen, A.L., Swatkoski, S., Gucek, M., Rusan, N.M., and Rogers, G.C. (2013). Polo-like kinase 4 autodestructs by generating its Slimb-binding phosphodegron. Current biology : CB *23*, 2255-2261.

Kleylein-Sohn, J., Westendorf, J., Le Clech, M., Habedanck, R., Stierhof, Y.D., and Nigg, E.A. (2007). Plk4-induced centriole biogenesis in human cells. Developmental cell *13*, 190-202.

Klingseisen, A., and Jackson, A.P. (2011). Mechanisms and pathways of growth failure in primordial dwarfism. Genes Dev *25*, 2011-2024.

Knoblich, J.A. (2008). Mechanisms of asymmetric stem cell division. Cell *132*, 583-597.

Kobayashi, T., and Dynlacht, B.D. (2011). Regulating the transition from centriole to basal body. J Cell Biol *193*, 435-444.

Kohl, J., Ng, J., Cachero, S., Ciabatti, E., Dolan, M.J., Sutcliffe, B., Tozer, A., Ruehle, S., Krueger, D., Frechter, S.*, et al.* (2014). Ultrafast tissue staining with chemical tags. Proceedings of the National Academy of Sciences of the United States of America *111*, E3805-3814.

Kraatz, S., Guichard, P., Obbineni, J.M., Olieric, N., Hatzopoulos, G.N., Hilbert, M., Sen, I., Missimer, J., Gonczy, P., and Steinmetz, M.O. (2016). The Human Centriolar Protein CEP135 Contains a Two-Stranded Coiled-Coil Domain Critical for Microtubule Binding. Structure *24*, 1358-1371.

Kratz, A.S., Barenz, F., Richter, K.T., and Hoffmann, I. (2015). Plk4-dependent phosphorylation of STIL is required for centriole duplication. Biol Open *4*, 370-377.

Kredel, S., Oswald, F., Nienhaus, K., Deuschle, K., Rocker, C., Wolff, M., Heilker, R., Nienhaus, G.U., and Wiedenmann, J. (2009). mRuby, a bright monomeric red fluorescent protein for labeling of subcellular structures. PLoS One *4*, e4391.

Lacey, K.R., Jackson, P.K., and Stearns, T. (1999). Cyclin-dependent kinase control of centrosome duplication. PNAS *96*.

Lam, A.J., St-Pierre, F., Gong, Y., Marshall, J.D., Cranfill, P.J., Baird, M.A., McKeown, M.R., Wiedenmann, J., Davidson, M.W., Schnitzer, M.J*., et al.* (2012). Improving FRET dynamic range with bright green and red fluorescent proteins. Nat Methods *9*, 1005-1012.

Lambrus, B.G., Uetake, Y., Clutario, K.M., Daggubati, V., Snyder, M., Sluder, G., and Holland, A.J. (2015). p53 protects against genome instability following centriole duplication failure. J Cell Biol *210*, 63-77.

Lancaster, M.A., Renner, M., Martin, C.A., Wenzel, D., Bicknell, L.S., Hurles, M.E., Homfray, T., Penninger, J.M., Jackson, A.P., and Knoblich, J.A. (2013). Cerebral organoids model human brain development and microcephaly. Nature *501*, 373-379.

Lattao, R., Kovacs, L., and Glover, D.M. (2017). The Centrioles, Centrosomes, Basal Bodies, and Cilia of Drosophila melanogaster. Genetics *206*, 33-53.

Lawo, S., Hasegan, M., Gupta, G.D., and Pelletier, L. (2012). Subdiffraction imaging of centrosomes reveals higher-order organizational features of pericentriolar material. Nature cell biology *14*, 1148-1158.

Lee, H., Simon, J.A., and Lis, J.T. (1988). Structure and expression of ubiquitin genes of Drosophila melanogaster. Molecular & Cellular Biology *8*, 4727-4735.

Leidel, S., Delattre, M., Cerutti, L., Baumer, K., and Gonczy, P. (2005). SAS-6 defines a protein family required for centrosome duplication in C. elegans and in human cells. Nature cell biology *7*, 115-125.

Leidel, S., and Gonczy, P. (2003). SAS-4 Is Essential for Centrosome Duplication in C. elegans and Is Recruited to Daughter Centrioles Once per Cell Cycle. Developmental cell *4*, 431-439.

Levine, M.S., Bakker, B., Boeckx, B., Moyett, J., Lu, J., Vitre, B., Spierings, D.C., Lansdorp, P.M., Cleveland, D.W., Lambrechts, D*., et al.* (2017). Centrosome Amplification Is Sufficient to Promote Spontaneous Tumorigenesis in Mammals. Developmental cell *40*, 313-322 e315.

Lin, M.Z., and Wang, L. (2008). Selective labeling of proteins with chemical probes in living cells. Physiology (Bethesda) *23*, 131-141.

Lin, Y.C., Chang, C.W., Hsu, W.B., Tang, C.J., Lin, Y.N., Chou, E.J., Wu, C.T., and Tang, T.K. (2013). Human microcephaly protein CEP135 binds to hSAS-6 and CPAP, and is required for centriole assembly. EMBO J *32*, 1141-1154.

Lindsley, D., and Zimm, G.G. (1992). The genome of Drosophila melanogaster (Academic Press).

Loncarek, J., Hergert, P., and Khodjakov, A. (2010). Centriole reduplication during prolonged interphase requires procentriole maturation governed by Plk1. Current biology : CB *20*, 1277-1282.

Loncarek, J., Hergert, P., Magidson, V., and Khodjakov, A. (2008). Control of daughter centriole formation by the pericentriolar material. Nature cell biology *10*, 322-328.

Lopes, C.A., Jana, S.C., Cunha-Ferreira, I., Zitouni, S., Bento, I., Duarte, P., Gilberto, S., Freixo, F., Guerrero, A., Francia, M.*, et al.* (2015). PLK4 trans-Autoactivation Controls Centriole Biogenesis in Space. Developmental cell *35*, 222-235.

Los, G.V., and Wood, K. (2007). HaloTag: A Novel Protein Labeling Technology for Cell Imaging and Protein Analysis. Methods in Molecular Biology *356*, 195-208.

Lucas, E.P., and Raff, J.W. (2007). Maintaining the proper connection between the centrioles and the pericentriolar matrix requires Drosophila centrosomin. J Cell Biol *178*, 725-732.

Mahmood, S., Ahmad, W., and Hassan, M.J. (2011). Autosomal recessive primary microcephaly (MCPH): clinical manifestations, genetic heterogeneity and mutation continuum. Orphanet Journal of Rare Diseases *6*, 1-15.

Mahowald, A.P., and J.M., S. (1970). Intercellular migration of centrioles in the germarium of Drosophila melanogaster: an electron microscopic study. The Journal of Cell Biology *45*, 306-320.

Margaritis, L.H., Kafatos, F.C., and Petri, W.H. (1980). The eggshell of Drosophila melanogaster. I. Fine structure of the layers and regions of the wild-type eggshell. Journal of Cell Science *43*, 1-35;.

Marshall, W.F. (2009). Centriole evolution. Curr Opin Cell Biol *21*, 14-19.

Martell, J.D., Deerinck, T.J., Sancak, Y., Poulos, T.L., Mootha, V.K., Sosinsky, G.E., Ellisman, M.H., and Ting, A.Y. (2012). Engineered ascorbate peroxidase as a genetically encoded reporter for electron microscopy. Nat Biotechnol *30*, 1143-1148.

Matsumoto, Y., Hayashi, K., and Nishida, E. (1999). Cyclin-dependent kinase 2 (Cdk2) is required for centrosome duplication in mammalian cells. Current Biology *9*, 429-432.

McEvoy, A.L., Hoi, H., Bates, M., Platonova, E., Cranfill, P.J., Baird, M.A., Davidson, M.W., Ewers, H., Liphardt, J., and Campbell, R.E. (2012). mMaple: a photoconvertible fluorescent protein for use in multiple imaging modalities. PLoS One *7*, e51314.

McLamarrah, T.A., Buster, D.W., Galletta, B.J., Boese, C.J., Ryniawec, J.M., Hollingsworth, N.A., Byrnes, A.E., Brownlee, C.W., Slep, K.C., Rusan, N.M.*, et al.* (2018). An ordered pattern of Ana2 phosphorylation by Plk4 is required for centriole assembly. J Cell Biol *217*, 1217-1231.

Megraw, T.L., Kao, L.-R., and Kaufman, T.C. (2001). Zygotic development without functional mitotic centrosomes. Current Biology *11*, 116-120.

Megraw, T.L., Li, K., Kao, L.-R., and Kaufman, T.C. (1999). The Centrosomin protein is required for centrosome assembly and function during cleavage in Drosophila. Development *126*, 2829-2839.

Mennella, V., Agard, D.A., Huang, B., and Pelletier, L. (2014). Amorphous no more: subdiffraction view of the pericentriolar material architecture. Trends Cell Biol *24*, 188-197.

Mennella, V., Keszthelyi, B., McDonald, K.L., Chhun, B., Kan, F., Rogers, G.C., Huang, B., and Agard, D.A. (2012). Subdiffraction-resolution fluorescence microscopy reveals a domain of the centrosome critical for pericentriolar material organization. Nature cell biology *14*, 1159-1168.

Meraldi, P., Lukas, J., Fry, A.M., Bartek, J., and Nigg, E.A. (1999). Centrosome duplication in mammalian somatic cells requires E2F and Cdk2-cyclin A. Nature cell biology *1*, 88-93.

Mitchison, H.M., and Valente, E.M. (2017). Motile and non-motile cilia in human pathology: from function to phenotypes. J Pathol *241*, 294-309.

Moyer, T.C., Clutario, K.M., Lambrus, B.G., Daggubati, V., and Holland, A.J. (2015). Binding of STIL to Plk4 activates kinase activity to promote centriole assembly. J Cell Biol *209*, 863-878.

Muller, H., Schmidt, D., Steinbrink, S., Mirgorodskaya, E., Lehmann, V., Habermann, K., Dreher, F., Gustavsson, N., Kessler, T., Lehrach, H.*, et al.* (2010). Proteomic and functional analysis of the mitotic Drosophila centrosome. EMBO J *29*, 3344-3357.

Naveed, M., Kazmi, S.K., Amin, M., Asif, Z., Islam, U., Shahid, K., and Tehreem, S. (2018). Comprehensive review on the molecular genetics of autosomal recessive primary microcephaly (MCPH). Genet Res (Camb) *100*, e7.

Nigg, E.A. (2007). Centrosome duplication: of rules and licenses. Trends Cell Biol *17*, 215-221.

Nigg, E.A., Cajanek, L., and Arquint, C. (2014). The centrosome duplication cycle in health and disease. FEBS Lett *588*, 2366-2372.

Nigg, E.A., and Holland, A.J. (2018). Once and only once: mechanisms of centriole duplication and their deregulation in disease. Nat Rev Mol Cell Biol *19*, 297-312.

Nigg, E.A., and Raff, J.W. (2009). Centrioles, centrosomes, and cilia in health and disease. Cell *139*, 663-678.

Nonaka, S., Tanaka, Y., Okada, Y., Takeda, S., Harada, A., Kanai, Y., Kido, M., and Hirokawa, N. (1998). Randomization of Left–Right Asymmetry due to Loss of Nodal Cilia Generating Leftward Flow of Extraembryonic Fluid in Mice Lacking KIF3B Motor Protein. Cell *95*, 829-837.

Novak, Z.A., Conduit, P.T., Wainman, A., and Raff, J.W. (2014). Asterless licenses daughter centrioles to duplicate for the first time in Drosophila embryos. Current biology : CB *24*, 1276-1282.

Novak, Z.A., Wainman, A., Gartenmann, L., and Raff, J.W. (2016). Cdk1 Phosphorylates Drosophila Sas-4 to Recruit Polo to Daughter Centrioles and Convert Them to Centrosomes. Developmental cell *37*, 545-557.

O'Connell, K.F., Caron, C., Kopish, K.R., Hurd, D.D., Kemphues, K.J., Li, Y., and White, J.G. (2001). The C. elegans zyg1 gene encodes a regulator of centrosome duplication with distinct maternal and paternal roles in the embryo. Cell *105*, 547-558.

Ohta, M., Ashikawa, T., Nozaki, Y., Kozuka-Hata, H., Goto, H., Inagaki, M., Oyama, M., and Kitagawa, D. (2014). Direct interaction of Plk4 with STIL ensures formation of a single procentriole per parental centriole. Nat Commun *5*, 5267.

Ohta, M., Watanabe, K., Ashikawa, T., Nozaki, Y., Yoshiba, S., Kimura, A., and Kitagawa, D. (2018). Bimodal Binding of STIL to Plk4 Controls Proper Centriole Copy Number. Cell Rep *23*, 3160-3169 e3164.

Ormo, M., Cubitt, A.B., Kallio, K., Gross, L.A., Tsien, R.Y., and S.J., R. (1996). Crystal Structure of the Aequorea victoria Green Fluorescent Protein. Science *Orm 273*, 1392-1395.

Paintrand, M., Moudjou, M., Delacroix, H., and Bornens, M. (1992). Centrosome organization and centriole architecture: their sensitivity to divalent cations. Journal of Structural Biology *108*, 107-128.

Peel, N., Stevens, N.R., Basto, R., and Raff, J.W. (2007). Overexpressing centriole-replication proteins in vivo induces centriole overduplication and de novo formation. Current biology : CB *17*, 834-843.

Pelletier, L., O'Toole, E., Schwager, A., Hyman, A.A., and Muller-Reichert, T. (2006). Centriole assembly in Caenorhabditis elegans. Nature *444*, 619-623.

Pelletier, L., Ozlu, N., Hannak, E., Cowan, C., Habermann, B., Ruer, M., Muller-Reichert, T., and Hyman, A.A. (2004). The Caenorhabditis elegans centrosomal protein SPD-2 is required for both pericentriolar material recruitment and centriole duplication. Current biology : CB *14*, 863-873.

Qiao, R., Cabral, G., Lettman, M.M., Dammermann, A., and Dong, G. (2012). SAS-6 coiled-coil structure and interaction with SAS-5 suggest a regulatory mechanism in C. elegans centriole assembly. EMBO J *31*, 4334-4347.

Rand, M.D., Kearney, A.L., Dao, J., and Clason, T. (2010). Permeabilization of Drosophila embryos for introduction of small molecules. Insect Biochem Mol Biol *40*, 792-804.

Reider, C.L., Faruki, S., and Khodjakov, A. (2001). The centrosome in vertebrates: more than a microtubule- organizing center. Trends in Cell Biology *11*, 413-419.

Reiter, J.F., Blacque, O.E., and Leroux, M.R. (2012). The base of the cilium: roles for transition fibres and the transition zone in ciliary formation, maintenance and compartmentalization. EMBO Rep *13*, 608-618.

Renz, M. (2013). Fluorescence microscopy-a historical and technical perspective. Cytometry A *83*, 767-779.

Richens, J.H., Barros, T.P., Lucas, E.P., Peel, N., Pinto, D.M., Wainman, A., and Raff, J.W. (2015). The Drosophila Pericentrin-like-protein (PLP) cooperates with Cnn to maintain the integrity of the outer PCM. Biol Open *4*, 1052-1061.

Riparbelli, M.G., and Callaini, G. (2003). Drosophila parthenogenesis: a model for de novo centrosome assembly. Developmental Biology *260*, 298-313.

Roberts, D. (1986). Drosophila, a practical approach (Oxford: IRL Press).

Rodrigues-Martins, A., Bettencourt-Dias, M., Riparbelli, M., Ferreira, C., Ferreira, I., Callaini, G., and Glover, D.M. (2007a). DSAS-6 organizes a tube-like centriole precursor, and its absence suggests modularity in centriole assembly. Current biology : CB *17*, 1465-1472.

Rodrigues-Martins, A., Riparbelli, M., Callaini, G., Glover, D.M., and Bettencourt-Dias, M. (2007b). Revisiting the Role of the Mother Centriole in Centriole Biogenesis. Science *316*, 1046-1050.

Rodriguez, E.A., Campbell, R.E., Lin, J.Y., Lin, M.Z., Miyawaki, A., Palmer, A.E., Shu, X., Zhang, J., and Tsien, R.Y. (2016). The Growing and Glowing Toolbox of Fluorescent and Photoactive Proteins. Trends in Biochemical Sciences.

Rogers G.C., Rusan N.M., Peifer M., and S.L., R. (2009). A multicomponent assembly pathway contributes to the formation of acentrosomal microtubule arrays in interphase Drosophila cells. Molecular & Cellular Biology *19*, 3163-3178.

Rogers, G.C., Rusan, N.M., Roberts, D.M., Peifer, M., and Rogers, S.L. (2009). The SCF Slimb ubiquitin ligase regulates Plk4/Sak levels to block centriole reduplication. J Cell Biol *184*, 225-239.

Roque, H., Saurya, S., Pratt, M.B., Johnson, E., and Raff, J.W. (2018). Drosophila PLP assembles pericentriolar clouds that promote centriole stability, cohesion and MT nucleation. PLoS Genet *14*, e1007198.

Roque, H., Wainman, A., Richens, J., Kozyrska, K., Franz, A., and Raff, J.W. (2012). Drosophila Cep135/Bld10 maintains proper centriole structure but is dispensable for cartwheel formation. J Cell Sci *125*, 5881-5886.

Sakaue-Sawano, A., Kurokawa, H., Morimura, T., Hanyu, A., Hama, H., Osawa, H., Kashiwagi, S., Fukami, K., Miyata, T., Miyoshi, H.*, et al.* (2008). Visualizing spatiotemporal dynamics of multicellular cell-cycle progression. Cell *132*, 487-498.

Satish Tammana, T.V., Tammana, D., Diener, D.R., and Rosenbaum, J. (2013). Centrosomal protein CEP104 (Chlamydomonas FAP256) moves to the ciliary tip during ciliary assembly. J Cell Sci *126*, 5018-5029.

Saurya, S., Roque, H., Novak, Z.A., Wainman, A., Aydogan, M.G., Volanakis, A., Sieber, B., Pinto, D.M., and Raff, J.W. (2016). Drosophila Ana1 is required for centrosome assembly and centriole elongation. J Cell Sci *129*, 2514-2525.

Savoian, M.S., Goldberg, M.L., and Rieder, C.L. (2000). The rate of poleward chromosome motion is attenuated in Drosophila zw10 and rod mutants. Nature cell biology *2*, 948-952.

Schermelleh, L., Ferrand, A., Huser, T., Eggeling, C., Sauer, M., Biehlmaier, O., and Drummen, G.P.C. (2019). Super-resolution microscopy demystified. Nature cell biology *21*, 72-84.

Schermelleh, L., Heintzmann, R., and Leonhardt, H. (2010). A guide to super-resolution fluorescence microscopy. J Cell Biol *190*, 165-175.

Schmidt, T.I., Kleylein-Sohn, J., Westendorf, J., Le Clech, M., Lavoie, S.B., Stierhof, Y.D., and Nigg, E.A. (2009). Control of centriole length by CPAP and CP110. Current biology : CB *19*, 1005-1011.

Schneider, I. (1972). Cell lines derived from late embryonic stages of Drosophila melanogaster Development *27*, 353-356.

Schnell, U., Dijk, F., Sjollema, K.A., and Giepmans, B.N. (2012). Immunolabeling artifacts and the need for live-cell imaging. Nat Methods *9*, 152-158.

Schnerch, D., and Nigg, E.A. (2016). Structural centrosome aberrations favor proliferation by abrogating microtubule-dependent tissue integrity of breast epithelial mammospheres. Oncogene *35*, 2711-2722.

Shaner, N.C., Campbell, R.E., Steinbach, P.A., Giepmans, B.N., Palmer, A.E., and Tsien, R.Y. (2004). Improved monomeric red, orange and yellow fluorescent proteins derived from Discosoma sp. red fluorescent protein. Nat Biotechnol *22*, 1567-1572.

Shaner, N.C., Lambert, G.G., Chammas, A., Ni, Y., Cranfill, P.J., Baird, M.A., Sell, B.R., Allen, J.R., Day, R.N., Israelsson, M.*, et al.* (2013). A bright monomeric green fluorescent protein derived from Branchiostoma lanceolatum. Nat Methods *10*, 407-409.

Shaner, N.C., Lin, M.Z., McKeown, M.R., Steinbach, P.A., Hazelwood, K.L., Davidson, M.W., and Tsien, R.Y. (2008). Improving the photostability of bright monomeric orange and red fluorescent proteins. Nat Methods *5*, 545-551.

Sharma, A., Aher, A., Dynes, N.J., Frey, D., Katrukha, E.A., Jaussi, R., Grigoriev, I., Croisier, M., Kammerer, R.A., Akhmanova, A.*, et al.* (2016). Centriolar CPAP/SAS-4 Imparts Slow Processive Microtubule Growth. Developmental cell *37*, 362-376.

Shcherbo, D., Merzlyak, E.M., Chepurnykh, T.V., Fradkov, A.F., Ermakova, G.V., Solovieva, E.A., Lukyanov, K.A., Bogdanova, E.A., Zaraisky, A.G., Lukyanov, S.*, et al.* (2007). Bright far-red fluorescent protein for whole-body imaging. Nat Methods *4*, 741-746.

Shcherbo, D., Murphy, C.S., Ermakova, G.V., Solovieva, E.A., Chepurnykh, T.V., Shcheglov, A.S., Verkhusha, V.V., Pletnev, V.Z., Hazelwood, K.L., Roche, P.M.*, et al.* (2009). Far-red fluorescent tags for protein imaging in living tissues. Biochem J *418*, 567-574.

Shimomura, O., Johnson, F.H., and Saiga, Y. (1962). Extraction, Purification and Properties of Aequorin, a Bioluminescent Protein from the Luminous Hydromedusan, Aequorea. J Cell Comp Physiol *59*, 223-239.

Shinoda, H., Ma, Y., Nakashima, R., Sakurai, K., Matsuda, T., and Nagai, T. (2018). Acid-Tolerant Monomeric GFP from Olindias formosa. Cell Chem Biol *25*, 330-338 e337.

Shu, X., Lev-Ram, V., Deerinck, T.J., Qi, Y., Ramko, E.B., Davidson, M.W., Jin, Y., Ellisman, M.H., and Tsien, R.Y. (2011). A genetically encoded tag for correlated light and electron microscopy of intact cells, tissues, and organisms. PLoS Biol *9*, e1001041.

Shu, X., Shaner, N.C., Yarbrough, C.A., Tsien, R.Y., and Remington, S.J. (2006). Novel Chromophores and Buried Charges Control Color in mFruits. Biochemistry *45*, 9639-9647.

Shukla, A., Kong, D., Rajasekaran, V., and Loncarek, J. (2016). Centriole reduplication block is lost in prophase and coupled with degrations of the centrsomal proteins in mitosis.

Sillibourne, J.E., Tack, F., Vloemans, N., Boeckx, A., Thambirajah, S., Bonnet, P., Ramaekers, F.C.S., Bornens, M., and Grand-Perret, T. (2010). Autophosphorylation of Polo-like Kinase 4 and Its Role in Centriole Duplication. Molecular Biology of the Cell *21*, 547-561.

Singla, V., and Reiter, J.F. (2006). The primary cilium as the cells antenna signaling at the sensory organelle. Science *313*, 629-633.

Sir, J.H., Putz, M., Daly, O., Morrison, C.G., Dunning, M., Kilmartin, J.V., and Gergely, F. (2013). Loss of centrioles causes chromosomal instability in vertebrate somatic cells. J Cell Biol *203*, 747-756.

Slevin, L.K., Nye, J., Pinkerton, D.C., Buster, D.W., Rogers, G.C., and Slep, K.C. (2012). The structure of the plk4 cryptic polo box reveals two tandem polo boxes required for centriole duplication. Structure *20*, 1905-1917.

Sonnen, K.F., Gabryjonczyk, A.M., Anselm, E., Stierhof, Y.D., and Nigg, E.A. (2013). Human Cep192 and Cep152 cooperate in Plk4 recruitment and centriole duplication. J Cell Sci *126*, 3223-3233.

Sonnen, K.F., Schermelleh, L., Leonhardt, H., and Nigg, E.A. (2012). 3D-structured illumination microscopy provides novel insight into architecture of human centrosomes. Biol Open *1*, 965-976.

Spektor, A., Tsang, W.Y., Khoo, D., and Dynlacht, B.D. (2007). Cep97 and CP110 suppress a cilia assembly program. Cell *130*, 678-690.

Stevens, N.R., Dobbelaere, J., Brunk, K., Franz, A., and Raff, J.W. (2010a). Drosophila Ana2 is a conserved centriole duplication factor. J Cell Biol *188*, 313-323.

Stevens, N.R., Raposo, A.A., Basto, R., St Johnston, D., and Raff, J.W. (2007). From stem cell to embryo without centrioles. Current biology : CB *17*, 1498-1503.

Stevens, N.R., Roque, H., and Raff, J.W. (2010b). DSas-6 and Ana2 coassemble into tubules to promote centriole duplication and engagement. Developmental cell *19*, 913-919.

Strnad, P., Leidel, S., Vinogradova, T., Euteneuer, U., Khodjakov, A., and Gonczy, P. (2007). Regulated HsSAS-6 levels ensure formation of a single procentriole per centriole during the centrosome duplication cycle. Developmental cell *13*, 203-213.

Tang, C.J., Fu, R.H., Wu, K.S., Hsu, W.B., and Tang, T.K. (2009). CPAP is a cell-cycle regulated protein that controls centriole length. Nature cell biology *11*, 825-831.

Tang, C.J., Lin, S.Y., Hsu, W.B., Lin, Y.N., Wu, C.T., Lin, Y.C., Chang, C.W., Wu, K.S., and Tang, T.K. (2011). The human microcephaly protein STIL interacts with CPAP and is required for procentriole formation. EMBO J *30*, 4790-4804.

Tinevez, J.Y., Perry, N., Schindelin, J., Hoopes, G.M., Reynolds, G.D., Laplantine, E., Bednarek, S.Y., Shorte, S.L., and Eliceiri, K.W. (2017). TrackMate: An open and extensible platform for single-particle tracking. Methods *115*, 80-90.

Tsou, M.F., and Stearns, T. (2006). Mechanism limiting centrosome duplication to once per cell cycle. Nature *442*, 947-951.

Tsutsumi, M., Yokoi, S., Miya, F., Miyata, M., Kato, M., Okamoto, N., Tsunoda, T., Yamasaki, M., Kanemura, Y., Kosaki, K.*, et al.* (2016). Novel compound heterozygous variants in PLK4 identified in a patient with autosomal recessive microcephaly and chorioretinopathy. Eur J Hum Genet.

van Breugel, M., Hirono, M., Andreeva, A., Yanagisawa, H., Yamaguchi, Y., Nakazawa, Y., Morgner, N., Petrovich, M., Ebong, I.-O., Robinson, C.V.*, et al.* (2011). Structures of Sas6 suggests its organisation in centrioles. Science *331*, 1196-1199.

van Breugel, M., Wilcken, R., McLaughlin, S.H., Rutherford, T.J., and Johnson, C.M. (2014). Structure of the SAS-6 cartwheel hub from Leishmania major. eLife *3*, e01812.

Varmark, H., Llamazares, S., Rebollo, E., Lange, B., Reina, J., Schwarz, H., and Gonzalez, C. (2007). Asterless is a centriolar protein required for centrosome function and embryo development in Drosophila. Current biology : CB *17*, 1735-1745.

Vicente, C. (2013). Elucidating the pathway of centrosome formation. In Sir William Dunn School of Pathology (Oxford: University of Oxford), pp. 277.

Vitre, B., Holland, A.J., Kulukian, A., Shoshani, O., Hirai, M., Wang, Y., Maldonado, M., Cho, T., Boubaker, J., Swing, D.A.*, et al.* (2015). Chronic centrosome amplification without tumorigenesis. Proceedings of the National Academy of Sciences of the United States of America *112*, E6321-6330.

Vulprecht, J., David, A., Tibelius, A., Castiel, A., Konotop, G., Liu, F., Bestvater, F., Raab, M.S., Zentgraf, H., Izraeli, S.*, et al.* (2012). STIL is required for centriole duplication in human cells. J Cell Sci *125*, 1353-1362.

Wakefield, J.G., Huang, J., and Raff, J.W. (2000). Centrosomes have a role in regulating the destruction of cyclin B in early Drosophila embryos. Current biology : CB *10*, 1367-1370.

Wang, J.T., Kong, D., Hoerner, C.R., Loncarek, J., and Stearns, T. (2017). Centriole triplet microtubules are required for stable centriole formation and inheritance in human cells. eLife *6*.

Wang, S., Moffitt, J.R., Dempsey, G.T., Xie, X.S., and Zhuang, X. (2014). Characterization and development of photoactivatable FP for single molecule based superresolution imaging. PNAS *111*, 8452-8457.

Wang, W.-J., Acehan, D., Jane, W.-N., Uryu, K., and Tsou, B. (2015). De novo centriole formation in human cells is error-prone and does not require SAS-6 self- assembly. eLife.

Wang, W.J., Soni, R.K., Uryu, K., and Tsou, M.F. (2011). The conversion of centrioles to centrosomes: essential coupling of duplication with segregation. J Cell Biol *193*, 727-739.

Water, A.M., and Beales, P.L. (2011). Ciliopathies: an expanding disease spectrum. Pediatric Nephrology *26*, 1039-1056.

Waterhouse, A.M., Procter, J.B., Martin, D.M., Clamp, M., and Barton, G.J. (2009). Jalview Version 2--a multiple sequence alignment editor and analysis workbench. Bioinformatics *25*, 1189-1191.

Wegel, E., Gohler, A., Lagerholm, B.C., Wainman, A., Uphoff, S., Kaufmann, R., and Dobbie, I.M. (2016). Imaging cellular structures in super-resolution with SIM, STED and Localisation Microscopy: A practical comparison. Sci Rep *6*, 27290.

Winey, M., and O'Toole, E. (2014). Centriole structure. Philos Trans R Soc Lond B Biol Sci *369*.

Yang, T.T., Chong, W.M., Wang, W.J., Mazo, G., Tanos, B., Chen, Z., Tran, T.M.N., Chen, Y.D., Weng, R.R., Huang, C.E.*, et al.* (2018). Super-resolution architecture of mammalian centriole distal appendages reveals distinct blade and matrix functional components. Nat Commun *9*, 2023.

Yao, K.-M., and White, K. (1994). Neural Specificity of elav Expression: Defining a Drosophila Promoter for Directing Expression to the Nervous System. Journal of Neurochemistry *63*, 41-51.

Zhang, R., Alushin, G.M., Brown, A., and Nogales, E. (2015). Mechanistic Origin of Microtubule Dynamic Instability and Its Modulation by EB Proteins. Cell *162*, 849-859.

Zhou, F., and Roy, S. (2015). SnapShot: Motile Cilia. Cell *162*, 224-224 e221.

Zhu, F., Lawo, S., Bird, A., Pinchev, D., Ralph, A., Richter, C., Muller-Reichert, T., Kittler, R., Hyman, A.A., and Pelletier, L. (2008). The mammalian SPD-2 ortholog Cep192 regulates centrosome biogenesis. Current biology : CB *18*, 136-141.

Zitouni, S., Francia, M.E., Leal, F., Montenegro Gouveia, S., Nabais, C., Duarte, P., Gilberto, S., Brito, D., Moyer, T., Kandels-Lewis, S*., et al.* (2016). CDK1 Prevents Unscheduled PLK4-STIL Complex Assembly in Centriole Biogenesis. Current biology : CB.

Zitouni, S., Nabais, C., Jana, S.C., Guerrero, A., and Bettencourt-Dias, M. (2014). Polo-like kinases: structural variations lead to multiple functions. Nat Rev Mol Cell Biol *15*, 433-452.